

**CHARACTERISTICS OF LATERAL-
FRONTAL MORaine FORMED BY
ARCTIC AND ALPINE GLACIERS**

Toby N. Tonkin

A thesis submitted in partial fulfilment of the requirements of
Nottingham Trent University for the degree of Doctor of
Philosophy

January 2016

Copyright Statement

This work is the intellectual property of the author (Note: if there are other owners of the IP, as a consequence of any statement issued under paragraph 12 of Section 14A, they must also be named here). You may copy up to 5% of this work for private study, or personal, non-commercial research. Any re-use of the information contained within this document should be fully referenced, quoting the author, title, university, degree level and pagination. Queries or requests for any other use, or if a more substantial copy is required, should be directed in the owner(s) of the Intellectual Property Rights.

Abstract

Recent climatic amelioration during the 20th and 21st centuries has stimulated the recession of glaciers world-wide. Moraines developed by valley glaciers provide a sedimentary record of their past response to climatic forcing. Despite the use of moraines for understanding the character and behaviour of former glaciers, our understanding of moraine development is lacking largely due to limited opportunities to study active moraine formation. This thesis reports on internal structure and sedimentary composition of lateral-frontal moraine at two Arctic (Austre Lovénbreen, Svalbard and Isfallsglaciären, Sweden) glaciers and one Alpine (Schwarzberggletscher, Switzerland) glacier and aids understanding of their palaeo-environmental significance.

The internal structure and sedimentary architecture of Arctic lateral-frontal moraine is documented using ground penetrating radar (GPR) and via shallow excavation. Lateral-frontal moraine at both Arctic sites are shown to contain buried ice within their lateral zones, but not within their frontal zones, although the volumetric content of the buried ice and potential origin varies between sites. Frontal zones are therefore likely to be better preserved in the geomorphological record following complete de-icing, whereas lateral zones, which may also be subject to de-icing and external censoring from slope processes, may be poorly preserved. As the internal structure is dissimilar across Arctic sites, it is argued that the processes involved in the development of landforms by Arctic polythermal glaciers vary between high-Arctic and continental Scandinavian settings. Arctic lateral-frontal moraine are also distinct from those found at Alpine sites which are organised into stacked diamicton units that dip away from the lateral margin of the glacier. The sedimentary signature of Arctic and Alpine lateral-frontal moraine are investigated and compared. All moraines investigated exhibit clast-form gradients which is interpreted to relate to the relative significance and spatial variation of 'active' and 'passive' debris transport mechanisms within Arctic and Alpine valley glacier landsystems. However, the climatic, glaciological, and topographic regimes in which the moraines form influence the resulting character of the landform. The evolution of a degrading ice-cored moraine at Austre Lovénbreen is investigated using repeat photogrammetric topographic surveys. Relict glacier ice is undergoing moderate rates of degradation, predominately via down-wastage and could potentially be preserved as an archive of former high-Arctic glacier characteristics.

This thesis also contributes to the wider body of knowledge in relation to the use of unmanned aerial vehicles (UAVs) and 'Structure-from-Motion' (SfM) photogrammetry for geomorphological research. The multi-technique approach employed by this research has allowed for the glaciological significance of subsets of lateral-frontal moraine ('Controlled', 'Østrem' and 'Alpine' type) within in glaciated valley landsystem to be better understood. Conceptual models accounting for landform development are presented and aid Quaternary studies that seek to identify and use lateral-frontal moraine for dating past glacier activity and determining palaeo-glacier characteristics.



Brøggerhalvøya, Svalbard

Acknowledgements

Nottingham Trent University are thanked for funding this project through a VC bursary scholarship and for providing additional funding for fieldwork and equipment. Most significantly, I would like to thank Dr. Nicholas Midgley for initially encouraging me to conduct geomorphological research, joining me on field-work, and mostly for persisting with my pessimism over the last three years! I am sincerely grateful for the opportunity and hope the publications that follow this research are adequate recompense. Additional thanks go to my second and third supervisors; Dr. Jill Labadz and Dr. David Graham. I would also like to thank Dr. David Graham and the Department of Geography at Loughborough University in general for providing access to equipment and resources. I would also like to thank my examiners Prof. Neil Glasser and Dr. Ben Clutterbuck for a challenging, but enjoyable viva, and for providing comments which helped improve the thesis.

The following organisations are thanked for providing logistical support whilst in the field; Norsk Polarinstutute for research in Svalbard under winter conditions; Nick Cox and the BAS/NERC for research in Svalbard under summer conditions; and Prof. Gunhild Rosqvist and the staff at Tarfala Research Station (Stockholm University) for summer and winter research in Arctic Sweden. Research in Arctic Sweden received additional funding from the European Union Seventh Framework Programme [FP7/2007-2013] under grant agreement n° 262693 [INTERACT].

Access to Cwm Idwal was granted by the National Trust. Field assistance provided by Anya Wicikowski, Dr. Simon Cook, Alex Walkinshaw, Emma Jolly, Luke Tonkin, Steven Clough, Rob Davis and Tom Biddulph is gratefully acknowledged. Thanks is extended to the research students at Trent; specifically to Dr Louis Phipps and Dr Tim Stratton for sharing in the PhD journey. Esther Kettel is thanked for her support during the final stages of the write up. Finally, I would like to thank my family and friends for their support over the past three years.

Table of Contents

1. Introduction and research context.....	1
1.1 Introduction	1
1.2 Overview of existing research	3
1.2.1 Alpine and high-mountain moraine development	3
1.2.2 Arctic and high-Arctic ice-cored ‘controlled’ moraines.....	9
1.2.3 ‘Østrem’ snowbank type ridges in Scandinavia.....	15
1.3.4 Push moraine and glaciotectonism.....	16
1.5 Rationale	18
1.6 Aim and objectives.....	18
1.6.1 Research aim.....	18
1.6.2 Research questions.....	18
1.6.3 Research objectives	19
1.7 Overview of the thesis.....	19
2. Research methods	22
2.1 Overview	22
2.2 Research approach	22
2.3 Study site selection.....	23
2.3.1 Overview of study site selection	23
2.3.2 Cwm Idwal.....	23
2.3.3 Schwarzberggletscher, Switzerland.....	23
2.3.4 Isfallsgläciären, Sweden	24
2.3.5 Austre Lovénbreen, Svalbard	24
2.4 Ground-penetrating radar	27
2.4.1 Introduction	27
2.4.2 Physics of ground-penetrating radar	27
2.4.3 Field data acquisition.....	28
2.4.4 Post-processing.....	31
2.4.5 Semblance analysis	34
2.4.6 Interpretation of radar datasets.....	34
2.5 Sedimentology	35
2.5.1 Introduction	35
2.5.2 Description of texture	36
2.5.3 Clast form analysis.....	38
2.5.4 Clast macrofabric analysis	40
2.5.5 Grain-size analysis	40
2.6 Geomorphological mapping.....	42
2.6.1 Overview and approach.....	42
2.6.2 Photogrammetry and UAV-based mapping	43
2.7 Structural glaciological mapping and interpretation.....	44

3. The potential of unmanned aerial vehicles and structure-from-motion for topographic surveys: a test of emerging integrated approaches at Cwm Idwal, North Wales.....	46
3.1 Introduction	46
3.2 Study area.....	47
3.3.1 Image and data acquisition.....	50
3.3.2 Image processing and analysis.....	53
3.4 Results.....	54
3.5 Discussion.....	57
3.5.1 Causes of vertical disagreement.....	57
3.5.2 Benefits and practical considerations	61
3.5.3 UAVs and SfM as a tool for geomorphological mapping and monitoring morphometric change.....	62
3.6 Conclusions and summary	63
4. Debris supply, transport and moraine development in high-mountain environments: an example from Schwarzbergletscher, Switzerland.....	65
4.1 Introduction and site specific methods	65
4.1.1. Chapter overview.....	65
4.1.2. Site specific methods.....	66
4.2 Study site and historical records of glacier change	67
4.2.1 Overview	67
4.2.2 Archive ground-level imagery	69
4.2.3 Historical maps.....	71
4.2.4 Glacier length measurements.....	73
4.3 Results.....	74
4.3.1 Moraine descriptions and reference codes	74
4.3.2 Proximal-slope morphometry	78
4.3.3 Sedimentology	81
4.3.4 Structural glaciology.....	96
4.4 Discussion.....	101
4.4.1 Synthesis of structural glaciological interpretation and debris transport.....	101
4.4.2 Dumping	103
4.4.3 Subglacial lodgement and traction	104
4.4.4 Debris transport and clast-form	104
4.4.5 Moraine morphology and topographic controls	106
4.4.6 Landform stability and preservation potential	106
4.5 Summary	109
5. The character and significance of ice-cored moraine complexes at the margins of polythermal Arctic glaciers: insights from a multi-technique approach at Isfallsglaciären, Sweden	110
5.1 Introduction	110
5.2 Study site description	111
5.3 Site specific methodology	114
5.4 Results.....	115
5.4.1 Radar-wave velocities.....	115

5.4.3 Internal structure.....	119
5.4.4 Sedimentology	123
5.5. Interpretation	127
5.5.1 Radar wave velocities and likely composition.....	127
5.5.2 Internal structure and sedimentology	129
5.6. Discussion.....	131
5.6.1 Development and chronology of moraines at Isfallsglaciären	131
5.6.2 Reconciling existing geochronologies and structural data.....	134
5.6.3 The potential of high-resolution topographic data for future research.....	135
5.7 Summary	135
6. Structural character, sedimentology and evolution of a high-Arctic lateral-frontal moraine: Austre Lovénbreen, Svalbard	136
6.1 Introduction	136
6.2 Study Site and site specific methods	137
6.2.1 Site overview.....	137
6.2.2 Site specific methods.....	138
6.3 Results.....	143
6.3.1 Internal structure.....	143
6.3.2 Radar wave propagation velocities	143
6.3.3 Glacier change and moraine development: 1892-2003 AD	151
6.3.4 Lithofacies descriptions.....	164
6.3.5 Clast-form analysis	171
6.3.6 Moraine evolution: 2003-2014.....	175
6.4 Discussion.....	180
6.4.1 Structural character and origin of buried-ice	180
6.4.2 Lateral-zone formation and evolution	182
6.4.3 Frontal-zone formation.....	183
6.4.4 Influences on rates of moraine disintegration.....	187
6.4.5 Limitations and issues related to the application of UAV topographic surveys and SfM Photogrammetry	190
6.5 Summary	191
7. Discussion and conclusions	193
7.1 Introduction	193
7.2 Discussion of study objectives.....	193
7.3 Limitations	202
7.4 Future research	203
7.6 Conclusions	204
8. References.....	206

Appendix I:

Tonkin, T.N., Midgley, N.G., Graham, D.J. and Labadz, J.C. 2014. The potential of small unmanned aircraft systems and structure-from-motion for topographic surveys: A test of emerging integrated approaches at Cwm Idwal, North Wales. *Geomorphology*, 226, 35-43

Appendix II:

Midgley, N.G., Cook, S.J., Graham, D.J. and Tonkin, T.N. 2013. Origin, evolution and dynamic context of a Neoglacial lateral–frontal moraine at Austre Lovénbreen, Svalbard. *Geomorphology*, 198, 96-106.

Appendix III:

Cook, S.J., Tonkin, T.N., Midgley, N.G., and Wicikowski, A. 2015. Analysis of 'hummocky moraine' using Structure-from-Motion photogrammetry. *North West Geography*, 15 (1), 9-18.

Appendix IV:

Tonkin, T.N., Midgley, N.G., Cook, S.J. and Graham, D.J. 2016. Ice-cored moraine degradation mapped and quantified using an unmanned aerial vehicle: A case study from a polythermal glacier in Svalbard. *Geomorphology*, 158, 1-10.

List of Figures

Fig. 1.1. Block diagram of a glacier and associated lateral-frontal moraine within the glacier foreland.	1
Fig. 1.2 Debris transport in high-Arctic glaciers adapted from Hambrey <i>et al.</i> (1999).	11
Fig. 2.1 Location map for the three glaciers and one formerly glaciated site investigated by this project.....	26
Fig. 2.2 GPR survey configurations redrawn from Neal (2004). Common offset surveys are also referred to as reflection surveys. Common mid-point, common source and common receiver survey configurations are used in this thesis to determine the propagation velocity of radar-waves. The latter two require either the transmitter or receiver to remain in a fixed location.	30
Fig. 2.3 Simplified overview of post-processing method used here.	32
Fig. 2.4 Example of uncorrected, and corrected topographic of a radar transect. Note the reorientation of the dipping reflectors following correction to a velocity of 0.17 m ns^{-1} . 33	33
Fig. 2.5 A schematic showing the effect of wow, and the result of its removal. Illustration is redrawn from Cassidy (2009).	33
Fig. 2.6 Radar terminology in relation to nine distinct radar signatures from Pellicer and Gibson (2011).	35
Fig. 2.7 Classification adopted by this thesis for the description of poorly sorted sediments. Classification adapted from Hambrey and Glasser (2012).	37
Fig. 3.1 Maps showing the study site location in relation to (A) North-west Europe and (B) North Wales. ©Crown Copyright/database right 2014. An Ordnance Survey/EDINA supplied service. (C) A ground-level panoramic photograph of the moraine-mound complex which is located on both the left and right of Llyn Idwal.	49
Fig. 3.2 A schematic drawing of the S800 hexacopter	52
Fig. 3.3 Maps displaying the topographic data and analysis of vertical disagreement. (a) The distribution of 7761 ground-survey points and 19 SfM ground-control points across the survey area. Two zones (Z1 and Z2) of distinct ground cover are delimited. (b) A hillshaded DSM at 0.088 m per pixel resolution derived from the UAV-SfM survey. (c) A raster surface of vertical difference produced using an ordinary kriging function at a resolution of 2.1 m per pixel. The spatial extent of the spot heights is delimited by the dashed line.	56
Fig. 3.4 Histograms of vertical difference for the east and west sections of Cwm Idwal	58

Fig. 3.5 The occurrence of vertical difference in association with: (a) vegetation, (b) near vertical and in places partially overhanging bedrock rafts, and (c) positional misregistration close to near vertical slopes.....60

Fig. 4.1 Schwarzberggletscher. (A) The glaciers location in relation to Switzerland. (B) Ground-level image of the terminus from the left-lateral moraine in 2013. (C) An orthorectified aerial image of the glacier in 2009 from Swisstopo. (D) Location of the study site with moraine indicated by the thick red line.68

Fig. 4.2 Historical Illustrations and photographs of Schwarzberggletscher. (A) An illustration by M. de Meuron dated to 1822 looking north along Saastal with Schwarzberggletscher in the middle distance, and Allalingsletscher in the far distance. (B) An illustration by E.Lafon dated to 1859, looking south-west towards the margin of Schwarzberg from the surface of Allalingsletscher. (C) An image of the upper terminus by Otto Lütschg dated to 1915. (D) A 1919 image of the glacier terminus. (E) An image of Schwarzberggletscher and Hangendgletscher dated to October 4, 1921. (F) An image of Schwarzberggletscher abutting the left-lateral moraine in 1922. All images are taken from the ETH-Bibliothek's Image Archive (2013) and are licensed under Creative Commons.70

Fig. 4.3 Historical maps of Schwarzberggletscher. (A) The Dufour map (1863). (B) The Siegfried map (1924). (C) National map of Switzerland (1968). The red circle shows the excavated area of moraine following the construction of the Mattmark dam.72

Fig. 4.4 Length change measurements of Schwarzberggletscher from 1880 to 2014 from SCNAT (2015).73

Fig. 4.5 Moraine locations and reference codes used within the text. Red dashed line is the bedrock step.....76

Fig. 4.6 Ground-level imagery of the lateral moraines of Schwarzberggletscher. (A) A single (older) linear ridge (M2) outside the upper-lateral complex and partially coalescing valley-side debris fans. (B) A series of 4 ridges located on the distal slope of the upper-lateral complex (M3-6). (C) Inset lateral-frontal ridges developed close to the current terminus (M7 and M8). (D) The distal slope of the lower left-lateral moraine complex which anastomoses into multiple distinct ridges (M10-M14). (E) An overview of the glacial terminus in August 2013. Note the extensive supraglacial debris cover to the right of the image. In contrast, a thin valley-side drape of sediment which constitutes the right lateral moraine of Schwarzberggletscher is visible to left of the photo. Volumetrically, these moraines show a marked asymmetry to the left-lateral moraines complex (to the right of the image).....77

Fig. 4.7 Five characteristic topographic profiles from the lateral moraine complex. T₁ is adjacent to the current glacier terminus, and T₅ is the furthest down moraine.79

Fig. 4.8 Sediment sampling locations84

Fig. 4.9 Exemplar sedimentary logs. (a) Gravelly sand lithofacies SCH-02 and SCH-05 (b) diamicton sedimentary exposures. SCH-35 and SCH-44.85

Fig. 4.10 Ground-level photography displaying the location of angular gravel surface lithofacies. (a) Angular gravel forming the supraglacial lateral moraine on the true left of Schwarzberggletscher and a drape of sediment in front of the receding glacier terminus. (b) Close up of the angular gravel lithofacies on the glacier surface with the author for scale. Note the abundance of angular slabby and elongate clasts.....	86
Fig. 4.11 Further visualisation of <2mm fraction of glacial sediment sampled at Schwarzberggletscher. (a) A ternary diagram showing the grain-size distribution of moraine samples. (b) Mean grain size plotted against the sorting coefficient for each sample.....	89
Fig. 4.12 Clast fabric data. Nine clast fabrics taken from the inner ice-proximal slopes of the lateral-frontal complex. Principle eigenvalues (S_1 , S_2 & S_3) are presented by each sample. All data is projected using lower hemisphere equal area Schmidt nets.	92
Fig. 4.13 Bivariate plot of clast fabric data (including SCH-02) with envelopes from Dowdeswell and Sharp (1986). Samples 18, 44L and 44U show clustering whereas other samples overlap with a range of depositional environments with clasts lacking preferred orientation and dip.....	93
Fig. 4.14 RA/C ₄₀ plot of 42 clast samples of $n = 50$ sorted by depositional environment .	94
Fig. 4.15 Linear and polynomial regression plots investigating the modification of various clast-form parameters with Euclidean distance down-valley from ice-proximal exposures.	95
Fig. 4.16 Structural interpretation of Schwarzberggletscher (B) derived from 2009 orthorectified aerial imagery (A).	97
Fig. 4.17. (A) Ground level photograph of the glacier terminus in 2004. (B) An interpretation of key features including the identification of debris-bearing structures melting out close to the terminus which are no longer present at the glacier terminus.	102
Fig. 4.18. Conceptual model for the development of lateral moraine at the margin of Schwarzberggletscher. Glacier flow is perpendicular to the cross-section.	108
Fig. 5.1 Study site location. (A) The location of the Kebnekaise Mountains in relation to Scandinavia. (B) Glaciers located on the Eastern flank of Kebnekaise. (C) Ground-level photograph of Isfallsgläciären and the moraine complex from Tarfala Research Station in 2013.....	113
Fig. 5.2 (A) Lantmateriet orthorectified image of the study area dated to 2009. (B) Geomorphological interpretation of the Lantmateriet orthorectified image.....	114
Fig. 5.3 High-resolution topographic data and the locations of radar surveys undertaken in spring 2013.....	116
Fig. 5.4 Exemplar WARR and CMP surveys demonstrating contrasting sub-surface conditions on the southern-lateral complex and frontal moraines. Patches of purple indicate clustering of stacked GPR velocities (e.g. the average propagation velocity which	

reflect the sub-surface sedimentology and characteristics). The frontal ridges show slower velocities ($\sim 0.11 \text{ m ns}^{-1}$) than lateral ridges ($0.15 \text{ to } 0.17 \text{ m ns}^{-1}$) indicating different subsurface conditions.	118
Fig. 5.5 100 MHz common offset radargrams. Data is topographically migrated using a propagation velocity of 0.15 m ns^{-1} for transects 1-3 and a velocity of 0.10 m ns^{-1} for profiles 4-7. Profile 7 has not been topographically migrated to more readily distinguish the sub-parallel reflectors. The actual topography is gentle sloping from left to right. Locations are highlighted in Fig 5.3.....	121
Fig. 5.6 Interpreted radargrams with surface sedimentology and velocity surveys highlighted. The radargrams were qualitatively assessed and coherent reflectors were digitised.	122
Fig. 5.7 (a) Clast form and (b) matrix particle size of lithofacies within the Isfallsglaciären moraines. Sampled material has a limited clay content.....	126
Fig. 5.8 (A) Ground-level photography taken by Enquist in 1910. (B) Interpretation of the ground-level photography showing debris run-out over the moraine distal slope of the inner-frontal ridge.....	132
Fig. 5.9 Conceptual model for the development and chronology of moraines at Isfallsglaciären.	133
Fig. 6.1 Location of the landforms studied in this research. (A) The location of Kongsfjorden in relation to Svalbard. (B) The position of Austre Lovénbreen in relation to Ny-Ålesund and adjacent glaciers.....	139
Fig. 6.2 Geomorphological interpretation of the Austre Lovénbreen lateral-frontal complex from 2014 topographic data with the approximate locations of hillshaded DEMs as shown Fig. 6.3 A and B.	140
Fig. 6.3 Hill-shaded DEM illustrating morphological characteristics of the lateral-frontal complex. (a) Surface linearity. (b) Surface irregularity ('hummocks').....	141
Fig. 6.4 Ground-level photograph illustrating morphological characteristics of the lateral-frontal complex. (A) Increasing topographic irregularity in frontal sections of the moraine complex. (B) Surface linearity in lateral sections of the landform.....	142
Fig. 6.5 The locations of nine GPR reflection surveys on the eastern lateral-frontal moraine in relation to the glacier terminus.	144
Fig. 6.6 100 MHz Reflection surveys transversely dissecting the western lateral-frontal ridge. (A) Transects 1-3. (B) Transects 4-6. (C) Transects 7-9 (Fig. 4 in Midgley <i>et al.</i> , 2013).	145
Fig. 6.7 Interpreted radar grams of the 9 100 MHz Reflection surveys (Fig. 4 in Midgley <i>et al.</i> , 2013). The radargrams were qualitatively assessed.	148

Fig. 6.8 Examples of CMP semblance analysis from (a) transect 2 and (b) transect 9 (Fig. 3 in Midgley <i>et al.</i> , 2013). Radar-wave velocity is not consistent across the study area, indicating variable subsurface characteristics.....	150
Fig. 6.9 (A) Vestre, Midtre and Austre Lovénbreen in 1892 as mapped by Hamberg (1894). (B) Debris-bearing features emerging from the terminus and subsequently contributing to moraine construction at Midtre Lovénbreen (Fig 9. in Hambrey <i>et al.</i> , 2005).	152
Fig. 6.10 Early historical imagery and interpretation of Austre Lovénbreen in 1907 taken from Isachsen (1912). (A) Austre Lovénbreen viewed from Bloomstrand. (B) Austre Lovénbreen viewed from the west.	154
Fig. 6.11 Neighbouring Midtre Lovénbreen in 1918 as viewed from Ny-Ålesund. Note the steep glacier terminus, with emerging debris structures visible above the Neoglacial moraine rampart.....	156
Fig. 6.12 Interpretation of Austre Lovénbreen in 1936 from an oblique aerial image obtained from the Norwegian Polar Institute (image S36 1553). This diagram appears in Midgley <i>et al.</i> (2013) as Fig. 6. (A) Original image. (B) Interpretation.	159
Fig. 6.13 Interpretation of Austre Lovénbreen in 1948 from aerial imagery obtained from the Norwegian Polar Institute (image S48 752). (A) Original image. (B) Interpretation.	161
Fig. 6.14 Interpretation of Austre Lovénbreen in 2003 from orthorectified aerial imagery obtained by the NERC ARSF. (a) Original image. (b) Interpretation.....	163
Fig. 6.15 Locations of excavations (numbered) across the lateral-frontal moraine with the position of the glacier terminus is noted (AL). Hillshaded DEM extracted from aerial imagery acquired in 2003 by the UK Natural Environment Research Council (NERC) Airborne Research and Survey Facility (ARSF) are provided courtesy of NERC via the NERC Earth Observation Data Centre (NEODC).....	167
Fig. 6.16 Summary of the structural relationships between lithofacies on the Austre Lovénbreen lateral-frontal moraine complex. Scale increments in metres.	168
Fig. 6.17 Physical properties of the ice sample extracted from the Austre Lovénbreen true-left lateral-frontal moraine. (A) Shape and roundness of clasts removed from the ice. (B) Photograph and interpretation of sampled ice.	170
Fig. 6.18 Clast form plots from Austre Lovénbreen. (a) RA/C40 plot. (b) The % RA plotted against the % striated discriminating samples obtained from two locations: subglacial controls and two samples from the frontal zone of the moraine.....	173
Fig. 6.19 Clast roundness on the lateral-frontal complex. Note the increase in SA-R clasts towards frontal sections of the landform. Geomorphology as mapped in section 6.2...174	174
Fig. 6.20 (A) DEM of differences for 2003-2014. Contour data are derived from the 2014 DEM and are displayed in metres. The locations of three additional zones of analysis (Z1, Z2 and Z3) are shown. (B) Surface change from 2003 to 2014 in relation to area and volume. Red represents surface lowering, gray represents thresholded change (error) and blue	

represents surface gain. (C) Average net surface change from 2003 to 2014 for areas Z₁, Z₂ and Z₃. This appears as Fig. 3 in Tonkin *et al.* (in press).178

Fig. 6.21 Surface evolution over the 11-year study period demonstrated by three topographic profiles. (A) The locations of the three profiles. (B) Surface change along profiles 1-3 between 2003 and 2014. This appears as Fig. 4 in Tonkin *et al.* (in press)....179

Fig. 6.22 A process-form model for the development of the ice-cored lateral moraine complex at Austre Lovénbreen. Glacier flow occurs obliquely to the cross-section. (A) Supraglacial debris transport and concentration at the Neoglacial Maximum. (B) Thinning of the terminus. (C) Present day downwastage following extensive glacier recession. For illustrative purposes the bed is depicted as horizontal. In reality it is gently sloping down-glacier.184

Fig. 6.23 Conceptual flow diagram showing pertinent feedbacks controlling the deglaciation process of ice-cored 'controlled' moraine. (A) Positive and negative feedbacks involved in the degradation of ice-cored moraine and (B) the rate of ice loss over time in relation to two hypothetical warming scenarios.185

Fig. 6.24 A potential process-form model for the development of ice-free frontal sections of the moraine complex related to the oscillation of the glacier terminus and the supply of basally derived material via debris-rich thrust propagation at the terminus (e.g. Hamberg, 1894). Material is dumped from the steepened ice-cliff. T₁ and T₂ indicate the chronology of the two moraine deposits, with T₁ formed first.186

List of Tables

Table 2.1 Overview of glaciers investigated in this thesis.....	25
Table 2.2 Overview of datasets reported in each chapter.....	25
Table 2.3 Summary of frequencies, configurations, and suggested maximum depth where sedimentary structures can be observed.....	28
Table 2.4 Glacigenic sediment compaction assessment scheme adopted from Hubbard and Glasser (2005).....	36
Table 2.5 The Goodsell <i>et al.</i> (2005a) schema for identifying glacier structures from aerial photography.....	45
Table 3.1 Statistics for the vertical difference (m) between the Cwm Idwal topographic datasets.....	59
Table 3.2 Calculated RMSE for vertical difference (m) binned by slope angle.....	59
Table 3.3 Comparative table of known vertical differences between small-format aerial image based topographic surveys and various validation datasets in a range of geomorphological environments.....	64
Table 4.1 Summary of proximal slope characteristics in relation to other alpine sites.....	80
Table 4.2 Summary table of gravel lithofacies.....	87
Table 4.3 Summary table of ice-proximal diamicton exposures.....	87
Table 4.4 Summary table of diamicton samples obtained from the various outer ridges of the lower-lateral complex.....	88
Table 4.5 Eigenvalues and vectors for 9 samples taken from the inner ice-proximal slopes of Schwarzberggletscher left-lateral moraine. Samples ordered by distance from the current glacier margin.....	91
Table 5.1 Summary table of radar-wave velocities on the Isfallsglaciären moraines derived from semblance analysis.....	117
Table 5.2 Summary table of sedimentary facies within the Isfallsglaciären moraine complex.....	125
Table 5.3 Summary table of radar profiles and their characteristics.....	128
Table 5.4 Estimated thickness for the USL. The locations for d_{\min} and d_{\max} are presented for each profile in Fig. 5.3.....	129

Table 6.1 Semblance analysis of CMP data obtained along 100 MHz radar transects 1-9. Note the decline in CMP velocity with increasing distance along the moraine rampart (Table 1 in Midgley <i>et al.</i> , 2013).	149
Table 6.2 Summary table of assessed lithofacies on the Austre Lovénbreen true-left lateral-frontal moraine complex and their structural configuration.....	166
Table 6.3 Summary of clast-rich sandy diamicton facies.....	169
Table 6.4 Summary of surface gravel facies.....	169
Table 6.5 Summary of clast-rich muddy diamicton facies.....	169
Table 6.6 Statistical differences between the CDF of four sets of two clast samples taken from a coarse surficial angular drape and an underlying diamicton facies.....	174
Table 6.7 Summary table of evidence used to deduce the likely origin of buried-ice structures within the Austre Lovénbreen left-lateral-frontal moraine	182
Table 7.1 Contrasting characteristics at the three sites investigated.	200

Glossary of selected terminology

Controlled moraine Used to refer to moraine with an ice-core which exerts an influence on the moraine morphology when de-icing. See Evans (2009).

Digital Surface Model (DSM) A model of the earth terrain including surface features such as vegetation and buildings.

Englacial debris Debris located within a glacier. Material can be entrained within an englacial position where material is deposited on a glacier from extraglacial valley side debris sources in the accumulation area, or alternatiely subglacially via a range of processes such as thrusting.

Englacial debris septa Non-genetic term used by Lukas and Sass (2011) to refer to debris features located within glacier ice, which potentially link to the elevation of material from the base of the glacier (see thrust).

Equilibrium line altitude The altitude on a glacier where accumulation is equal to ablation over a one year period.

Glaciated An area formerly subject to occupation by glaciers.

Glacierised An area currently occupied by glaciers.

Glaciotectonism Deformation of glacial materials by a glacier related to the transmission of stress to ice-marginal and sub-marginal sediments. Related to the development of push moraine.

Ground penetrating radar A geophysical method for imaging sub-surface materials through the use of electro-magnetic energy.

Lateral-frontal moraine Non-genetic term referring to a moraine on the basis of its location in relation to the parent glacier. The term **frontal moraine** refers to features occurring transverse or oblique to the direction of former or current ice-flow. **Lateral moraine** refers to features occurring parallel to the direction of former or current ice-flow. **Lateral-frontal moraine** are used to describe a continuous or discontinuous rampart that encircles a contemporary or former glacier forefield and margin.

Palaeosol A relict soil buried under sediment. In a glacial context, they are often incorporated within the structure of moraines.

Permafrost Ground which remains frozen (at or below 0c) perinially. Ground typically has to be frozen for two consecutive years to be classified as permafrost.

Photogrammetry The science of taking measurements from photography.

Piedmont glacier A glacier which is non-longer constrained by topography (e.g. valley walls) resulting in a lobate terminal zone.

Polythermal glacier A glacier which contains ice both at and below the pressure melting point.

Small unmanned aerial vehicle Rotary or fixed wing craft typically 1-5 kg in weight used to collect small format low-level aerial imagery.

Structure-from-Motion An automated digital photogrammetric technique that can be used in conjunction with metric and non-metric cameras.

Subglacial (basal) debris Debris found at the bed of a glacier. Typically clasts of subglacial origin shown evidence of transport at the glacier bed (e.g. rounding and striae).

Supraglacial debris Debris found on the surface of a glacier. Typically sourced from valley side extraglacial debris sources and angular or very angular in character

Surge-type glacier A glacier which is subject to short lived faster than normal flow conditions resulting in the rapid advance of the terminus. Surge activity is punctuated by a quiescent phase.

Thrust Low angle fault resulting from compression in glacier ice. Associated with the elevation of basal debris to the glacier surface and the formation of moraine-mound complexes.

Valley glacier A glacier constrained by topography (e.g. valley walls)

1. Introduction and research context

1.1 Introduction

Valley glaciers are important geomorphic agents in moderate and high-relief mountain environments. A key product of glacial activity in mountain chains are large lateral-frontal moraine complexes (Boulton and Eyles, 1979; Spedding and Evans, 2002; Benn *et al.*, 2003; Fig. 1.1). Research seeking to understand the significance and formation of such ice-marginal landforms is longstanding and extensive (e.g. Agassiz, 1840; Collomb, 1847; Lamplugh, 1911; Galloway, 1956; Østrem, 1964; Röthlisberger and Schneebeli, 1978). Despite this long history of research, improvements in our understanding of the formation and significance of these features is ongoing due to the diversity of ice-marginal processes operating globally across different glacierised basins (Hambrey and Glasser, 2012). Additionally, opportunities to study these features actively forming are rare (e.g. Whalley, 1973; Matthews *et al.*, 1995; Winkler and Matthews, 2010), due to the widespread and on-going recession of mountain glaciers globally (Paul *et al.*, 2004; Kaser *et al.*, 2006; Masiokas *et al.*, 2008; Nesje *et al.*, 2008; WGMS, 2012).

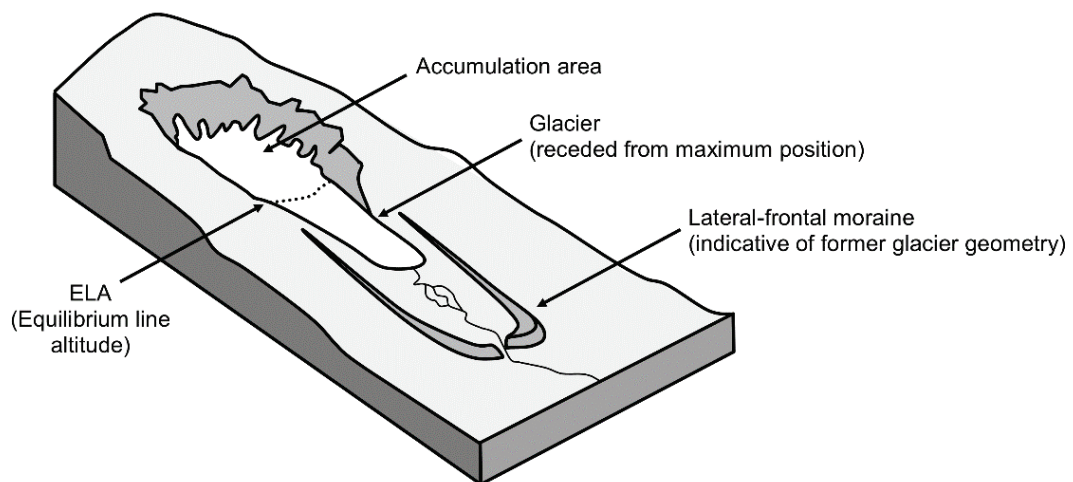


Fig. 1.1. Block diagram of a glacier and associated lateral-frontal moraine within the glacier foreland.

Nomenclature to describe moraine formation objectively is inconsistent and diverse (Bennett and Glasser, 2009). Specifically, researchers have sought to classify features on the basis of their position in relation to a body of glacier-ice (e.g. non genetic terms such

as lateral, frontal, terminal, recessional etc.) or through genetic terminology, which highlights process-form relationships (e.g. dump and glaciotectonic moraine). A diverse taxonomy for glacial landforms can in part be seen as a consequence of regionally specific case studies (e.g. Napieralski *et al.*, 2007) or complex morphological and sedimentological landform characteristics, which reflect the range of environmental conditions involved in the development of these features (e.g. Østrem, 1964; Osborn, 1978; Small, 1983; Bennett *et al.*, 2000; Lyså and Lønne, 2001; Benn *et al.*, 2003; Burki, 2009; Evans, 2009; Curry *et al.*, 2009; Evans, 2010; Winkler and Matthews, 2010).

Lateral-frontal moraine can be considered to be terrestrial sinks for glacial debris (Reinardy *et al.*, 2013), and are regularly used as a proxy for obtaining past glaciological and climatic information (e.g. Kirkbride and Winkler, 2012). However, moraines are not ubiquitous in terms of their form, structure or sedimentology, which vary greatly between different glacial landsystems (Benn *et al.*, 2003). A robust understanding of moraine forming processes has been demonstrated to be important when considering the potential utility of such features for palaeoclimatic reconstruction (Kirkbride and Winkler, 2012; Barr and Lovell, 2014). As a consequence, studies which investigate moraine formation in a range of contemporary environments are important if the significance of formerly glaciated areas during the Quaternary are to be correctly interpreted and understood (Hambrey and Glasser, 2012). Precise understanding is confounded by the fact that a large number of valley glaciers are currently receding (WGMS, 2012), meaning that only limited observations of active landform development have been made (Whalley, 1973; Krüger, 1985; Matthews *et al.*, 1995). As lateral-frontal moraines are frequently used in the Quaternary sciences for dating past-glacier activity and for determining past glacier characteristics (e.g. Kirkbride and Winkler, 2012; Osborn *et al.*, 2015), the origin and processes of moraine development require thorough investigation. This is especially pertinent where moraines are used to inform our interpretation of past glaciers and their associated dynamics (Benn and Lukas, 2006), where moraine chronologies are developed from dated moraine sediment (Kirkbride and Winkler, 2012), or where moraines are used to estimate past palaeoclimatic conditions (e.g. Kerschner *et al.*, 2000). The need for research characterising the development of lateral-frontal moraine under a range of environmental conditions is apparent if these features are to be effectively used by Quaternary scientists. This thesis aims to address this research gap.

1.2 Overview of existing research

1.2.1 *Alpine and high-mountain moraine development*

1.2.1.1 *Introduction*

Large Alpine type lateral moraines develop following repeated reoccupation of mountain valleys by glacier ice (Röthlisberger and Schneebeli, 1979; Lukas et al., 2012) and are distinct in character from moraine ridges developed at the margins of high-Arctic glaciers (e.g. Bennett et al., 1996; Midgley et al., 2007) and valley glaciers across Arctic Scandinavia (e.g. Østrem, 1964; Matthews and Shakesby, 1984). The use of the word alpine or Alpine (emphasis on the capitalisation) requires clarification of the definition within the context of this research. The use refers to those occurring within the European Alps (e.g. a geographical region), rather than high-mountain environments in general. Whilst such research may be broadly applicable to other mountain chains, it is acknowledged that Alpine/alpine moraines represent one type of landform generated in high-mountain glacial landsystems. For example, landforms produced in alpine ('high-mountain') environments of Norway (e.g. Winkler and Matthews, 2010) or Himalaya (e.g. Benn and Owen, 2002) do not necessarily produce landforms similar to those found within the European Alps geographic region.

Alpine moraines are characterised by their large size (topographic prominence of up to ~100 metres and lengths extending into the kilometre range), sharp crestlines, asymmetric form, and regularly over-steepened ice-proximal slopes which are reported to locally exceed 70° (Lukas *et al.*, 2012). This morphological distinctiveness has been used as a criteria for distinguishing debris-dominant moraine complexes from their ice-cored counterparts for the purpose of assessing the probability of catastrophic proglacial lake drainage (McKillop and Clague, 2007). Dumping is regarded as an important mechanism for the formation of Alpine type lateral moraines (Röthlisberger and Schneebli, 1979; Small, 1983), and refers to the process of sub-aerial debris transfer of material from a supraglacial to an ice-marginal position. The terminology 'dump' moraine is an umbrella descriptor that includes debris transfer via falls, slumps, slides and flowage (Benn *et al.*, 2003).

1.2.1.2 Age and palaeoenvironmental significance

The age and significance of Alpine moraines have been subject to considerable research. Large lateral-frontal complexes have been dated by a range of geochronological techniques. Notably, research was conducted in the 1970s which used buried organic layers to radiocarbon date past fluctuations in glacier extents (e.g. Rothlisberger and Schneebli, 1979). Recent developments in geochronological techniques have also led to the application of cosmogenic dating to determine the age and significance of Alpine moraines. Cosmogenic dating involves the measurement of radionuclides, which are concentrated in relation to the time a rock surface is exposed to cosmic radiation (Ivy-Ochs and Kober, 2008). Commonly used cosmogenic nuclides for Quaternary studies include ^{10}Be , ^{36}Cl and ^{26}Al . At certain sites, Alpine moraine formations have yielded dates suggesting their initial development, and subsequent preservation as moraines throughout the Holocene (11.5 kyr BP to present). A comprehensive review of known Alpine glacier fluctuations is presented by Ivy-Ochs *et al.* (2009). However, since this review, additional cosmogenic nuclide studies have been completed. For example, moraines at Steingletscher (Switzerland) appear to have developed as early as 11-10 kyr BP, with subsequent moraine building episodes also identified (Schimmelpfennig *et al.*, 2013). Similar patterns of glacier occupation are recorded at Tsidjoire Nouve, a valley glacier located in the Arolla valley, Valais. There, ^{10}Be dating of moraine deposits revealed the occupation of ice as early as 11.4 kyr BP, and subsequent advance, similar in spatial extent *c.* 3.8 kyr BP (Schimmelpfennig *et al.*, 2014).

Alpine moraines have also been used as palaeoclimatic indicators (Kerschner *et al.*, 1999; Kerschner *et al.*, 2000; Kerschner and Ivy-Ochs, 2008). Key to these studies is the use of moraines to delimit the past geometry of Alpine glaciers. Such data can be used to infer the likely ELA (equilibrium line attitude) of a given glacier which typically relies on inferences with regard to the likely area accumulating, or ablating on a past glacier surface (Kerschner and Ivy-Ochs, 2008). In turn, these data can be used to estimate likely palaeo-precipitation and mean summer temperatures. However, such reconstructions can be problematic in high-mountain environments where mass balance may be sensitive to supraglacial debris loads or localised topo-climatic controls (e.g. Clark *et al.*, 1994; Benn and Lehmkuhl, 2000) or where topographic controls are a determining factor on moraine formation (Barr and Lovell, 2014). Moraine assemblages may present a fragmentary

record of palaeoglacier change. Given the range of dates given by geochronological studies, a level of landform stability is evident. Several studies have sought to understand landform stability, and the paraglacial response of Alpine moraines to deglaciation (e.g. Curry *et al.*, 2006; Curry *et al.*, 2009). Curry *et al.* (2006) reported paraglacial processes operating on Alpine moraine, and debris mantled slopes. Gullies were found to stabilise 80-140 years following deglaciation.

In summary, a wide body of knowledge derived from dating moraine assemblages at the margins of Alpine glaciers exists. Dates derived from a range of techniques demonstrate the composite nature of Alpine moraine assemblages. There is robust evidence which demonstrates that Alpine moraines reflect varied, and temporally extensive (timescales extending into 11 ka range) environmental history.

1.2.1.3 Landform development and sedimentology

Humlum (1978) documented moraine structural characteristics from glacier forefields in the Austrian Alps, and noted that for moraine formation to occur the glacier surface must exceed the elevation of the moraine surface for material to be deposited on distal slopes. Whilst the moraines reported by Humlum (1978) show a linear aggraded structure, later research identified a wider range of structural configurations that develop within alpine landsystems (e.g. Rothlisberger and Schneebli, 1979; Boulton and Eyles, 1979). Importantly, Rothlisberger and Schneebli (1979) used the terminology 'accretion' and 'superposition' processes to describe the range of moraine end products developed by Alpine glaciers. Key to these conceptual models is the role topography plays in the resulting morphology of a given moraine complex. The key control determining the development of accretion type or superposition type moraines was said to be the moraine barrier, and whether a given glacier advance is significant enough to surmount topographic obstacles. Interrupted periods of moraine construction via superimposition were recognised to result in the preservation of organic materials such as palaeosols to within moraine structure. Such material can be used to produce a minimum age for glacier recession and maximum ages for renewed moraine construction (thus glacier advance) (Kirkbride and Winkler, 2012). The use of buried organic material for dating alpine glacier activity is now widespread (Osborn, 1978; Reyes *et al.*, 2006; Le Roy *et al.*, 2015).

Small (1983) introduced further taxonomy to distinguish the various elements of lateral moraine systems. The term 'abandoned dump moraine' is used to distinguish dumped accumulations of material on the valley side from thin layers of material resting on active glacier-ice ('supraglacial lateral moraine') (Small, 1983). Later work by Small (1987) used clast-form analysis to determine the passive and active debris transport components of moraines at Glacier de Tsidjiore Nouve. An overview of clast form analysis is presented in chapter 2. Small (1987) suggested limited field evidence for subglacial debris sources and estimated that up to 80% of debris included within the northern lateral ridge to be of supraglacial origin.

In contrast to observations of highly angular debris at high altitude sites in the European Alps, clast-form gradients have been recorded at a number of low altitude sites in Scandinavia and Iceland where roundness has been found to decrease with distance from the former glacier terminus (Matthews and Petch, 1982; Benn and Ballantyne, 1994; Spedding and Evans, 2002). Matthews and Petch (1982) postulated that the composition of lateral moraines is related to subglacial transport and/or the pushing of pre-existing valley side paraglacial debris. However the authors questioned the significance of both hypotheses on the basis that (i) low debris volumes have been observed within the basal transport zone of temperate glaciers in the Jotunheimen region; (ii) push mechanisms in isolation are unlikely to develop large moraine ridges and (iii) the composition of valley-side debris and lateral moraines often exhibit different clast-form properties.

Matthews and Petch (1982) also discussed causes for the within-valley asymmetry exhibited by many lateral-frontal moraines. Notably they suggested that the distribution of pre-existing valley-side sediment was an important control on the size of moraines where the reworking of material via a pushing occurs. Subsequent research appears to corroborate this assessment. For example, research on the drift mantled slopes of Faberdalen, Norway, by Ballantyne and Benn (1994) revealed that alternating periods of glacial and paraglacial sediment recycling occurred throughout the Holocene as a consequence glacier fluctuations. Furthermore, Burki (2009) reported on the clast-form properties of lateral moraines in the Jotunheimen area, and concluded that sediment reworking constituted a considerable debris source for lateral moraine construction during the Little Ice Age maxima (c. 1755 AD).

Whilst the entrainment of pre-existing sediment is undoubtedly an important control on lateral moraine construction, within-valley asymmetry has also been reported as a consequence of variable cross-valley debris supply. Differential debris supply to the glacier surface is suggested to relate to (1) changes in lithology; (2) the distribution of rockwalls at the glaciers axis; or (3) cross-valley changes in glacier dynamics (resulting from shading effects or the distribution of accumulation area at the glaciers head), leading to the concentration of deposition, although total debris volume of moraines across the valley may be equal (Benn, 1989; Benn *et al.*, 2003).

Research by Benn and Owen (2002) examined the landforms, sediments and earth-surface processes associated with Himalayan glaciers in the Lahul region. Himalayan glaciers carry a high supraglacial debris load (Benn *et al.*, 2003), and although their thermal character is understudied they are likely to be polythermal (Hambrey and Glasser, 2012), distinguishing them from Alpine sites. The authors report that Himalayan glaciers often develop continuous lateral-frontal ramparts as a consequence of high debris transfer relative to ice-discharge. Large lateral moraine ramparts may constrict glacier expansion where debris deposition exceeds or matches rates of glacier thickening (Benn and Owen, 2002). Observations of moraine structure are therefore proposed to allow an interpretation of palaeoenvironmental conditions where aggrading sedimentary layers indicate a positive mass balance hence deposition, whereas unconformities derived from moraine erosion can be interpreted evidence of glacier recession.

Lateral-frontal moraines at various Himalayan sites were found to comprise of (1) stratified or massive matrix support diamict units, depleted of fines; (2) stacked massive diamict units dipping away from the glacier at 10° on distal slopes; (3) debris flow units, indicated by the concentration of clasts beneath a lens of fine-grained sediment and (4) various glacio-fluvial sedimentary units that occur more frequently with distance for the former ice-margin (Benn and Owen, 2002). In their findings, clasts sampled from a supraglacial position exhibited both an elongate and slabby form, and high angularity. Whilst it would be expected that lateral moraine sediment share similar clast-form characteristics, moraines were found to have markedly different clast angularity and shape. Although the dominance of high-level debris transport on Himalayan glaciers is documented, Benn and Owen (2002) hypothesise that actively worked debris may be

elevated to the glacier surface by englacial debris septa running parallel to the bed at the margin of the glacier, and mixed with passively transported debris, prior to deposition.

Further research within high-mountain environments was conducted by Hambrey *et al.* (2008) who examined glacial sedimentology of the Mount Everest region. Unlike previous studies, sediments were assessed against a modified Montclieff (1989) classification to more readily distinguish between different units of poorly sorted sediment. Lateral moraine facies were mainly found to comprise of sandy boulder-gravels, a facies that was also associated with lateral moraine in earlier work at various high-Alpine catchments in the Mount Cook region, New Zealand (Hambrey and Erhmann, 2004). Hambrey *et al.* (2008) report that lateral moraines development corresponded to sediment inputs from rockfall material, and debris derived from traction at the valley-sides. More frontal sections of moraines were noted to develop due to the shearing, thrusting and folding of sediment in response to longitudinal compression where Little Ice Age moraine ramparts constricted ice-flow (Hambrey *et al.*, 2008).

In recent years the association between lateral-frontal moraines and passive supraglacial debris transport pathways have been challenged. Lukas *et al.* (2012) reported on the sedimentology of large lateral moraines developed at the margin of Findelgletscher. Here, moraine sediment has an anomalously low angular and very angular (RA) component (between 0% and 32%) and clasts are frequently striated. Lukas *et al.* (2012) attributed these anomalous clast form parameters to the prominence of sediment delivery via englacial debris septa. These serve to elevate subglacial material to a supraglacial position, thus making it available for the construction of lateral 'dump' moraines. Here, the glacier's structural configuration exerts a control on the resulting sedimentary signature of a moraine. However, it is unclear whether processes documented here can be broadly applied to a range of alpine glacier basins.

The use of Alpine moraine assemblages as proxies for glacier change, hence perturbations in past climate, is well established in Quaternary science. Future geomorphological studies can aid interpretation of the character and behaviour of former glaciations by examining the sedimentary signature of moraine complexes. However, recent studies may suggest a strong glaciological structural control on the sedimentary signature of some Alpine moraine complexes, with ice-proximal units potentially strongly influenced by glaciotectonic processes (the deformation of sediment) in the lateral-subglacial domain

(e.g. Lukas and Sass, 2011; Lukas *et al.*, 2012). Given the diversity of moraines, additional studies investigating the geomorphology of Alpine moraines complexes can be seen as beneficial for our understanding and interpretation of absolute dates, which in turn are used to inform studies of palaeo-environmental conditions.

1.2.2 Arctic and high-Arctic ice-cored 'controlled' moraines

1.2.2.1 Introduction

The term 'ice-cored' moraine is used as a descriptor to refer to a body of dead-ice (e.g. where glacier ice is no longer under motion) insulated by debris that is preserved in the glacier forefield. Ice-cored moraines have been recognised as widespread features common to a range of contemporary glacial environments, including Canada (e.g. Østrem and Arnold, 1970; Johnson, 1971; Hooke, 1973; Driscoll, 1980; Mattson and Gardner, 1991), Iceland (e.g. Krüger and Kjær, 2000; Kjær and Krüger, 2001; Evans, 2010; Bennett and Evans, 2012), the Norwegian high-Arctic (e.g. Bennett *et al.*, 2000; Lyså and Lønne, 2001; Sletten *et al.*, 2001; Lønne and Lyså, 2005; Lukas *et al.*, 2005; Schomacker and Kjær, 2008; Midgley *et al.*, 2013), and Antarctica (e.g. Pickard, 1983; Carrivick *et al.*, 2012a). Ice-cored moraines have also been reported to occur in temperate glacial environments, albeit with minimal preservation potential (Brook and Paine, 2012).

Use of the term 'ice cored moraine' has attracted some debate over the last decade. Lukas *et al.* (2007) suggest that the term should be strictly reserved for moraines where the ice is detached from the main glacier body. Given the extensive occurrence of dead-ice in glacier forelands subject to permafrost conditions, this application of the terminology would limit the use of the terms application to environments where significant geophysical and structural surveys have been completed to verify the detached nature of potential buried ice. Evans (2009), however, rejects Lukas' (2007) criteria, applying a more general application of the terminology which does not require buried-ice to be detached from the main glacier body. Key to this argument, Evans (2009) highlights that the term 'moraine' does not imply detachment of a landform from the glacier terminus (e.g. medial moraines).

1.2.2.2 Origin of debris septa

As the subsequent melt out of debris bands is important in terms of the morphological expression of a resulting landform (Evans 2009), the structural glaciology and transport

of debris through Arctic glaciers can be seen as an important aspect of landform generation. The structural glaciology of valley glaciers in Svalbard has been subject to considerable research (e.g. Bennett *et al.*, 1996; Hambrey and Glasser, 2003; Hambrey *et al.*, 2005; Roberson and Hubbard, 2010). Rockfall debris sourced from valley sides and headwalls are subject to folding and burial in composite glaciers with converging flow units (Glasser and Hambrey, 2003). Reorganisation and melt out of extraglacially derived debris within the ablation areas is reported to form linear supraglacial debris stripes ('medial moraine') (Fig. 1.1; Glasser and Hambrey, 2003). Where surge-type behaviour occurs, supraglacial debris may be deformed into looped structures (e.g. Pedersenbreen; see Bennett *et al.*, 1996 and Glasser *et al.*, 2004).

Further entrainment and transport has been suggested to occur via the mechanism of thrusting, which describes the faulting of ice under compression (Hambrey, 1994). Thrusts have been documented to occur within land terminating (e.g. Hambrey *et al.*, 1996; 1997; Huddart *et al.*, 1998), and calving glaciers in Svalbard (e.g. Murray and Booth, 2010). Thrusts may propagate onto the glacier surface within the ablation zone bringing basal debris to the glacier surface (Huddart and Hambrey, 1996). Longitudinal compression has been cited as a causal mechanism for the development of thrusts in glacier ice (Swift *et al.*, 2006). In glaciated environments, longitudinal compression may be initiated by a reverse bedrock slope or the transition from warm to cold based ice in polythermal glaciers, which may reduce ice sliding velocities (Hambrey *et al.*, 1997). Thrusting represents one mechanism which is suggested to be applicable to high-Arctic glaciers. Reviews of additional debris entrainment mechanisms are presented in Alley *et al.* (1997) and Knight (1997) which include: regelation, freeze-on, and glaciohydraulic supercooling. Regelation involves the re-freezing of ice and debris in the low pressure lee of subglacial obstacles, or freezing of pore water within the subglacial sediment layer, if the overlying ice is at higher pressure (Benn and Evans, 2010). Freeze-on occurs in relation to its association with the thermal properties of glacier ice with bulk freeze-on related to the advection of cold ice from winter cold (Alley *et al.*, 1997), or in relation to the thermal configuration of polythermal glaciers where the transition from warm-based ice to a cold terminus permits the freeze-on (Weertman, 1961; Boulton, 1972).

Debris transport in high-Arctic valley glaciers (from Hambrey *et al.* 1999)

CROSS-SECTION

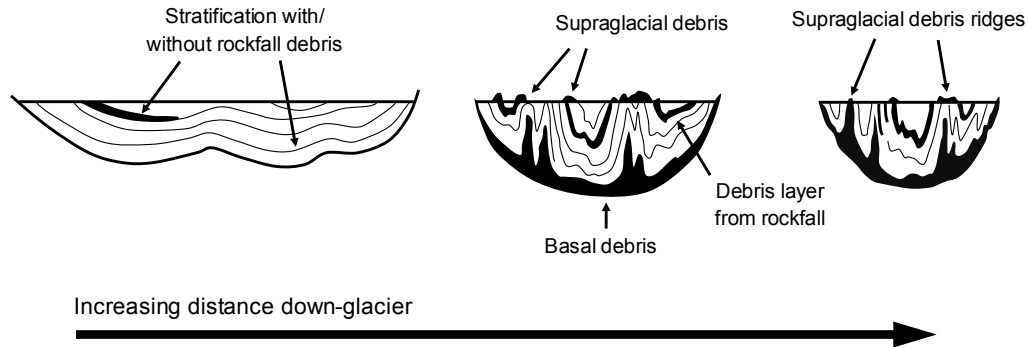


Fig. 1.2 Debris transport in high-Arctic glaciers adapted from Hambrey *et al.* (1999).

1.2.2.3 Landform development and sedimentology

The genesis of lateral moraine at high-Arctic sites has been discussed in relation to a range of glacier-permafrost interactions (e.g. Etzelmüller *et al.*, 1996; Etzelmüller *et al.*, 2000; Etzelmüller and Hagen, 2005). Unlike temperate glaciers with high turnovers, high-Arctic glaciers are typically characterised by low rates of accumulation, polythermal or cold-based ice and short ablation seasons (Benn and Evans, 2010). According to Etzelmüller and Hagen (2005) cold-based ice may be present in a glacier where the ELA sits at or below the regional lower limit of permafrost, thus when the regional limit sits well below the terminus, a glacier is likely to be entirely cold-based. Specifically, the thinning and recession of glaciers from their Neoglacial maximum position (*c.* 1900) is suggested to have, and continue to, promote the transition from polythermal to cold-based thermal regimes at some sites (e.g. Glasser and Hambrey, 2001; Hambrey *et al.*, 2005).

Numerous studies have investigated morphologically similar lateral-frontal moraines, developed by high-latitude, low-relief valley glaciers (Lyså and Lønne, 2001; Lønne and Lyså, 2005; Lukas *et al.*, 2005; Ewertowski *et al.*, 2012). Notably Lyså and Lønne (2001) presented a conceptual model for the formation of lateral moraines from their observations at the valley glacier, Reiperbreen (Svalbard). This model is similar to that

developed by Small (1983) for moraine development in the European Alps, and considers debris from sub-, en- and supraglacial sources. However, the inclusion of dead-ice appears to be more extensive than that envisaged by Small (1983), which is explained by the burial of glacier ice by debris fall/flows from valley side material following the down wastage of the glacier surface.

The development of 'controlled' ridges involves the melt-out of material from the glacier surface. Evans (2009) refers to ice-cored features as 'controlled' moraine due to the influence of debris bearing structures within buried glacier-ice exert on the resulting morphology of the moraine. The term is useful for describing ice-cored landforms which specifically have morphological characteristics that form in response to the melt-out of debris. Debris transport within glaciers can concentrate material into 'depocentres' at the glacier terminus. This may be due to the melt-out of englacial debris-bearing structures within the ablation area of a glacier, or as a result of the accumulation of debris within supraglacial transport. Where sufficiently thick, supraglacial debris will insulate buried-ice from further ablation. Stagnant or dead-ice that is buried below the depth of seasonal thaw will be preserved (Waller *et al.*, 2012). Where affected by seasonal thaw, ablation derived moraines can undergo 'secondary deglaciation' (Everest and Bradwell, 2003).

1.2.2.4 Preservation and stability

The most prominent consequence of glacier-permafrost interactions is the wide-spread inclusion of dead-ice into moraine structure. However, the presence of dead ice is not restricted to moraines, and may partially underlie entire proglacial zones (e.g. Irvine-Fynn *et al.*, 2011). It is generally considered that ice-cored moraines develop under low ice-activity and moderate levels of debris input (e.g. Whalley, 2009). For example, Lukas *et al.* (2005) reported on the morphology and sedimentology of lateral-frontal moraine ridges developed by three small valley glaciers (Nordenskiöldtoppenbreen / Platåbreen, Longyearbreen and Larsbreen) located near Longyearbyen, Svalbard. Dead-ice within moraine structure and across the pro-glacial areas of interest are reported to be extensive with moraines grading into in-distinct debris-covered zones (Lukas *et al.*, 2005). Surface debris thickness were found not to exceed 0.15 m, and contained very angular and angular clasts, indicative of rockfall from valley sides (Lukas *et al.*, 2005).

Ewertowski *et al.* (2012) and Ewertowski (2014) reviewed moraine development at Ragnarbreen. Ewertowski *et al.* (2012) reported on the sedimentology and geomorphology of the moraine complex at this glacier. Here, sediment ridges within the lateral-frontal complex contained deformed laminated fines, which are interpreted as evidence of topographic inversion, resulting from the differential melting out of material surrounding a previous ponded surface water body. Ewertowski (2014) used repeat historical aerial imagery to understand rates of change within the high-Arctic environment. Observations of landform generation and paraglacial alteration are used to develop a model specific to the site. Lateral moraines at Ragnarbreen, as reported by Ewertowski (2014), are known to have developed from; (1) the accumulation of debris from extraglacial sources on the glacier surface; and (2) differential ice melting resulting in the deposition of ice-cored valley side ridges. Subsequent debris flowage, resulting in exposed ice-cores and downwasting are responsible for paraglacial modification and re-sedimentation at this site. The situation at Ragnarbreen is similar to the small land terminating valley glacier, Rieperbreen, as reported in Lyså and Lønne (2001). However, Lyså and Lønne (2001) reported on potential sub- and englacial debris sources related to the melt out of debris septa within buried ice.

The surface processes associated with ablating moraine ice-cores have also been subject to considerable research interest (Schomacker, 2008). Two key ablation processes are commonly defined; (1) downwasting, and (2) backwasting and associated gravity driven mass movements. Downwasting refers to the thinning of dead ice from either top or bottom melt (Schomacker, 2008). Back wastage involves the lateral mass-wastage of exposed ice-walls. Sections of dead-ice can be fully or partially exposed (Krüger and Kjær, 2000). The coupling of fluvial and slope processes have been emphasised as important agents of ice-cored moraine disintegration (Etzelmüller *et al.*, 2000; Lukas *et al.*, 2005). Rates of ice-melt have been quantified in a range of studies (Krüger and Kjær, 2000; Lukas *et al.*, 2005; Irvine-Fynn *et al.*, 2011; Ewertowski and Tomczyk, 2015). For example, Schomacker and Kjær (2008) found ice-cored moraine at the margin of Holmströmbreen downwasted at a rate of -0.9 ma^{-1} over a 20 year period spanning 1984 to 2004. Similar rates were observed at Midtre Lovénbreen by Irvine-Fynn *et al.* (2011). Here the western lateral (true medial) moraine was quantified to be down wasting at $-0.65 \pm 0.2 \text{ ma}^{-1}$ between 2003 and 2005.

Notably, Schomacker (2008) reviewed the controls on dead-ice ablation by correlating a range of climatic variables (e.g. mean annual and air temperature, total positive degree days, mean annual and summer precipitation) against annual backwasting measurements obtained from various dead-ice environments. Mean annual air temperature was shown to have the strongest correlation with backwasting ($R^2 = 0.65$; 95 % CI). However, other climatic variables exhibited weaker correlations with annual rates of backwasting. This is interpreted by Schomacker (2008) to signify the importance of topography and surface processes on de-icing progression in glacial environments. However, the aspect of a given near-vertical backwasting ice-exposure is important with respect to its sensitivity to climatic forcing (Krüger and Kjær, 2000). Topography appears to be a key driver of secondary deglaciation (Schomacker, 2008).

Recent work by Ewertowski and Tomczyk (2015) reported on ablating ice-cored moraine at the Svalbard glacier Ragnarbreen and Ebbabreen over the 2012-2014 period. Where a combination of backwasting, and downwasting occurred, higher rates of surface lowering were observed ($>1.8 \text{ ma}^{-1}$) in comparison to where ice was ablating by downwasting alone (0.3 ma^{-1}). Such findings reiterate the findings of Schomacker (2008) regarding the importance of local topography and surface processes in regulating the de-icing progress.

The efficient coupling of slope and fluvial process in permafrost environments is documented elsewhere (e.g. Bennett *et al.*, 2000). Lukas *et al.* (2005) argued that, as a result, the preservation of lateral-frontal moraine is perhaps limited to poorly defined ridges of dumped sediment following complete deglaciation, and thus provides an inappropriate analogue for landsystems in the Scottish Highlands. Bennett *et al.* (2000) observed the re-sedimentation of a large ice-cored lateral moraine developed on the southern margin of Kongsvegan, Svalbard. They found that the decaying ice-core promoted the development of sediment fans on proximal slopes. The authors suggested that, following complete deglaciation, only a thin veneer of matrix-supported diamicton and laminated silt and sand is likely to remain.

Degraded ancient lateral moraines in the British Isles have also been reported to exhibit a topographically indistinct morphology resulting from extensive para- and periglacial activity (e.g. Bennett, 1999a). Despite morphologically similar descriptions of moraine end-products following complete deglaciation, the use of Svalbard as an analogue for

Late Quaternary glacial landsystems in the British Isles is controversial (Lukas, 2007; Evans, 2009).

In summary, a key aspect to most studies of ice-cored moraines is the importance of back wasting, gravity-driven mass movements coupled with glacio-fluvial processes as agents of sediment remobilisation (e.g. Lukas *et al.*, 2005; Ewertowski and Tomczyk, 2015).

1.2.3 'Østrem' snowbank type ridges in Scandinavia

The moraines developed at glaciated sites across Scandinavia have a long history of geomorphological research (Schytt, 1959; Østrem, 1959; 1963; 1964; 1965; Karlén, 1973; Ackert, 1984; Hayman and Hattestrand, 2008). These features are identified as potentially atypical of other ice-cored ridges occurring in high-Arctic settings, containing moraine-distal snowbank ice within their structure (Østrem, 1964). In recent years, the term 'Østrem' type moraine has been introduced in the literature (e.g. Whalley, 2009; Whalley, 2012) to distinguish these ice-cored moraine systems from their high-Arctic counterparts, with the term aptly naming the moraines after the geoscientist who conducted initial investigations on ice-cored moraines during the 1950s and 1960s. These moraines often exhibit a complex morphology comprised of anastomosing ridge crests (Østrem, 1964).

Specifically, studies completed in the Tarfala valley have contributed to a wider understanding of moraine formation in the European Arctic by documenting their structural character, or by developing conceptual models accounting for moraine genesis (e.g. Østrem 1959; 1963; 1965; Karlén, 1973; Ackert, 1984). The identification of an ice-component in these moraines is long recognised. Schytt (1959) notes exposures of black 'dead-ice' following the reworking of material on the ice-proximal slopes of lateral-frontal moraine in the Tarfala valley following the removal of ice support. Schytt (1959) hypothesised that several up-glacier dipping slabs of dead-ice maybe incorporated within this ridge. Later research by Gunner Østrem investigated the internal structure of the southern lateral complex through the excavation of three pits (Østrem, 1963; 1964). Ice was found to occur under 2.5-3.6 m of surface debris (Østrem, 1964). By analysing the crystallographic content of sampled material, Østrem (1963) concluded that the ice was of meteoric origin, and originated as moraine-distal snowbanks, which were subsequently overridden and included into the internal structure of the landform. Strict

morphostratigraphic interpretations under this scenario would mean that distal ridges would be youngest in origin (Matthews *et al.*, 2014). Studies vary in terms of their interpretation of Scandinavian ice-cored moraines. For example, at other sites, ice-cored moraines have been conflated with rock-glaciers (e.g. Barsch, 1971). Whilst a polygenetic interpretation may be appropriate for some ice-cored moraines which may transition into rock glaciers (Whalley and Martin, 1992; Berthing, 2011), geomorphologically stable features deposited on near-level terrain were cited by Østrem (1971) as suitable criteria for classifying features as ice-cored moraine.

Karlén (1973) argued for 'proximal enlargement' as an important moraine forming process in northern Sweden based on interpretations of lichenometric data obtained from the Isfallsgläciären moraines. Karlén envisaged a scenario where moraine ramparts acted as topographic barriers for subsequent glacier advances, leading to the incremental stacking imbricate 'drift sheets' of different ages onto ice-proximal slopes. These 'drift sheets' were proposed to correspond to successive episodes of Holocene glacier expansion occurring c. 8000-5000 and 2700-2300 years BP and more recently during the Little Ice Age (various dates from c.1500-1916). Karlén favoured this hypothesis despite acknowledging ground-level photographic evidence from c. 1910 (Enquist images: 43/374 and 43/277) depicting both Isfallsgläciären and Storgläciären partially overriding their respective lateral-frontal moraine complexes. Later research by Ackert (1984) identified glacier ice within the moraines of the adjacent glaciers (Storgläciären and Kaskasatjakkaglaciären) leading him to suggest that ice of both origins can be incorporated into the internal structure of Scandinavian ice-marginal moraines.

1.3.4 Push moraine and glaciotectonism

Moraine genesis resulting from the deformation of submarginal and proglacial sediments by advancing glaciers are widely reported (e.g. Etzelmüller *et al.*, 1996; Bennett, 2001; Beedle *et al.*, 2009). Glaciotectonism occurs following the transmission of glacier stress to sediment at sub-marginal and ice-marginal positions (Van der Wateren, 2002). The size and morphology of ridges produced by glaciotectonic process vary (Bennett, 2001). Glaciotectonism is responsible for the production of a wide range of morainic forms. These include small seasonal ridges (Beedle *et al.*, 2009), composite moraine complexes (e.g. Etzelmüller *et al.*, 1996) and larger landform assemblages formed at the margins of former continental ice-masses (e.g. Hart, 1990; Lee *et al.*, 2013). The various properties of

deforming sediment are important with regard to the development of glaciotectonic ridges. One example is that pore-water pressure may determine whether proglacial sediments will be subject to ductile or brittle deformation with the proglacial area (Benediktsson, 2012). Permafrost is also identified as a control on proglacial deformation, where strong permafrost retarding the production of push ridges, and variability in the strength of weaker permafrost influencing the style of deformation (Etzelmüller *et al.*, 1996). Proglacial push moraines related to the deformation of permafrost affected gravels have been documented to produce distinctive 'thrust-block moraines' (e.g. Evans and England, 1991). Smaller ridges formed by pushing are associated with freeze-on processes. This is the process whereby slabs of basal sediment are entrained by the glacier terminus during cold winter conditions (Evans and Hiemstra, 2005). As the glacier undergoes a seasonally controlled re-advance, entrained slabs are transported. Where seasonal oscillations occur, but are superimposed on an overall trend of glacier recession, annual moraines may form (Kruger, 1995). If the ice margin remains stable, but seasonally oscillates, sediment slabs are stacked in an imbricate fashion forming composite moraine ridges (e.g. Kruger, 1994; Matthews *et al.*, 1995).

In relation to Østrem type ridges, deformation is suggested to be an important moraine forming mechanism. For example, recent research by Matthews *et al.* (2014) uses high-precision Schmidt hammer exposure-dating to interpret the age and significance of 'Østrem' type ridges in southern Norway. A series of progressively older dates moving in a down-glacier direction are argued to falsify earlier interpretations that the outer-ridges are youngest in age. This site was used by Østrem (1964) to formulate ideas surrounding the genesis of Scandinavian ice-cored moraine complexes and, importantly, the mechanism of ice incorporation. On this basis, Matthews *et al.* (2014) consider the ice-cored moraine complexes in question to be of glaciotectonic origin related to interaction of the advancing of polythermal glacier onto alpine permafrost. However, Matthews *et al.* (2014) highlight the need for structural data before ice-marginal processes relevant to landform development can be determined. Ice-marginal processes, such as glaciotectonism and dumping may occur simultaneously. For example Kruger *et al.* (2002) report on moraine formation at the advancing margin of Kötlujökull between 1982 and 2001. Here, the thrusting of pre-existing outwash sediments and the pushing of dumped

material as it was transferred from the ice-margin led to the development of a polygenetic moraine ridge.

1.5 Rationale

Understanding the apparent diversity of lateral-frontal moraine is important due to the usage of ice-marginal moraines to determine local and regional glacier change through time and to obtain meaningful palaeoclimatic data where landforms are used for environmental reconstruction (e.g. Nesje, 1992; Benn and Lehmkuhl, 2000; Ramage *et al.*, 2005; Carr *et al.*, 2010). For example, boulder-size rock fragments located on lateral moraines are commonly used for cosmogenic radionuclide (CRN) investigations to obtain absolute dates for past fluctuations in glacier extent (e.g. Banard *et al.*, 2004; Everest and Kubik, 2006; Rood *et al.*, 2011). Due to their obvious importance in Quaternary science, a number of studies provide detailed sedimentological and structural data on these landforms (e.g. Small, 1983; 1987; Curry *et al.*, 2009; Lukas and Sass, 2011). The processes by which they form under differing environmental conditions and their preservation potential could, however, be better understood by investigating further landforms within their respective localised contexts.

1.6 Aim and objectives

1.6.1 Research aim

The aim of this project is to document the structural characteristics of lateral-frontal moraines developed by glaciers in Arctic and Alpine environments and to better understand the formation, and associated glaciological and climatic significance of these features.

1.6.2 Research questions

This thesis will attempt to answer the following research questions:

- How does the character of lateral-frontal moraine vary within different sub-sets of the glaciated valley landsystem?
- What do the geomorphological characteristics of the three sites investigated tell us about: (1) the nature/dynamics of the glaciers that formed them; (2) earth surface processes operating during the Neoglacial; (3) the preservation potential of these landforms in the geomorphological record?

- What implications do the findings have on our palaeo-glaciological interpretation of late Quaternary landform assemblages?

1.6.3 Research objectives

The following objectives are used to fulfil the aim and research questions of this thesis:

- **Objective 1:** To investigate the novel integrated use of UAV and SfM technologies for geomorphological research and apply the technique to contemporary glacial environments.
- **Objective 2:** To assess the internal structure of lateral-frontal moraine using ground-penetrating radar (GPR) or direct observations.
- **Objective 3:** To use sedimentological techniques to assess the debris transport histories and origin of material contained within moraine, and to allow important moraine forming processes to be identified.
- **Objective 4:** To develop models of moraine formation to account for subsets of lateral-frontal moraine formation in Arctic and Alpine environments
- **Objective 5:** To assess how the morphology and internal composition of lateral moraine may change following climatic amelioration or deglaciation and to identify any implications this may have on interpretations of the Quaternary landform record.

1.7 Overview of the thesis

This thesis contains four data chapters. Data chapters IV-VI solely focus on the theme of lateral-frontal structure and morphology, whereas Chapter III is a methodological study which helps to inform later research within this thesis. Findings from these research components are integrated in a general discussion (Chapter VII). A brief summary of the contents of each chapter is provided below.

Chapter II outlines the sites and research methods used within this research. Four research methods are described: (1) geophysical surveys; (2) sedimentological surveys; (3) geomorphological mapping and (4) glaciological mapping.

Chapter III investigates the potential of small unmanned aerial vehicles (UAVs) and structure-from-motion (SfM) based photogrammetry for supporting geomorphological investigations at Cwm Idwal, north Wales, through the comparison and validation of a

SfM derived topographic dataset with a total station survey of the moraine-mound complex obtained by Graham and Midgley (2000a). Insights gained from this chapter inform later data collection of UAV aerial imagery in contemporary glacial forefields and the production and analysis of UAV derived datasets from these settings. This chapter was published as an original research article in *Geomorphology* (Tonkin *et al.*, 2014).

Chapter IV investigates the sedimentology and morphology of a lateral moraine complex developed at the temperate Alpine glacier, Schwarzberggletscher, located at the head of the Saas valley, Valais (Swiss Alps). In this chapter current theories of landform genesis relevant to Alpine sites are tested. Basin-wide debris transport is considered through the mapping of glacier structures and debris coverage from 2009 SwissTopo aerial imagery. This chapter is currently being prepared for submission within the target journals of *Geografiska Annaler: Series A* or *Zeitschrift für Geomorphologie*.

Chapter V explores the development of 'Østrem type' ice-cored lateral-frontal moraine at the margin of the polythermal glacier, Isfallsglaciären, located in Tarfala Valley, Arctic Sweden. A multi-technique approach is used, including the analysis of sedimentological and geophysical (ground-penetrating radar) datasets. As a result of these new datasets, the likely development, glaciological significance and chronology of these landforms are re-evaluated.

Chapter VI investigates the structure, sedimentology and morphological evolution of a large ice-cored moraine developed at the margins of polythermal high-Arctic glaciers through the use of geophysics, field-sedimentology and UAV-photogrammetry. The main feature investigated in this chapter is the true-left lateral-frontal moraine at Austre Lovénbreen. Geophysical data from the lateral-frontal moraine are reported in Midgley *et al.* (2013). Additional findings are reported here from surveys of surficial sedimentology. The geomorphological response and de-icing progression of the Austre Lovénbreen true-left lateral-frontal moraine over an 11 year study period is assessed. Aerial imagery obtained in 2014 is used to contrast NERC ARSF imagery from 2003. DEMs are produced and differenced to give volumetric estimates of landform evolution. The landform evolution section of this chapter has been accepted in *Geomorphology* as an original research article (Tonkin *et al.*, 2016).

Chapter VII synthesises the findings of this thesis in relation to the research objectives and considers how current understanding of Quaternary sites can benefit from insights obtained at the three contrasting sites assessed in chapters IV, V and VI. Consideration is given to the sedimentological, and morphological signature of 'Alpine', 'Østrem' and 'controlled' (ice-cored) type moraines and the potential significance of relict features from a palaeoglaciological perspective. A synthesis of the research is presented and its limitations are considered. Recommendations for future research are provided.

2. Research methods

2.1 Overview

This chapter provides an introduction to the various methods used and details the selection of the three sites investigated.

2.2 Research approach

This research adopts both an inductive and deductive approach for the purposes of investigating lateral-frontal moraine development. The inductive approach refers to the process of making observations, forming generalisations and ultimately models which explain a given phenomenon (Goudie and Viles, 2010). An example of this would be where a range of observations are combined to explain landform development at a certain site. The explanation may then be used to explain the wider formation of a set of landforms under similar environmental conditions. Whilst this is important in light of the site specific sites investigated here, a deductive approach is also useful. The deductive approach is relevant where existing models have been developed to explain the formation, sedimentology and morphology of a landform under a prescribed set of environmental conditions. Under this circumstance, it is important to 'test' and refine existing models and their relevance to the given study site (Miall, 2010). The latter approach is particularly important.

Benn (2006) highlights that a purely inductive approach can be limiting due to researchers looking to fit their preconceived ideas to the available evidence ('confirmation bias'). This can be problematic given the highly interpretative element of geomorphological research in glacial sedimentary environments and may not always lead to the development of robust understanding of geomorphological phenomena. Therefore a key element of this research will involve evaluating/testing existing ideas in light of new, and potentially enlightening datasets derived from novel or previously unused research methods (e.g. UAVs, SfM photogrammetry, and ground-penetrating radar). In line with good practice, interpretations are separated from reporting of the results throughout this research (Benn, 2006).

2.3 Study site selection

2.3.1 Overview of study site selection

To aid generalisations of lateral-frontal moraine development, study sites are needed to be suitably diverse in terms of their topographic and climatic setting. As identified in the literature review, large lateral-frontal complexes have been differentiated in terms of the mode of formation, sedimentology and structure in both Alpine and Arctic glacial landsystems. Therefore, to gain an understanding of moraine formation under different conditions, an example study site from each category was selected. Initial site selection was aided by aerial imagery assessed in Google Earth. The location and accessibility of potential study sites was important from a logistical perspective. One formerly glaciated site is also included in this study, for the purpose of testing the UAV-SfM approach for conducting topographic surveys. Given the use of geophysical (GPR) and remote sensing (UAV-photogrammetry), access to mains electricity for charging equipment was an important consideration. The locations of the glacierised sites are displayed in Fig. 2.1. Table 2.1 compares the character of the glaciers at the three sites. Table 2.2 provides an overview of the application of the methods with respect to each of the study sites.

2.3.2 *Cwm Idwal*

This site was selected to validate the integrated UAV and SfM approach to topographic data acquisition which is used in this thesis to examine the geomorphology and evolution of contemporary moraine formations. The main determining factor for choosing this study site was an existing high resolution topographic survey completed by Graham and Midgley (2000a) allowing for the new technique to be compared with an existing ground based survey method. The co-benefit of this site is that it is formerly glaciated, with analogues drawn between the character of the moraines used and high-Arctic valley glacier landsystems investigated in chapter VII.

2.3.3 *Schwarzberggletscher, Switzerland*

This site was selected to provide an Alpine example of lateral-frontal moraine formation. Although studies have investigated the character of moraines in the Valais region, few geomorphological studies have been completed at Schwarzberggletscher. The site located >15 km from Gornergletscher, and Findelgletscher, whose moraines have been subject to recent investigations (e.g. Lukas and Sass, 2011; Lukas *et al* 2012). This site is therefore ideal for investigating the applicability of conceptual models developed at these

glaciers. Furthermore, the most significant research contribution to our understanding of the Schwarzberggletscher moraines is that of Bircher (1982). This research predates the development of standardised sedimentological techniques for glacial geomorphological research, and is heavily focused on general glacier geochronology, rather than geomorphological and glaciological processes within the basin.

2.3.4 *Isfallsglaciären, Sweden*

This site is selected to provide an example of moraine formation within an Arctic polythermal setting of moderate relief (i.e. less mountainous than Alpine terrain; Hambrey and Glasser, 2012). Whilst the glaciers of the Kebnekaise region have been subject to significant glaciological research (e.g. Schytt, 1962; 1966; Holmlund *et al.*, 1996a; Holmlund and Jansson, 1999; Zemp *et al.*, 2010; Rippin *et al.*, 2011; Gusmeroli *et al.*, 2012), research seeking to understand the geomorphological significance of their moraines is largely lacking (e.g. Østrem, 1964; Etienne *et al.*, 2003; Heyman and Hättestrand, 2006; Pomeroy, 2014). This is at odds with the importance of these sites for contextualising current and future glacier change. Furthermore, the origin of ice contained within these moraines distinguishes them from their high-Arctic counterparts, yet little research attention has been directed at understanding the significance of these potentially rare geomorphological features. A modern investigation of the characteristics of these features is warranted. An additional co-benefit of this site is the logistical support offered by Tarfala Research Station which facilitated the completion of geophysical and UAV-photogrammetric surveys at the site.

2.3.5 *Austre Lovénbreen, Svalbard*

This site provides an example of ice-cored 'controlled' moraine (e.g. Evans, 2009) which can be contrasted with the Arctic landsystems of Northern Sweden and the Alpine high-mountain glacial environment of Schwarzberggletscher. Furthermore, there is ongoing debate regarding the applicability of our understanding of 'hummocky' moraine assemblages in high-Arctic landsystems to the British Younger Dryas. Key unresolved issues revolve around the perseveration potential of ice-cored landforms. Additionally, the location of this site (e.g. its close proximity to Ny-Ålesund) aids the completion of geophysical, UAV surveys and safer working conditions in the high-Arctic environment.

Table 2.1 Overview of glaciers investigated in this thesis.

Glacier	Location	Length (Neoglacial max)	Thermal regime	Dynamic status	Terminus Elevation
Austre Lovénbreen	78°53' N 12°08' E	c. 5 km	Polythermal (transitioning)	Receding	100 m.a.s.l
Isfallsglaciären	67°54' N 18°34' E	c. 2.5 km	Polythermal (transitioning)	Receding	1285 m.a.s.l
Schwarzberggletscher	46°00' N 07°57' E	c. 5.5 km	Temperate	Receding	2710 m.a.s.l

Table 2.2 Overview of datasets reported in each chapter.

Glacier	Sedimentology	Morphology	Geophysics	Geomorphological Evolution
Austre Lovénbreen	✓	✓	✓	✓
Isfallsglaciären	✓	✓	✓	
Schwarzberggletscher	✓	✓		

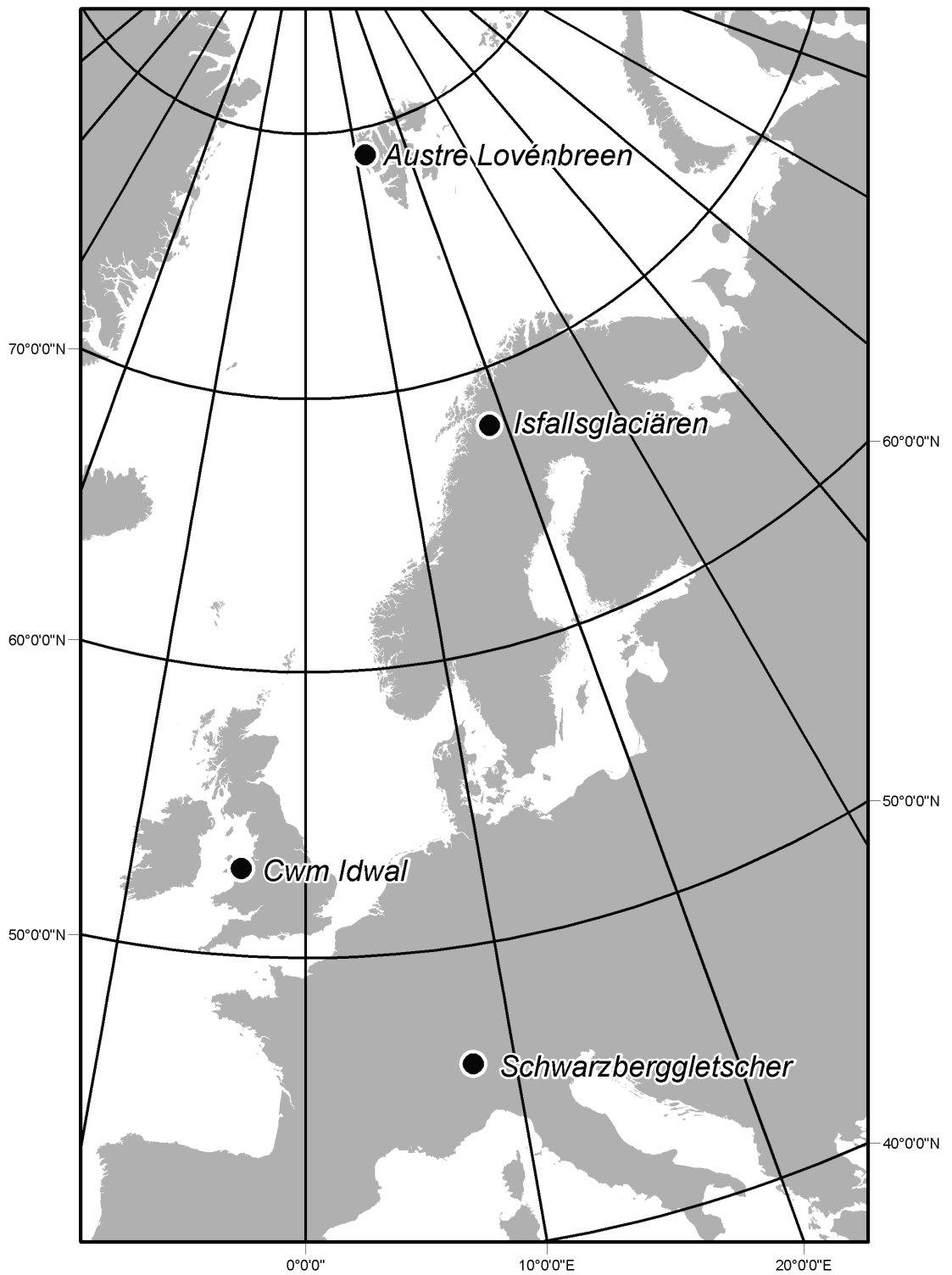


Fig. 2.1 Location map for the three glaciers and one formerly glaciated site investigated by this project

2.4 Ground-penetrating radar

2.4.1 Introduction

Ground-penetrating radar and its use in sedimentology is well established (Neal, 2004). Over the last decade the technique has been demonstrated to be effective in glacial sedimentary environments (Bakker and Van Der Meer, 2003; Sadura *et al.*, 2006; Brandt *et al.*, 2007; Burki *et al.*, 2010; Lukas and Sass, 2011; Midgley *et al.*, 2013) despite potential constraints on the effectiveness of the technique in coarse, or silt and clay rich substrates. One of the main benefits of ground-penetrating radar is that the technique is non-invasive, which is particularly useful for field sedimentology in environments where sedimentary exposures are rare or non-existent. Here the technique is applied to lateral-frontal moraine. Recently the use of ground-penetrating radar to assess the sedimentology of glacial moraines has been advocated (e.g. Lukas and Sass, 2011).

2.4.2 Physics of ground-penetrating radar

The technique exploits the interaction between the transmission of electromagnetic energy and the properties of a given substrate. The velocity that electromagnetic energy propagates is dependent on the properties of the sub-surface material. Important properties include the electrical conductivity (σ), magnetic permeability (μ) and dielectric permittivity (ϵ) of a material (Neal, 2004; Cassidy, 2009). Changes in these properties influence the propagation velocities of transmitted electromagnetic energy and result in reflections between contrasting sub-surface materials. Materials with strongly contrasting properties lead to the high-amplitude reflections (Conyers, 2012). A key aspect of this relationship is that certain materials have known velocities, which may vary depending on their thermal state (frozen or unfrozen), and the degree to which the material is water saturated (Davies and Annan, 1989). The propagation velocity of the electromagnetic energy can therefore be used as an indirect proxy for the sub-surface composition and material properties with the properties of a range of geological media well defined within the literature (Reynolds, 2011).

Where the velocity of the propagating electromagnetic energy is defined, depth can be estimated from two-way travel time (TWTT) (Robinson *et al.*, 2013). The thickness of a bed can be determined by measuring the travel time from the top to the bottom of a sedimentary unit, and calculating the TWTT difference (Δt) (e.g. Annan, 2003; Núñez-Nieto *et al.*, 2014). Propagation depth can therefore be solved using the following equation:

$d = v \times t / 2$, where v is the propagation velocity, t is the TWTT and d is the estimated depth.

For glacial sedimentary environments, 50 and 100, and 200 MHz antennae configurations have shown to be effective when surveying diamicton and gravel substrates. The antenna configuration used dictates the step-size, and subsequent spatial resolution of a dataset. Step-size refers to the distance the equipment is moved between the acquisition of an individual trace. The 100 MHz configuration uses a 0.25 m step size, whereas, a 50 MHz configuration will use a 0.5 m step-size (Table 2.3). Despite this trade-off, lower frequencies are associated with greater penetration, which is a key constraint of the technique in some glacial environments. For example Smith and Jol (1995) identified a linear relationship between the frequency of the antenna used, and the maximum depth structure could be observed within a Quaternary sedimentary substrate. However, a secondary trade-off is the resolution of the resulting radar data. Higher frequencies are associated with higher resolution subsurface data, but rapid signal attenuation, whereas lower frequencies attenuate less rapidly, but producing coarser resolution subsurface imaging (Annan, 2003).

Table 2.3 Summary of frequencies, configurations, and suggested maximum depth where sedimentary structures can be observed.

Frequency	Step-size	Antenna Separation	Suggested max probable depth of propagation ¹	Spatial resolution of reflectors ²
200 MHz	0.1 m	0.5 m	28 m	0.25 m
100 MHz	0.25 m	1 m	37 m	0.5 m
50 MHz	0.5 m	2 m	47 m	1 m

¹ Values derived from Fig. 7 in Smith and Jol (1995) for Quaternary sediments

² Taken from Annan (2003) with a dielectric constant of 9.

2.4.3 Field data acquisition

Radar data was collected using a Pulse EKKO Pro GPR. Reflection surveys were undertaken with an 100 MHz antenna configuration. A 0.25 m step size between traces and a 1 m transmitter/receiver separation distance was used. All surveys reported in this thesis were undertaken under winter conditions (frozen ground conditions) in an attempt

to circumvent potential scattering issues related to the presence of liquid ground-water. For all surveys, the transmitter and receiver were set up in a consistent manner, with the transmitter leading in the direction of the reflection survey. In adverse weather conditions the transmitter and receiver were insulated with polyethylene foam to improve performance and operational duration of the lead acid gel batteries. Where snow depth was deep enough to permit, both the control unit and transmitter-receiver were mounted to plastic pulks to improve the efficiency of the survey.

A distance of >5 m was kept between the DVL (digital video logger) control unit and transmitter/receiver setup to avoid unnecessary signal interference. Snow shoes were found to produce ringing at depth within the GPR reflection profiles, thus were not worn whilst surveying. A time-window of 750-800 ns was found to be sufficient for each trace. Traces were manually triggered using either the control unit interface or CANBUS electrical beeper. Surveys were conducted along a 100 m tape to ensure the correct step-size was maintained throughout the survey. To correct radar profiles for topography, surveys were conducted on each transect using a Leica NA700 automatic level. The start and finish location of a given survey was recorded by using a Garmin GPS 62. Waypoint averaging was used to reduce positional error. During CMP/WARR surveys the fibre optic cables (each of which were 20 m in length) limited the maximum separation to 38 m. WARR surveys were conducted using a common receiver configuration. The various survey configurations are illustrated in Fig. 2.2.

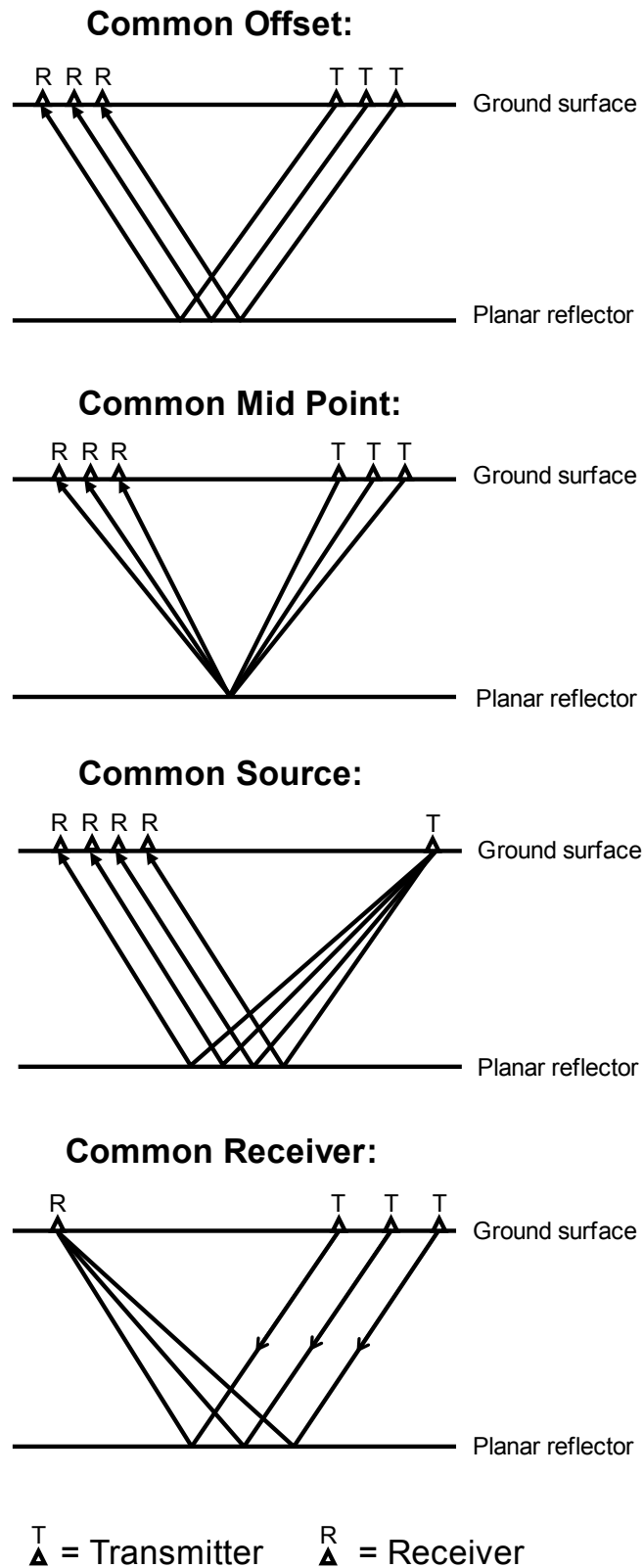


Fig. 2.2 GPR survey configurations redrawn from Neal (2004). Common offset surveys are also referred to as reflection surveys. Common mid-point, common source and common receiver survey configurations are used in this thesis to determine the propagation velocity of radar-waves. The latter two require either the transmitter or receiver to remain in a fixed location.

2.4.4 Post-processing

An overview of the post-processing steps used within this thesis is presented in Fig. 2.3 and explained below. The amount of post-processing was kept to a minimum in accordance with best practice to avoid operator bias (Cassidy, 2009). The three main post-processes (dewow, topographic correction and the application of gain) were applied.

The topographic correction (e.g. Fig. 2.4) process involves the horizontal repositioning of traces to allow for geometry of subsurface reflectors to account for changes in surface topography (Neal, 2004). The average velocity for a section is needed prior to correction of the radar data (Annan, 2003). Fig. 2.4 shows a radar profile prior to, and after topographic correction using a velocity of 0.17 m ns^{-1} . Methods for determining velocity are discussed in section 2.4.5. When corrected a fixed velocity was applied to the radar gram, which is a limitation of the software used for post-processing.

The dewow process involves the removal of a low frequency decaying signal trend (Robinson *et al.*, 2013; Fig. 2.5). The initial low-frequency 'wow' is caused by saturation of signals by early returns such as the ground or airwave (Neal, 2004; Cassidy, 2009). Without the application of dewow, the colour filling used to highlight the positive or negative amplitude of a given trace will be distorted as it will not be reset to a mean of zero (Cassidy, 2009). Dewow removal is achieved through the application of an averaging filter prior to any additional post-processing (Annan, 2003).

The application of gain as a post-process facilitates the identification and clarity of subsurface structure. Where radar signal propagates at depth, reflectors at depth may be obscured, or poorly visible due to signal attenuation. Signal attenuation may be particularly problematic in clay and silt rich substrates due to the dielectric properties of the material (Overgaard and Jakobsen, 2001). Several types of gain are available for use including automatic gain control (AGC), constant gain, and spreading and exponential compensation (SEC). AGC applies gain to boost the visibility of weak reflectors. The amount of gain applied is inversely proportional to the signal strength (Annan, 2003). The potential use of amplitude as an indicator of the strength of a given reflection event is removed once AGC is applied. The process can therefore be seen as a method equalising signals within a trace. Cassidy (2009) notes that AGC offers a trade-off between amplifying noise and displaying weak reflectors at depth, thus has the potential to be problematic when applied to poorly sorted glacial sediments. Within the EKKO view

software used for post processing the data presented in this thesis, the maximum and minimum amplitude that can be assigned to a trace using gain is ± 32767 . Constant gain is the simplest of the gain functions used. Within the EKKO view software constant gain is applied, multiplying signal strength by a specified value (Annan, 2003). For example if this parameter was set to 5, all signals would be multiplied by this amount. As the multiplication is applied to all signals, excessive gain may be applied to the least attenuated signals within the trace, therefore leading to over-amplified shallow signals. SEC applies gain in an exponential fashion along a trace. As radar-wave energy may attenuate in exponential manner at depth, this gain function attempts to account for this, and therefore preserve the relative amplitude of reflectors within a section (Annan, 2003)

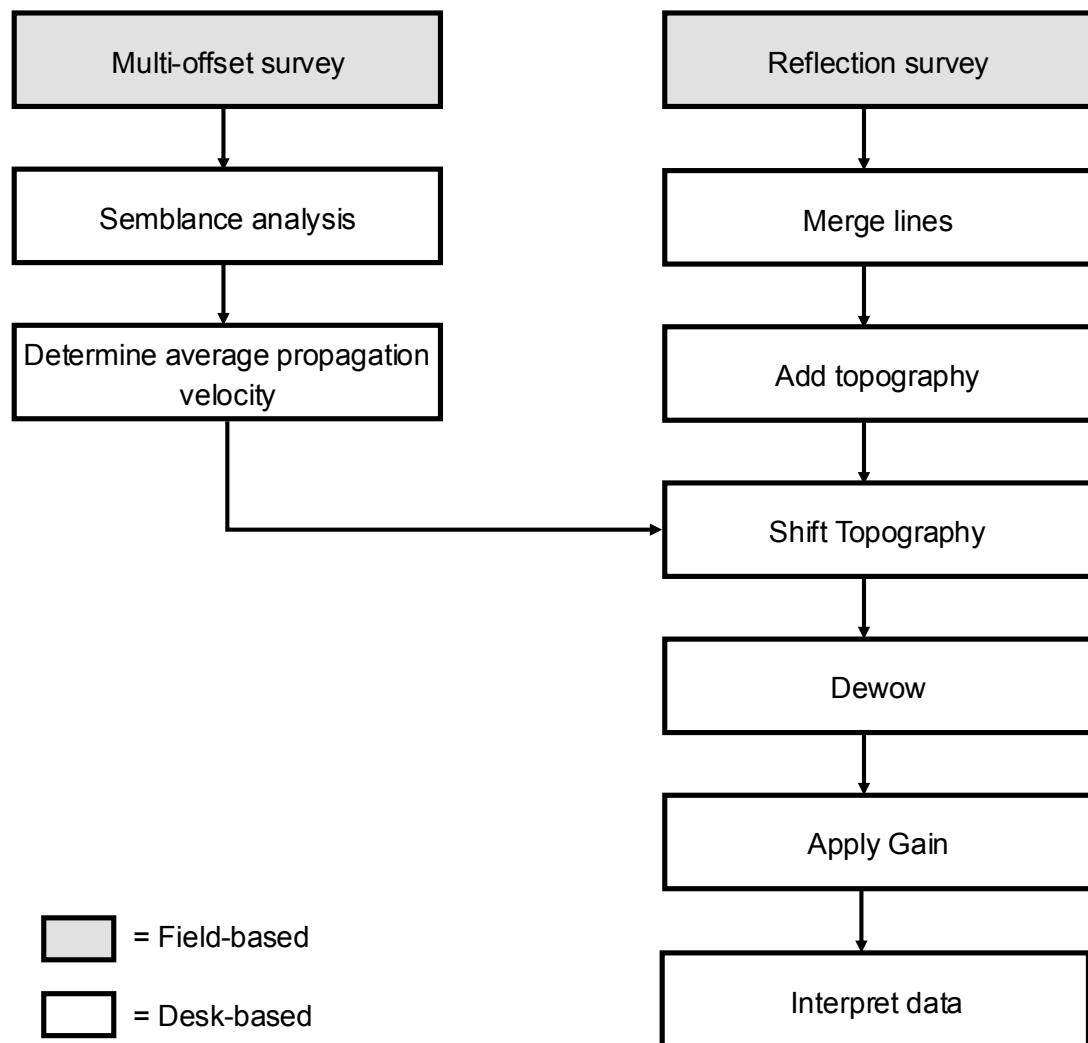


Fig. 2.3 Simplified overview of post-processing method used here.

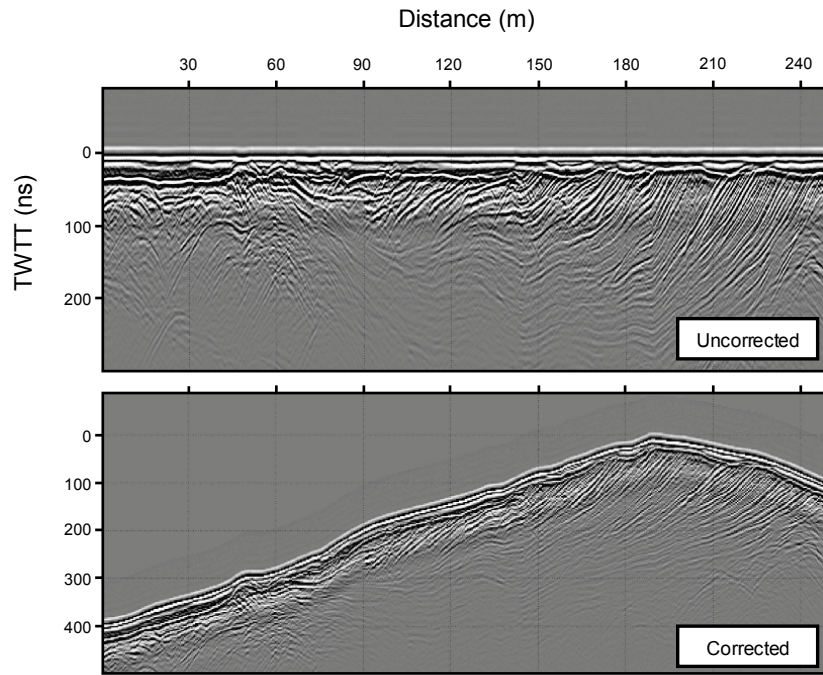


Fig. 2.4 Example of uncorrected, and corrected topographic of a radar transect. Note the reorientation of the dipping reflectors following correction to a velocity of 0.17 m ns^{-1} .

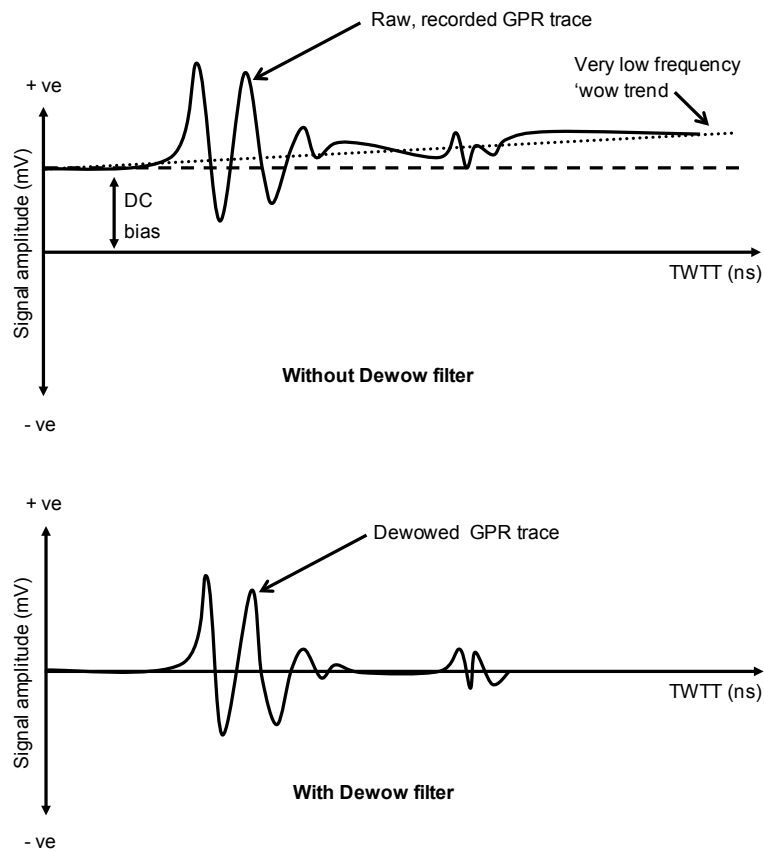


Fig. 2.5 A schematic showing the effect of wow, and the result of its removal. Illustration is redrawn from Cassidy (2009).

2.4.5 Semblance analysis

Multi-offset data derived from common mid-point and wide angle reflection and refraction surveys were analysed using semblance analysis to provide data on radar-wave propagation velocities. Within the Sensors and Software EKKO View deluxe software package, semblance analysis is referred to as CMP analysis. Annan (2003) defines the process as a method where traces derived from CMP or WARR surveys are stacked at a range of radar velocities. This results in high amplitude signals where the correct velocities are stacked, and low amplitudes where incorrect velocities are stacked (Annan, 2003). The resulting data output were plotted against the variables time (in nanoseconds) and depth (in metres) using a colour scale showing the amplitude (thus occurrence of a particular velocity) of the stacked traces.

2.4.6 Interpretation of radar datasets

The radar datasets were interpreted qualitatively following post-processing. Interpretations were made by digitising features present on the processed radargrams (e.g. Lukas and Sass, 2011; Lindhorst and Schutter, 2014). Reflectors were described based on their geometry. Four main characteristics for reflectors were noted; (1) the reflector shape (planar, wavy, convex, concave), (2) the reflector dip (e.g. horizontal, or either up or down glacier dipping), (3) the relationship between different reflectors within a radargram (e.g. parallel, subparallel, oblique, chaotic) and the continuity of reflectors within a radargram (continuous, moderately continuous and discontinuous). The terminology used to describe radar facies and surfaces was adopted from Neal (2004) and Pellicer and Gibson (2011) (Fig. 2.6).

Terminology for description of radar signatures

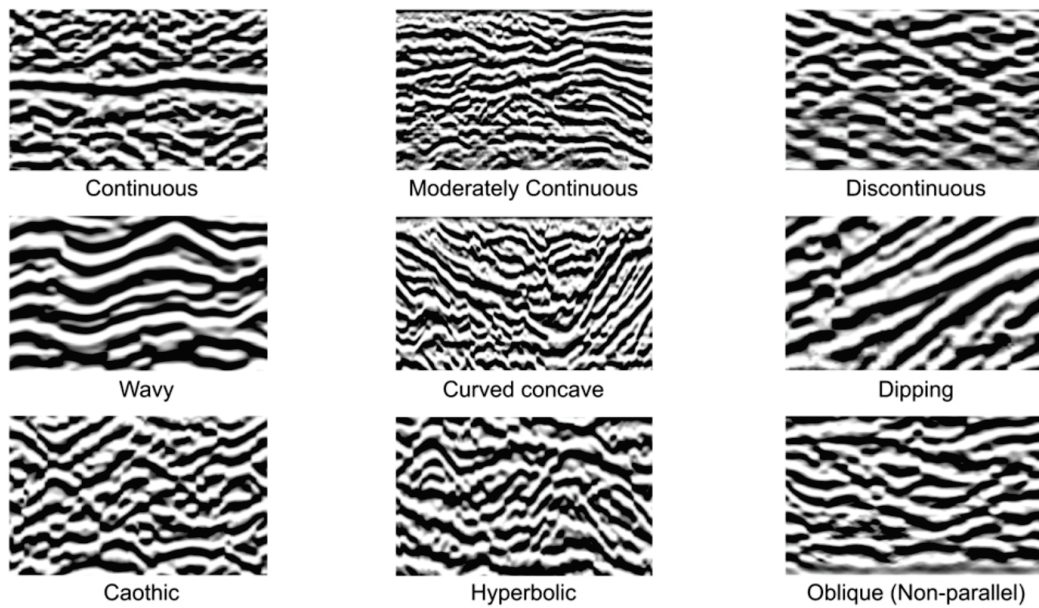


Fig. 2.6 Radar terminology in relation to nine distinct radar signatures from Pellicer and Gibson (2011).

2.5 Sedimentology

2.5.1 Introduction

Investigations into the sedimentology of moraines at Alpine and Arctic glaciers are used to interpret ice-marginal geomorphological processes, including the origin and transport pathways of moraine sediment, modes of deposition and any subsequent disturbance of lithofacies. This research uses standardised techniques in glacial sedimentology allowing the collected data to be compared with a wider population of glacial landsystems. To this end, the following techniques were used:

- I. Description of texture
- II. Logging of sedimentary structures and spatial relationships between lithofacies
- III. In-the-field measurement of lithofacies clast fabric
- IV. Sampling of clasts and assessment of clast morphology
- V. Sampling and laboratory assessment of matrix grain-size to supplement in-the-field assessment of lithofacies texture.

2.5.2 Description of texture

The Hambrey and Glasser (2012) modified Moncrieff (1989) classification was used to characterise poorly-sorted sediments (Fig. 2.6). This entailed estimating the percentage of sand, mud and clasts within a sedimentary exposure. Descriptive terminology used to refer to lithofacies throughout the thesis is therefore derived from this classification. The percentage sand contained within the matrix (particles <2 mm) was later verified through the analysis of samples using laser granulometry. Structural features such as displacements, laminations and lenses were also recorded using sedimentary field logs. Photographs of key sedimentary features were also taken to aid later interpretation of sedimentary units. Compaction was assessed using the descriptive scheme presented in Hubbard and Glasser (2005).

Table 2.4 Glacigenic sediment compaction assessment scheme adopted from Hubbard and Glasser (2005)

Description	Terminology
Loose	Unconsolidated
Crumbles easily between fingers	Very friable
Rubbing with fingers free numerous grains; gentle blow with a geological hammer disintegrates sample	Friable
Grains can be separated from sample with a steel probe; breaks easily when hit with a geological hammer	Hard

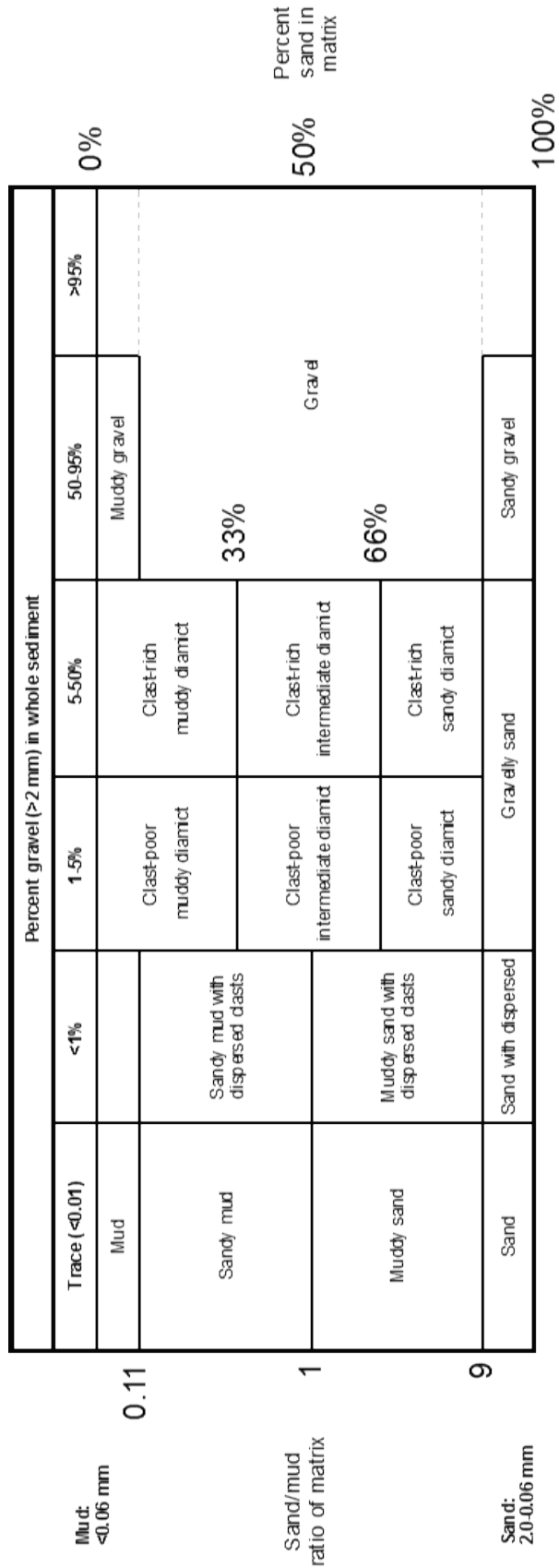


Fig. 2.7 Classification adopted by this thesis for the description of poorly sorted sediments. Classification adapted from Hambrey and Glasser (2012).

2.5.3 Clast form analysis

2.5.3.1 Overview

Clast morphological characteristics reflect their transport histories. Three parameters of clast morphology are commonly assessed. These include shape, roundness, and surface features (sometimes referred to as texture) (Benn, 2004a). Shape entails measurement of the three orthogonal axis to produce the relative dimensions of a clast. Roundness as a clast form parameter refers to degree of rounding (curvature) on the edges of a given clast. This classification assigns clasts to one of the six roundness categories through a subjective visual assessment. Clasts can be assigned to these categories using a visual (e.g. Powers, 1953) or descriptive criteria (e.g. Benn, 2004). A range of surface features (e.g. striae and polished surfaces) can be recorded, which reflect the erosional transport and depositional history of the clast. The presence or absence of striae, for example, can be used to determine an 'active' subglacial transport pathway (Hambrey, 1994).

Lithology is known to exert an influence on clast morphology (Lukas *et al.*, 2013). Recently, Lukas *et al.* (2013) have advocated the use of a single lithology to maximise the discriminatory power of the technique. However, mixed lithologies have been widely used by a range of studies, and are still found to provide robust discrimination between the various glacial transport pathways (e.g. Hambrey and Glasser, 2012). For example, in high-Arctic glacial environments, Bennett *et al.* (1997) found lithology to have limited influence on clast morphology. Furthermore, pragmatically, restricting sampling to single lithologies may not be possible if clasts are sampled from a spatially limited facies or a facies with a dispersed clast content. Here, mixed lithologies with higher sample sizes are likely to be more robust than simple lithologies of low sample sizes.

2.5.3.2 Field methods

Clast-form properties were assessed using the measurement of three superimposed parameters: shape, roundness and surface features (Benn and Ballantyne 1993; 1994; Bennett *et al.*, 1997). For shape, digital callipers were used to measure the long, intermediate, and short (L, I, & S) orthogonal axis of each clast. Measurements were undertaken on predominantly the pebble component of moraine sediments using size classes as defined by Wentworth (1922). Therefore clasts with a long orthogonal axis

falling outside the 40-64 mm range were excluded from analysis. Roundness was assessed using the visual scale published by Powers (1953).

Clast surface features were assessed by recording the presence or absence of striae on each clast within a sample. The fine component within glacial sediments can obscure clast angularity and preclude the identification of striae. Clasts were therefore thoroughly washed prior to analysis. Mixed lithology sample sizes of $n = 50$ were used, except in sedimentary facies with dispersed clast. Here, insufficient numbers of clasts were sourced to complete a sample of 50. At each study location, control samples from known environments were obtained for comparison with moraine sedimentology. These included samples from extraglacial (e.g. scree), subglacial (obtained from *in situ* extraction at the terminus), and glacio-fluvial settings taken from outwash stream at various distances from current glacier margin (e.g. Brook and Lukas, 2012). To characterise coarse boulder facies, which have a limited or absent quantity of clasts falling within the standard sizes (as defined by Wentworth, 1922) a modified approach was used. Boulders were assessed by measuring the roundness and intermediate axis of 50 clasts located at one metre intervals along a randomly placed 50 metre tape. The percentage of clasts exhibiting striae along the tape were also recorded.

2.5.3.3 Data analysis

Shape was graphically displayed using the Graham and Midgley (2000b) Microsoft Excel™ spreadsheet, which generates Sneed and Folk (1958) ternary diagrams. To aid discrimination between sediment transport pathways, co-variance RA-C₄₀ graphs were produced by plotting the percentage of very angular (VA), and angular (A) clasts in each sample (RA) against the percentage of clasts where the ratio of the S/L axis was ≤ 0.4 (C₄₀; Benn and Ballantyne, 1994). This is a standardised, and widely adopted approach to analysing clast form data (Benn, 2004a), and allows findings to be compared to existing studies. Where needed, the percentage of rounded and well-rounded clasts were also plotted against the C₄₀ index to assist discrimination between glacio-fluvial and subglacial transport pathways (e.g. Brook and Lukas, 2012; Lukas *et al.*, 2013). Additional clast form analysis is provided through the use of a two tailed Kolmogorov-Smirnov statistical test which compares the cumulative distribution functions (CDF) of two samples to aid discrimination. The statistical test was manually calculated using Microsoft Excel. This test has previously been used to distinguish a statistical difference

between the roundness of clasts from different populations (e.g. Spedding and Evans, 2002; Swift *et al.*, 2006). This is a non-parametric test, where equal sample sizes are not a pre-requisite (Borradaile, 2003).

2.5.4 *Clast macrofabric analysis*

A compass-clinometer was used to measure the dip and orientation of elongated clast axis. Samples of $n = 50$ are typically considered to produce statistically significant datasets, therefore were used as a minimum during data collection (Benn, 1994; 2004b). Clasts were selected randomly approximately over a 50 x 50 cm area to avoid sampling bias related to planar surfaces, whereby clasts which protrude, rather than run parallel to the exposure surface may be over-represented within a dataset (Millar and Nelson, 2001a; Chandler and Hubbard, 2008). Particle fabric can be weakened by repeated freeze-thaw cycles which are known to cryoturbate subsurface sediments (Millar and Nelson, 2001b; Chesworth *et al.*, 2008). To reduce this issue, samples were collected at *c.* 1 metre depth. To allow the direction of dip to be clearly distinguished an in-the-field visual assessment of shape was conducted where clasts with an axial L:I ratio of <1.5:1 were excluded (e.g. Millar and Nelson, 2003; Benn, 2004b). Following the removal of individual clasts, a pencil was inserted, to clearly delimit a plane for the measurement of particle dip and direction with the compass-clinometer. All metallic items were removed from the study area to avoid issues with instrument accuracy. Whilst it has been highlighted that there is significant overlap existing between fabric datasets of different origins (Hicock *et al.*, 1996; Bennett *et al.*, 1999b), fabric datasets are used in-combination (rather than in isolation) with other techniques to discern depositional/ice-marginal processes. The resulting data was presented using equal area lower-hemisphere Schimdt nets using the Stereonet 8 (Allmendinger *et al.*, 2012). Eigenvalues and vectors were calculated using as a quantitative method to analyse fabric data.

2.5.5 *Grain-size analysis*

2.5.5.1 *Overview*

The size of sedimentary particles allows for interpretation of erosional, transport, and subsequent depositional history. Grain size may reveal details on the relative energy of a given depositional environment (Hubbard and Glasser, 2005). Laser granulometry is one potential technique that can be used to determine the percentage volume of particles of

different sizes within a sample. Unlike sieving techniques, laser granulometry is achieved by passing a laser beam through a fluid module containing a sediment sample, and measuring the degree of scattering. Samples are entrained within a fluid chamber which results in random particle orientation relative to the laser (Beuselinck *et al.*, 1998). The degree of scattering is measured by a bank of detectors. The LS 13 320 used in this research has 126 detectors (Beckman Coulter Inc, 2011). One limitation of the method is that the shape of a grain will affect the resulting particle size distribution. This occurs as the area of particles will be averaged over a range of possible orientations, which results in possible over reporting of the coarser particle size of coarser non-spherical particles (Konert and Vandenberghe, 1997; Eshel *et al.*, 2004). Conversely, the volume of clay size material may be underestimated where the Fraunhofer optical model is used, with underestimation particularly pronounced in poorly sorted sediment types (Blott *et al.*, 2004). The resulting data may not be directly comparable to those produced using other methods (Hoey, 2004). Whilst organic matter can be removed prior to analysis using hydrogen peroxide, Beuselinck *et al.* (1998) found that removing the organic material from soil samples had a statistically limited effect on the resulting grain size distribution when analysed using laser diffraction. Significant variation exists between measurements derived using different laser diffraction instruments and other particle size analysis techniques (e.g. Eztler and Deanne, 1997; Hoey, 2004). The clay component is under-reported by this technique (Konert and Vandenberghe, 1997; Beuselinck *et al.*, 1998). Therefore findings from this analysis are predominantly used to aid the correct identification of diamicton units against the Hambrey and Glasser (2012) modified Moncrieff (1989) classification.

2.5.5.2 Field and laboratory methods

The matrix component of moraine sediment (sand and mud) was sampled in the field and retained in air tight plastic sample bags for later laboratory analysis. Approximately 15 g of sediment was taken from each facies. Where exposures were found to cross-cut several sedimentary facies, multiple samples were taken. Particle size was then quantified using a Beckman Coulter LS 13 320 laser diffraction analyser which measured particles size between 2000 and 0.375 μm . As the LS 13320 cannot process particles greater than 2000 μm , for diamicton samples, a wet sieve was used to exclude the granular component from the analysis. To ensure the accurate measurement of particle size by the device,

samples were dispersed/disaggregated using a solution of calgon. Although smaller concentrations have been recommended (e.g. Blott *et al.*, 2004), 5% concentrations were found to be acceptable for consistently dispersing the samples without introducing bubbles into the fluid module. The 5% calgon solution was prepared following the procedure outlined in Head (1992) by adding 35 g of sodium hexametaphosphate and 7 g sodium carbonate to 1 litre of distilled water. Samples were prepared into a homogenised paste to ensure good sample representation. To further aid sample disaggregation and dispersal, each sample was agitated in a sonic bath for 15 minutes, prior to transfer into the fluid module. Prepared samples were incrementally loaded into the diffraction analyser until an optimal obscuration of 8-12% was reached. The analysis was conducted using the Fraunhofer standard optical model. The instrument pump speed was consistently set to 60%, which produced sufficient particle entrainment without generating bubbles. The polarisation intensity differential scattering (PIDS) system was disabled. This allows for larger quantities of sediment to be added to the universal liquid module, which is particularly important to gain representative samples (e.g. Blott *et al.*, 2004). Additional statistical data was generated using the Blott and Pye (2001) Microsoft Excel™ GRADISTAT spreadsheet.

2.6 Geomorphological mapping

2.6.1 Overview and approach

Geomorphological field mapping used here serves to organise field observations into a GIS (geographic information system) and allow for features to be identified and interpreted (e.g. Knight *et al.*, 2011). Field observations ground-truth the spatial extent of landforms, document active surface processes and subtle geomorphological features. Two approaches are used: (1) conventional field mapping supplemented by existing base-maps or orthorectified aerial imagery (e.g. Hubbard and Glasser, 2005); and (2) novel UAV based image acquisition, and the subsequent programmatic processing of imagery into GIS datasets. Such datasets aid geomorphological mapping of moraines, and allow for morphometric change to be quantified. Mapped features include the ridge crests of moraines and the location of observable surface processes (e.g. gullying, back wasting faces, and debris flowage). A Garmin GPSMAP 62 was used to record the position of such features in the field. The following datasets were used for geomorphological mapping:

Schwarzberggletscher:

- ALTI3D DEM. 2m Resolution. Obtained from the Swiss Federal Office of Topography
- Orthophoto. 0.5 m resolution. Acquisition year: 2009. Obtained from the Swiss Federal Office of Topography.

Isfallsglaciären:

- Orthophoto. 0.5 m resolution. Acquisition year: 2008. Obtained from Lantmäteriet.
- SfM DEM. 0.5 m resolution. Acquisition year: 2013. Derived from UAV imagery.

Austre Lovénbreen:

- SfM DEM. 0.5 m resolution. Acquisition year: 2014. Derived from UAV imagery.
- SfM DEM. 0.5 m resolution. Acquisition year 2003. Derived from NERC aerial imagery.
- SfM orthophoto. 0.5 m resolution. Acquisition year 2003. Derived from NERC aerial imagery.

2.6.2 Photogrammetry and UAV-based mapping

For UAV surveys photogrammetrically produced imagery and elevation data was used for geomorphologically mapping. Photogrammetry is the process of producing measurements from photography (Aber et al. 2010). The technique itself has a long history of development with early attempts to use photogrammetry documented in the late 19th and early 20th Centuries. Traditionally, where the position of a camera location is known the 3D position of two features visible on overlapping photography can be estimated by triangulating the rays from the two camera positions. In recent years new approaches to photogrammetry have been developed. Specifically what is often referred to as 'Structure-from-Motion' photogrammetry has been adopted in the geosciences (Westoby *et al.*, 2012). Using this approach, the camera locations can be automatically resolved by detecting matching points between photography. The automated aspect of the workflow integrates efficiently with the use of small-format low level imagery such as imagery derived from UAV surveys and is capable of producing very high resolution topographic data sets (Fonstad *et al.*, 2013). Due to the novelty of UAV based image acquisition integrated with SfM photogrammetry, Chapter III is dedicated to assessing

the potential of this method for geomorphological research. An overview of the digital photogrammetric approach used and the data acquisition process in relation to each study site is provided in their respective chapters sections.

2.7 Structural glaciological mapping and interpretation

Structural glaciological mapping and interpretation can be used to understand debris entrainment, transport and deposition within glacier landsystems (e.g. Goodsell *et al.*, 2002). It is of importance due to the influence debris supply and transport has on controlling the rate and style of ice-marginal moraine formation (Benn and Evans, 2010). Information on the structural configuration of a given glacier can aid understanding of the subsequent distribution of lithofacies within a glacier forefield (e.g. Roberson, 2008). The use of this technique at high-Arctic polythermal glaciers has been particularly important in furthering our understanding of the significance of structural glaciological controls on landform development (Glasser *et al.*, 1998; Hambrey and Glasser, 2003; Hambrey *et al.*, 2005). Structural mapping is particularly effective where glacier-ice accounts for the constituent part of a moraine complex ('ice-cored moraine') as englacial structures exert an influence on resulting moraine morphology in ice-cored terrain (e.g. Evans, 2009; 2010). Midgley *et al.* (2013) demonstrated that the structural information obtained from relict-ice contained within moraine complexes also provides information on the character of glaciers at the time of moraine formation. However contemporary observations of glacier structures are needed to aid interpretations of relict glacier-ice structures contained within 'controlled' moraines.

Goodsell *et al.* (2005a) provided a schema for identifying glacier structures from aerial photographs (Table 2.5) and defined seven non-genetic features and their likely interpretations which are readily identifiable on aerial photography. This schema is adopted in this research to allow for the mapping of glacier structures from aerial imagery. Structural mapping was undertaken in Quantum GIS version 2.2. The contrast and brightness of the raster datasets were manipulated to aid identification of structure from the raster datasets. Additional units not defined by Goodsell *et al.* (2005a) are also mapped. These relate to the nature of supraglacial debris coverage on a given glacier. These units are mapped within a GIS from orthorectified aerial imagery to allow for their areal extent to be reported. Two types of debris coverage are qualitatively assessed: sporadic and extensive. Sporadic debris coverage is defined as debris where ice can still be readily

observed through the material on the aerial imagery. Extensive debris units are used to highlight where thick supraglacial debris are present on the glacier surface, and no ice is observed on the aerial photography.

Table 2.5 The Goodsell *et al.* (2005a) schema for identifying glacier structures from aerial photography

Non-genetic Name	Interpretation	Identification on aerial photography
Systematic layering	Primary stratification	Parallel layering usually found in the upper glacier basin, sometimes parallel to snowline.
Discontinuities in layering	Unconformity	A break in the normal systematic layering of the primary stratification.
Structural discontinuity	Flow unit boundary	A junction that separates structures rotated in one orientation from structures rotated in a different orientation.
Crevasses	Crevasses	Either as straight white lines (snow filled) or straight dark lines (non-snow filled or water filled), with cross-cut features.
Transverse/arcuate structures	Crevasse traces	First found in areas of crevassing as straight dark lines, can be followed down glacier as deforming dark lines, cross-cutting previously formed structures.
Steeply dipping longitudinal structure	Longitudinal Foliation	Long linear pervasive layered structure parallel to ice movement, which can be traced discontinuously.
Folding	Folding	Large-scale folding is identified as curves in linear features which do not follow surface topography.

3. The potential of unmanned aerial vehicles and structure-from-motion for topographic surveys: a test of emerging integrated approaches at Cwm Idwal, North Wales

3.1 Introduction

The use of small unmanned aerial vehicles (UAVs) and structure-from-motion (SfM) digital photogrammetry presents a new methodological frontier for topographic data acquisition and is of interest to scientists researching in a range of geomorphological environments (Westoby *et al.*, 2012; Carrivick *et al.*, 2013; Hugenholtz *et al.*, 2013; Tarolli, 2014). Traditionally low-level aerial photography has been acquired using a variety of unmanned platforms including small lighter-than-air blimps, kites, and model fixed-wing and single rotor aircraft (e.g. Wester-Ebbinghaus, 1980; Rango *et al.*, 2009; Smith *et al.*, 2009; Watts *et al.*, 2010; Hugenholtz *et al.*, 2013; Ryan *et al.* 2015). More recently lightweight (< 5 kg), relatively low-cost multi-rotor aerial platforms have been used to capture low-level imagery (Harwin and Lucieer, 2012; Niethammer *et al.*, 2012; Rosnell and Honkavaara, 2012; Mancini *et al.*, 2013; Lucieer *et al.*, 2014). These UAVs can be programmed to fly semi-autonomously at fixed altitudes along flight lines, ensuring optimal image overlap for digital photogrammetry. A key strength of the integrated UAV and SfM approach is the degree of automation involved. Previously, a high degree of user experience was a prerequisite for both the operation of aerial platforms and the application of photogrammetric methods to extract meaningful topographic data from aerial imagery (Aber *et al.*, 2010). The premise of SfM as a digital photogrammetric technique is that three-dimensional coordinates can be extracted from sufficiently overlapping photography without the need for camera spatial information (Snavely *et al.*, 2008; Westoby *et al.*, 2012). The integration of SfM with UAV camera platforms offers a rapid and increasingly cost effective option for geomorphologists to produce digital surface models (DSMs), with resolution and data quality proposed to be on-par with, or better than LiDAR (Carrivick *et al.*, 2013; Fonstad *et al.*, 2013). Topographic surveys derived from UAV imagery have recently been used for a variety of geoscientific

applications including quantifying rates of landslide displacement (Lucieer *et al.*, 2013), mapping vegetation spectral dynamics (Dandois and Ellis, 2013), producing DEMs (digital elevation models) of agricultural watersheds (Ouédraogo *et al.*, 2014), quantifying coastal erosion rates (James and Robson, 2012), and measuring rates of glacier motion and thinning (Whitehead *et al.*, 2013). The potential of SfM to aid geomorphological mapping, derive measurements of landforms (morphometry) and quantify geomorphological change is evident. Numerous software packages for SfM are now available and include cloud-based processing, which has the additional benefit of not requiring a high-specification consumer computer capable of handling the image processing.

Whilst a range of recent studies have sought to quantify data quality and associated error of SfM techniques (Harwin and Lucieer, 2012; Turner *et al.*, 2012; Westoby *et al.*, 2012; Dandois and Ellis, 2013; Fonstad *et al.*, 2013; Hugenholtz *et al.*, 2013; Ouédraogo *et al.*, 2014), further research is beneficial due to the diverse nature of the aerial platforms and consumer-grade digital cameras available for the production of topographic data using this methodology. Existing reports on the effectiveness of integrated multi-rotor based UAV–SfM approaches describe surveys conducted from relatively low altitudes (< 50 m). The objectives of this chapter are to: (1) provide a systematic account of the data acquisition process associated with this new integrated technique; (2) compare vertical spot heights obtained from the UAV–SfM survey to those obtained from a total station ground survey; (3) highlight important considerations for researchers seeking to use UAV image acquisition and SfM approaches to acquire data for topographic investigations; and (4) provide a baseline for the potential spatial resolutions when using a consumer-grade 18 MP compact digital camera at a target flight altitude of 100 m. This chapter addresses objective 1 of the thesis.

3.2 Study area

The test was undertaken at Cwm Idwal, North Wales in September 2013 ($53^{\circ} 6' 50.89''$ N; $4^{\circ} 1' 38.38''$ W; Fig. 3.1), a large cirque that was last occupied by a glacier during the Younger Dryas Stadial (c. 12.9-11.7 ka BP; Bendle and Glasser, 2012). The study area is located on the cirque floor and covers an altitudinal range of approximately 370 to 410 m (above Ordnance Datum). The geomorphology of the site is characterised by a moraine-mound complex ('hummocky moraine') located on both the east and west of Llyn [lake] Idwal (Fig. 3.1c). These moraines have been the subject of numerous investigations

(Darwin, 1842; Escritt, 1971; Gray, 1982; Addison, 1988; Graham and Midgley, 2000a; Bendle and Glasser, 2012) due to their importance for understanding the significance of Younger Dryas glaciers in the British Uplands. The majority of the moraines are 8 to 80 m in length, with the exception being a set of discontinuous stream-breached ridges totalling ~450 m in length which are stacked against the western cirque wall. In places the morphology of the moraines is influenced by glacially abraded bedrock. The prominence of some of the landforms is also disguised by a peat infill. The southern section of the survey area is characterised by a relatively flat lake infill and steep glacially abraded bedrock slopes. Vegetation on the eastern side of the cwm is typically restricted to short swards of grass, whereas livestock grazing exclosures erected in the 1950s and 1960s on the western side of Llyn Idwal have promoted the growth of vegetation including a thick cover of common heather (*Calluna vulgaris*), western gorse (*Ulex gallii*), and the occasional rowan (*Sorbus aucuparia*) and silver birch (*Betula pendula*) (Rhind and Jones, 2003). A large part of the moraine-mound complex and surrounding area was surveyed with a total station by Graham and Midgley (2000b). A similar area was surveyed by a UAV to allow a direct comparison between total station based data acquisition, and the UAV-SfM method used for this study.

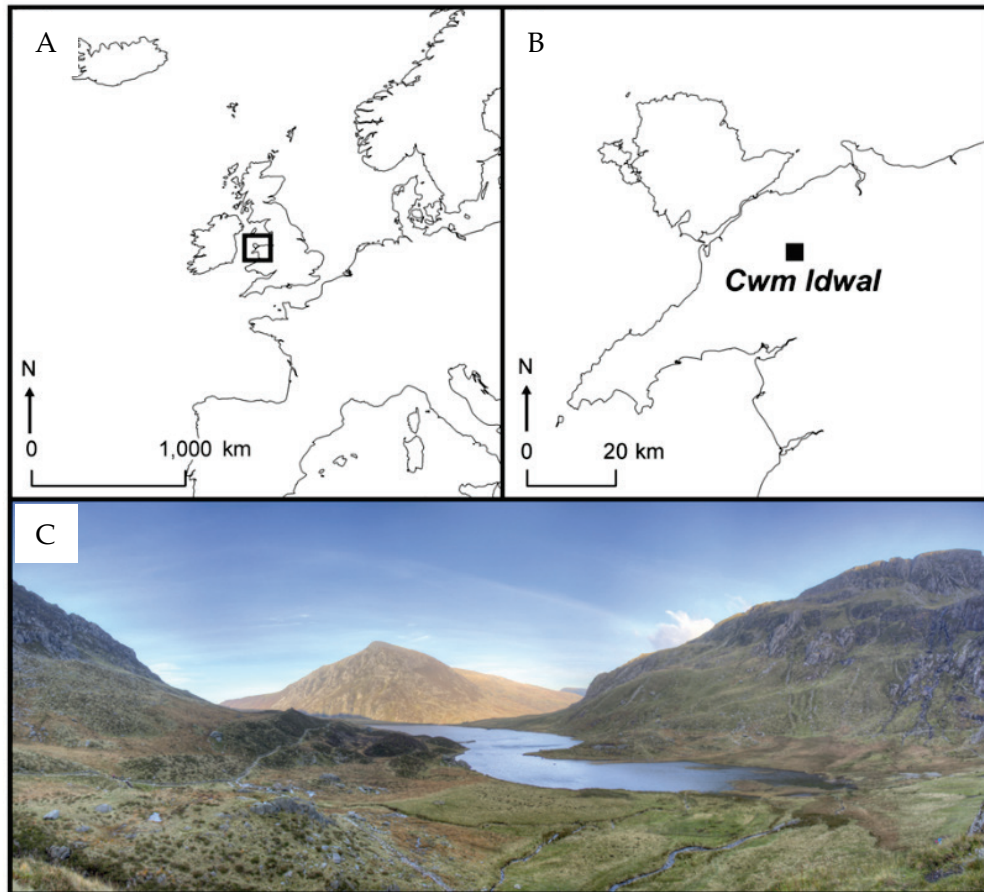


Fig. 3.1 Maps showing the study site location in relation to (A) North-west Europe and (B) North Wales. ©Crown Copyright/database right 2014. An Ordnance Survey/EDINA supplied service. (C) A ground-level panoramic photograph of the moraine-mound complex which is located on both the left and right of Llyn Idwal.

3.3 Methods and materials

3.3.1 Image and data acquisition

Aerial imagery was acquired using a Canon EOS-M 18 MP camera suspended from a DJI S800 Hexacopter (Fig. 3.2). A Photohigher AV130 servo driven gimbal maintained the camera angle close to the nadir (e.g. the camera was pointing down). The hexacopter was equipped with a Wookong-M GPS assisted flight controller which allowed for semi-autonomous surveys. Survey flight lines were pre-programmed via the DJI Ground-Station software package. For all surveys the UAV was set to a target altitude of 100 m above ground level (AGL) and horizontal ground speed of 2.5 ms^{-1} . The target altitude is calculated in the DJI Ground-Station software using elevation data derived from Google Earth. Parallel flight lines were programmed to have an image sidelap of 80%, whilst taking into account the camera sensor size ($22.3 \times 14.9 \text{ mm}$) and focal length (22 mm). The intervalometer function of the Magic Lantern third-party camera firmware was set to acquire imagery every 2 s along parallel flight lines. Actual image acquisition was every ~ 4 s, resulting in image capture approximately every 10 m along flight lines. Although image capture can be triggered using the DJI flight controller, an intervalometer was used for its improved reliability and potential to capture excess imagery along flight lines. This allowed for blurred or poor quality imagery to be removed whilst ensuring that an image onlap in excess of 80% was maintained. The camera was set to shutter-priority mode and used a $1/1000 \text{ s}$ shutter speed. To provide the required image coverage the survey area had to be split between four flights. The UAV had a flight-time of ~ 14 min whilst carrying its payload (using an 11 Ah, 22.2 V, 6 cell lithium polymer battery). A generous overhead (~ 2 min) was left in order to safely land the UAV. In the UK unaided visual line of sight (VLOS) has to be maintained whilst operating UAVs (CAA, 2012). Therefore the ground equipment and launch position were moved between flights to allow the UAV to be easily observed, and manually controlled if necessary.

The total station dataset was previously acquired over multiple survey sessions in 1997 and 1998 using a Leica TC600 by Graham and Midgley (2000). An assessment of error for this data set is unavailable. However, measurement accuracies (expressed as standard deviation) for the TC600 are defined by Leica (1997), with distance measurements accurate to $2 \text{ mm} \pm 2 \text{ ppm}$ and angle (horizontal and vertical) measurements to 1.5 mgon . As the original total station dataset was collected for the purpose of characterising the

overall shape of the moraine-mound complex, individual points were collected rapidly. Points recorded whilst the prism pole was not perfectly vertical have the potential to result in misregistration between the two datasets. The extent of the resulting error will be exacerbated by slope steepness and the height of the reflector on the detail pole. The SfM dataset was tied into the same arbitrary co-ordinate system and datum through the use of two brass pin benchmarks located on exposed bedrock on the east and west of Llyn Idwal. Point densities for the validation points reach as high as 20 per 100 m² over the moraine-mound complex (Graham and Midgley, 2000a). For the UAV survey, 19 SfM ground-control points (GCPs) were distributed across the survey area (Fig. 3.3a). White laminated A3 size targets (297 × 420 mm) were used as GCPs and were found to be adequately visible on the aerial imagery. These GCPs were surveyed with a Leica TC407 total station to a precision of <1 mm and estimated accuracy of <3 cm.

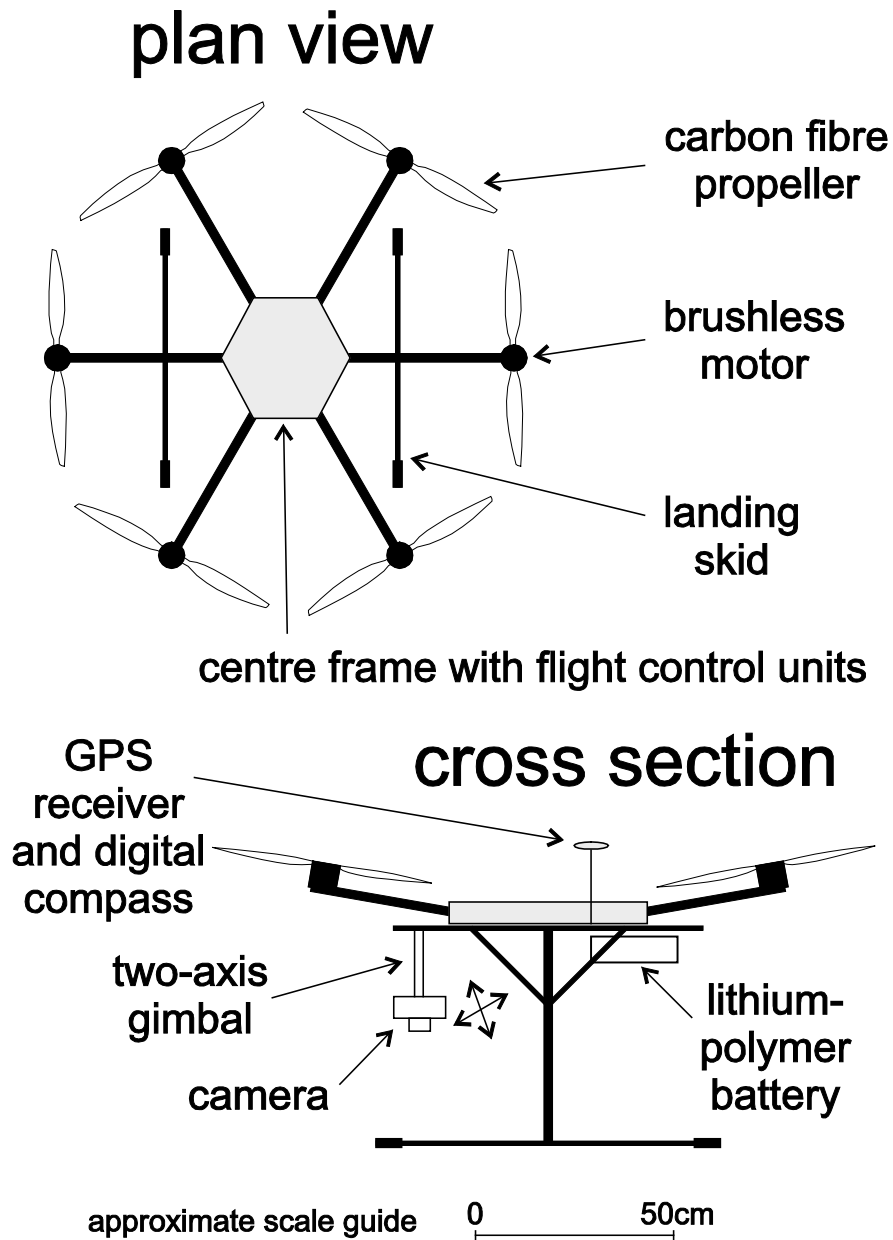


Fig. 3.2 A schematic drawing of the S800 hexacopter

3.3.2 Image processing and analysis

From the original set of 824 images, 543 images were selected for model reconstruction using the Agisoft Photoscan 1.0.0 (build 1795) software package. Images were visually assessed for quality and blurry images were removed prior to processing. Image processing followed the recommended procedure outlined by Agisoft (2013). Image processing was conducted on a HP Z820 workstation equipped with dual Intel Xeon E5-2690 processors, 128 GB RAM, and nVidia 680 graphics card. As GPS information for camera positions were not collected, images were aligned using the 'Generic Pair Preselection' parameter. This parameter detects matching features between images at a lower accuracy first, to reduce overall processing time (Agisoft, 2013). Photoscan provides nominal parameters for setting the target accuracy to which the images are aligned. Here the 'high' setting was used to obtain the best possible image alignment accuracy. Nineteen GCPs were then identified on imagery within the software a total of 674 times, with the XYZ coordinates input for each point. The sparse point cloud was optimised using a marker accuracy of 0.001 m and focal parameters (Fy and Fx) defined in the image headers. Camera radial and tangential distortion coefficients (K_1 , K_2 , K_3 , P_1 and P_2) were automatically estimated by Photoscan. A dense point cloud was then produced using the 'medium' quality setting. Again, this is a nominal setting that relates to the geometric accuracy of the target dense point cloud produced within Photoscan. Aggressive depth filtering was used to remove outliers from the dense point cloud (Agisoft, 2013). The dense point cloud and polygonal mesh was generated using a target point count of 3×10^5 . An additional sparse point cloud and a DSM were produced for comparative purposes. An orthorectified aerial image was produced using the 'orthophoto' and 'mosaic' parameters with colour correction enabled. Where image overlap occurs, the 'mosaic' parameter ensures that images with pixels closest to the image centre are used preferentially for orthophoto generation (Agisoft, 2013).

Data handling and the analysis of geographic data were conducted using QuantumGIS 2.0 and ArcGIS 10.1. SfM height (SfMz) was subtracted from ground height (GSz) for 7761 independently surveyed data validation spot heights derived by total station survey (Fig. 3.3a) providing a vertical difference. The vertical difference was converted into a raster surface with a 2.1 m cell size using an ordinary kriging function (default settings: spherical semivariogram, variable search radius, 12 points) in ArcGIS 10.1. This allowed

the vertical difference to be visualised. RMSE (root mean square error) and MD (mean difference) were calculated for the vertical difference (SfMz–GSz). Two zones of contrasting vegetation cover (Z1 and Z2; Fig. 3.3a) were mapped from orthorectified aerial imagery, and used to quantify vertical difference associated with contrasting vegetation types. Z1 is characterised by a continuous ground cover of heather, gorse, and occasional shrub and is located on the western side of Llyn Idwal. Z2 consists of grassland and exposed bedrock, and is also located on the western side of Llyn Idwal.

3.4 Results

The dense point cloud was composed of 31,474,859 unique points. With the exception of the extremities of the model, the effective overlap was > 9 images per point. ‘Noisy’ anomalies are present where the surface of reflective water-bodies are reconstructed. The orthorectified images had a 0.022 m per pixel resolution, and the DSM as seen in Fig. 3.3b had a 0.088 m per pixel resolution. These resolutions were achieved from an average flight altitude of 117.282 m AGL as reconstructed from the imagery. Discrepancy between the target flight attitude and actual flight attitude is likely to be caused by the use of low resolution Google Earth elevation data for flight planning, and error associated with the use of barometric pressure sensors for determining relative height (see DJI, 2013). Photoscan reported a total RMSE value of 0.033 m calculated from the 19 SfM GCPs (errors ranging from 0.011 to 0.062 m reported for individual points). The total x and y RMSE values reported by Photoscan were 0.019 and 0.020 m respectively. The total vertical RMSE value was 0.018 m.

Spot heights (n = 7761) from the ground survey (GSz) and DSM (SfMz) are in broad agreement, although the vertical difference is a higher than that reported by the 19 SfM GCPs used during the image processing stage. The vertical difference is visualised in Fig. 3.3c. The dense point cloud provides a vertical RMSE value of 0.517 m (Table 3.1). The differences for the DSM are offset from zero, with a mean difference of 0.454 m. The majority of the height values on the DSM were within the ± 1 m range (99.8%). However, only 55.4% of the SfM DSM values were within ± 0.5 m of the ground survey data. Isolated spot heights were found to be as much as 0.705 m under the actual ground survey (GSz) and as much as 4.347 m over. When vertical RMSE is calculated separately, RMSE for the east (less densely vegetated) is significantly lower (RMSE = 0.200; n = 1988), than the west

(RMSE = 0.588; n = 5773) with 98.8% of height values for the east falling within the ± 0.5 m range (Fig. 3.4).

Two contrasting vegetation zones (Z1 and Z2 in Fig. 3.3a) were investigated. Z1 had an RMSE value of 0.789 m (n = 244). In contrast, Z2 produced a lower RMSE value of 0.362 m (n = 205). The calculated RMSE values for slopes gentler than 20° and those steeper than or equal to 20° were examined for both patches. The values are 0.031 and 0.030 m higher for slopes steeper than 20° regardless of the vegetation type. Where RMSE was calculated for separate 10° bins for the entire dataset (7761 observations), excluding the $60\text{--}70^\circ$ bin, the reported RMSE value increases on progressively steeper slopes (0.444 to 0.838; Table 3.2). The $80\text{--}90^\circ$ bin comprised one observation, which shows a high vertical difference (2.222 m). An additional analysis of the DSM derived from the sparse point cloud (2,058,037 points) was conducted. The sparse point cloud produced a coarser resolution DSM at 0.258 m per pixel. Unlike the dense point cloud, the sparse point cloud did not produce 'noisy' anomalies related to reflective water-bodies. Points from the SfM DSM and the ground survey data were also in broad agreement with 98.9% of the data within the ± 1 m range, and 58.5% of the data in the ± 0.5 m range. The total vertical RMSE value was 0.505 m. The sparse point cloud derived DSM produced a wider range of outlying values, with minimum and maximum anomalies of -3.416 and 3.782 m.

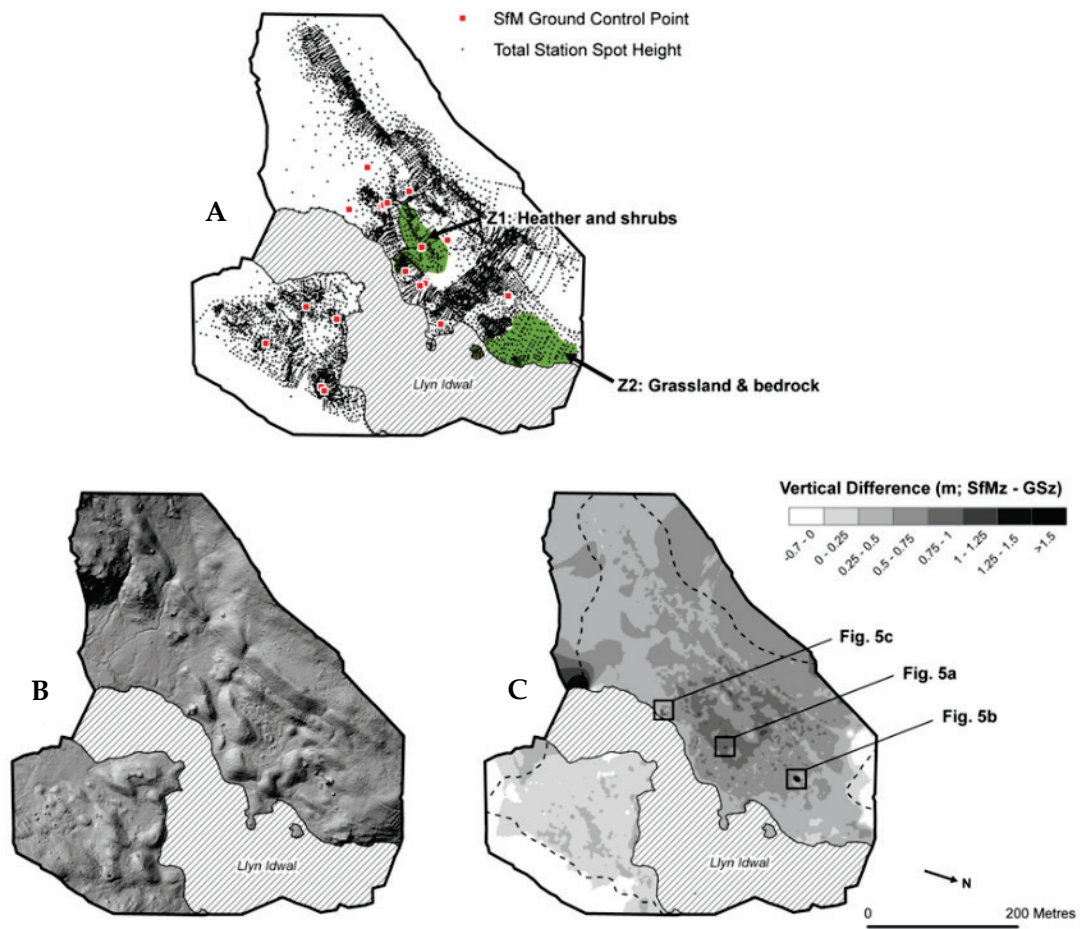


Fig. 3.3 Maps displaying the topographic data and analysis of vertical disagreement. (a) The distribution of 7761 ground-survey points and 19 SfM ground-control points across the survey area. Two zones (Z1 and Z2) of distinct ground cover are delimited. (b) A hillshaded DSM at 0.088 m per pixel resolution derived from the UAV-SfM survey. (c) A raster surface of vertical difference produced using an ordinary kriging function at a resolution of 2.1 m per pixel. The spatial extent of the spot heights is delimited by the dashed line.

3.5 Discussion

3.5.1 Causes of vertical disagreement

Causes of poor surface representation and vertical disagreement between the two data sets have been investigated and include: (1) vegetation; (2) slope angle; and (3) unintentional random error related to the acquisition of the original total station dataset. Vegetation is a known cause of poor surface representation in DEMs derived from both photogrammetry (Lane, 2000; Marzoff and Poesen, 2009), and airborne LiDAR (Lui, 2008; Spaete *et al.*, 2011; Hladik and Alber, 2012). A visual assessment of high vertical difference against the orthorectified imagery shows that error is particularly pronounced around trees, and in areas vegetated with heather (Fig. 3.5a). Dense vegetation types obstruct line-of-sight of actual ground level, thus generate a vertical difference between the two datasets (Table 3.1). This difference generated by vegetation is also apparent when the east (sparsely vegetated) and west (densely vegetated) are visualised together (Fig. 3.3c) or where RMSE is calculated for the two zones of contrasting vegetation (Z1 and Z2). For the examples of Z1 (heather and other shrubs) and Z2 (grasses and exposed bedrock), the presence of a thick covering of vegetation produces an additional 0.434 m RMSE value (Table 3.1). Whilst the total station data provides information that can be used to produce a bare earth DEM of the moraines, the data presented from SfM photogrammetry accounts for the surface plus vegetation, and therefore represents a DSM. Fig. 3.5a exemplifies this error, showing how a ground survey point located under a silver birch generates a vertical difference between the two datasets. Similarly, in other areas of the Cwm Idwal DSM, this problem arises due to tilted bedrock rafts with near vertical and in places overhanging sides (Fig. 3.5b), generating the outlying vertical difference of 4.347 m. As DSMs are essentially 2.5 dimensional representations of the Earth's surface and associated surface features, true 3 dimensional representation of overhanging surfaces is not possible (Bernhardsen, 2002). If the same SfM approach was applied to un-vegetated terrain (e.g. braided channels in Javernick *et al.*, 2014), a significantly lower degree of vertical difference would be expected.

Further vertical differences between the two topographic datasets is also likely to be the result of unintentional random errors in the ground survey dataset caused by the reflector detail pole not being held perfectly level during point acquisition. The vertical difference caused by this operational error appears to be exacerbated on steep slopes (Table 3.2). For

example, on a perfectly horizontal surface, if the reflector (with the detail pole set to the minimum high of 1.3 m) was inclined at 10° from vertical opposed to being perfectly vertical, the calculated positional and vertical errors would be 0.226 and 0.020 m respectively. However, if the detail pole was inclined at 10° from vertical on a slope of 30° , the expected vertical error would reach the decimetre range. As 16.3% of the 7761 observations were made on slopes $>30^\circ$, additional errors should be expected. An example where positional misregistration between the two datasets has occurred is presented in Fig. 3.5c. Here points taken in the vicinity of a steep-sided tilted bedrock raft with near vertical slopes have resulted in vertical disagreement exceeding 1 m. In this circumstance, sub-decimetre positional errors on the ground survey data or poorly resolved features on the SfM DSM promote a high degree of localised vertical disagreement between the two datasets.

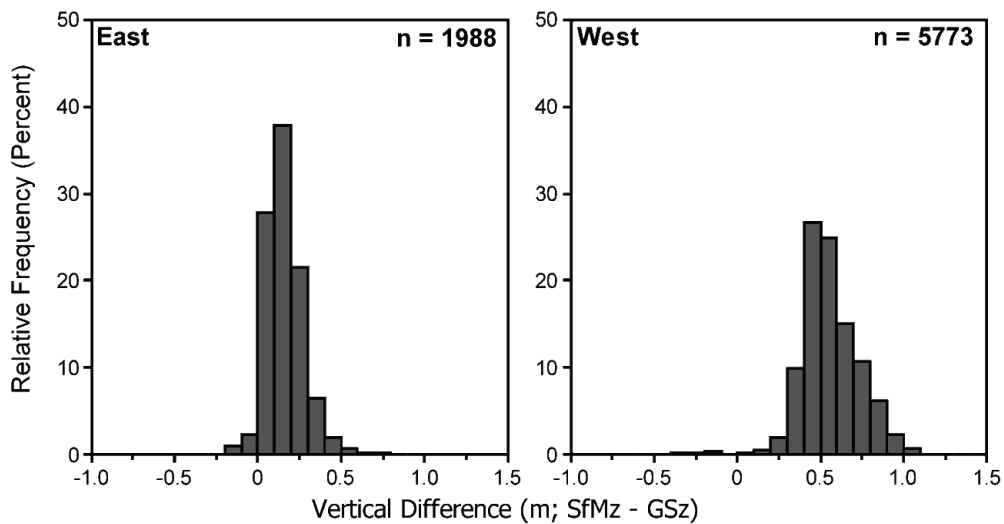


Fig. 3.4 Histograms of vertical difference for the east and west sections of Cwm Idwal .

Table 3.1 Statistics for the vertical difference (m) between the Cwm Idwal topographic datasets

Area	Total Observations (n)	RMSE	Mean	RMSE (<20°)	RMSE (≥20°)
All	7761	0.517	0.454	0.468 (n = 4527)	0.578 (n = 3234)
East	1988	0.200	0.155	0.169 (n = 1306)	0.247 (n = 682)
West	5773	0.588	0.557	0.544 (n = 3222)	0.639 (n = 2551)
Z1	244	0.796	0.820	0.789 (n = 102)	0.821 (n = 142)
Z2	205	0.362	0.341	0.354 (n = 152)	0.384 (n = 53)

Table 3.2 Calculated RMSE for vertical difference (m) binned by slope angle.

Bin	RMSE	Observations (n)
0 – 9	0.444	1864
10 – 19	0.482	2662
20 – 29	0.543	1967
30 – 39	0.603	952
40 – 49	0.678	263
50 – 59	0.739	36
60 – 69	0.729	10
70 – 79	0.838	6
80 – 90	2.222	1

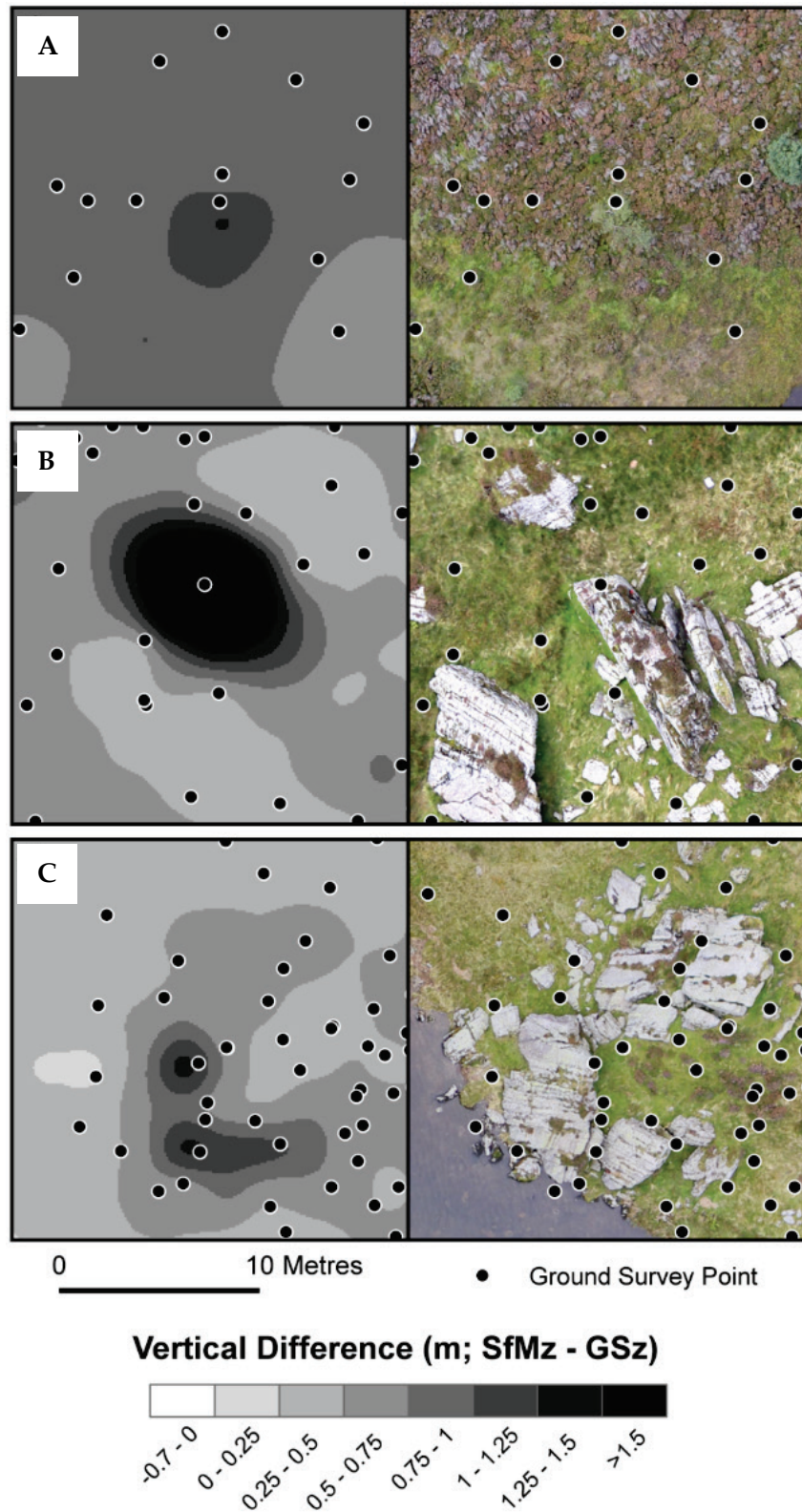


Fig. 3.5 The occurrence of vertical difference in association with: (a) vegetation, (b) near vertical and in places partially overhanging bedrock rafts, and (c) positional misregistration close to near vertical slopes

3.5.2 Benefits and practical considerations

The UAV-SfM technique is in many ways superior to a conventional total station ground survey and performed comparably to a range of recent SfM data validation studies (Table 3.3). Whilst the total station topographic survey reported by Graham and Midgley (2000) took approximately 15 field-days, this aerial survey was completed in 3 days and also provided high-resolution aerial imagery. The standalone UAV survey could have feasibly been completed in one day, however this survey needed to be tied into the arbitrary coordinate system and datum used by Graham and Midgley (2000a). Operation of the UAV is unfortunately restricted to dry conditions, with relatively low wind speeds ($< 8 \text{ ms}^{-1}$). Despite specific weather requirements, multi-rotor based systems appear to be well-suited to mountain settings. They can be deployed where there is limited space for take-off and landing, and offer a high-degree of control, which is beneficial when surveying in close proximity to steep slopes. Regardless of the UAV platform used for image acquisition, the technique lends itself to surveying unstable or inaccessible terrain where traditional survey methods would be unfeasible or unsafe.

UAV based image acquisition has clear benefits over existing full-scale airborne image acquisition as the low survey altitude circumvents much of the weather dependency (particularly cloud coverage) that affect full-scale airborne surveys (Baltsavias, 1999). UAVs also have the additional co-benefits of being less costly to deploy in comparison to full scale airborne surveys and have the ability to produce data products that are more scale appropriate for micro topographic investigations than those provided by airborne LiDAR (Laliberte and Rango, 2009; Anderson and Gaston, 2013). However, application of the SfM technique may be limited in some geomorphological environments due to the presence of texturally 'smooth' or reflective surfaces (e.g. snow cover or sand) which prohibit the extraction of meaningful topographic data (Fonstad *et al.*, 2013). Further work to investigate the performance of automated image alignment over more texturally homogenous surfaces may be beneficial where GPS information for camera positions are not available. Care must be taken when acquiring coordinates for the GCPs used during the image processing stage, due to the potential for erroneous readings to propagate through the various derivative data products. Providing that the GCPs are accurately surveyed, the automated nature of the approach is beneficial as it reduces the potential for unintentional random error (e.g. as found to occur in the total station dataset).

Although the production of a DSM from a dense point cloud produced a sub-decimetre DSM, a coarser DSM (0.258 m per pixel) can be reconstructed from a sparse point cloud of 2 million points with comparable error to that derived from a dense point cloud of 30 million points. Where computational resources for both image processing and data handling are limited or where data are not required at sub decimetre resolution, producing DSMs from lower point densities maybe desirable. The DSM presented here required ~7 h to point match and align the 543 images. An additional 43 min of processing time was needed to derive the dense point cloud. Research to investigate the influence of point cloud density and the resulting DSM error merits further investigation, although all DSMs should be regarded as an abstraction, with some associated uncertainty (Fisher and Tate, 2006; Wechsler, 2007).

3.5.3 UAVs and SfM as a tool for geomorphological mapping and monitoring morphometric change

The UAV–SfM based approach appears to be a useful research tool that aids the production of accurate geomorphological maps. A variety of data sources can be used to compile geomorphological maps (Oguchi *et al.*, 2011), with remotely sensed data often requiring ground-truthing to ensure that landforms are accurately recognised within a study area (Hubbard and Glasser, 2005; Knight *et al.*, 2011). From this perspective the recent availability of high-resolution airborne LiDAR datasets are seen to be beneficial for the production of more accurate geomorphological maps (Jones *et al.*, 2007; Bishop *et al.*, 2012), yet the limited coverage of LiDAR surveys mean researchers do not always have access to high-resolution data. In such cases the UAV–SfM approach could be utilised by researchers who wish to produce their own ultra-high-resolution DSMs and orthophotos to aid field-mapping campaigns. Researchers should determine whether the spatial coverage offered by UAVs is useful for their investigation. Here, a localised area of 0.211 km² was surveyed over four separate flights. This is unlikely to be sufficient for all geoscientific applications, however as UAV technology improves, greater survey coverage per flight may be permitted.

A further application of UAV–SfM based surveys is morphometric change detection due to how readily the technique can be deployed for use. Quantification of geomorphological change through the comparison of multi-temporal DEMs is a well-established practice applied to a range of geomorphological settings (coastal, glacial, hillslope, fluvial, etc.; e.g.

Pyle *et al.*, 1997; Schiefer and Gilbert, 2007; Dewitte *et al.*, 2008; Marzolff and Poesen, 2009; Mitsova *et al.*, 2009; Hugenholtz, 2010; Irvine-Fynn *et al.*, 2011; Carrivick *et al.*, 2012b). In some cases quantifying morphometric change can be problematic where the rate of change is below or close to the achievable accuracy of a given topographic survey technique (Williams, 2012). SfM integrated with UAV based image acquisition has recently been used for change detection. For example, Whitehead *et al.* (2013) successfully completed repeat SfM surveys to report on the thinning and motion of Fountain Glacier (Alaska) over a one year period, with the first survey utilising a fixed wing UAV for image acquisition. Lucieer *et al.* (2013) also used UAV-photogrammetry, comparing multi-temporal, multi-rotor derived aerial images to monitor landslide displacements at sub-decimetre accuracies. The now widespread availability of aerial platforms and SfM packages adds the range of mapping and survey techniques available to geomorphologists. The technique is a logical choice due to the achievable survey accuracies (errors in the decimetre range) and potential to monitor geomorphological change at smaller spatial scales remotely.

3.6 Conclusions and summary

The integrated use of UAVs and SfM technologies for the acquisition of sub-decimetre resolution DSMs has been investigated. The technique is shown to be superior to a conventional total station survey in terms of resolution, time required for data acquisition, and has the additional benefit of providing ultra-high-resolution orthorectified aerial imagery. DSM spatial resolutions of 0.088 m were achieved from an approximate flight altitude of 117 m AGL whilst using a consumer-grade 18 MP digital camera. Unintentional random error on the total station dataset, vegetation and steep terrain are shown to promote vertical disagreement between the two datasets. Where vegetation is sparse, a vertical difference of 0.200 m RMSE was achieved. Overall, the technique is shown to provide exceptionally high-resolution topographic datasets and aerial imagery. The repeatability of the technique where surveys can be benchmarked or georeferenced using dGPS could offer not only unprecedented spatial resolutions, but also high temporal resolution for monitoring on-going geomorphological processes in a range of environments.

This chapter has elucidated some of the logistical and practical challenges associated with the use of this technique, and facilitated understanding of potential error margins. As a

result the methods described in this chapter are appropriate for investigating contemporary glacial environments. Given the scarcity of vegetation in proximity to receding glaciers, lower error may be permitted at other sites than observed at Cwm Idwal. This technique has subsequently been adopted for use at other field sites investigated by this thesis (Chapters 5 and 6).

Table 3.3 Comparative table of known vertical differences between small-format aerial image based topographic surveys and various validation datasets in a range of geomorphological environments

Study	Setting	Camera	Platform	Survey Altitude (m AGL)	Validation Data	Vertical Difference
Westoby <i>et al.</i> (2012)	Coastal	SLR: Model not specified	None	Ground-level	Terrestrial Laser Scanner	94% points values within +/- 1 m
Hugenholtz <i>et al.</i> (2013)	Aeolian	Olympus PEN Mini E-PM1	Fixed-wing UAV	200	RTK GPS	RMSE = 0.29 m
Fonstad <i>et al.</i> (2013)	Fluvial and bedrock	Canon A480	Helikite	10-70	LiDAR	RMSE = 1.05 m
Javernick <i>et al.</i> (2014)	Fluvial (Braided Channel)	Canon (10.1 MP): Model not specified.	Full-scale helicopter	600-800	RTK GPS	RMSE = 0.13 – 0.37 m
This study	Glacial landforms (Vegetated)	Canon EOS-M (18 MP)	Multi-rotor UAV	117 (average)	Total Station	RMSE = 0.517 m

4. Debris supply, transport and moraine development in high-mountain environments: an example from Schwarzberggletscher, Switzerland

4.1 Introduction and site specific methods

4.1.1. Chapter overview

Large 'Alpine type' lateral moraines develop following repeated reoccupation of mountain valleys by glacier ice (Röthlisberger and Schneebeli, 1979; Lukas *et al.*, 2012). In the context of past and future change, alpine lateral moraines represent important geomorphological features that contribute to our understanding of the dynamics and response of glaciers to past climatic perturbations. Alpine lateral moraines may document glacier change over hundreds of years, and in many cases millennial timescales (Kirkbride and Winkler, 2012). A range of studies have utilised these features for dating glacier advances (e.g. Röthlisberger and Schneebeli, 1979; Joerin *et al.*, 2006; Ivy-Ochs *et al.*, 2009; Schimmelpfenni *et al.*, 2013). Despite this, there are relatively few studies investigating the geomorphological and sedimentological diversity of these features (Humlum, 1978; Osborn, 1978; Boulton and Eyles, 1979; Small, 1983; Small, 1987; Lukas and Sass, 2011; Lukas *et al.*, 2013). Thus an apparent discrepancy has been argued for in relation to the widespread use of alpine moraines as geomorphological proxies for past climates, despite a deficit of studies offering specific models explaining landform development (e.g. Lukas *et al.*, 2012).

As a result, relatively few process-form models are available in the literature (e.g. Röthlisberger and Schneebeli, 1979; Lukas *et al.*, 2012). Typically, 'Alpine type' lateral moraines have been associated with passive supraglacial transport pathways and the direct deposition (dumping) of paraglacial material from a subaerial position (Humlum, 1978; Osborn, 1978; Boulton and Eyles, 1979; Small, 1983). The composite nature of these features may be demonstrated by successively overtopped crestlines and buried organic layers within moraine structure (Osborn, 1986; Reyes *et al.*, 2006). However, limited description of these features from a sedimentology perspective is at odds with their obvious utility for understanding environmental change over the Quaternary. In line

with the recommendations of recent studies (Lukas and Sass, 2011; Lukas *et al.*, 2012), here the origin and significance of moraines within a single Alpine catchment are considered.

This component of the research contributes to the research questions in section 1.6 and assesses the sedimentology and morphology of the Schwarzberggletscher lateral moraine complex in order to understand important ice-marginal processes, debris transport pathways and establish patterns of local glacier change over the Holocene within the Schwarzberg basin. In the absence of direct observation of moraine forming processes, historical maps and photographs are used to inform interpretations of moraine sedimentology. This chapter will therefore: (1) assess historical ground-level imagery and maps for recent glacier change and its role in the development of the Schwarzberggletscher lateral-frontal moraine; (2) map and glacial landforms within the Schwarzberg; (3) characterise the morphology of the lateral-frontal moraine; (4) characterise the sedimentology of the lateral-frontal moraines and provide sediment-landform associations that link moraine sedimentology to prevalent ice-marginal processes; and (5) investigate debris transport pathways through the use of clast from analysis and structural glaciological mapping. The findings will allow current conceptual models of landform development at Alpine sites to be critiqued and aid the development of an appropriate model for the Schwarzberg glacier.

4.1.2. Site specific methods

Geomorphological and sedimentological surveys were undertaken at this site using the methods detailed in Section 2.4 and Section 2.5. Survey work was undertaken in August 2013. Measurements of landform morphology and orientation were conducted in ArcGIS using the ALTI3D 2 m resolution DEM obtained from the Swiss Federal Office of Topography. The DEM was used to extract topographic profiles to determine slope angle and curvature. Raster cell values for the profiles were sampled in ArcGIS 10.2.1 and analysed in Microsoft Excel™, where basic descriptive statistics were produced (mean, maximum and minimum values) to characterise landform slope angle and profile curvature. The results are compared against the Alpine sites from Curry *et al.* (2006). Structural glaciological mapping (see Section 2.6) was conducted using a 0.5 m resolution orthophoto acquired in 2009 by the Swiss Federal Office of Topography.

4.2 Study site and historical records of glacier change

4.2.1 Overview

Schwarzberggletscher (46° 01' N; 7°56' E) is a ~3 km long alpine valley glacier located in Saastal, Switzerland (Fig. 4.1). The head of the accumulation basin represents the border with neighbouring Italy. This glacier is situated in a high-mountain setting. The prominent peak Schwarzberghorn (3609 m.a.s.l) is located at the head of the accumulation basin. The glacier flows in a NNE direction. Fluchhorn (3795 m.a.s.l) is located on the true left of Schwarzberggletscher. The south-west flank of this mountain hosts three smaller discrete bodies of glacier ice: Hangendegletscher, and two unnamed masses of ice. The glacier is currently undergoing recession. Evidence of glacier change is reviewed in this section.

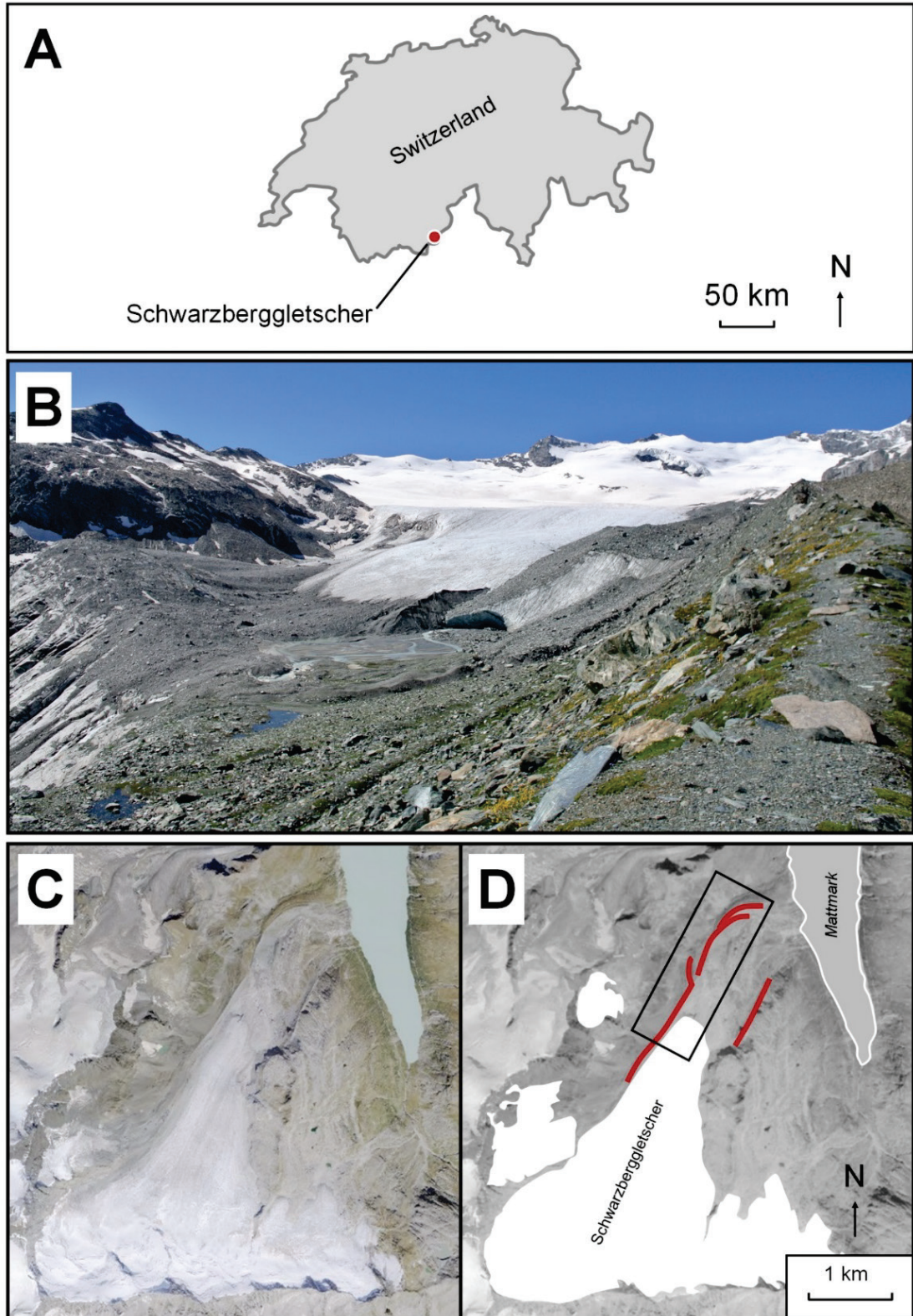


Fig. 4.1 Schwarzberggletscher. (A) The glaciers location in relation to Switzerland. (B) Ground-level image of the terminus from the left-lateral moraine in 2013. (C) An orthorectified aerial image of the glacier in 2009 from Swisstopo. (D) Location of the study site with moraine indicated by the thick red line.

4.2.2 Archive ground-level imagery

All images are taken from the ETH-Bibliothek's Image Archive (2013) and are licensed under Creative Commons. Early evidence of glacier change is presented in an illustration by M. de Meuron which depicts both a heavily crevassed Schwarzberggletscher and Allalingletscher extending into the Mattmark basin during the summer of 1822 (Fig. 4.2a). The extent of Schwarzberg appears to be somewhat unchanged in a later field sketch by Escher von der Linth dated to 18 August 1842. A further illustration by E. Lafon in 1859 (Fig. 4.2b) looking south-west from the surface of Allalingletscher shows the terminus of Schwarzberggletscher still extending into the Mattmark basin but not as extensively as documented by E.Lafon or Escher von Linth. In Otto Lütschg's 1915 photograph of the upper basin the extent of recession of the true right of the glacier is delimited, with the terminus located behind a small inset ridge of the right lateral complex (moraine R3/4; Fig. 4.2c). In this photograph the glacier-profile is irregular, with the lower snout showing a smooth but partially crevassed morphology, contrasting the heavily crevassed and topographically prominent upper profile of the glacier. This photo corresponds with a period of positive cumulative length change as recorded in the length change dataset obtained from SCNAT (2015) (section 4.2.4). It is unclear whether this is related to underlying subglacial topography or a surface bulge indicative of surge type movements. Surge type movements are rarely reported in the European Alps, however, they have been documented near-by at Ghiacciaio del Belvedere (Haeberli *et al.*, 2002) where glacier flow rapidly accelerated in 2001/2, leading to crevasse development and moraine overriding.

A ground-level image taken by an unknown photographer dated *c.* 1919 shows the lower terminus since the 1859 E. Lafon illustration (Fig. 4.2d). Again, the rate of recession of the true-right of the glacier appears to be more extensive, in comparison to the left. The true left of the glacier abuts the inner-proximal ridge of the lower-lateral complex, and an extensive supraglacial debris cover is readily observable in the photography. An additional image dated to October 4, 1921 by an unknown photographer displays Hangendgletscher as a detached ice-mass within the Schwarzberg catchment (Figure 4.3e). Figure 4.1f is dated to 1922. This photograph documents the position of Schwarzberggletscher as it abuts its left-lateral moraine. Unfortunately snow-cover disguises the glaciers supraglacial debris coverage at this date.

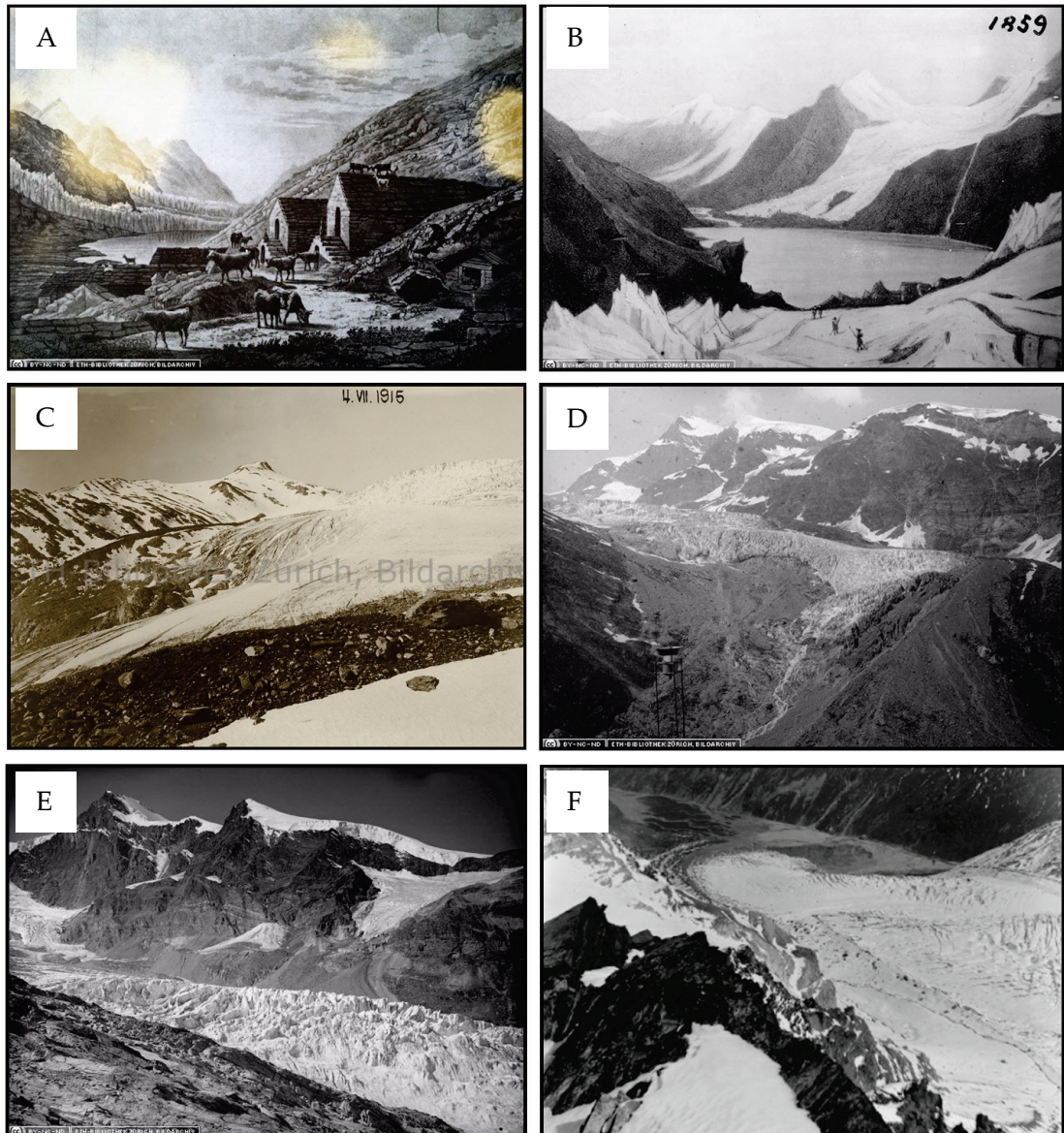


Fig. 4.2 Historical Illustrations and photographs of Schwarzberggletscher. (A) An illustration by M. de Meuron dated to 1822 looking north along Saastal with Schwarzberggletscher in the middle distance, and Allalingletscher in the far distance. (B) An illustration by E.Lafon dated to 1859, looking south-west towards the margin of Schwarzberg from the surface of Allalingletscher. (C) An image of the upper terminus by Otto Lütschg dated to 1915. (D) A 1919 image of the glacier terminus. (E) An image of Schwarzberggletscher and Hangendgletscher dated to October 4, 1921. (F) An image of Schwarzberggletscher abutting the left-lateral moraine in 1922. All images are taken from the ETH-Bibliothek's Image Archive (2013) and are licensed under Creative Commons.

4.2.3 Historical maps

Three historical maps were reviewed to provide context to the recent development and evolution of moraines within the Schwarzberg catchment (Fig. 4.3). The oldest reviewed here is the Dufour series published in 1863 (sheet 23) at a scale of 1:100 000. Here, the terminus displays a bifurcating morphology, with the true-left of the glacier extending into the Mattmarksee basin (*c.* 2200 m; Fig. 4.3a). The second reviewed is the Siegfried map (sheet 534) published in 1924 at a scale of 1:50 000. Topography is represented by 30 m contours, with the elevation of the glacier terminus identified at *c.* 2350 m (Fig. 4.3b). Considerable recession is recognisable between the two maps (*c.* 600 m), however in the Siegfried map, the glacier terminus is depicted to form a single tongue, opposed to the bifurcated morphology displayed in the Dufour map. In both maps, Hangendgletscher is delimited as a detached body of ice located on the true left of the Schwarzberg basin. The third map reviewed is the 1968 National Map of Switzerland (sheet 268) which was originally published at a scale of 1:50 000 (Fig. 4.3c). In this map, a detached linear body of debris covered ice is seen abutting the proximal slope of the lower lateral moraine complex. This ice is located in an altitudinal range *c.* 2400 to 2500 m elevation, and appears to be dead glacier-ice, which became detached as the glacier receded up a steep bedrock step. Significant anthropogenic alteration of the moraine is also identified, and appears to be related to the development of the Mattmark and Schwarzbergalp access roads. Specifically the true-left lower lateral-complex is extensively excavated (red circle in Fig. 4.3C).

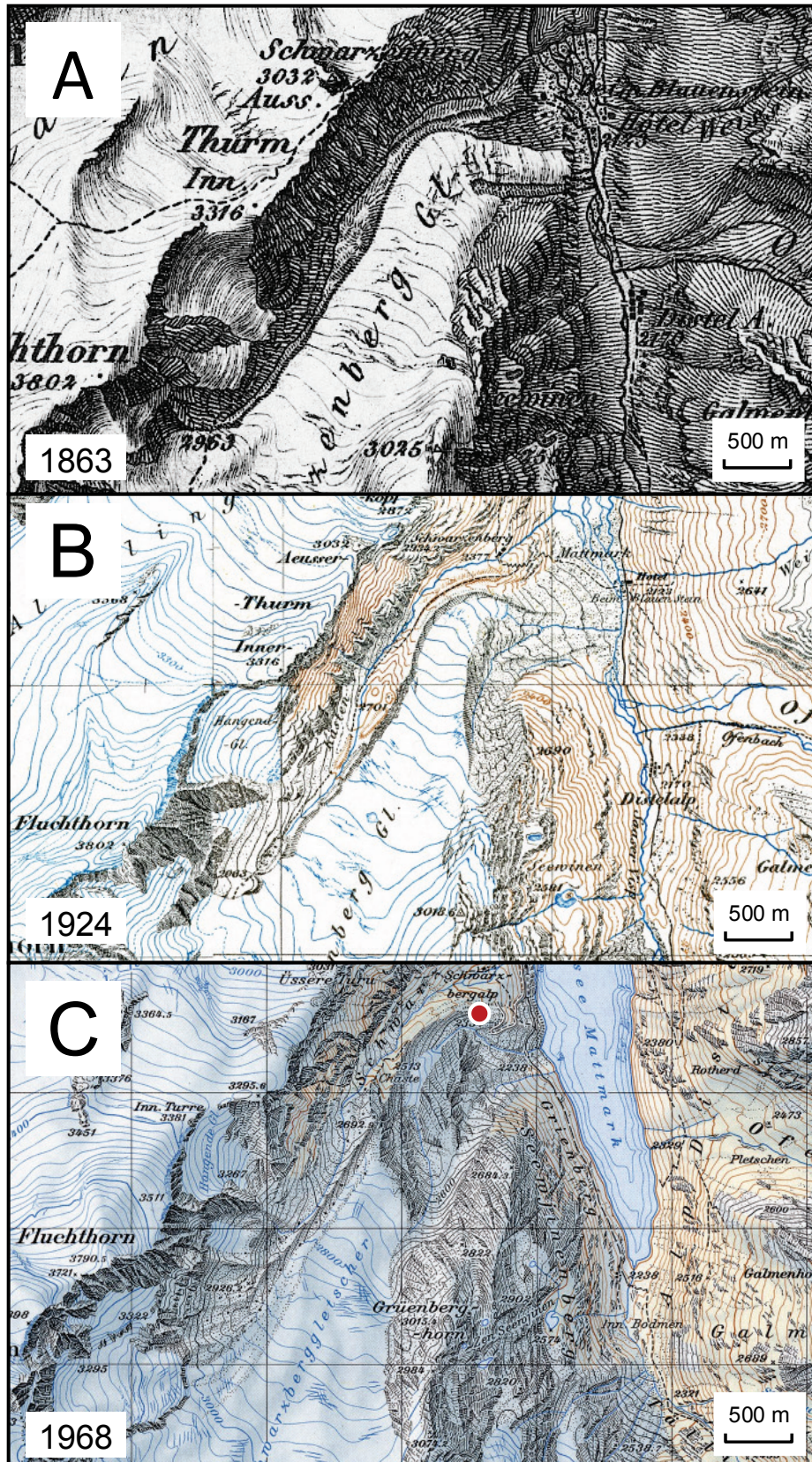


Fig. 4.3 Historical maps of Schwarzberggletscher. (A) The Dufour map (1863). (B) The Siegfried map (1924). (C) National map of Switzerland (1968). The red circle shows the excavated area of moraine following the construction of the Mattmark dam.

4.2.4 Glacier length measurements

As Schwarzberggletscher is part of the Swiss Glacier Monitoring Network. A record of length change for the glacier is available from SCNAT (2015) (Fig. 4.4). Since monitoring began the glacier has predominantly receded with a total cumulative length change of -649 m (1880-2013; Fig. 4.4). The overall trend of recession is punctuated by a series of advances. The oldest records have the lowest temporal resolution, with changes of +150 m between 1880-1909 (Fig. 4.4), followed by a period of recession between 1909 and 1915 (-140 m). Over a 6 year period, between 1918 and 1924, the glacier advanced by a total of 132 m. The onset of this advance is potentially delimited in ground-level photography (Fig. 4.2c), although no data for the terminus position is available for the years 1916-17. An 8 year period, between 1976 and 1984, saw the glacier terminus advance by 79 m. The advance of Schwarzberggletscher in the late 1970s and early 1980s appears to have occurred analogously with a range of monitored glaciers across the Swiss Alps (Zemp *et al.*, 2006). The last recorded minor advance of Schwarzberggletscher occurred between 1989 and 1991, where the recorded glacier length change was +14 m. In recent decades the glacier has continued receding, with the average annual rate of recession of 13 m per year for the period between 1991 and 2013.

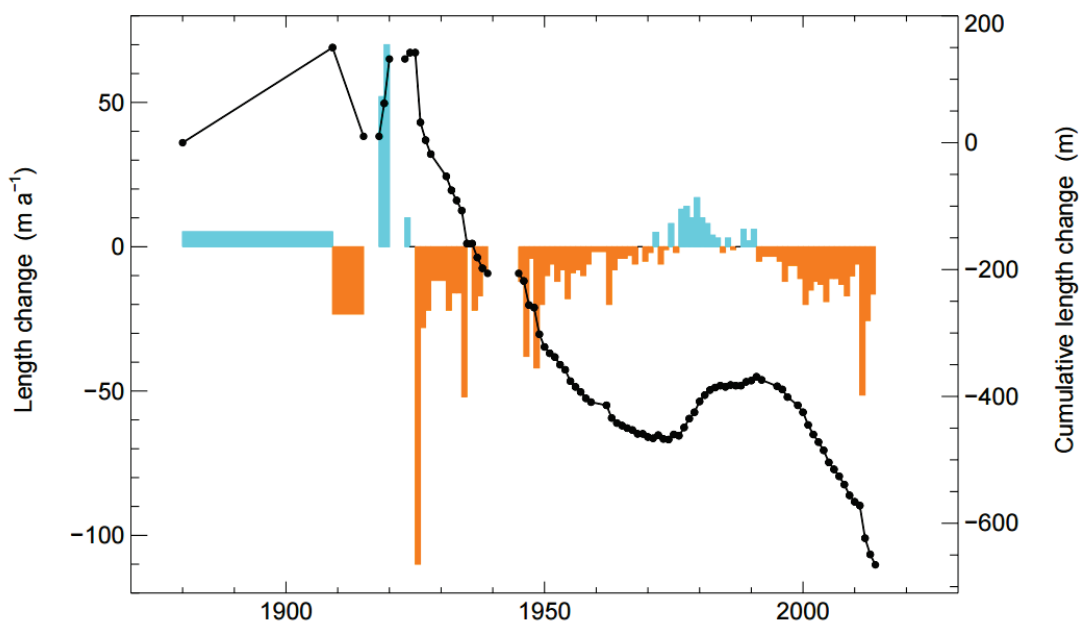


Fig. 4.4 Length change measurements of Schwarzberggletscher from 1880 to 2014 from SCNAT (2015).

4.3 Results

4.3.1 Moraine descriptions and reference codes

Here, the morphology of the moraines are described. The moraine codes presented in this section relate to Fig. 4.5. Ground level photography from 2013 is presented in Fig. 4.6.

Two major sections of the left-lateral frontal moraine are recognised: (1) the upper left-lateral complex; and (2) the lower left-lateral complex. The lateral sections are dissected by a bedrock step which runs approximately transverse glacier flow (*c.* 160/340°). The upper lateral complex exhibits an angular profile typical of 'Alpine' type lateral moraines. The upper lateral-ridge crestline (M1) is oriented at 032-037/212-217°. The main upper lateral ridge (M1) can be traced ~1.2 km up on the true left of the glacier margin where it eventually becomes indistinguishable from supraglacial and valley side debris units. Outside the main upper lateral ridge a ~180 m long ridge located between coordinates 638548/97522 and 638478/97366 runs contiguous to valley-side debris with a crest orientation of 25/205° (M2). An additional four moraine ridges are located NNW of M1 (Fig. 4.6.; M3–M6). In places, some of the ridges are less topographically defined and form a series of benches on the moraine distal slope. Unlike the main upper lateral ridge, the crestline of features M3-M6 are oriented between 011/191° and 171/351° and appear to delimit the extent of a series of glacier advances prior to the deposition of the larger main lateral-ridge, which would have served as an obstruction to more recent advance(s) of Schwarzberggletscher. Several inset moraine ridges on the ice-proximal slope of the main upper lateral ridge and current proglacial area are identified. Two of these features (M7 and M8) can be traced to the current glacier margin. The upper ridge (M7) runs a total length of ~200 m approximately parallel to the direction of ice-flow and the ridge crest of the main upper moraine ridge (31/211°).

A lower ridge (M8) is curvilinear and extends as a bench of sediment which is located on the ice-proximal slope of the main upper lateral ridge. This ridge extends into a more topographically distinct ridge where it attains ~2-3 metres prominence above the surrounding proglacial area. Unique to the lower ridge is a 'notch' (located at 6387545/97547). This 'notch' also corresponds to changes in surface sedimentology with up-valley sections characterised by a surface drape of angular gravel devoid of fine material (Fig. 4.6c), and lower sections by gravelly sand (further details given in section

4.3.3). A further curvilinear inset ridge (M9; Grid coordinate: 638798/97723) is located on the ice-proximal slope of the lateral complex. This feature is identified down-valley of M8.

The lower lateral complex (M10-M18) is characterised by a large curvilinear moraine rampart which reaches ~1.3 km in length and ~300 m in width. The up valley sections of the ridge are characterised by an angular morphology, with a single 'sharp' crestline (M10). At 450 m along the crestline the moraine anastomoses into four main ridges. The distal-most ridge (M17) becomes topographically indistinct down-moraine. Smaller benches of sediment superimposed onto the proximal slope are also identified (M15 and M16). These ridges appear to be oriented parallel to the direction of former ice-flow and range from 045/225 to 68/248°. Outside the distal slope of the lower lateral-rampart, two additional <5 m high moraine ridges are identified (M17 and M18). Further down-valley, several additional moraine features can be identified, however they appear to be extensively modified as a result of the construction of the Mattmarksee dam and the Schwarzbergalp access roads during the 1960s (See Grech and Semenenok, 1969). Due to the extent of the disturbance to the sedimentology and morphology of these features, they are not investigated in this study.

On the right side of the glacier several features can also be identified. A linear lateral ridge runs parallel to ice-flow. In places, the lateral contiguity of the landform is interrupted by protruding bedrock, which separates the upper and lower sections of the ice-proximal moraine slope (R2). The proximal slopes of R2 are ice-cored. Remobilisation of ice-proximal sediments was observed in the field.

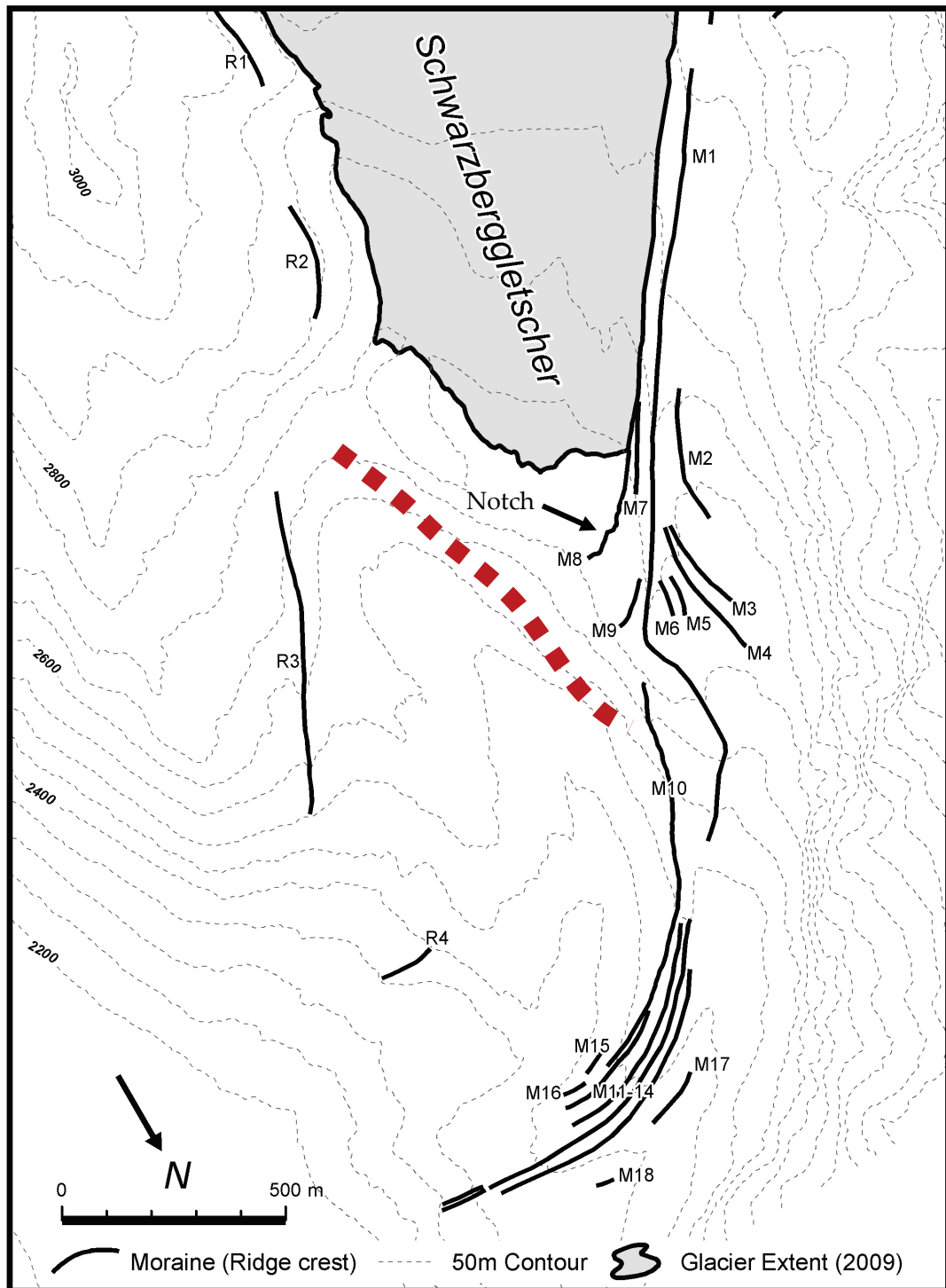


Fig. 4.5 Moraine locations and reference codes used within the text. Red dashed line is the bedrock step.

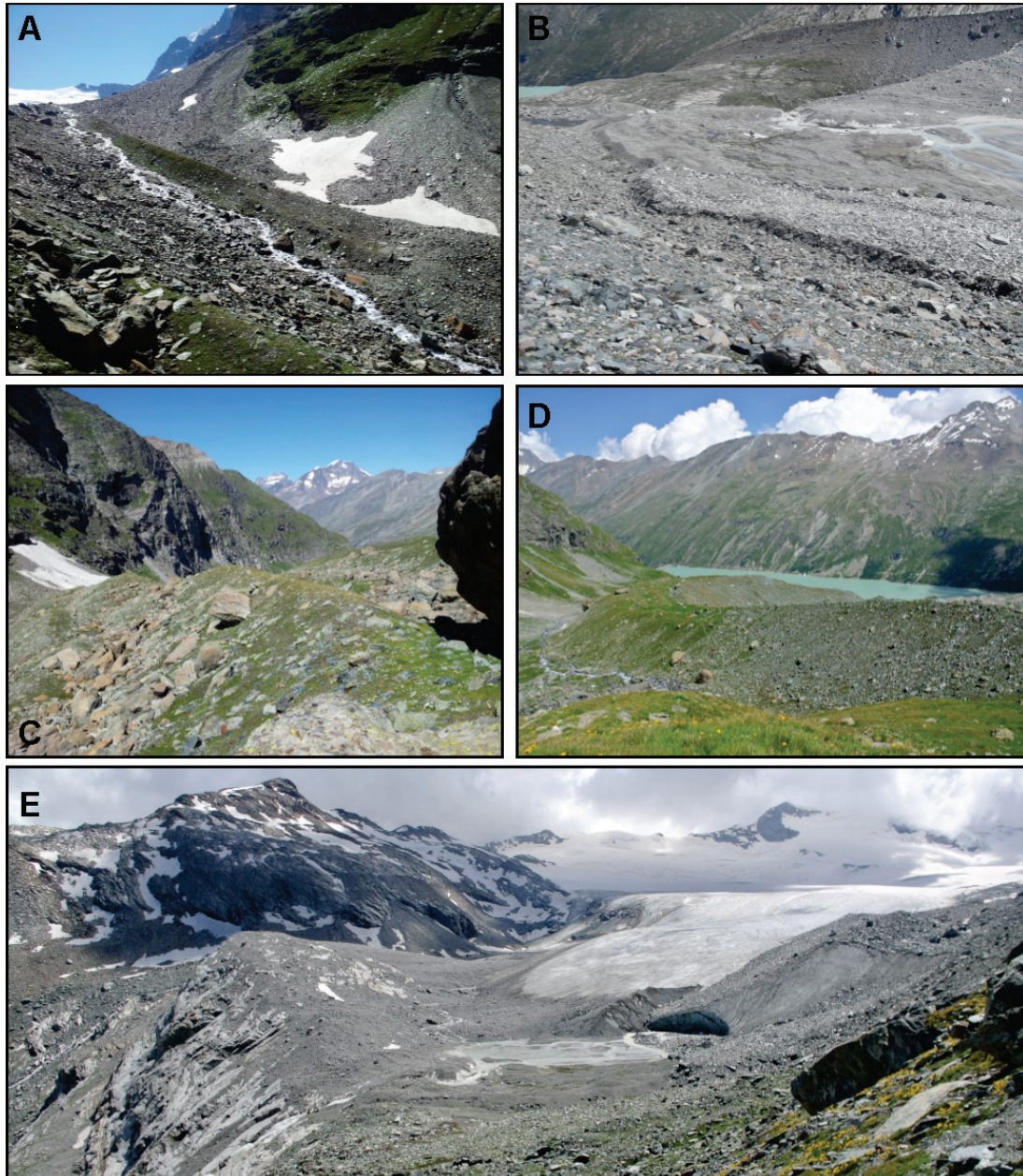


Fig. 4.6 Ground-level imagery of the lateral moraines of Schwarzberggletscher. (A) A single (older) linear ridge (M2) outside the upper-lateral complex and partially coalescing valley-side debris fans. (B) A series of 4 ridges located on the distal slope of the upper-lateral complex (M3-6). (C) Inset lateral-frontal ridges developed close to the current terminus (M7 and M8). (D) The distal slope of the lower left-lateral moraine complex which anastomoses into multiple distinct ridges (M10-M14). (E) An overview of the glacial terminus in August 2013. Note the extensive supraglacial debris cover to the right of the image. In contrast, a thin valley-side drape of sediment which constitutes the right lateral moraine of Schwarzberggletscher is visible to left of the photo. Volumetrically, these moraines show a marked asymmetry to the left-lateral moraines complex (to the right of the image).

4.3.2 Proximal-slope morphometry

Five exemplar profiles were assessed for their morphology (Fig. 4.7; Table 4.1). Fluvial incision of the proximal slopes in the vicinity of T₁ and T₂ appears to be limited. Slopes in the vicinity of T₃ show the greatest degree of gully incision, but have an overall low gully density index (1 is equal to <10 gullies per kilometre; e.g. Curry *et al.*, 2006). Unlike transects T₁, T₂ and T₃, patches of grassy vegetation can be found on the proximal slopes of T₄ and T₅. Mean profile curvature values for the ice-proximal sections were calculated from raster cells located along each of the transects (T₁ to T₅). T₁ and T₂ are 0.6 ($n = 26$) and 1.0 ($n = 76$) respectively highlighting an overall concave slope morphology with superimposed convex elements. Profiles T₃ ($c = -0.6$; $n = 89$) and T₄ ($c = -1.3$; $n = 93$) exhibit somewhat 'straight' morphologies with an absence of both convex and concave elements. T₅ has the lowest mean curvature ($c = -1.5$; $n = 68$) related to convex curvature as a result of several undulations along the slope profile.

Maximum slope angle values for the ice-proximal sections were calculated from raster cells located along each of the transects (T₁ to T₅). The maximum DEM slope angle along each transects vary from 41.7° to 53.6°. The maximum DEM slope angle is attained by T₃. There is no tendency for the maximum DEM slope angle to vary with respect to distance down-valley. The mean slope angles for T₁, T₃, T₄ and T₅ vary between 28.2° and 31.7°. T₂ has the lowest mean slope angle at 18.6°. T₂ is located immediately adjacent to the glacier terminus. Unlike T₃, T₄ and T₅, whose proximal slopes are truncated at their base by a proglacial stream (Schwarzbergbach), the proximal slope of T₂ extends as a contiguous gently sloping unit onto a relatively level outwash plain. The proximal slope height varies between 26 and 105 m. A summary of the Schwarzberggletscher ice-proximal moraine slopes are presented in Table 4.1 alongside examples from other Alpine moraines from Curry *et al.* (2006).

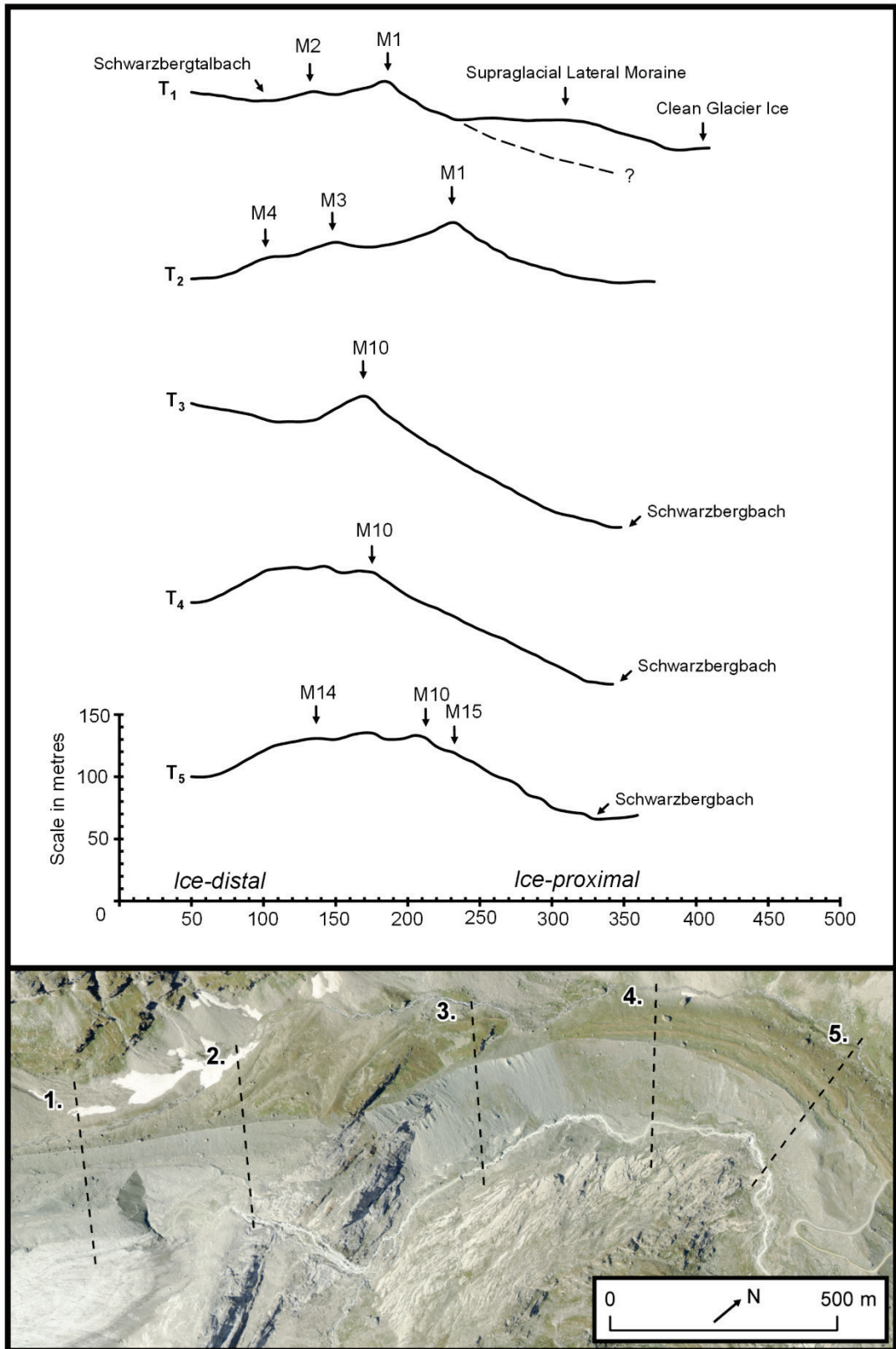


Fig. 4.7 Five characteristic topographic profiles from the lateral moraine complex. T₁ is adjacent to the current glacier terminus, and T₅ is the furthest down moraine.

Table 4.1 Summary of proximal slope characteristics in relation to other alpine sites.

Profile	Average gradient	Max gradient	Crest Elevation (m)	Slope height (m)	Vegetated	Gully Index ^a	Topographic Setting
Schwarzberggletscher							
T ₁	31°	50°	2761	26	No	1	combination
T ₂	19°	45°	2710	58	No		
T ₃	32°	54°	2480	91	No		
T ₄	27°	42°	2532	105	Partially		
T ₅	28°	51°	2439	67	Partially		
Tsidjoure Nouve ^b							
--	30°	--	2300 ^c	50 ^d	--	2	valley floor
Findelgletscher ^b							
--	34°	--	2550 ^c	120 ^d	--	3	combination
Bas Glacier d'Arolla ^b							
--	31°	--	2150 ^c	150 ^d	--	3	valley side
Feegletscher North (s) ^b							
--	22°	--	2125 ^c	80 ^d	--	1	combination
Glacier du Mont Mine ^b							
--	32°	--	2050 ^c	180 ^d	--	3	valley floor

^a Gully index from Curry *et al.* (2006). 1 = <10 gullies per km; 2 = 10-40 gullies per km; 3 = >40 gullies per km;

^b Data from Curry *et al.* (2006);

^c Average crest elevation;

^d Maximum slope height

4.3.3 Sedimentology

4.3.3.1 Lithofacies descriptions

Three major sedimentary facies were documented within the Schwarzbergletscher left-lateral moraine. These include diamicton (three types), angular gravel, and gravelly sand. Descriptions of the three major facies are provided below. Section logs for exemplar moraine lithofacies are provided in Fig. 4.8. Summaries for each facies are provided in Tables 4.2-4.4. Each sample site is assigned a sample ID.

Angular Gravel: This facies forms a uniformly distributed drape across the left-hand side of the Schwarzbergletscher proglacial area and extends onto the lower proximal slope of the lateral moraine. Concentrated deposits of angular gravel also form a small inset ridge superimposed on the left lateral moraine (M8). The angular gravel drape has an RA index of 100 %, with 33% clasts falling within the very angular roundness category. The C_{40} value of the sample is 92 %, with the most frequent clast shape classes (after Sneed and Folk, 1958) are defined as 'platy' and 'bladed' (comprising 26 and 28 % of the sample, respectively). Angular gravel is also abundantly found on the surface of Schwarzbergletscher, with debris concentrated on the left of the glacier to form an extensive supraglacial lateral moraine (Fig. 4.11). The character of supraglacial angular gravel is much the same as that found in front of the glacier terminus. With the exception of sample SCH-26 (RA = 90 %), clasts are exclusively angular and very angular (RA = 100 %; $n = 150$). Sampled clasts have high C_{40} indices typically ranging between 90 and 96% and exhibit a modal 'very bladed' shape category. The clast form of SCH-26 is distinguishable from other supraglacial samples and exhibits a lower C_{40} index of 72 % with a 'bladed' modal shape category.

Gravelly Sand: A summary sedimentary log for exposures at SCH-02 and SCH-05 can be found in Fig. 4.9. This lithofacies was found to occur within inset ridges on the proximal slope of the upper lateral moraine complex (as displayed within Fig. 4.8). At SCH-02, gravelly sand is crudely stratified and has an apparent dip of 30°. The sandy matrix is predominately composed of very coarse sand (51%), and classified as poorly sorted. Facies of gravelly sand are interspersed with lenses of fine material. The matrix visibly fines at the base of the assessed exposure. Clasts at SCH-02 are mostly sub-angular (74%) and contain low quantities of angular material (% RA=24). Clasts exhibit bladed (42%)

and platy (20%) morphologies and an overall C_{40} index of 58. 18% of sampled clasts were found to be striated. Gravelly sand at SCH-05 is capped by a ~10 cm thick drape of angular gravel. Similar to SCH-02, the matrix is predominantly composed of very coarse sand (40%; Fig. 4.10). At SCH-05, the characteristics of sampled clasts show a strong similarity to SCH-02, 20% of which fall within the RA category and 62 % with S/L axial ratios of ≤ 0.4 (C_{40}). Here, clasts are 30 % striated and also have a modal 'bladed' (38%) shape category.

Diamicton: Fifteen exposures in proximity to the crestline of the left-lateral moraine complex were assessed (Table 4.3). Exposures were accessed from the crestline of the proximal slope of the lateral complex. At this position, exposures are uniformly composed of a clast rich intermediate diamicton. The majority of clasts fall within the sub-angular and angular categories, with the percentage RA ranging between 50 and 82%. The percentage of striated clasts within samples are not consistent between sites. Samples in the upper section of the moraine complex, in closer proximity to the current glacier terminus are devoid of striated material. In contrast, striated material is found on the lower lateral moraine complex approximately below 2524 m elevation. Below this altitude, between 4 and 30% of sampled clasts were found to be striated. The C_{40} indices from clast samples range from 46 % to 80 %.

The diamicton is matrix supported and predominantly composed of a mix of sand and silt. The proportions (as % volume) are relatively consistent across samples. These range from 44-57 % for the sand component (< 2000 to $63 \mu\text{m}$) and 40-52 % for the silt component (< 63 to $2 \mu\text{m}$) (Fig. 4.11). The percentage volume clay within the matrix of proximal-crestline samples was found to vary between 3 to 4 %. The mean descriptive class for the samples are very coarse silt ($n = 9$) and very fine sand ($n = 7$). All matrix samples are classified as very poorly sorted and have geometric sorting coefficients ranging from 4.7 to 7.1 σ . Samples are polymodal ($n = 16$) with geometric means ranging from 43 to 96 μm and modal peaks ranging from 169 to 186 μm . With the exemption of SCH-35 and SCH-44 (upper/lower) all lithofacies appear to be massive. The structure of SCH-35 and SCH-44 are shown in Fig. 4.9. The upper and lower diamicton facies of SCH-44 are dissected by a palaeosol. Similar to other sample locations, a ~1m excavation at SCH-35 is characterised by a clast rich intermediate diamicton, however the matrix was found to be

interspersed with two bands of medium silt. The silt is tri-modal and symmetrically distributed with a modal particle size of 14 μm .

A further eight diamicton exposures were investigated on the distal ridges of the lower-left lateral moraine (Table 4.4). Shallow exposures (<1 m) exposed a single lithofacies of massive clast rich diamicton. At SCH-37 and SCH-39 the quantity of sand within the matrix is marginally higher (66% and 68%), and therefore distinguishes the diamicton within the investigated facies as 'sandy' (Fig. 4.11). All assessed exposures on the outer ridges are massively structured. The modal roundness category for all samples is angular. The proportion of clasts falling within the RA category varies between 56 and 58 %. Six of the samples contain low proportions of striated clasts (0-8%). In contrast, samples SCH-36 and SCH-34 have anomalously high proportions of striated material (16 and 18% respectively).

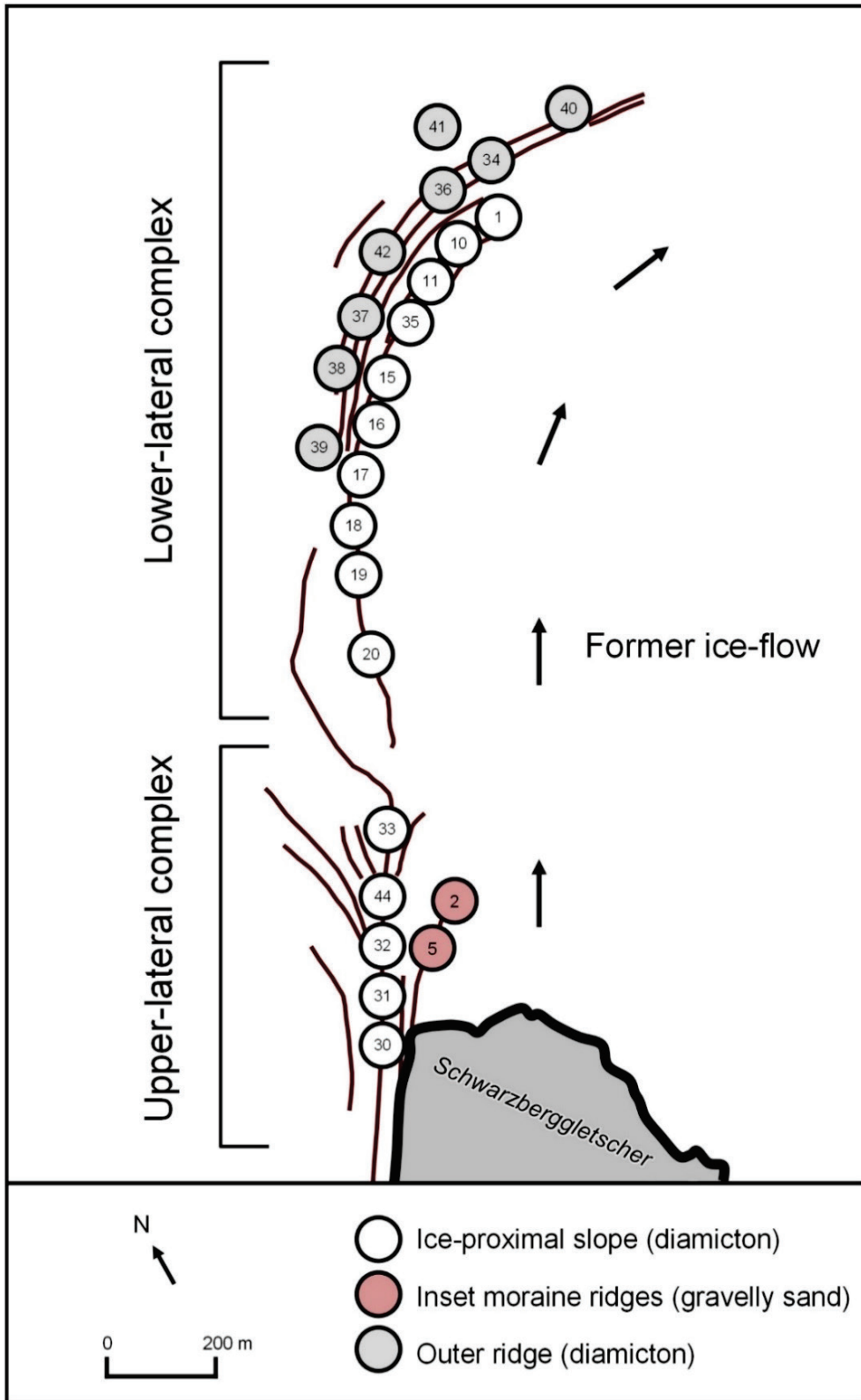


Fig. 4.8 Sediment sampling locations

A Inset ridge

B lateral-frontal moraine (ice-proximal face)

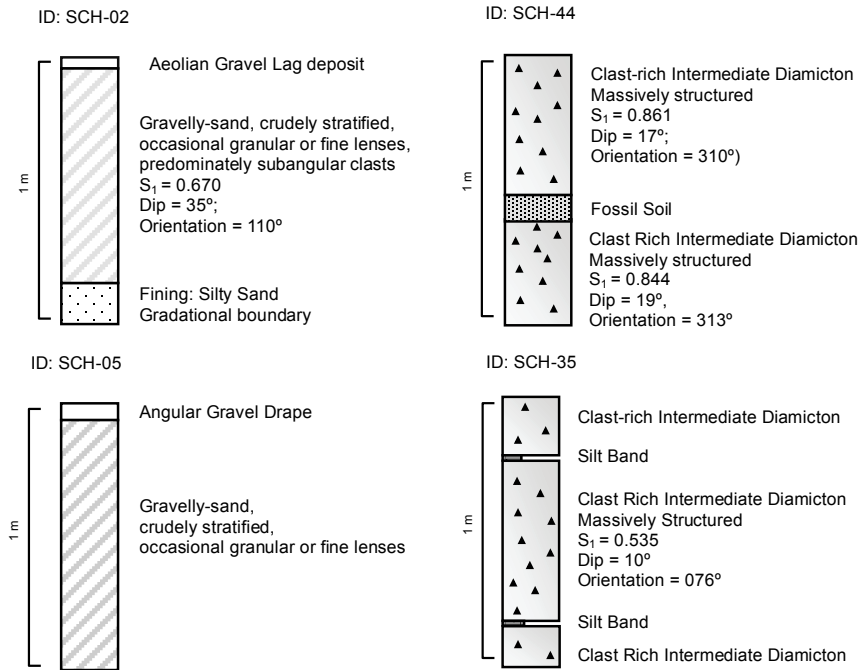


Fig. 4.9 Exemplar sedimentary logs. (a) Gravelly sand lithofacies SCH-02 and SCH-05 (b) diamicton sedimentary exposures. SCH-35 and SCH-44.

A



B



Fig. 4.10 Ground-level photography displaying the location of angular gravel surface lithofacies. (a) Angular gravel forming the supraglacial lateral moraine on the true left of Schwarzberggletscher and a drape of sediment in front of the receding glacier terminus. (b) Close up of the angular gravel lithofacies on the glacier surface with the author for scale. Note the abundance of angular slabby and elongate clasts.

Table 4.2 Summary table of gravel lithofacies.

ID	Location	Height (m)*	Character	% RA	% C ₄₀	% S	Matrix:%		
							Sand	Silt	Clay
SCH-25	638710 97471	2677	Coarse**	100	92	0	--	--	--
SCH-26	638466 97037	2767	Coarse**	90	72	0	--	--	--
SCH-27	638424 96950	2777	Coarse**	100	90	0	--	--	--
SCH-28	638747 96891	2745	Coarse**	100	92	0	--	--	--
SCH-29	638657 97221	2715	Coarse**	100	96	0	--	--	--
SCH-02	638779 97570	2664.5	Gravelly sand	24	58	18	96	4	0
SCH-05	638744 97551	2671.5	Gravelly sand	10	62	30	96	4	0

* Heights derived from the Swisstopo Alti^{3D} DEM.

** Supraglacial samples

Table 4.3 Summary table of ice-proximal diamicton exposures

ID	Location	Height (m)*	Notes	% RA	% C ₄₀	% S	Matrix: %		
							Sand	Silt	Clay
SCH-30	638560 97416	2747	Massive	70	52	0	55	42	3
SCH-31	638598 97479	2735	Massive	70	70	0	49	48	3
SCH-32	638671 97604	2721	Massive	70	74	0	50	47	3
SCH-44-U	638689 97631	2718	Palaeosol	68	66	0	51	46	3
SCH-44-L	638689 97631	2717	Palaeosol	72	58	0	44	52	4
SCH-33	638766 97748	2700	Massive	72	62	0	52	45	3
SCH-20	638899 98041	2571	Massive	64	52	0	50	47	3
SCH-19	638968 98200	2533	Massive	56	60	0	55	43	3
SCH-18	638990 98247	2524	Massive	70	46	4	57	40	3
SCH-17	639022 98332	2509	Massive	82	52	4	50	47	3
SCH-16	639103 98412	2489	Massive	64	68	12	57	41	3
SCH-15	639179 98490	2477	Massive	50	56	16	45	52	3
SCH-35	639284 98546	2452	Silt bands	60	60	30	45	51	4
SCH-11	639343 98591	2450	Massive	64	54	16	44	51	4
SCH-10	639375 98605	2444	Massive	72	80	14	49	48	3
SCH-01	639476 98616	2432	Massive	56	58	16	44	52	4

* Heights derived from the Swisstopo Alti^{3D} DEM.

Table 4.4 Summary table of diamicton samples obtained from the various outer ridges of the lower-lateral complex.

Sample ID	Location	Height (m)*	% RA	% C40	% S	Matrix:%		
						Sand	Silt	Clay
SCH-39	639027 98389	2499	68	72	0	66	31	2
SCH-38	639109 98511	2480	66	64	8	51	47	3
SCH-37	639188 98577	2467	68	58	6	68	30	2
SCH-42	639287 98656	2451	62	66	0	44	53	2
SCH-36	639436 98690	2428	66	62	16	46	50	4
SCH-34	639526 98695	2413	56	66	18	67	30	2
SCH-40	639707 98707	2372	62	44	6	47	50	3
SCH-41	639486 98806	2383	58	60	0	63	35	2

* Heights derived from the Swisstopo Alti^{3D} DEM.

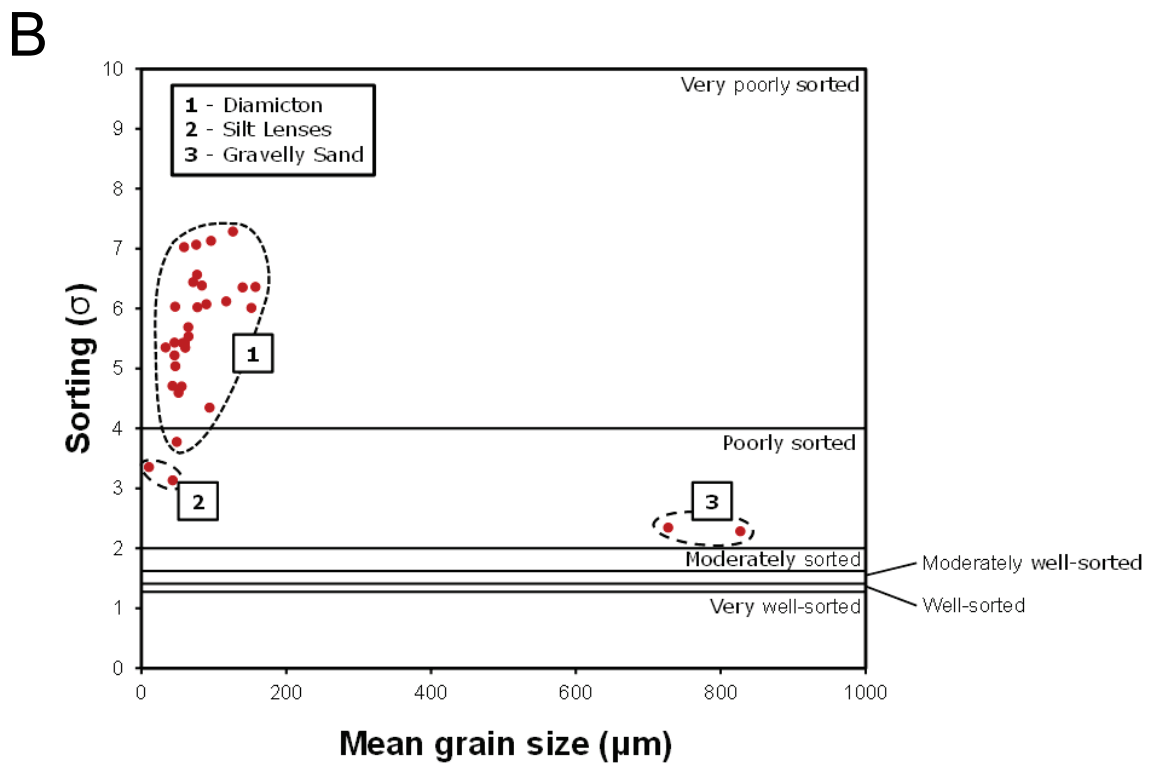
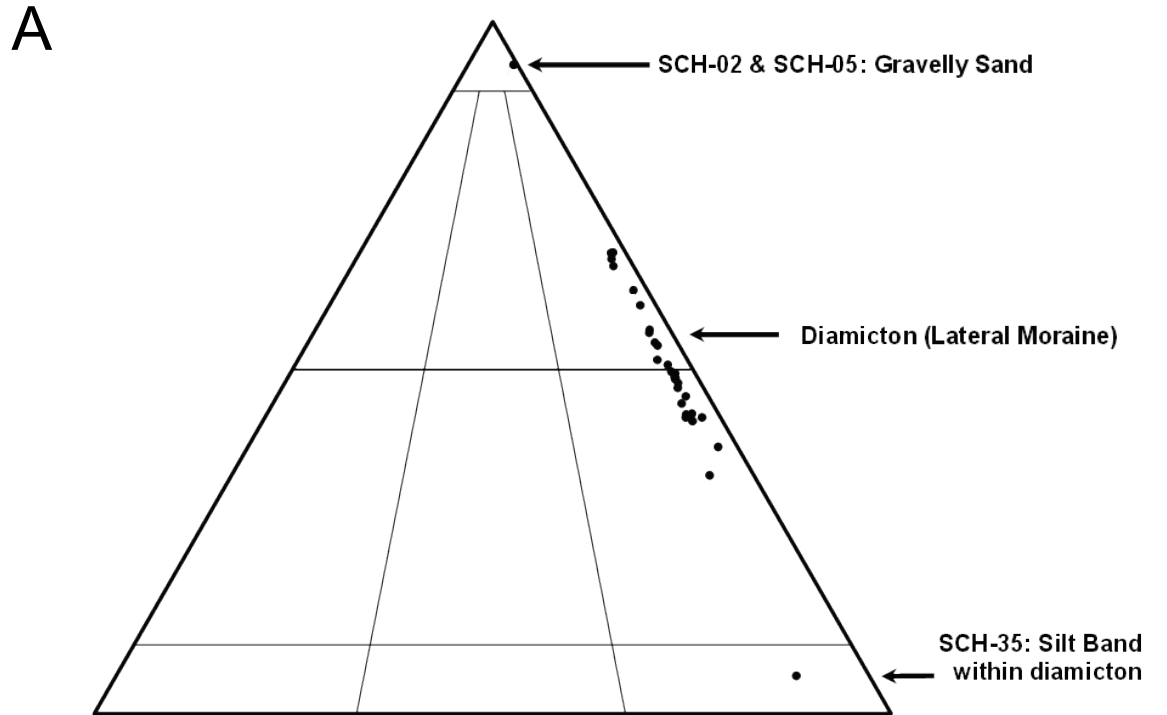


Fig. 4.11 Further visualisation of <2mm fraction of glacial sediment sampled at Schwarzberggletscher. (a) A ternary diagram showing the grain-size distribution of moraine samples. (b) Mean grain size plotted against the sorting coefficient for each sample.

4.3.3.2 *Clast macrofabrics*

The clast fabric characteristics for the inner proximal exposures are presented in Table 4.5 and Fig. 4.12. Clast fabrics show a moderate to strong preferred clast orientation ($S_1 = 0.861-0.535$). Samples taken in proximity to the current glacier terminus exhibit the strongest clast fabrics (e.g. SCH-44U/L, SCH-20, SCH-18) with S_1 values ranging between 0.795 and 0.861. Macrofabrics at these sites show a narrow range in terms of the orientation ($297.9-313.7^\circ$) and dip ($16.9-18.9^\circ$) of the principle eigenvector (V_1). The V_1 orientation (308.7°) and dip (11.1°) of SCH-16 is comparable to these samples, however the fabric lacks strength ($S_1 = 0.582$). The secondary eigenvector at SCH-16 appears to be broadly oriented down-valley and approximately parallel to the moraine crestline (41.8°). Macrofabric data obtained from the inset ridge (SCH-02; M8 in Fig. 4.4) is distinct from samples taken on the main lateral complex. Here, the preferred orientation and dip of clastic material is moderately consistent ($S_1 = 0.670$), however the principle eigenvector is oriented approximately transverse to former ice-flow ($V_1 = 109.5^\circ$) and dips towards the left-lateral complex at 34.5° . When fabric eigenvalues (S_1 and S_3) are displayed on a bivariate plot (Fig. 4.13), samples fall within a range of known environmental envelopes, as defined in Dowdeswell and Sharp (1986). SCH-44U, SCH-44L, and SCH-18 fall within the 'melt-out till' process field. SCH-10 and SCH-20 fall within the 'undeformed logdment till' process field. Other samples overlap with a range of predefined depositional settings (Fig. 4.13).

Table 4.5 Eigenvalues and vectors for 9 samples taken from the inner ice-proximal slopes of Schwarzbjerggletscher left-lateral moraine. Samples ordered by distance from the current glacier margin.

Sample	Eigenvalues	Eigenvectors	Dip	Moraine Orientation ^a	I ^b	E ^c
SCH-44-Upper	S ₁ : 0.861	V ₁ : 310.5	16.9	032/212	0.040	0.669
	S ₂ : 0.104	V ₂ : 219.5	3			
	S ₃ : 0.035	V ₃ : 119.8	72.8			
SCH-44-Lower	S ₁ : 0.844	V ₁ : 313.7	18.9	032/212	0.046	0.673
	S ₂ : 0.118	V ₂ : 223.1	1.8			
	S ₃ : 0.039	V ₃ : 127.7	71.1			
SCH-20	S ₁ : 0.689	V ₁ : 310.2	18.6	020/200	0.059	0.850
	S ₂ : 0.271	V ₂ : 043.4	9.5			
	S ₃ : 0.041	V ₃ : 159.1	69			
SCH-18	S ₁ : 0.795	V ₁ : 297.9	18.5	021/201	0.029	0.874
	S ₂ : 0.183	V ₂ : 028.6	2			
	S ₃ : 0.023	V ₃ : 124.6	71.3			
SCH-16	S ₁ : 0.582	V ₁ : 308.7	11.1	044/224	0.141	0.756
	S ₂ : 0.336	V ₂ : 041.8	15.4			
	S ₃ : 0.082	V ₃ : 184.3	70.8			
SCH-35	S ₁ : 0.535	V ₁ : 076.1	10.1	060/240	0.139	0.810
	S ₂ : 0.391	V ₂ : 170.3	22.3			
	S ₃ : 0.074	V ₃ : 323.3	65.3			
SCH-11	S ₁ : 0.529	V ₁ : 315.5	27.9	070/250	0.323	0.431
	S ₂ : 0.300	V ₂ : 060.0	25.2			
	S ₃ : 0.171	V ₃ : 185.2	50.7			
SCH-10	S ₁ : 0.728	V ₁ : 330.7	29.4	070/250	0.131	0.461
	S ₂ : 0.177	V ₂ : 071.5	18.4			
	S ₃ : 0.095	V ₃ : 189.1	54.3			
SCH-01	S ₁ : 0.541	V ₁ : 028.5	11.8	093/273	0.221	0.647
	S ₂ : 0.339	V ₂ : 121.1	12.6			
	S ₃ : 0.120	V ₃ : 256.6	72.7			

^a Observations derived from Swisstopo aerial imagery and elevation datasets.

^b Isotropy index ($I = S_3/S_1$)

^c Elongation index ($E = 1 - (S_2/S_1)$)

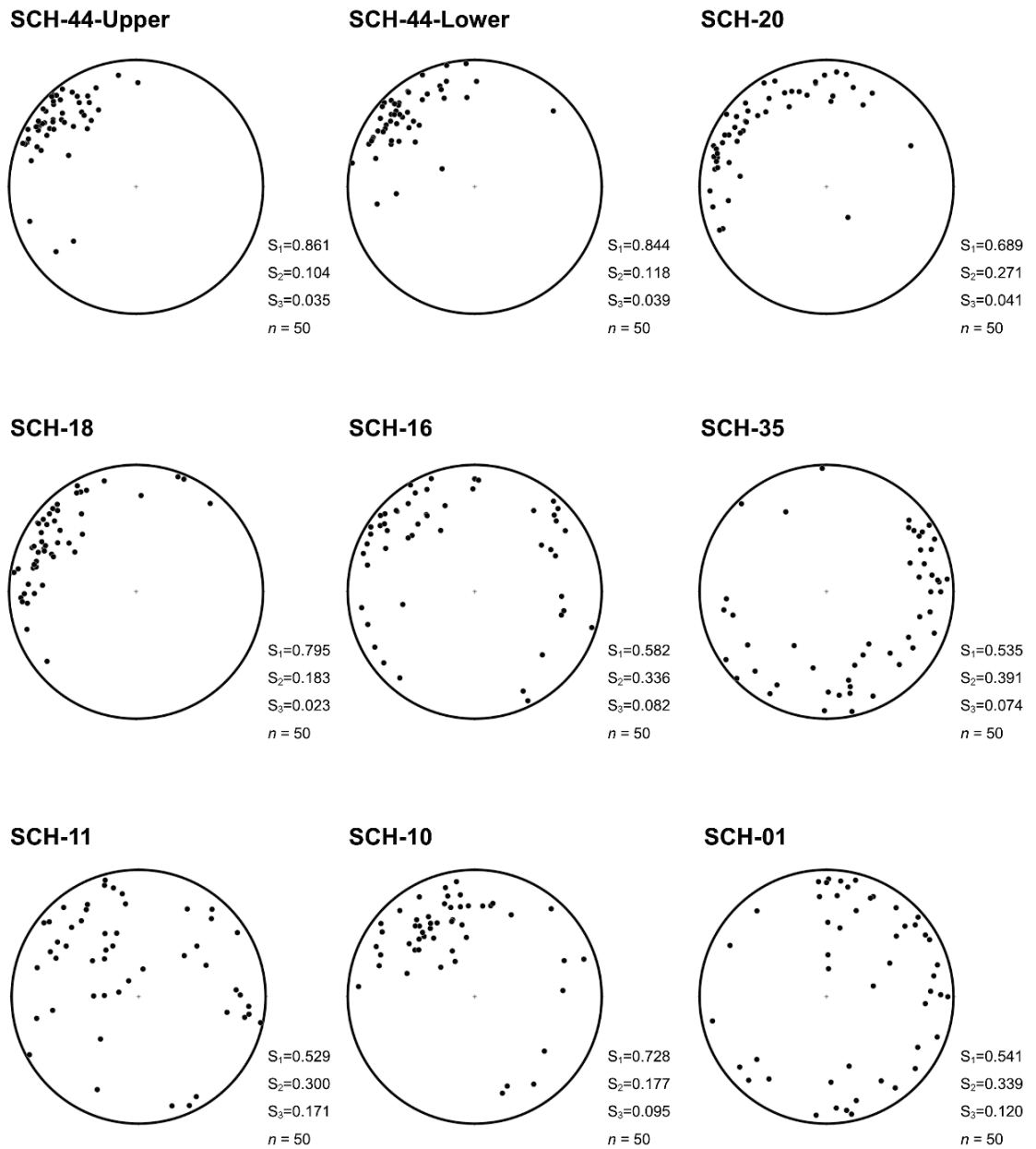


Fig. 4.12 Clast fabric data. Nine clast fabrics taken from the inner ice-proximal slopes of the lateral-frontal complex. Principle eigenvalues (S_1 , S_2 & S_3) are presented by each sample. All data is projected using lower hemisphere equal area Schmidt nets.

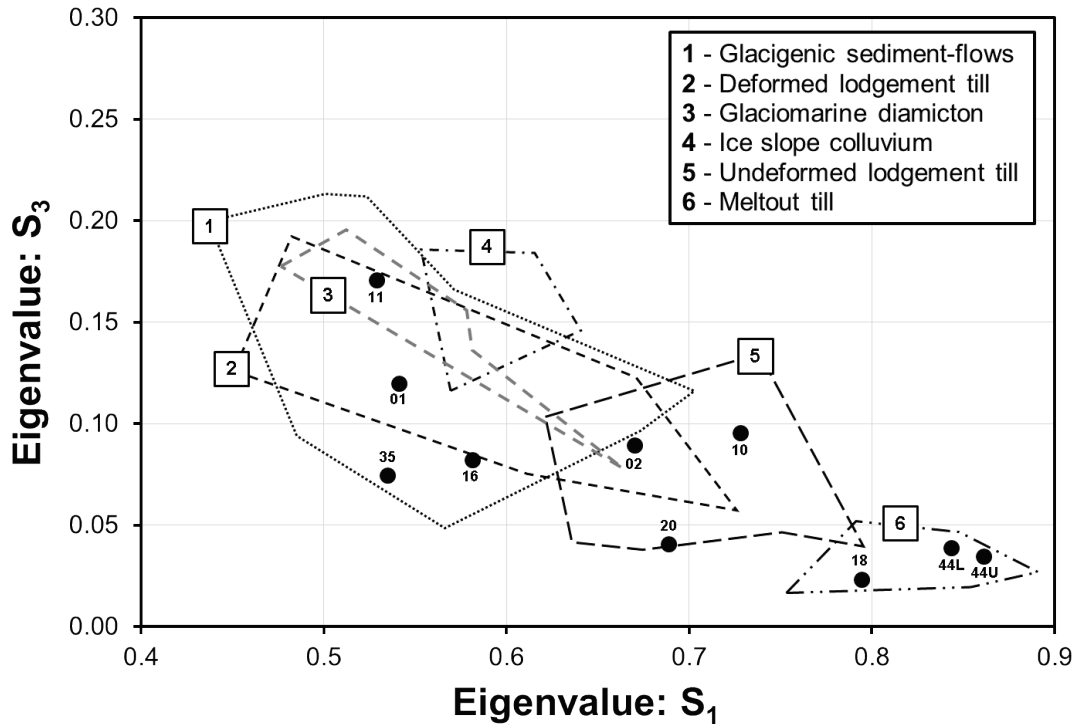


Fig. 4.13 Bivariate plot of clast fabric data (including SCH-02) with envelopes from Dowdeswell and Sharp (1986). Samples 18, 44L and 44U show clustering whereas other samples overlap with a range of depositional environments with clasts lacking preferred orientation and dip.

4.3.3.3 Clast-form analysis

A total of 42 clast samples were analysed. The % RA and % C_{40} indices are presented using a covariant plot in Fig. 4.14. Lateral moraine diamicton (clast-rich sandy and intermediate) have distinct clast-form indices, distinguishing it from control samples. All inner lateral moraine samples exhibit RA indices of 50-82% and C_{40} indices of 46-80%. Outer moraine samples show similar variability (% RA = 56-58; % C_{40} = 44-74). Diamicton samples are distinguishable from supraglacial (% RA = 90-100; % C_{40} = 72-96) and extraglacial control samples (% RA = 90-100; % C_{40} = 74-86). Samples from a small inset ridge contain a lower angular component (% RA = 20-24), yet exhibit similar shape indices to sediment from the main lateral complex (% C_{40} = 58-62). The inset ridges share some overlap with subglacial control samples obtained from a recently deglaciated fluted terrain (% RA = 12-32; % C_{40} = 36-56). Fluvial control samples have the highest degree of

edge rounding (% RA = 2-18), and a wide variability in terms of their shape characteristics (% C₄₀ = 26-64).

Clast form parameters were subject to regression analysis in Minitab 17 (e.g. Evans, 2010) to understand the statistical relationship between distance down-moraine and clast-form (Table 4.6; Fig. 4.15). The most statistically significant clast-form parameter to change with distance down-moraine was the percentage of striated clasts within a sample. The fitted polynomial regression model for this variable showed the best fit and statistical significance ($R^2 = 73.6\%$; $p = 0.065$) out of the analysed variables. 47.3% of the variability in terms of the percentage of very-angular clasts within a sample is explained by distance down-moraine, although the fitted polynomial regression is not statistically significant and falls outside the 95 % confidence interval ($p = 0.828$). Overall, none of the investigated parameters were statistically significant to within the 95% confidence interval (Table 4.6).

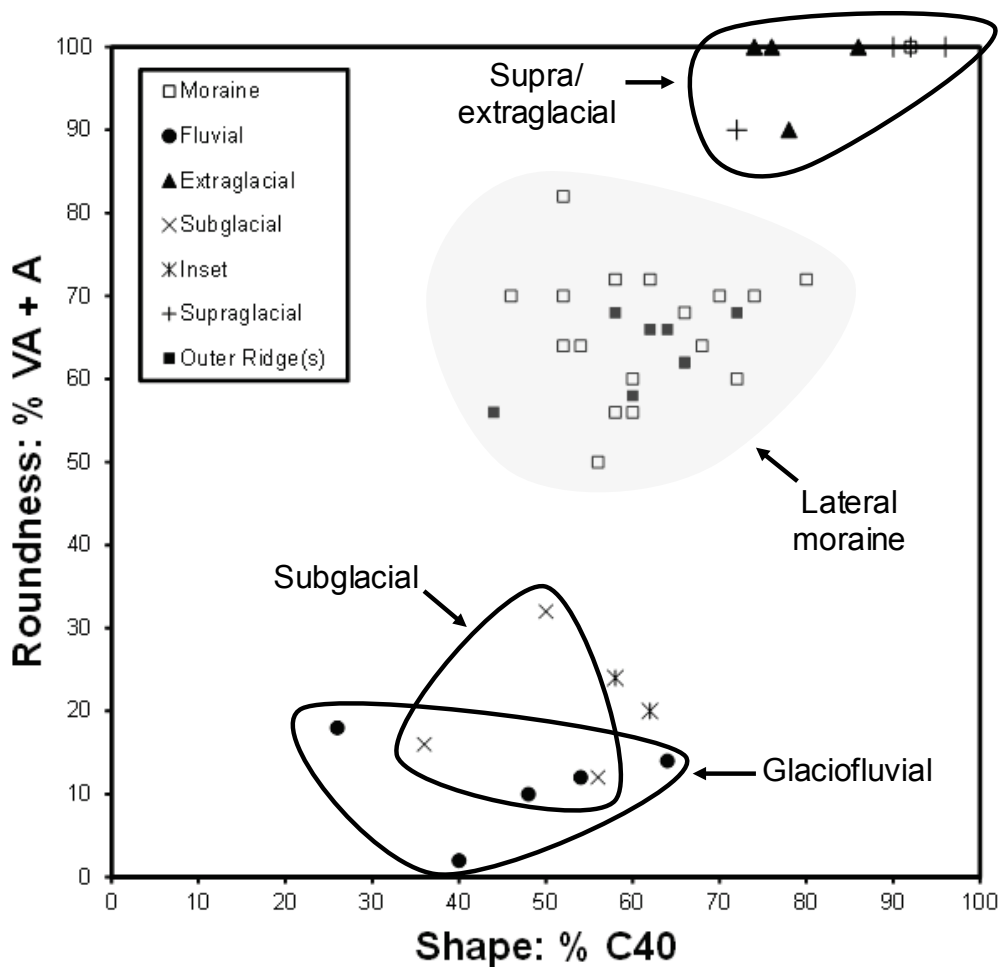


Fig. 4.14 RA/C₄₀ plot of 42 clast samples of $n = 50$ sorted by depositional environment

Table 4.6: Regression statistics of clast-form parameters and their relationship with distance-down from inner-proximal samples

Parameter	Analysis	R ²	P-value
% VA	Polynomial (2 nd Order)	0.473	0.828
% A	Polynomial (2 nd Order)	0.005	0.899
% SA	Polynomial (2 nd Order)	0.145	0.982
% RA	Polynomial (2 nd Order)	0.192	0.814
% C ₄₀	Linear	0.007	0.764
% Striated	Polynomial (2 nd Order)	0.736	0.065

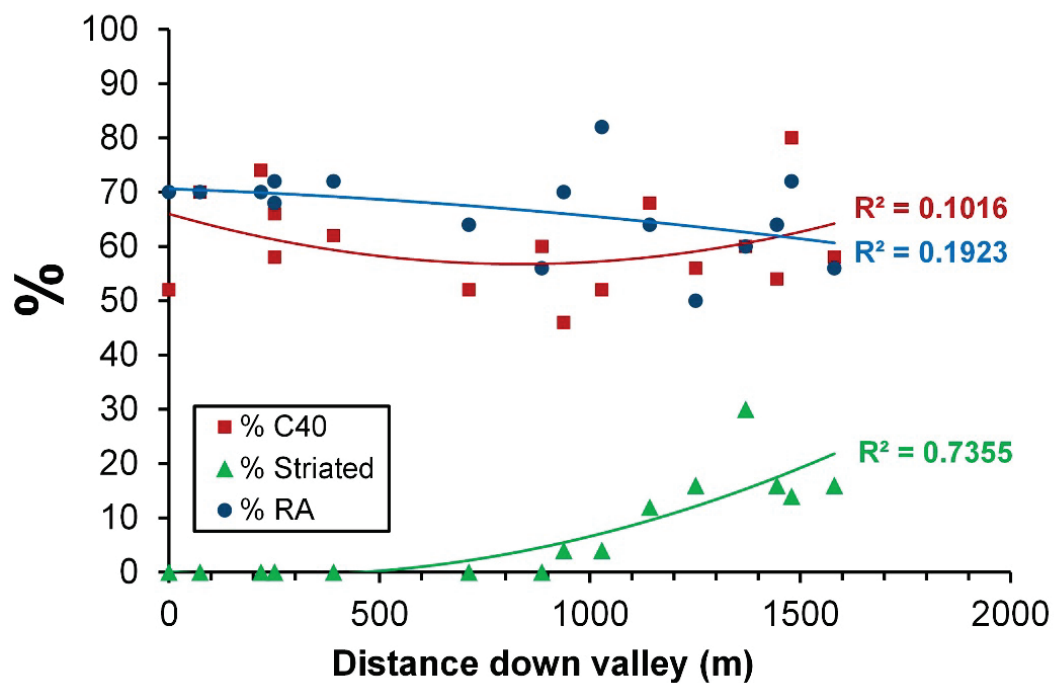


Fig. 4.15 Linear and polynomial regression plots investigating the modification of various clast-form parameters with Euclidean distance down-valley from ice-proximal exposures.

The roundness cumulative distribution functions of clast samples from the five depositional environments (supraglacial, extraglacial, lateral moraine and inset moraine ridges) are compared for similarity using the Kolmogorov-Smirnov two-sample test (Table 4.7). Moraine samples represent ice-proximal exposures only. The extraglacial sample populations are shown to have no statistical difference ($\alpha = 0.01$) to supraglacial samples in terms of their roundness characteristics ($D = 0.14$). Subglacial control samples show a statistical similarity to clasts sampled from an inset ridge in terms of the maximum discrepancy between their cumulative distribution functions ($D = 0.03$). Statistical differences are observed between all other sample populations. Although, not statistically significant, the CDF of moraine samples show some association with extraglacial debris ($D = 0.39$).

Table 4.7: Two-sample Kolmogorov-Smirnov matrix showing the maximum difference between sample populations. Clast samples are from the following depositional environments: (i) Moraine proximal exposures ($n = 1600$); (ii) Supraglacial ($n = 200$); (iii) Subglacial ($n = 150$); (iv) Extraglacial ($n = 400$); (v) Inset moraine ridge ($n = 100$). Bold text indicates no statistical difference between clast populations at 99% Confidence significance ($\alpha = 0.01$).

	i	ii	iii	iv	v
i	-	0.52	0.46	0.39	0.44
ii	-	-	0.78	0.14	0.76
iii	-	-	-	0.78	0.03
iv	-	-	-	-	0.76

4.3.4 Structural glaciology

4.3.4.1 Overview

The structural glaciology is interpreted from an orthorectified aerial image acquired in 2009 to aid understanding of the origin and transport history of moraine sediments. A total of four main structural categories were described and interpreted; (S_0) arcuate planar structures, (S_1) longitudinal planar structures, (S_2) fractures and traces. The areal extent of the supraglacial debris cover were mapped. A map displaying the main structural units is presented in Fig. 4.16.

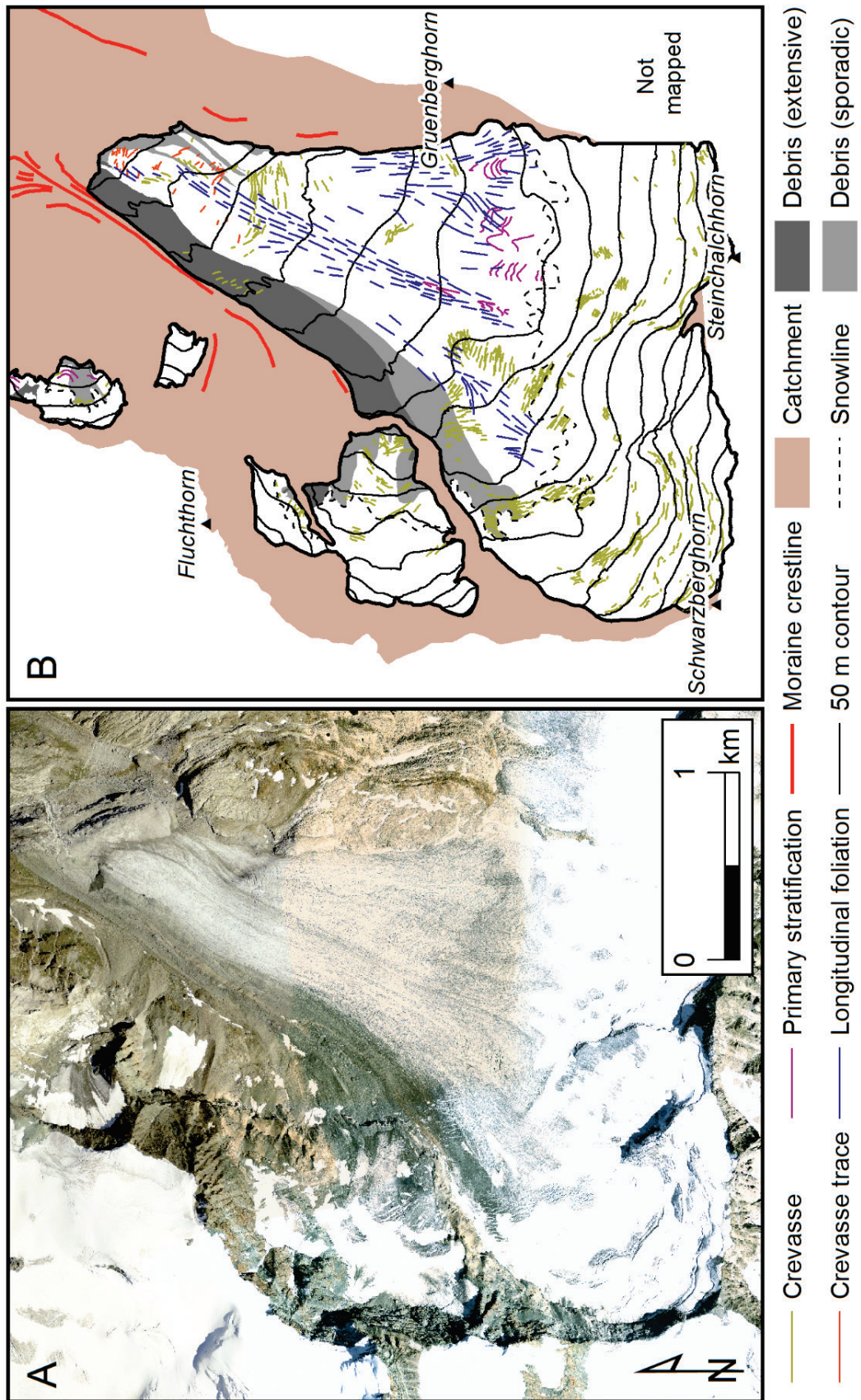


Fig. 4.16 Structural interpretation of Schwarzberggletscher (B) derived from 2009 orthorectified aerial imagery (A).

4.3.4.2 Arcuate planar structures (S_0)

Description: Continuous arcuate bands are observed within the upper section of Schwarzberggletscher, underneath the snowline at the point of aerial image acquisition. The full distribution of S_0 in the accumulation area is unclear, due to snow-cover obscuring structure on the aerial photography. In places, folded arcuate structures display a chevron planar form. These stronger folds appear to coincide with a flow unit boundary separating the two main accumulation areas of Schwarzberggletscher. These features are readily identified by their colouration on the aerial photography, which alternates between darker and lighter bands. The spacing of the lighter bands of clear ice located at the centre of the glacier is inconsistent, varying with distance down-glacier. The bands located up glacier reach a maximum width of 20 m. Banding on the true right of the glacier is typically more tightly spaced (>5m) down-glacier. The exact spacing between darker bands cannot be delimited given the coarse 0.5 metre resolution of the orthorectified aerial imagery. Close to the glacier centreline, the intensely folded arcuate structure becomes indistinguishable from longitudinal planar structures (S_1).

Interpretation: Arcuate planar structures are interpreted as primary stratification. Their visibility on the aerial photography is likely to relate to differences in properties of the ice, although, as mapping was undertaken remotely from aerial imagery, field observations of difference ice facies were not made. Principle differences controlling the visibility of primary stratification include the ice crystal size, bubble content, and debris content (Goodsell *et al.*, 2002; Roberson, 2008). Compacted snow during winter months is typically bubble-rich, whereas the melt and subsequent refreezing of snow during summer months facilitates the formation of debris-rich layering and allows water to infill pore space forming superimposed ice (e.g. Benn and Evans, 2010). Ductile structures exhibited by primary strata are interpreted to signify (1) moderate lateral compression down-glacier as the east and west accumulation basins coalesce and are topographically constrained and (2) differential flow within individual flow units (e.g. Hambrey and Lawson, 2000).

4.3.4.3 Longitudinal planar structure (S_1)

Description: The most extensive area of S_1 occurs down-glacier of intensely folded arcuate planar structures (S_0). Evidence of cross-cutting of longitudinal planar structure is by

arcuate planar structures (S_1) could not be identified on the aerial photography. Longitudinal planar structures can be traced down-glacier to the terminus, and are almost exclusively concentrated within a c. 100 m wide unit close to the glacier centre-line.

Interpretation: Longitudinal planar structures are interpreted as bands of longitudinal foliation. The spatial distribution of S_1 forms the basis of this interpretation. As S_1 occurs down-glacier of intensely folded arcuate planar structures it most likely signifies the transposition of primarily layering into longitudinal foliation parallel to ice-flow (e.g. Hambrey and Lawson, 2000). Longitudinal foliation is known to develop at the confluence between flow units, and in areas of lateral compression (related to the topographic controls on glacier geometry) (Hambrey and Lawson, 2000; Roberson, 2008; Jennings et al. 2014). The continuity between the two structures, and occurrence of S_1 at a flow unit boundaries appears to satisfactorily confirm this mechanism of formation, although additional investigations to comparing the crystallography properties of ice within each structure would be beneficial (e.g. Roberson, 2008).

4.3.4.4 Fractures (S_2) and traces (S_3)

Description: These features occur discontinuously across the glacier surface. The largest occur in the accumulation areas of Schwarzberggletscher, where they are aligned transverse to the direction of ice flow, exceed 200 m in length, and are often concave in plan form. The full extent of fractures in the accumulation area are unclear as snow-cover obscures structure on the aerial imagery. Occasional crevasses below the snowline are in filled by snow. The lower glacier tongue is largely fracture-free, although a series of fractures can be identified between 2750 and 2850 m elevation. Indistinct features are identified at the glacier terminus down-glacier of fractured areas (S_3). Some fractures are visible through the extensive supraglacial debris cover on the true-left of the glacier. These features are oblique to glacier flow, oriented between 340-350/160-170°, and linear in plan form. A series of indistinct longitudinal features (S_3) are readily distinguishable from foliation (S_1) and occur in proximity to the terminus.

Interpretation: S_2 and S_3 are interpreted as crevasse and crevasse traces forming in response to tensile and shear stresses. They therefore represent patterns of deformation within the glacier (e.g. Benn and Evans, 2010). Four types are distinguished here: (1) large 'bergschrunds' occurring in the upper accumulation area, (2) smaller (<100 m) linear or

concave open crevasses (S_2) (and subsequent traces; S_3) occurring in both the accumulation and ablation areas of the glacier, (3) linear (chevron) type crevasses occurring contiguously with the glacier margin (S_2), and (4) longitudinal crevasses/crevasse traces occurring close to the glacier terminus (S_2/S_3).

Large 'bergschrund' type crevasses, and smaller linear and concave open crevasses, are interpreted as evidence of an extensional flow regime related to the acceleration of ice over steep terrain (Hambrey and Lawson, 2000; Benn and Evans, 2010). Although mostly occurring in the upper reaches of the glacier, localised areas of transverse crevasses occur as the glacier profile steepens once more, allowing for further crevasses to open. Crevasses appear to be less defined in proximity to the terminus. These transverse features cross-cut existing structure and are typically found down-glacier of active crevasse fields, and therefore represent the closure of existing crevassing ('crevasse traces') (e.g. Goodsell *et al.* 2002).

Hambrey *et al.* (2005) present two mechanisms for the formation of crevasses traces. The first mechanism involves the refreezing of meltwater within the crevasses and can be distinguished by the presence of blue ice (Goodsell *et al.*, 2002). The second mechanism forms tensional veins and originates from the recrystallization of ice at adjacent fracture walls (Hambrey *et al.* 2005; Benn and Evans, 2010). Debris and snow can also be incorporated within closing crevasses (Gulley and Benn, 2007; Hambrey, 2011), however such features were not observed at Schwarzberggletscher.

Oblique linear (chevron) crevasses appear to indicate lateral shear stresses occurring at the glacier margin (e.g. Appleby *et al.*, 2010; Jennings *et al.*, 2012). However, the isolated occurrence of open chevron crevasses (e.g. to an area of extensive debris coverage and an absence on the true-right of the glacier) suggests limited lateral shear stress at the glacier margin. Evidence of longitudinal fractures and traces at the glacier margin represent the transverse extension of ice in respect to the direction of flow (e.g. Jennings *et al.*, 2014). The occurrence of longitudinal crevasses are interpreted to signify the diminishing lateral confinement of ice at in proximity to the glacier terminus.

4.3.4.5 Supraglacial debris

Supraglacial debris represent a significant component of the Schwarzberg glacier system. The areal coverage of extensive and sporadic debris on the main the glacier are mapped.

Extensive debris covers 0.4 km² of the glacier surface (8%) and is restricted to the true left of the glacier. Sporadic debris are observed along the glacier terminus. The right of the glacier is characterised by relatively 'clean' glacier ice. A summary of the sedimentology characteristics supraglacial debris is provided in section 4.3.3.

4.4 Discussion

4.4.1 Synthesis of structural glaciological interpretation and debris transport

Structural glaciological mapping from aerial imagery indicates no evidence of englacial septa propagation on the glacier surface. Debris accumulations of sub-angular gravelly material were found on the glacier surface at three locations during field surveys in 2013. Two of these accumulations are not visible on the 2009 aerial photography which is used for geomorphological and structural mapping. Therefore they appear to have only recently propagated onto the glacier surface. At present the potential for subglacial material to propagate onto the glacier surface appears to be limited at Schwarzberggletscher, thus limiting the availability of basally derived material for moraine building by debris flowage and dumping (Fig. 4.17). The areal coverage of supraglacial debris and the potential contributing area of extraglacial debris up-glacier are clearly linked to the prominence of the moraines down-valley and a clear control on the cross-valley moraine asymmetry at this site.

A



B

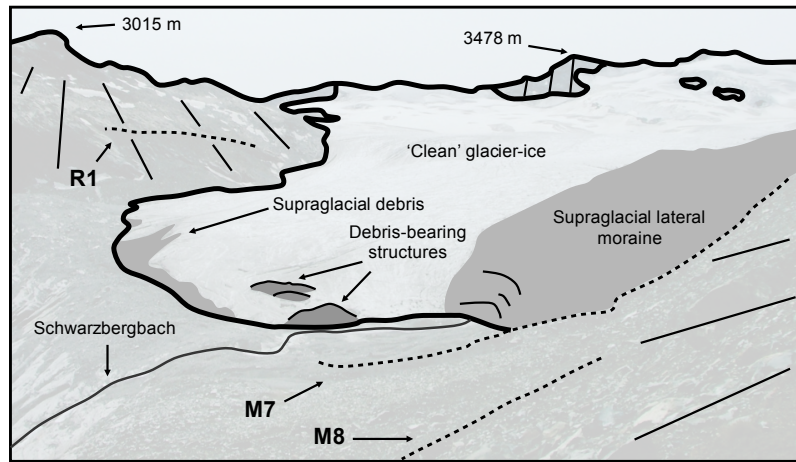


Fig. 4.17. (A) Ground level photograph of the glacier terminus in 2004. (B) An interpretation of key features including the identification of debris-bearing structures melting out close to the terminus which are no longer present at the glacier terminus.

4.4.2 Dumping

The formation of ice-marginal moraines by debris flowage and slumping of material from supraglacial positions is well documented in a range of glacial settings (Benn *et al.*, 2003) and appears to be a significant ice-margin process responsible for the construction of the Schwarzberggletscher moraine. The flowage and slumping of debris as moraine constructional processes have also been directly observed first hand in the Swiss Alps where localised glacier advances during the 1970s were significant enough to allow glacier-ice to overtop lateral moraines at Tsidjoire Nouve (Whalley, 1973; Small, 1983). Debris transfer via flows, slumps and slides from supraglacial to ice-marginal positions result in the production of crudely stratified diamictons, often resulting in strong-moderate macrofabrics dipping away from the former glacier surface (Humlum, 1978; Osborn, 1978; Benn and Owen, 2002; Curry *et al.*, 2009). Assessed facies (e.g. SCH-44U/L, SCH-20, and SCH-18) were found to exhibit these strong macrofabrics, typical of dumping and flowage.

Evidence of a buried palaeosol within exposure SCH-44 highlights multiple periods of moraine construction, whereby moraine-formation (thus the overtopping of an existing moraine rampart) was interrupted, allowing for ecological succession, and the onset of soil development (e.g. Rothlisberger and Schneebli, 1979). Whilst material from this palaeosol is currently undated, it is interpreted to signify a period of climatic amelioration and associated reduction in glacier. Bircher (1982) radiocarbon dated two fossil soils within the Schwarzberggletscher lower-left lateral moraine to 630 ± 60 and 950 ± 115 ^{14}C yr BP. These dates appear to correlate to lesser glacier coverage during onset of the Medieval warm Period (MWP) (e.g. Rothlisberger *et al.*, 1980), punctuated by minor glacier advances dated to between 1000-1100 yr AD (Grove and Switsur, 1994), and the later onset of the Little Ice Age during the 14th century AD (Ivy-Ochs *et al.*, 2009). Should this newly discovered palaeosol be dated, it would provide a minimum age for the recession of Schwarzberggletscher, and maximum age for later glacier overriding and subsequent moraine-construction (e.g. Kirkbride and Winkler, 2012). Models accounting for landform development and glacier change are presented in Fig. 4.18. It is currently unclear which glacier advance (Little Ice Age or earlier) these sedimentary units should be assigned to, however it is reasonable to assume that the Little Ice Age advance was extensive enough to permit the overtopping of the left-lateral moraine complex.

A further diagnostic characteristic of debris flowage is the incorporation of sorted lenses of sediment within diamicton units that typically signify reworking and subsequent sorting of the fine sediment fraction via glacio-fluvial surface processes which are incorporated into the moraine structure as units of diamicton are incrementally superimposed onto existing moraine structure (Benn and Owen, 2002). Here, diamicton deposits are typically massive, and lack crude stratification. Fine lenses of silt were only located at one exposure (SCH-35), which exhibits a macrofabric that is weakly parallel to former ice-flow and dipping down-slope. This facies may represent subsequent paraglacial disturbance, related to the loss of ice-support following glacier recession.

4.4.3 Subglacial lodgement and traction

Till lodgement and lateral-subglacial traction are identified as additional processes responsible for the modification of ice-proximal sedimentary units (Boulton and Eyles, 1979; Small, 1983; Lukas *et al.*, 2012). Characteristics of sedimentary units subject to such processes include over consolidation and the production of fissile structures related to the unloading of over consolidated till units. Exceptionally strong clustered fabrics parallel to ice flow have been interpreted as evidence of the incremental plastering ('lodgement') of primarily subglacial traction till on ice-proximal slopes (Lukas *et al.*, 2012). A tendency for clast orientations to align parallel to ice-flow is somewhat evident in select samples within the lower-lateral moraine complex (e.g. SCH-35; SCH-16; SCH-01), yet generally these fabrics lack the strength typically associated with lodgement at the ice-till interface (Benn and Evans, 2010). Despite this, sites with weakly developed fabrics also contain a striated clastic component, with striated material accounting for up to 30% of assessed clasts. All diamicton sedimentary units at Schwarzberggletscher are set within a highly friable, poorly consolidated silt-rich matrix, which disintegrates when extracted. This is at odds with over consolidated/compacted material or partially cemented material reported to occur in other alpine glacial landsystems (e.g. Whalley, 1975; Eyles *et al.*, 1983; Lukas *et al.*, 2012). The absence of clear diagnostic sedimentary characteristics provide somewhat equivocal evidence of subglacial till deformation in assessed facies at this site (e.g. Bennett *et al.*, 1999).

4.4.4 Debris transport and clast-form

The lower sections of the moraine contain the highest concentration of striated material (4-30%). Although these striated clasts may represent the comminution of clasts at the

interface between the glacier and ice-proximal moraine, several factors confound the interpretation of debris transport from clast-form parameters. For example, it is unclear whether this striated, sub-angular material is indicative of a complex debris transport related to the transfer of material from the bed, to the glacier surface. A range of conditions are known to initiate the transfer of material from the glacier-bed in alpine settings, including ice-flow over steep bedrock controlled topography (e.g. Goodsell *et al.*, 2002; Lukas and Sass, 2011) or folding and subsequent elevation of subglacial or glacio-fluvial debris following extensive longitudinal compression of individual flow units which may form dirt cones close to the glacier terminus (Goodsell *et al.*, 2005b). Ice-flow over a bedrock step which runs transverse to former glacier flow may have initiated the transfer of material from the base of the glacier, onto the glacier surface. A structurally controlled transport origin for worn and striated clasts (e.g. Gornergletscher/Findelgletscher; Lukas and Sass, 2011; Lukas *et al.*, 2012) is unclear based on structural mapping of Schwarzberggletscher. It is acknowledged that an absence of aerial photography from before 1967, and limited ground-level photography from the early 20th century impede mapping of glacier structures from a period where the lower lateral moraine would have been actively forming. Whilst a clear high-supraglacial debris component is identified on the true-left of the glacier on historical images, emerging debris-bearing structures are not identified.

Additionally, clast form parameters may have been modified by either; (1) minor reworking of material occurring over time-scales in excess of the Little Ice Age advance (e.g. Matthews and Petch, 1982; Evans, 1999; Burki, 2009) which produces homogenous units of diamicton which display subtle but distinguishable down-moraine clast-form parameters from ice-contact dumps; and (2) the active transport of clasts which cause progressive clast wear-down moraine related to the overriding of ice-proximal deposits within the 'active' lateral-subglacial domain with the traction of debris resulting in clast wear (e.g. Boulton and Eyles, 1979; Hambrey and Ehrmann, 2004; Hambrey *et al.*, 2008; Lukas *et al.*, 2012). The recycling of glacial material between glacier-retreat advance stages is documented to result in moraines which exhibit anonymous clast-form in relation to their genesis. Recycling is facilitated by bedrock steps and the presence of overdeepenings, which act to trap glacio-fluvial and subglacial material during periods of less glacier extent times (e.g. Burki *et al.*, 2010) and allow for material to be

subsequently remobilised and mixed with passively transported material prior to deposition. The potential for modification of clast form via reworking or *in situ* wear of clasts in the subglacial lateral domain are likely due to the clear geomorphological, sedimentological, and geochronological evidence (e.g. existing radiocarbon dating by Bircher, 1982) that indicate the repeated reoccupation of the moraine rampart over the Holocene.

An additional interesting characteristic of assessed lateral moraine facies is the overlap in terms of clast-form parameters between proximal samples (interpreted as youngest in age) with samples from the outer ridges on the lower lateral complex. This overlap appears to suggest that debris transport pathways responsible for moraine construction have remained much the same over multiple Holocene glacier-readvance stages, despite the potential for changing ice geometry within the accumulation basin of Schwarzberggletscher.

4.4.5 Moraine morphology and topographic controls

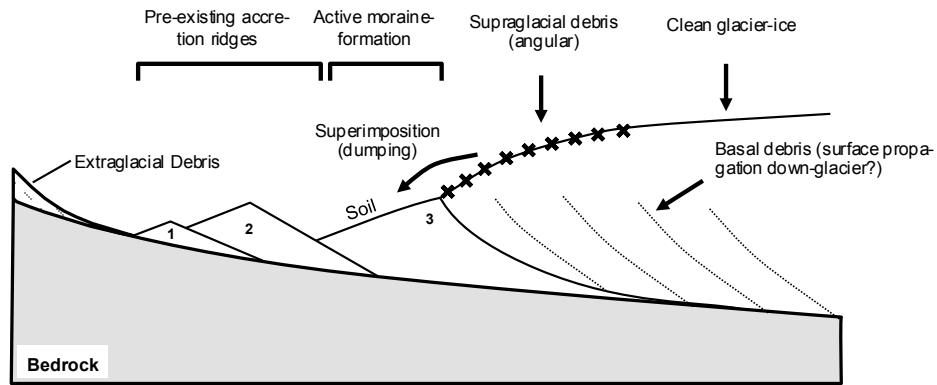
Geomorphological maps and sedimentology data appear to demonstrate the importance of topographic controls regulating not only initial moraine inception (e.g. Barr and Lovell, 2014), but also the resulting sedimentary signature of ice-marginal moraines in high-mountain environments. Schwarzberggletscher offers an excellent example where a mixture of lateral-accretion and superposition construct structurally complex ice-marginal ramparts. However, in more laterally constrained Alpine valleys, large moraine ramparts are responsible for restricting successive glacial advances, which appear to be a prerequisite for lateral-subglacial traction (e.g. Findelgletscher; Lukas *et al.*, 2012). Existing models of moraine genesis focusing on lateral accretion and superposition are applicable to a broad range of high-mountain catchments, however, consideration of topographic controls deserves attention to fully understand the nature of moraine formation and the resulting sedimentary signature of ice-marginal moraines.

4.4.6 Landform stability and preservation potential

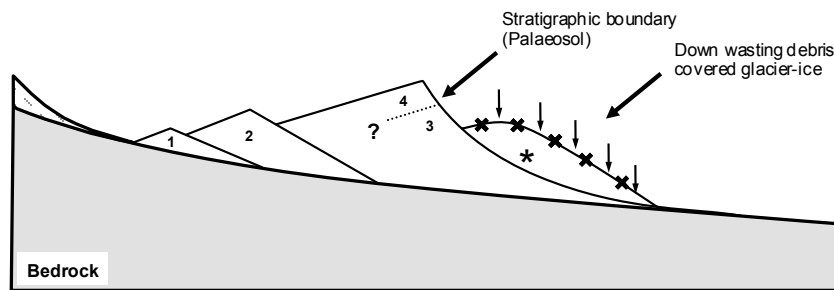
Moraine-forming processes appear to be key controls on the susceptibility of ice-proximal slopes to paraglacial reworking following the removal of ice-support. The absence of consolidated/compact or 'plastered on' diamicton is a plausible control on landform stability, explaining the gentle slope characteristics in comparison to other sites within the Valais region (Curry *et al.* 2006; Table 4.1). It is worth noting that gently dipping

macrofabrics have been linked to inherent landform stability, with Alpine lateral moraines known to remain in a quasi-stable state, typified by over-steepened upper proximal gullied slope sections (Curry *et al.*, 2009). Curry *et al.* (2009) suggest that the macrofabric of glacial material contained within Alpine moraines is instrumental in enhancing the stability of moraine proximal slopes. This is a response to the resistance of material to translational shear which often acts at near-perpendicular angles to the preferred fabric of *in situ* diamicton within Alpine moraines. However, at Schwarzberggletscher, strong developed dipping fabrics appear in proximity to the current glacier terminus and appear to result in no discernible difference in terms of the maximum slope angle attained by ice-proximal slopes. Additional features which have a low preservation potential include benches of diamicton deposited on ice-proximal slopes during the back, and downwastage of the glacier from its Neoglacial maximum position. Proximal diamicton units are sensitive to the collapse following the loss of ice support (e.g. Curry and Ballantyne, 1999; Curry *et al.*, 2006); and may be poorly distinguishable in the geomorphological record over centennial and millennial time scales.

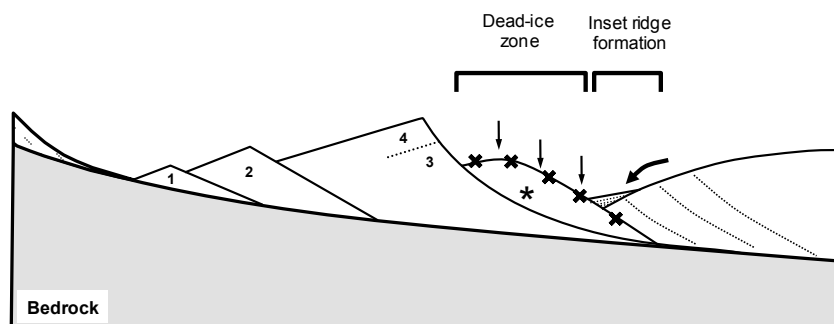
A Neoglacial Maximum? (Little Ice Age; c. 1850)



B Glacier recession (c. 1967)



C Minor glacier re-advance (c. 1970s)



D Present day (c. 2013)

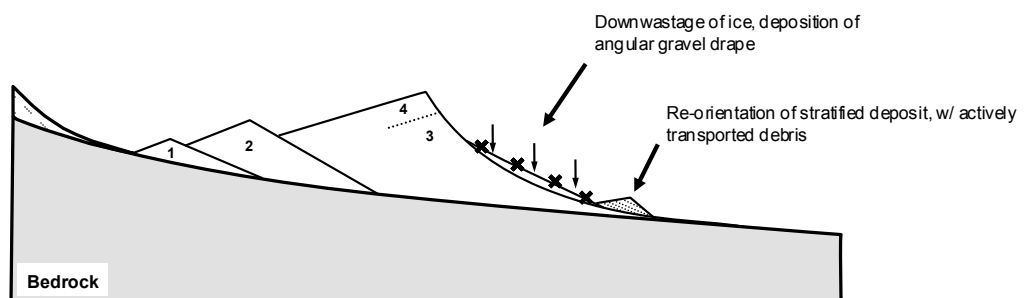


Fig. 4.18. Conceptual model for the development of lateral moraine at the margin of Schwarzberggletscher. Glacier flow is perpendicular to the cross-section.

4.5 Summary

Lateral moraines formed at Schwarzberggletscher provide a sedimentary record of glacier fluctuations, probably extending over millennia. Debris transport and lateral moraine development was investigated. Clasts within the moraine display high RA indices yet do not overlap with control samples of a known transport history. Extraglacial debris (e.g. scree, rockfalls from valley sides) are responsible for the primary provision material which is subsequently transferred into the moraine via 'passive' supraglacial transport. Differences in terms of extraglacial sediment input at the site have resulted in clear within-basin asymmetry. Up-moraine lithofacies show clear structural evidence of moraine overtopping and debris-dumping as the mode of formation, although the topographic influence of a pre-existing moraines are important within regard to the mode of formation. Down-moraine sites exhibit weak clast fabrics and readily contain striated clasts, indicating the contribution of actively transported material for moraine construction. Mechanisms responsible for the delivery of 'actively' transported, striated clasts were therefore considered.

The provision of actively transported debris at Alpine glaciers has been suggested to relate to englacial debris septa. At present, structural interpretation of the glacier highlights a lack of propagating debris-bearing features as the glacier continues to down and back-waste. It remains unclear how actively transported material was incorporated into the moraine, but is likely to reflect the propagation of englacial debris septa onto the glacier surface during the LIA maxima when the structural glaciology was likely considerably different to the present. The clast-form parameters (RA/C_{40}) of debris within the outer ridges are indistinguishable from the inner ridges, implying that transport pathways have remained fixed through multiple periods of glacier expansion. This study serves to provide additional information on the sedimentology signature of lateral moraine with respect to the former characteristics of Alpine valley glaciers.

5. The character and significance of ice-cored moraine complexes at the margins of polythermal Arctic glaciers: insights from a multi-technique approach at Isfallsglaciären, Sweden

5.1 Introduction

Moraines assumed to demarcate late Holocene glacier advances across Scandinavia are subject to on-going debate and ambiguity regarding their development, age and significance (Østrem, 1963; 1964; Karlén, 1973; Ackert, 1984; Matthews *et al.*, 2014). Moraines developed at the margins of some Scandinavian glaciers are identified to be potentially atypical of other ice-cored ridges occurring in high-Arctic settings, containing moraine-distal snowbank ice within their structure (Østrem, 1964). In recent years, the term ‘Østrem’ type moraine has been introduced in the literature (e.g. Whalley, 2009; Whalley, 2012) to distinguish these ice-cored moraine systems from their high-Arctic counterparts, with the term aptly naming the moraines after the geoscientist who conducted initial investigations on ice-cored moraines during the late 1950s and early 1960s.

Glaciers within the Tarfala valley, Northern Sweden are some of the most extensively studied globally (Holmlund *et al.*, 1996; Holmlund and Jansson, 1999). This is at odds with our understanding of moraine forming processes operating at the margins of these glaciers. Precise understanding of moraine stratigraphy, genesis, and age may result in a better understanding of Holocene glacier change within Scandinavia and moraine formation at the polythermal glacier margins. In comparison to Alpine type moraines whose structural characteristics are well documented (Rothlisberger and Schneebli, 1979; Small, 1983; Lukas *et al.*, 2012) current understanding of ‘Østrem’ type moraine is limited.

Ground-penetrating radar (GPR) offers a non-invasive method to characterise subsurface structure and composition (Neal, 2004). This technique has been demonstrated to have potential value in glacial sedimentary environments (Sadura *et al.*, 2006; Brandt *et al.*, 2007; Burki *et al.*, 2010; Midgley *et al.*, 2013). To bridge the gap in the current understanding of

these features, a multi-technique approach has been used to investigate the structure, morphology and sedimentology of a large 'Østrem' type moraine complex located at Isfallsglaciären, Tarfala Valley, Northern Sweden. The objectives of this study are therefore to: (1) use geophysical survey methods to determine the sub-surface structure/stratigraphy and composition of the Isfallsglaciären lateral-frontal moraine complex; (2) characterise the sedimentology of debris within the moraines to ground-truth radar facies, (3) interpret ice-marginal processes involved in the construction of the moraine and (4) characterise moraine morphology using high-resolution topographic data. The investigation of the moraine structure, sedimentology and geomorphology will aid understanding of former glacier characteristics.

5.2 Study site description

Isfallsglaciären is a c. 1.5 km long valley glacier located in the Kebnekaise Mountains in Arctic Sweden (Fig. 5.1; Fig. 5.2). The glacier has an easterly aspect, and has receded approximately 500 m from its 1920s position, where the glacier partially overrode its inner moraine ridge (e.g. Karlén, 1973). Similar to the neighbouring Storglaciären, Isfallsglaciären contains both temperate and cold ice (Eklund and Hart, 1996). Schytt (1962) recorded subfreezing temperatures from an artificially created tunnel at the glacier terminus. The neighbouring Storglaciären is currently under-going changes to its thermal configuration (Pettersson *et al.*, 2003), with one third of its cold surface layer lost over the 1989-2009 period (Gusmeroli *et al.*, 2012). These changes have been linked to recent climatic amelioration, such as increased winter air temperature since the 1980s (Pettersson *et al.*, 2003; Gusmeroli *et al.*, 2012). It is unclear whether the thermal regime of Isfallsglaciären is undergoing a similar evolution.

The moraines of Isfallsglaciären are subject to some morphological description in research presented by Schytt (1959) and Karlén (1973). Two frontal moraines are distinguished within the glacier forefield; an outer more subdued ridge with a relief of up to c. 10 m and a more topographically prominent inner-frontal ridge, which is partially overprinted with subglacial flutes. The inner ridge has a topographic prominence of up to 20 m, and together with the north and south lateral-complex, impound the current glacier forefield. Glaciofluvial run-off is restricted to one outlet stream which dissects this inner moraine ridge, separating the northern- and southern lateral-frontal complexes. The outer lateral-ridge on the northern-lateral-frontal exhibits a series of discontinuous mounds on its

distal slope of the outer ridge (Fig. 5.3). The southern lateral complex displays a furrowed morphology, and includes a prominent nested arcuate ridge. The northern-lateral ridge is dissimilar to the southern. Up-glacier the moraine forms a single embankment, which anastomoses into four nested ridges that adjoin the less topographically prominent outer-frontal ridge. Both the proximal and distal slopes of this feature reach up to 45°.

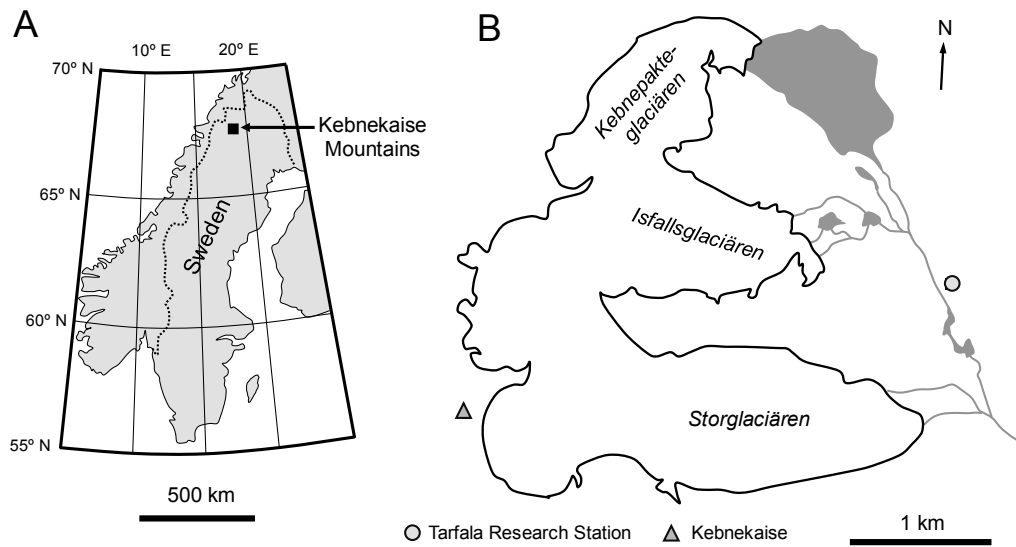


Fig. 5.1 Study site location. (A) The location of the Kebnekaise Mountains in relation to Scandinavia. (B) Glaciers located on the Eastern flank of Kebnekaise. (C) Ground-level photograph of Isfallsglaciären and the moraine complex from Tarfala Research Station in 2013.

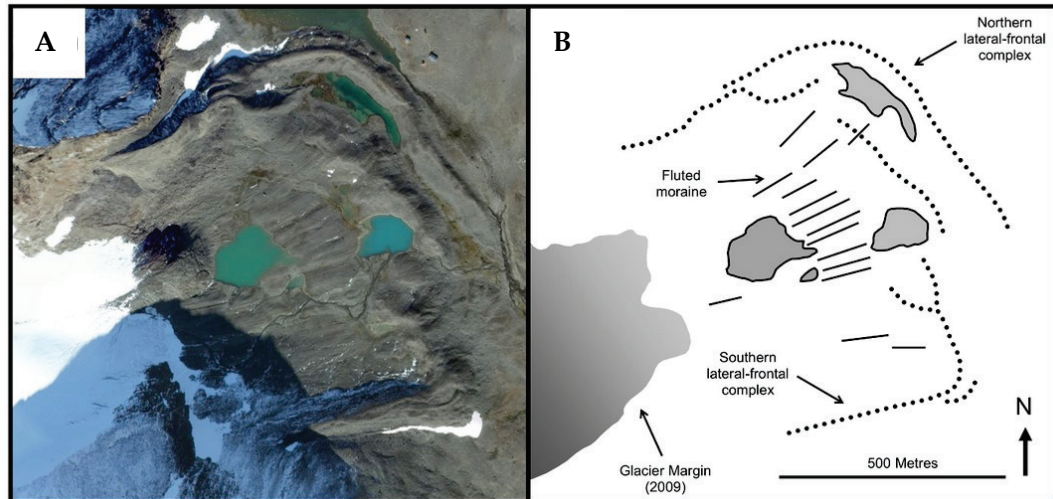


Fig. 5.2 (A) Lantmäteriet orthorectified image of the study area dated to 2009. (B) Geomorphological interpretation of the Lantmäteriet orthorectified image

5.3 Site specific methodology

Ground penetrating radar surveys were completed in spring 2013 using the methods outlined in section 2.4. Surveys were undertaken transverse to the orientation of the moraine, surveying from the ice-proximal to ice-distal slope (Profiles 1-6) and also approximately parallel to the moraine crestline surveying from an up-glacier to down-glacial position (Profile 7). Surveys were undertaken uniformly across the moraine to optimise the coverage.

The morphology of the moraines was assessed using high-resolution topographic data derived from 12 UAV surveys. The target flight altitude for the UAV was 100 m. Two DEMs are produced; one for the north-lateral-frontal moraine and one for the southern-lateral-frontal moraine (Fig. 5.3). GCPs were surveyed using a Leica Builder 300 total station. Following chapter 3 A3 paper targets were used as GCPs. The southern-lateral-frontal DEM was derived from 586 images. The total RMSE on this dataset following the application of 10 GCPs was reported at 0.08 m. The northern-lateral-frontal DEM was derived from 765 images. The total RMSE on this dataset following the application of 25 GCPs was reported at 0.06 m. Both DEMs were exported at a spatial resolution of 0.5 m per pixel. As the total station SfM ground control points used an arbitrary coordinate system, the resulting elevation data was georeferenced to SWE99TM using affine transformation (rotation, skew, scaling) in ArcGIS version 10.2.1. In practice, transformation introduced additional positional errors into this dataset, thus was

undertaken for illustrative purposes only (see Fig. 5.3) to enable the positions of sedimentological and geophysical surveys to be plotted over the resulting SfM datasets. Georeferencing was conducted using boulders visible on the high resolution topography and a 0.5 m spatial resolution Lantmateriet aerial image dated to 2009. All height data remains on an arbitrary datum. The datasets from Isfallsglaciären are produced solely to characterise the morphology of the lateral-frontal moraine, however future re-analysis of the dataset to quantify morphometric change is possible where independent data validation is conducted.

Sedimentological surveys follow the methods outlined in section 2.5. Clast macrofabric analysis was, however, not conducted at this site. Where coarse boulder facies were identified, surface sampling was undertaken as detailed in Section 2.5.3.2.

5.4 Results

5.4.1 Radar-wave velocities

Semblance analysis was conducted on 9 WARR, and 2 CMP datasets to obtain radar-wave velocities (Table 5.1; Fig. 5.3). Surveys were completed at various positions across the Isfallsglaciären moraines (Fig. 5.3; Table 5.1). Inner-frontal surveys A and D appear to be in agreement, providing values of 0.11 and 0.12 m ns⁻¹ at each site. Excluding survey B which shows high velocities of 0.22-0.23 at <50 ns, the inner-frontal ridge provided radar-velocity values of 0.10 and 0.11. The southern-lateral-frontal complex was broadly found to exhibit higher propagation velocities at depth, typically ranging from 0.13-0.19 m ns⁻¹ (Table 5.1). Site I was the exception, where radar-wave velocities as low as 0.10-0.11 m ns⁻¹ were found to occur at c. 70 ns. Sites F, G, H, J, and K have clear returns between 0.20 and 0.30 m ns⁻¹. These returns are restricted a time window of <70 ns. Example plots demonstrating the variable radar-wave velocities are presented in Fig. 5.4.

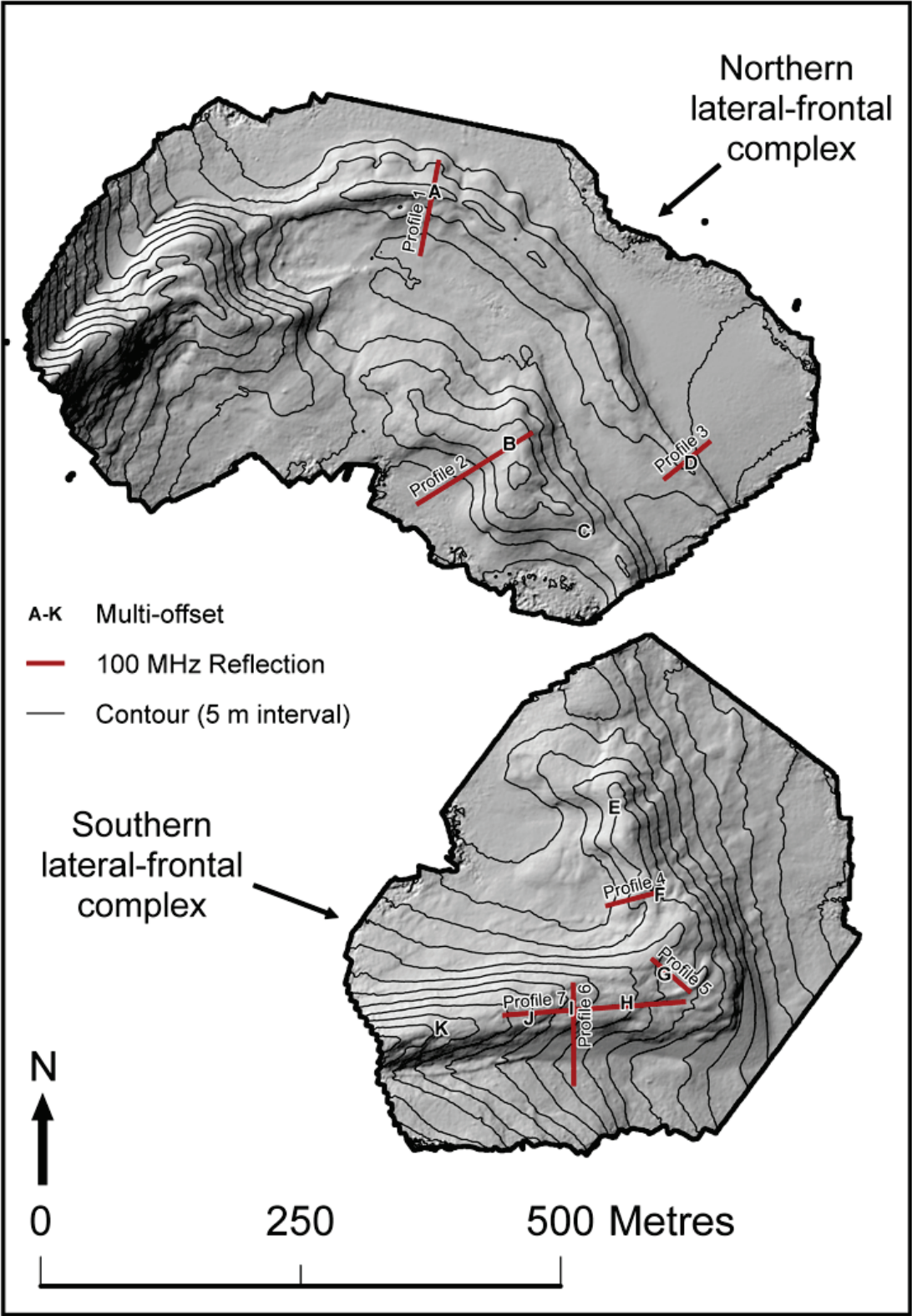


Fig. 5.3 High-resolution topographic data and the locations of radar surveys undertaken in spring 2013.

Table 5.1 Summary table of radar-wave velocities on the Isfallsglaciären moraines derived from semblance analysis.

DEM zone	Survey	Velocity (m ns ⁻¹)	Survey Configuration
Northern lateral-frontal	A	0.11-0.12	WARR
Northern Inner-frontal	B	0.22-0.23	WARR
Northern Inner-frontal	C	0.11	WARR
Northern lateral-frontal	D	0.11-0.12	WARR
Southern lateral-frontal	E	0.10	WARR
Southern lateral-frontal	F	0.14-0.15	WARR
Southern lateral-frontal	G	0.13-0.19	WARR
Southern lateral-frontal	H	0.13-0.19	WARR
Southern lateral-frontal	I	0.10-0.11; 0.13-0.15	CMP
Southern lateral-frontal	J	0.15-0.16	WARR
Southern lateral-frontal	K	0.14-0.17	CMP

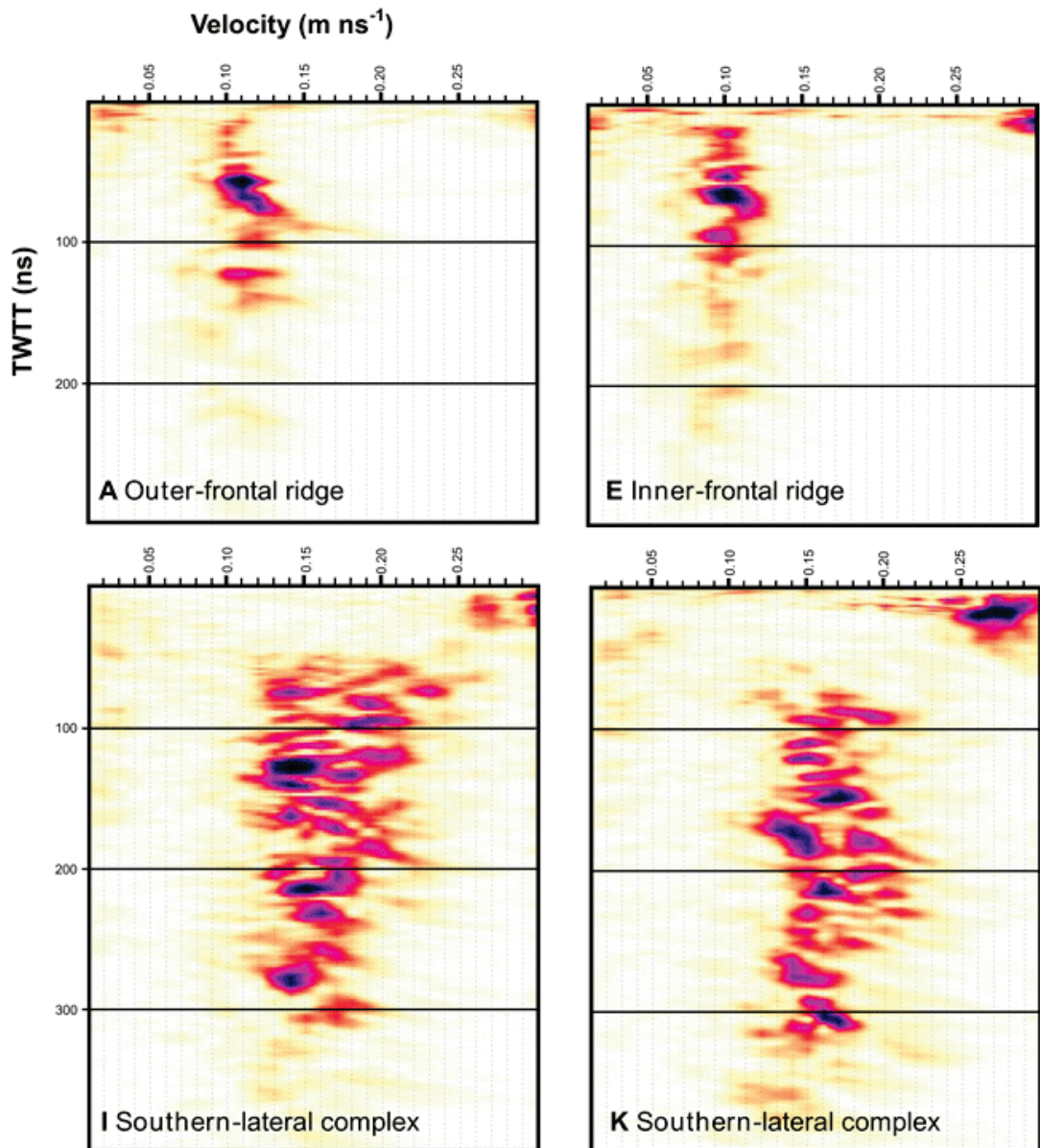


Fig. 5.4 Exemplar WARR and CMP surveys demonstrating contrasting sub-surface conditions on the southern-lateral complex and frontal moraines. Patches of purple indicate clustering of stacked GPR velocities (e.g. the average propagation velocity which reflect the sub-surface sedimentology and characteristics). The frontal ridges show slower velocities ($\sim 0.11 \text{ m ns}^{-1}$) than lateral ridges ($0.15 \text{ to } 0.17 \text{ m ns}^{-1}$) indicating different subsurface conditions.

5.4.3 Internal structure

5.4.3.1 Overview

Seven 100 MHz reflection profiles were surveyed to investigate the internal structure of the Isfallsglaciären moraines (Fig. 5.3; Fig. 5.5). Below, key structural features are discussed. A summary of the seven profiles is presented in Table 5.3.

5.4.3.2 Northern lateral-frontal complex

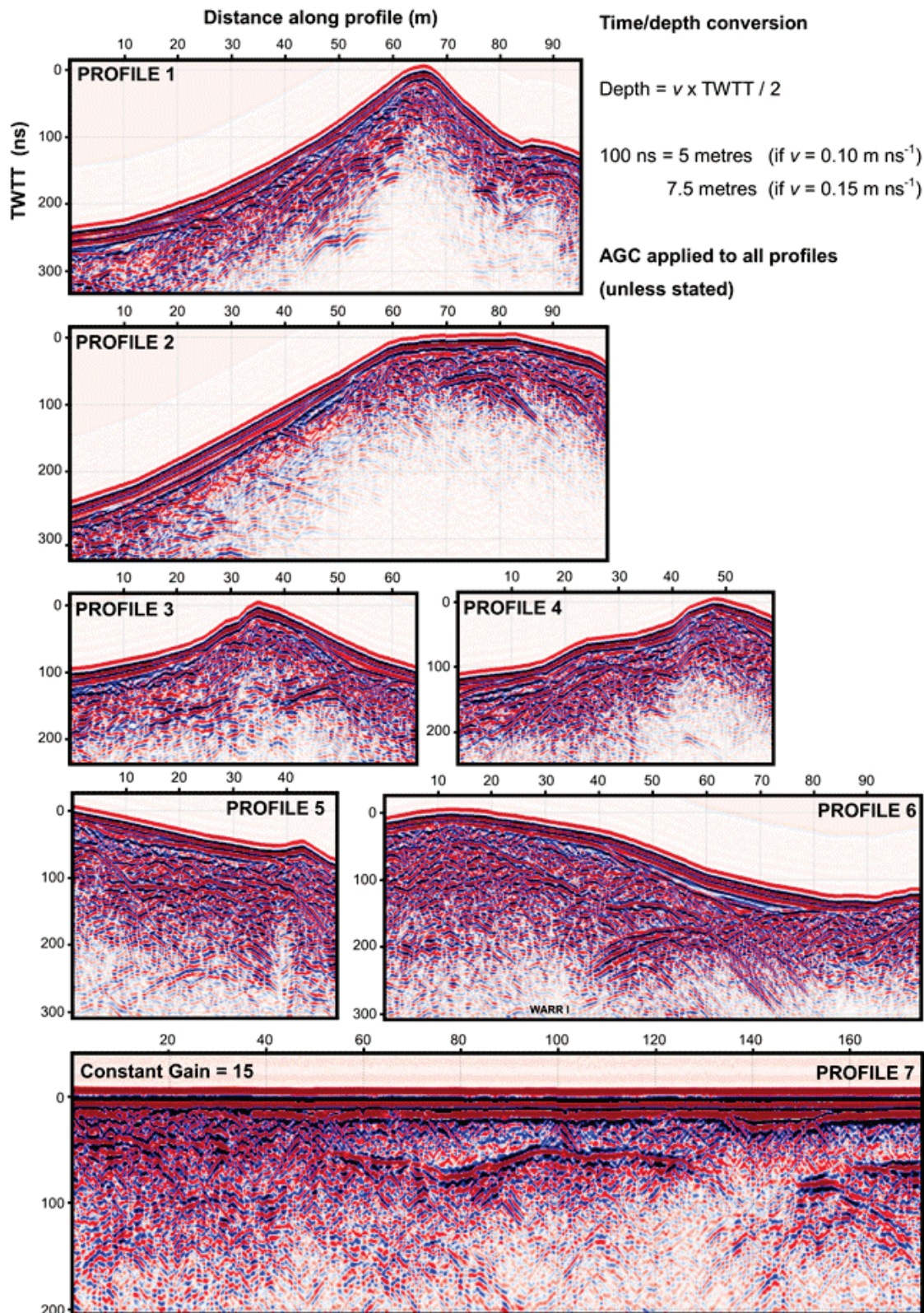
The northern outer-frontal ridge is presented in profiles 1 and 3 which both run transverse to the ridge crestline (Fig. 5.3; Fig. 5.5). Profile 1 appears to be more structurally diverse. The proximal slope of the landform is intersected by a clear up-glacier dipping reflector. Below this reflector a series of discontinuous, wavy up-glacier dipping reflectors are also visible. Additional reflectors are present between 23-30 m, and are contiguous with both ground and air wave. Reflectors within the crest of the landform are irregular and hyperbolic. On the distal slope of this landform, coherent, continuous reflectors are visible within a topographically prominent hummock. A double of this feature is also present c. 200 ns. Despite the application of AGC, structure is poorly defined at depth within the main ridge. Profile 3 displays multiple overlapping hyperbolic point diffractions and irregular medium and high amplitude reflectors. Unlike profile 1, a partially coherent down glacier dipping reflector appears to dissect the feature between c. 27 and 35 m and also corresponds with a change in surface morphology. Up-glacier dipping reflectors are present at depth within the landform and can be seen c. 20-30 m and 40-50 m along the profile.

The inner-frontal ridge was surveyed in profiles 2 and 4 (Fig. 5.3; Fig. 5.5). The crestline of profile 2 is overprinted with subglacial flutes. The main features of structural interest within this profile are coherent, high amplitude reflectors which are visible between c. 67 and 96 m. The reflectors run sub-parallel with the moraine surface, before dipping down-glacier. A second less coherent reflector is present at 88-96 m.

5.4.3.3 Southern-lateral-frontal complex

Profile 4 presents the sub-surface structure of the southern-lateral-frontal complex prior to where the ridge adjoins the lateral section of the landform (Fig. 5.3; Fig. 5.5). Atypical of other reflection surveys, continuous reflectors can be seen running sub-parallel to the

moraine surface. At 28 m along this transect two coherent reflectors can be seen to cross-cut each other. A radar facies characterised by irregular reflectors and overlapping hyperbolic point diffractions can be seen both above and below these coherent reflectors. Profiles 5, 6 and 7 display the sub-surface structure of the southern-lateral complex (Fig. 5.3; Fig. 5.5). Profile 5 runs oblique to the landform (but approximately parallel to the inferred direction of former ice-flow). Similar to other profiles, profile 5 displays hyperbolic (presumably related to subsurface point diffractions) and irregular reflectors. Reminiscent of profile 2, two coherent subsurface reflectors which initially run parallel sub-parallel to the moraine surface, and subsequently dip down glacier and are visible between c. 0-14 m and 25-47 m respectively. The resolution afforded by the use of 100 MHz antenna does not permit detailed imaging of structure within an arcuate nested ridge located on the moraines surface, however at the available resolution, reflectors can be described as irregular and discontinuous, with no clear preference in terms of alignment. Profile 6 runs transverse to the southern lateral moraine complex. Here, the main structural feature is a moderately continuous reflector at depth within the moraine. This reflector appears to run sub-parallel to the moraine surface and is both over- and underlain by hyperbolic, chaotic and irregular radar facies. A snowbank can be distinguished on the ice-distal slope of the landform. The base of the ice-distal slope is characterised by multiple strong point diffractions. Profile 7 runs approximately parallel to the ridge crest of the southern-lateral complex (Fig. 5.3; Fig. 5.5). The main structural feature of interest within this profile can be seen between c. 50 and 130 m along the profile and is located in the c. 50 to 70 ns time window. This feature runs sub-parallel to the moraine surface and appears to dissect an upper radar-facies consisting of hyperbolic and irregular point diffractions. A less coherent (partially due to the hyperbolic nature of the overlying radar-facies) continuation of this radar surface is present between 0 to c. 20 m at c. 45 ns.



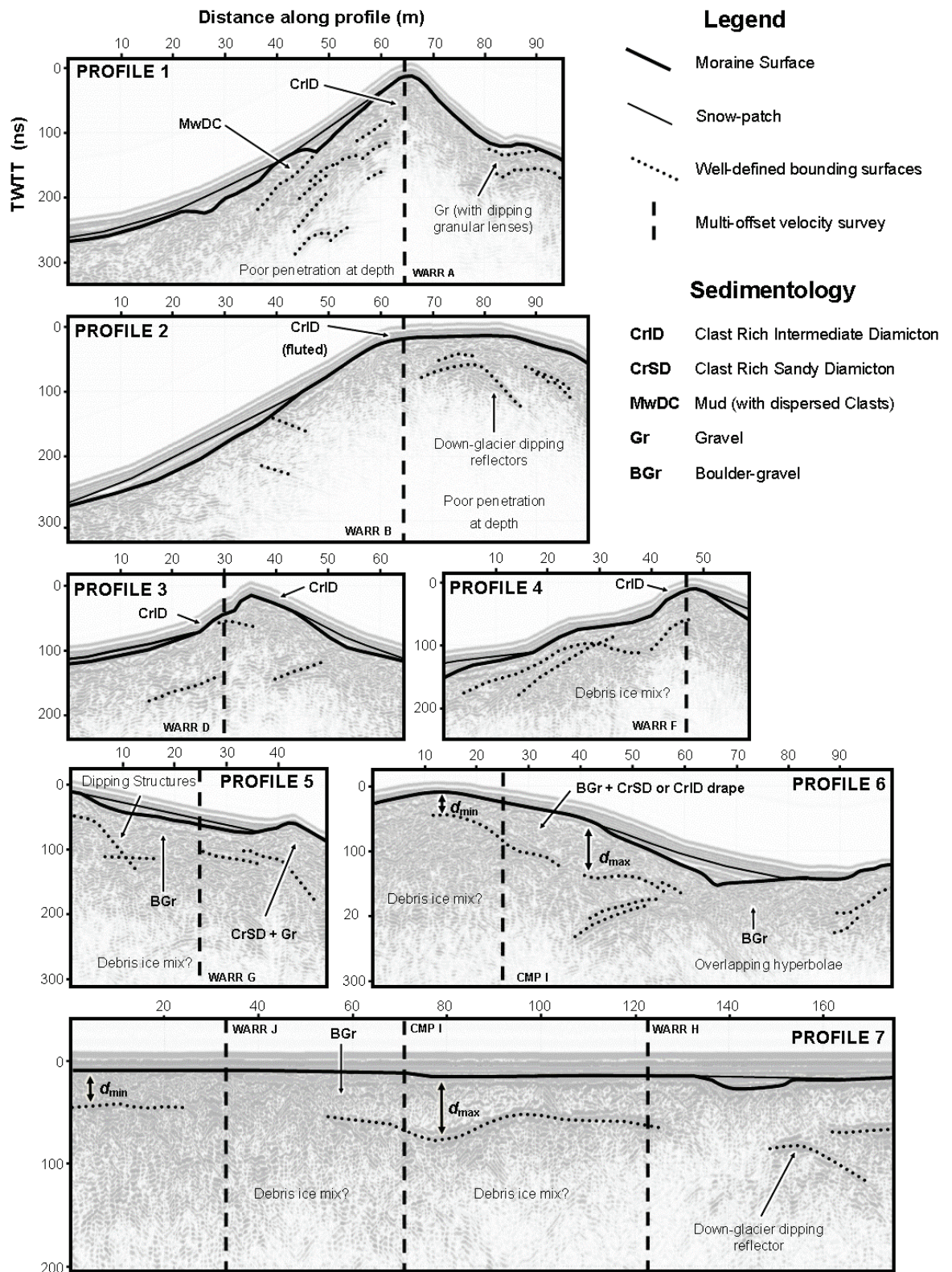


Fig. 5.6 Interpreted radargrams with surface sedimentology and velocity surveys highlighted. The radargrams were qualitatively assessed and coherent reflectors were digitised.

5.4.4 Sedimentology

Lithofacies found within the Isfallsglaciären moraines are summarised in Table 5.3 and Fig. 5.7 and are described below. The position of lithofacies in relation to the 100 MHz reflection transects are also highlighted in Fig. 5.6.

5.4.4.1 Southern lateral-frontal complex

The most abundant lithofacies on the southern-lateral complex is boulder-gravel. The sedimentology of this facies was assessed via five surface surveys at various positions along the moraine complex in proximity to profile 7. In this unit the clast intermediate axis were found to range in size from 0.03 m to 1.67 m. Sampled boulder gravels fall within the VA, A and SA roundness categories. The modal category is not consistent between boulder-gravel sample sites, with an increase in the SA component and corresponding decrease in the RA component down-moraine (% RA = 48-96; % SA = 4-52; $n = 5$). Isolated ice-proximal boulders were found to exhibit a polished finish, with well-defined striae. Whilst these facies have little or no interstitial component, occasional patches of fine and granular material were observed in proximity to disintegrating clasts of amphibolite. Isolated draped units of angular clast-rich intermediate or sandy diamicton are found to intersperse this boulder-gravel facies. A water-saturated clast-rich intermediate diamicton facies were identified above a melting moraine-distal snow-patch. The sedimentology of the prominent nested arcuate ridge visible in profile 5 was investigated (Fig. 5.3; Fig. 5.6). Here, a clast-rich sandy diamicton with granular lenses is overlain by deposits of gravel and sand with dispersed clasts. All clasts within this ridge are unstriated and predominantly angular (% RA = 62-86).

5.4.4.2 Northern lateral-frontal complex

The north lateral ridge contains a range of lithofacies including gravel (with muddy component), sandy gravel, and clast-rich sandy diamicton. Poor field conditions prohibited the collection of GPR data from this area. Clasts sampled from these facies exhibit highly angular morphology (% RA = 86-94), but surprisingly low C_{40} values (18-26). All facies appear to be massively structured. Evidence of ice-proximal slope failure is identified on this ridge, revealing an exposure of sandy gravel. An additional facies of boulder-gravel was found in the upper reaches of the moraine before it anastomoses. This

facies exhibits an almost exclusively very angular and angular clasts (% RA = 98) with intermediate axis that range between 0.07 and 1.25 m in length.

Investigations revealed six lithofacies in proximity to the northern-lateral-frontal zone which are detailed in profile 1 and WARR A (Fig. 5.3; Fig. 5.5). On the distal hummocks, lithofacies include crudely stratified sandy gravel and sand interspersed with alternating muddy or gravelly lenses that gently dip down-glacier. Clasts contained within the sandy gravel and down-glacier dipping gravelly lenses exhibit angular morphologies (% RA = 72-80) and are unstriated. The crest of the landform is composed of a clast-rich intermediate diamicton, containing clasts with moderate angularity (% RA = 52) and striae (12%). Three sedimentary units are superimposed onto the ice-proximal slope. These include a mud with dispersed clasts. Clasts within this unit show moderate angularity (% RA = 62) and are 12% striated. Two ice-proximal diamicton (clast-rich sandy, and clast-rich muddy) units were also found adjacent to the mud with dispersed clasts. Clastic material in both facies is unstriated, and exhibit moderate angularity (% RA = 60).

Four exposures were assessed on the outer-frontal ridge. The internal structure of this feature is investigated in profile 3 and by WARR D (Fig. 5.3; Fig. 5.6). These moraines appear to be uniformly composed of a clast-rich intermediate diamicton. Samples here show some edge rounding (% RA = 60-76) in comparison to supraglacial controls (Fig. 5.6a), they are however are unstriated. The distal slope of the outer-frontal ridge contains a boulder-drape.

Excavations on the inner-frontal ridge revealed lithofacies of clast-rich sandy and intermediate diamictons interspersed with granular lenses (profiles 2 and 4). These appear to show slightly reduced angularity (% RA = 46-60) in comparison to the outer-frontal ridge and are up to 8 % striated. Flutes are superimposed (i.e. in proximity to radar profile 2) onto this landform.

Table 5.2 Summary table of sedimentary facies within the Isfallsgläciären moraine complex.

Lithofacies	Relative Abundance	% RA	% C ₄₀	% Striated	Matrix (<2mm fraction)		
					% Sand	% Silt	% Clay
Clast-rich sandy diamicton	*****	62-100	12-38	0-2	71-89	9-26	2-3
Clast-rich intermediate diamicton	*****	46-84	12-32	0-12	47-64	31-44	3-10
Clast-rich muddy diamicton	*	60	18	0	24	68	8
Gravel	****	66-94	10-26	0	55-80	18-35	2-10
Sandy gravel	*	92	18	0	92	6	2
Boulder gravel	*****	48-100	--	0-2	--	--	--
Mud (with dispersed clasts)	*	64	14	12	8-28	66-80	5-12
Sand (with dispersed clasts)	*	86	14	0	66	28	6

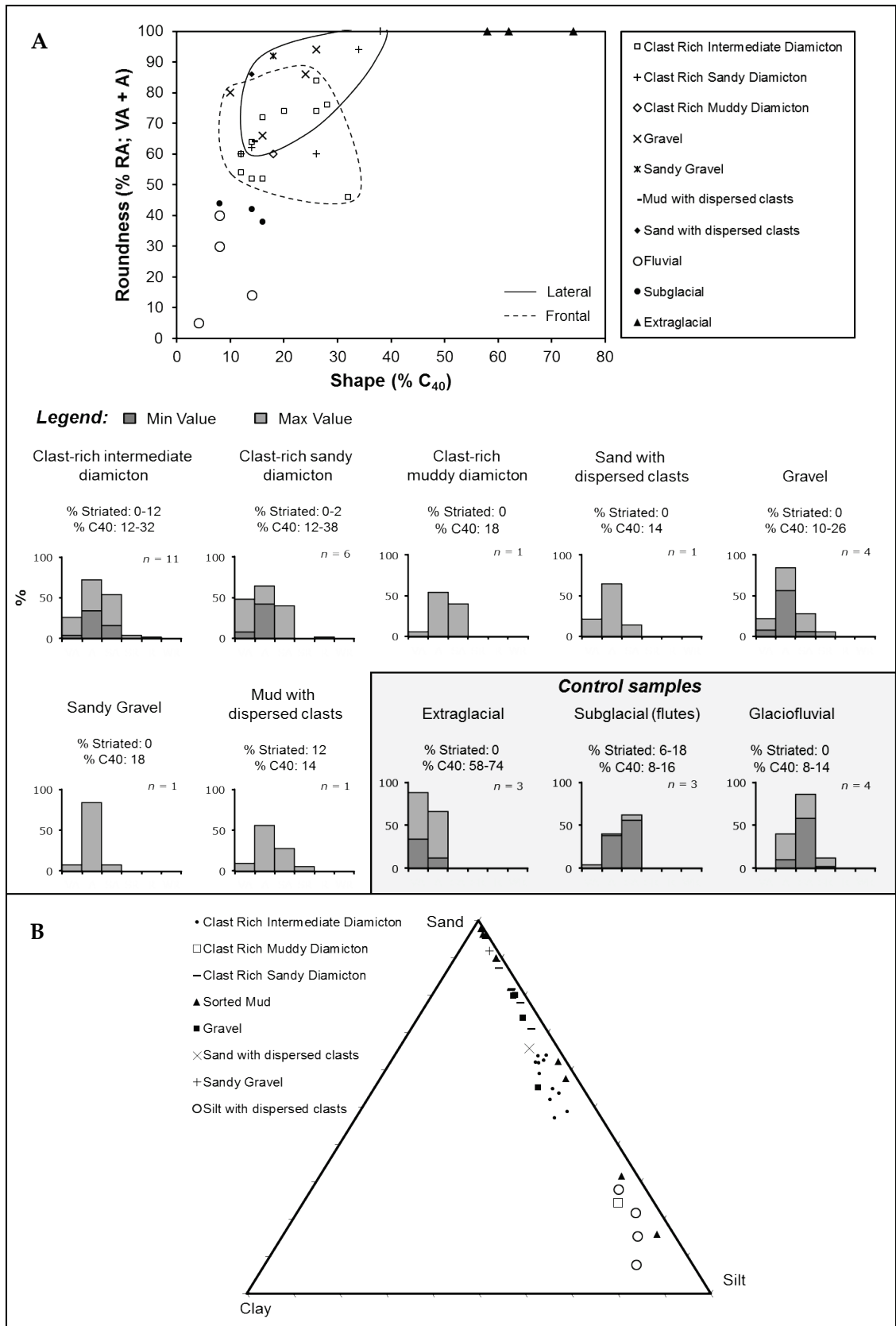


Fig. 5.7 (a) Clast form and (b) matrix particle size of lithofacies within the Isfallsgläciären moraines. Sampled material has a limited clay content.

5.5. Interpretation

5.5.1 Radar wave velocities and likely composition

Moraine composition appears to vary spatially across the lateral-frontal complex. Velocities from the outer-frontal ridge (surveys A and D; 0.11-0.12 m ns⁻¹; Fig. 5.7) were found to correspond with deposits of clast-rich intermediate diamicton. Radar-wave propagation velocities vary depending on their saturation and thermal state (e.g. frozen or unfrozen) (Neal, 2004; Lukas and Sass, 2011). Schwamborn *et al.* (2007) found frozen diamicton (with 10% pore water) to have a radar-wave velocity of 0.125 m ns⁻¹ (determined from a CMP survey). This contrasts with unfrozen diamictons and till which can exhibit variable propagation velocities ranging between 0.06-0.09 (e.g. Burki *et al.*, 2010; Lukas and Sass, 2011). Given that the moraines were frozen at the time of the survey, slightly higher velocities are to be expected, especially if sediment is partially saturated prior to winter freezing. The frontal moraine is, therefore, suggested to be debris dominant in composition (Table 5.3), although lower frequency surveys (e.g. 50 MHz or less) may achieve greater propagation depths, and allow for additional sub-surface conditions to be determined. High concentrations of silt are associated with poor signal penetration (e.g. Overgaard and Jakobsen, 2001). This is evident in profiles composed of clast-rich intermediate diamicton which become highly attenuated at depth. Sub-surface conditions at site B relate to known velocities for polar snow (0.194–0.252 m ns⁻¹; Reynolds, 2011), and appear to mask the radar signature of the clast-rich intermediate diamicton found in proximity to this survey.

The structural composition for the southern-lateral complex is unclear. Here, the wide range of radar propagation velocities are likely to relate to variability in terms of the porosity, amount of interstitial ice and fine material within the landform. Given the coarse nature of the surficial sediments (boulder-gravel facies) and known inclusion of ice within the landform (e.g. Østrem, 1964), radar-wave velocities derived from rock-glaciers are likely to serve as a useful proxy for sub-surface composition. For example, Monnier and Kinnard (2013) explain velocities of 0.15-0.17 m ns⁻¹ within surficial deposits of rock glaciers as evidence of significant quantities of air (high porosity), and calculate that a velocity of 0.16 m ns⁻¹ are equivalent to 22% air content. Whilst this may explain high-velocities within up-glacier sections of the Isfallsglaciären southern lateral moraine, similar velocities are also identified at depth (<100 ns) within the landform. Values

ranging between 0.13 and 0.19 m ns⁻¹ are therefore interpreted to indicate a variable composition at depth. Buried glacier-ice at the margins of high-Arctic glaciers may produce velocities of 0.15-0.17 m ns⁻¹ (Brandt *et al.*, 2007; Midgley *et al.*, 2013). However, the ice within the southern-lateral complex is suggested to originate as a moraine distal-snowbank (Østrem, 1964). As the snow is likely to be of considerable age (potential age ranging from centuries to millennia; e.g. Karlén, 1973), recrystallisation, compression and mixing with debris may have occurred, resulting in lower than expected radar-wave propagation velocities for snow.

Table 5.3 Summary table of radar profiles and their characteristics.

P ¹	Zone ²	Radar-surface geometries ³	Radar facies	Signal attenuation	Likely composition
1	OF	DuG; Sh	Chaotic	High	Debris
2	IF	DdG; Sh	Chaotic	High	Debris
3	OF	DuG; DdG	Chaotic	High	Debris
4	IF	DuG; Sh	Chaotic	Moderate	Debris-ice mix
5	SLF	DdG	Chaotic; Hyperbolic	Low	Debris-ice mix
6	SLF	DdG; Sh	Chaotic; Hyperbolic	Low	Debris-ice mix
7	SLF	DdG; Sh	Chaotic; Hyperbolic	Low	Debris-ice mix

¹ Profile number

² OF = Outer-frontal, IF = Inner-frontal and SLF = Southern lateral-frontal complex

³ DuG = dipping up-glacier; DdG = dipping down-glacier; Sh = subparallel to the moraine surface

5.5.2 Internal structure and sedimentology

Sub-horizontal reflectors such as those seen in profile 7 are likely to indicate the interface between the surficial deposits of diamicton and boulder-gravel, and frozen sediment and ice at depth. This interpretation is also partially based on the field-observations of Østrem (1964), who excavated the southern-lateral complex, and found ice at 2.2, 2.5 and 2.8 m depth. Results of the radar surveys are in broad agreement with these findings. The estimated depth to the reflector, thus thickness of the upper surface layer (USL) in question ranges from between 2.25 (d_{\min}) and 4.5 (d_{\max}) metres in profile 7, and on the distal slope of profile 6 is located up to 6 m below the moraine surface (Fig. 5.5; Table 5.4). Karlén (1973) suggested that structurally, the moraines consist of imbricately stacked units of poorly sorted glacial sediment ('drift sheets'). Given this scenario, it is reasonable to assume that up-glacier dipping reflectors to highlight bounding layers between stacked sediment units within the radar transects. Such bounding layers would represent a change in sedimentology related to wash/aeolian lag or cryoturbation surfaces (e.g. Etienne *et al.*, 2003) where stacked sedimentary units are subject to surface processes prior to subsequent burial during a later glacier advance. However, such structures are not ubiquitous across the moraine complex, with some profiles conversely exhibiting down-glacier dipping structures (profiles 2, 3 and 5).

Table 5.4 Estimated thickness for the USL. The locations for d_{\min} and d_{\max} are presented for each profile in Fig. 5.3.

Profile	USL Thickness (ns)	Velocity	Estimated USL Thickness (m)
7	$T_{\min} = 30$	0.15 m ns^{-1}	$d_{\min} = 2.25$
	$T_{\max} = 60$		$d_{\max} = 4.50$
6	$T_{\min} = 30$	0.15 m ns^{-1}	$d_{\min} = 2.25$
	$T_{\max} = 80$		$d_{\max} = 6.00$

Profile 1 provides a clear example of where sedimentary units have been deposited on the ice-proximal slope of an existing moraine ridge. Here, the main moraine ridge is massively structured and consists of a clast-rich intermediate diamicton sourced from a presumed combination of sub- and supraglacial transport pathways. Subsequent recession of the glacier margin forms terraces of massive mud with dispersed clasts on the ice-proximal slope of the outer ridge with clasts showing moderate angularity and

striae, indicating a mixed transport history. The distal-slope moraine hummocks are interpreted as ice-contact fans resulting from both gravitational flows and glacio-fluvial deposition (e.g. Lukas, 2005), with the position of individual coalescing hummocks controlled by former supraglacial debris concentrations and the distribution of supraglacial drainage systems (e.g. Krzyszkowski and Zieliński, 2002). The alternating gravelly and muddy lenses indicate changing energy-level related to a variable supply of water to the ice-contact feature. The largely angular, unstriated character of clasts within gravelly lenses highlight a potential supraglacial transport origin (% RA = 72) for debris within this ridge. The geochronology of the distal hummocks are unclear.

However, ice-proximal deposition appears to be spatially limited across the ridge. The morpho- and lithostratigraphic relationships between sedimentary units suggest that at profile 3 the glacier partially overrode an existing ridge, resulting in two stacked units of clast-rich intermediate diamicton of different ages, and a coarse bouldery drape on the distal slope of the landform. For the southern-lateral complex, the limited reflectors revealed by the 100 MHz radar survey are interpreted as evidence of a predominantly coarse and massive structural configuration. Nested ridges and similar dipping structures (e.g. profile 5) to those documented on the frontal-ridge are interpreted as evidence of overriding and distal deposition on the southern-lateral complex. Small moraine ridges such as the arcuate ridge visible in profile 5 can develop in response to the dumping, pushing or squeezing of material at the ice-margin (e.g. Price, 1970; Birne, 1977; Boulton and Eyles, 1979; Bennett, 2001; Krüger *et al.*, 2010), or the freeze on of sediment related to annual oscillations of the ice-front (Krüger, 1995). Unstriated and angular clast-rich sandy diamicton with linear granular lenses and sand-rich gravels within the moraine may indicate a supraglacial and glacio-fluvial origin related to the dumping of material from the ice-margin, with sorted linear lenses representing wash horizons. Pushing as a moraine forming mechanism is unlikely here as (1) dominant ice-proximal sediments are dissimilar to those contained within the ridge; (2) coarse angular boulder facies have high shear strengths, thus are not particularly conducive to push moraine formation (Cook *et al.*, 2013), and (3) granular lenses are linear in form and lack displacement structures associated with ice-marginal stress.

5.6. Discussion

5.6.1 Development and chronology of moraines at Isfallsglaciären

Conceptually, Isfallsglaciären is clearly distinguishable from alpine temperate glacial landsystems which produce distinct asymmetric ice-contact ramps resulting from the flowage of debris from supraglacial positions (Humlum, 1978; Boulton and Eyles, 1979; Röthlisberger and Schneebeli, 1979; Small, 1983; Lukas and Sass, 2011; Lukas *et al.*, 2012). The morphological characteristics of the moraines share some similarity with multi-crested 'controlled' ice-cored moraine complexes documented to occur in some high-Arctic and Icelandic glacial landsystems (Evans, 2009; 2010; Ewertowski *et al.*, 2012; Midgley *et al.*, 2013). However, at Isfallsglaciären, debris supply and transport is likely to represent a constricting factor controlling moraine-formation. A key observation related to debris transport can be made from ground-level photography provided by Enqvist (1910; Fig. 5.8): the glacier surface appears to be relatively free of supraglacial debris leading to well-exposed subglacial sediments within the forefield (e.g. Pomeroy, 2014), however, debris can be seen emerging from subglacial and englacial debris pathways at the ice-front. Whilst Karlén (1973) disregarded the ground-level photography taken by Enqvist, the structural characteristics (down-glacier dipping structures) lend support to the hypothesis of overtopping and distal deposition of debris. Assuming the ice-margin remains stable over multiple years, mixtures of debris and potentially distal snow may be distally incorporated into the structure of the moraine or a drape of debris may be deposited over a pre-existing snowbank (e.g. Østrem, 1964; Fig. 5.9). However, given the limited supraglacial debris visible in the 1910 ground-level photography, the ice-margin would need to remain stationary over a considerable period of time for efficient moraine construction (Boulton and Eyles, 1979; Benn *et al.*, 2003; Benn and Evans, 2010).

Topographic influences on glacier geometry by pre-existing moraine ramparts is an important factor controlling styles of moraine development (e.g. Spedding and Evans, 2002; Barr and Lovell, 2014). For the neighbouring Storglaciären, initial moraine formation c. 2500 yrs BP is suggested (Karlén 1973; Ackert 1984; Etienne *et al.*, 2003). On the assumption that the Isfallsglaciären moraines formed analogously, the landforms are highly likely to have exerted a topographic influence on later glacier advance stages. Glacier advances between 2700 and 2000, 1900 and 1600, 1200 and 1000, and 700 and 200 cal. years BP are suggested for Northern Sweden by Karlén and Kuylenstierna (1996) with

the valley glaciers attaining their largest Little Ice Age extent during the 17th and 18th centuries (e.g. Karlén, 1988; Nesje, 2009). Further known ice-marginal positions demarcated by the previously discussed historical ground-level photography (e.g. Enqvist, 1910) and by measurements from 1915 provided by Hamberg *et al.* (1930) which highlight sustained overriding of the inner moraine ridge, over a five year period between 1910 and 1915 (see Schytt, 1959 for a full review of historical glacier records). Whilst overriding is clearly important for the development of the inner-ridge (Fig. 5.9), differences in terms of the size and morphology of the north-lateral ridge are indicative of additional ice-marginal processes. The topographic prominence of this ridge is likely to have restricted the lateral extent of Isfallsglaciären during its various Neoglacial advances leading to proximal stacking of glacial debris (e.g. as argued for by Karlén, 1973), with potential push-deformation mechanisms that have been applied to the high-alpine moraine complexes of southern-Norway likely to be relevant here (e.g. Matthews and Shakesby, 1984; Shakesby *et al.*, 1987; 2004; Matthews *et al.*, 2014). Unfortunately, no geophysical data was obtained from this ridge to confirm this assertion.

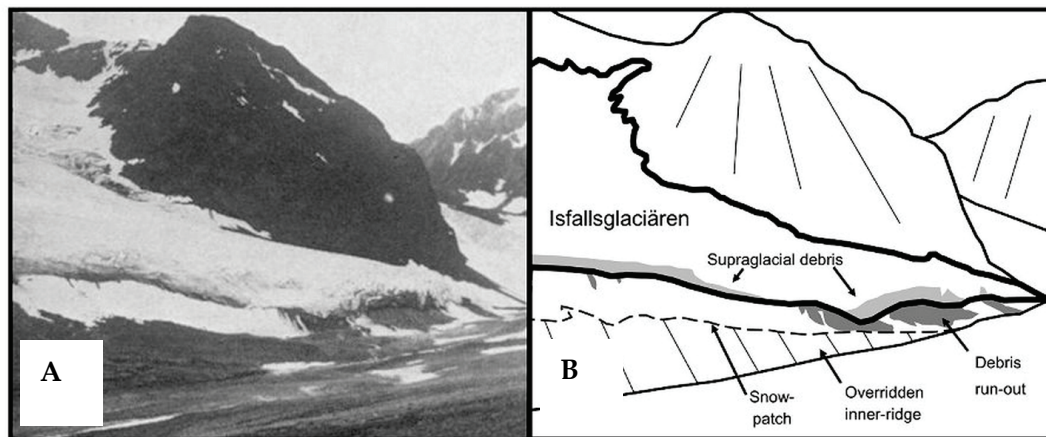


Fig. 5.8 (A) Ground-level photography taken by Enquist in 1910. (B) Interpretation of the ground-level photography showing debris run-out over the moraine distal slope of the inner-frontal ridge.

It is clear that the Isfallsglaciären moraines relate to a range of topographically controlled ice-marginal processes that operated in a spatially variable manner along the former ice-front. The moraines are, therefore, polygenetic as a result of the repeated reoccupation of ice and may be described as ‘palimpsest’ features. Unlike active temperate glacier margins where the sedimentary signature of proglacial deformation is well preserved,

the coarse nature of the deposits can be seen as a prohibitive factor, limiting registration of certain ice-marginal processes within the terrestrial geomorphological record.

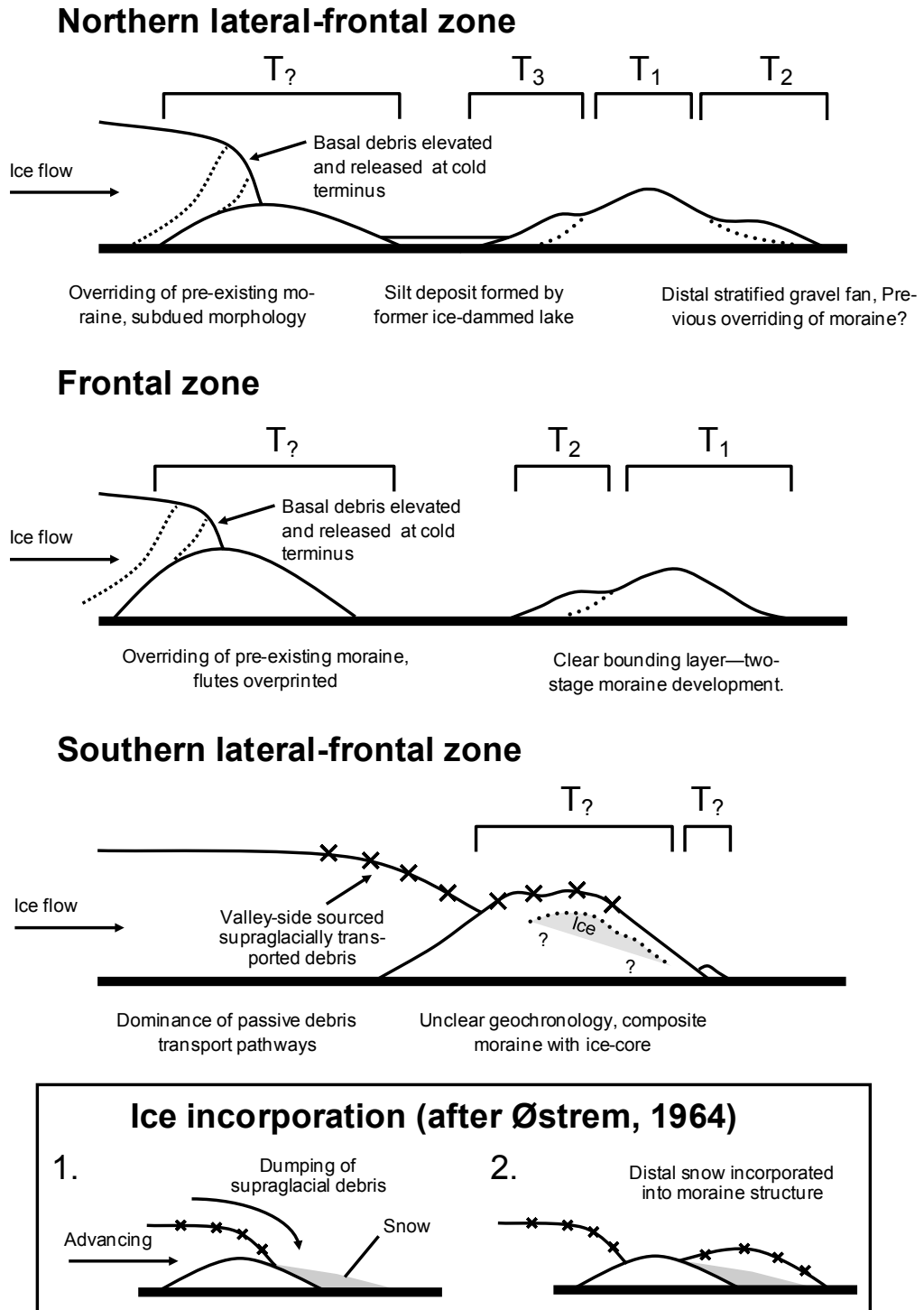


Fig. 5.9 Conceptual model for the development and chronology of moraines at Isfallsglaciären.

5.6.2 Reconciling existing geochronologies and structural data

It is worth noting that the lichenometric trends identified by Karlén (1973) may be misleading in terms of their environmental and geomorphological significance. It is probable that the extensive coverage of ice-marginal snowbanks visible within historical photography would have either served to limit the growth of lichens on the lateral-frontal complex or alternatively kill off and remove any pre-existing lichens (Benedict, 1993). Recently the use of lichens to produce robust absolute dates has been criticised, with ages >160 years suggested to be spurious (Osborn *et al.*, 2015). However, to date, the only dating evidence relating to moraine chronologies for Isfallsglaciären are developed from lichenometric data provided by Karlén (1973).

Hormes *et al.* (2004) presented radiocarbon dates from a small valley glacier c. 6 km north of Isfallsglaciären. Unlike many moraine systems in the Kebnekaise region, palaeosol were identified within the stratigraphy of these landforms. From the analysis of organic material, Hormes *et al.* (2004) advocated four periods of soil formation at Nipalsglaciären: 7800–7580, 6300–4080, 2450–2000 and 1170–740 cal. yr BP. Similar responses of Isfallsglaciären during these periods are likely. However, it is acknowledged that the two glaciers will respond differently to environmental change due to differences in the aspect, hypsometry and topography. However, in the absence of robust dating controls at Isfallsglaciären, and issues related to censoring (e.g. Gibbons *et al.*, 1984), moraine chronologies will remain uncertain. Further work could apply additional dating controls (e.g. Schmidt hammer dating, exposure dating), however, issues related to the recycling of glacial debris, and overriding of pre-existing materials may also result in problematic or inconclusive datasets. Future work to document structural characteristics of a wider range of Scandinavian moraines is a worthwhile endeavour, which may further assist understanding of their glaciological significance. In summary, it is suggested that current evidence used to construct Neoglacial moraine chronologies at the margins of glaciers in the Kebnekaise region are currently insufficient. A combination of moraine overriding, by the most recent glacier advance stages serve to further conflate the issue. Without new geochronological work, models of landform development should be considered sceptically at best.

5.6.3 *The potential of high-resolution topographic data for future research*

The de-icing of ice-cored moraines have been documented in a range of glacial environments (Schomacker and Kjær, 2007; Irvine-Fynn *et al.*, 2011; Tonkin *et al.*, 2016; chapter 6). However, to the author's knowledge no recent quantitative observations of de-icing have been made on the 'Østrem' type moraines studied here. The high-resolution dataset can, therefore, be used as a benchmark for future geomorphological studies on these moraines. Whilst the current debris cover may permit limited melting of incorporated ice, future climatic amelioration may promote further melting.

5.7 Summary

Similar to high-Arctic ice-cored moraines, buried ice is restricted to lateral zones of the moraine complex. The frontal moraines appear to be debris dominated and are predominantly composed of a clast-rich intermediate diamicton. The landforms are multicrested in form. It is unclear whether the ridges represent former ice-marginal positions resulting from late Holocene glacier readvances or the transmission of stress onto pre-existing moraine ridges ('push deformation moraine').

GPR data appear to demarcate the spatial extent and depth at which ice within the southern-lateral complex is buried. Radar-depth conversions are in broad agreement with the reported findings of Østrem (1964). Given that previously destructive methods were used to investigate moraine structure, the GPR is shown to be a valuable tool for documenting the structure of glacial landforms. Nine main lithofacies are identified within the lateral-frontal moraine complex. Lateral facies are notably coarse and angular, whereas, frontal deposits are predominantly composed of massive clast-rich intermediate diamicton which exhibit evidence (e.g. striae, sub angularity) of active glacial transport.

The topography appears to have exerted a strong control on the resulting landform structure with morpho- and stratigraphic relationships between sedimentary units indicative of synchronous proximal enlargement and overriding and stacking of sedimentary units at various position along the former ice-front.

Further research to apply additional dating controls on the moraines (e.g. Schmidt Hammer exposure dating), and assessment of the internal structure of further ice-cored moraine complexes is recommended and would facilitate future interpretations of the geomorphological record in this region.

6. Structural character, sedimentology and evolution of a high-Arctic lateral-frontal moraine: Austre Lovénbreen, Svalbard

6.1 Introduction

The morphology and character of ice-marginal landsystems developed at the margins of high-Arctic polythermal glaciers have been subject to considerable research (Boulton *et al.*, 1999; Bennett *et al.*, 2000; Sletten *et al.*, 2001; Lyså and Lønne, 2001; Lukas *et al.*, 2005; Lønne and Lyså, 2005; Ewertowski *et al.*, 2012; Ewertowski, 2014). One motivation for such research is that contemporary glacial landsystems can be used as analogues for former Quaternary glaciation occurring at lower altitudes (Hambrey *et al.*, 1997; Hambrey and Glasser, 2012). Specifically, some ice-marginal landforms and landsystems in high-Arctic settings have been suggested to bear some similarity to relict Younger Dryas glacial landforms found in the British Isles (Hambrey *et al.*, 1997; Graham and Midgley, 2000a; Graham and Hambrey, 2007). Specifically hummocky areas, which are considered by Evans (2009) to represent a type of ‘controlled’ moraine. However, the use of the high-Arctic glaciers as an analogue for the British Younger Dryas has been debated (Lukas, 2005a; Lukas, 2007; Graham *et al.*, 2007). A key area of uncertainty remains in regards to the preservation potential of ice-cored landforms following the completion of de-icing (Evans, 2009). Despite this, it is clear that glacier structure exerts a significant influence in resulting geomorphological signature. This is especially true for high-Arctic valley glaciers.

Evans (2009) promotes the term ‘controlled moraine’ as a descriptor for such ice-cored geomorphological systems. This term implies that englacial debris contained within the relict glacier ice will exert some influence on the resulting landform morphology, with landforms often exhibiting linearity related to incorporated debris structures within ice (Evans, 2009). Furthermore, Midgley *et al.* (2013) suggested that buried relict glacier-ice may serve as a useful proxy for past glaciological conditions. Determining former glaciological conditions is especially pertinent for aiding understanding of the potential

response of high-Arctic glaciers (including polythermal surge type glaciers) to future climatic amelioration.

This chapter examines the structure, sedimentology and geomorphology of lateral-frontal moraine developed at the high-Arctic glacier Austre Lovénbreen. The lateral-frontal moraine is investigated using a multi-proxy approach. The structure is investigated through the deployment of a 100 MHz ground-penetrating radar system (section 6.3.1). Glacier change is reported based off interpretation of historical aerial and ground-level photography (section 6.3.3). The results of a field sedimentological campaign are reported, providing data on debris transport at Austre Lovénbreen and for characterising the surficial debris drape of ice-cored landforms (sections 6.3.4 and 6.3.5). High-resolution topographic datasets documenting the evolution of the landform are reported (section 6.3.6). It is worth noting that this chapter is partially based on the following published papers:

Midgley, N.G., Cook, S.J, Graham, D.J. and Tonkin, T.N. 2013. Origin, evolution and dynamic context of a Neoglacial lateral–frontal moraine at Austre Lovénbreen, Svalbard. *Geomorphology*, **198**: 96-106.

Tonkin, T.N., Midgley, N.G., Cook, S.J. and Graham, D.J. 2016. Ice-cored moraine degradation mapped and quantified using an unmanned aerial vehicle: a case study from a polythermal glacier in Svalbard, *Geomorphology*, **158**, 1-10.

6.2 Study Site and site specific methods

6.2.1 Site overview

Austre Lovénbreen is a 5 km long valley glacier located in the Kongsfjorden on Spitsbergen, Svalbard (78°53'12"N 12°08'50"E; Fig. 6.1). The glaciers thermal regime was polythermal in 2010 based on interpretation of GPR profiles presented by Saintanoy *et al.* (2013). The extent of temperate ice appears to be exceptionally spatially limited with the glacier being close to entirely cold-based. Austre Lovénbreen has a strong negative mass balance, with Friedt *et al.* (2012) reporting that between 1962 and 1995 the glacier experienced a mean ablation rate of 0.43 ma⁻¹, which increased to 0.70 ma⁻¹ for the 1995-2009 period.

The glacier is composite, being fed by four main accumulation basins. The glacier is surrounded by mountainous terrain with peaks ranging from 583 m.a.sl (Slattofjellet) to

879 m.a.s.l (Nobilefjellet) at the head of the basin. The forefield is characterised by a large arcuate lateral-frontal moraine that is stream-breached at two locations, which currently act as the main outlets for glaciofluvial run-off. The moraines are inferred to demarcate the Neoglacial limit. The glacier has receded *c.* 1 km from this position. Within the Neoglacial limit several areas of mound-moraine complex (“hummocky moraine”) are identified. Fluted diamicton plains and linear accumulations of supraglacial debris (e.g. Hambrey *et al.*, 1997) have developed as Austre Lovénbreen has receded from its Neoglacial position. The character of the glacier forefield is mapped at low resolution and briefly described in Hambrey *et al.* (1997) and additional field observations are documented in Graham (2002). The landform studied is present on the true-left of Austre Lovénbreen and is part of a semi-continuous lateral-frontal loop which encircles the glacier forefield, but is stream-breached at several locations.

The lateral-frontal moraine is morphologically diverse. Up-glacier (lateral) sections of the landform are distinct in comparison to down-glacier (frontal) sections. Principally the up-glacier sections appear as a series of linear and curvilinear ridges which are aligned transverse or oblique to the inferred direction of former ice-flow (Fig. 6.2; Fig. 6.3; Fig. 6.4). The ridges are somewhat discontinuous in terms of their surface expression and range from *c.* 80-200 m in length. There is a clear cross-sectional landform asymmetry. Ice-distal slopes are steep, with material likely to be at the angle of repose, whereas ice-proximal slopes are more gently sloping in form. Frontal sections of the landform contain a series of hummocks (Fig. 6.4a) which appear to be ‘perched’ on the moraine complex. However, as significant excavation was not undertaken, this structural observation cannot be confirmed. Areas of less well developed moraine hummocks are also observed on the lower ice-proximal slopes of lateral-sections of the landform.

6.2.2 Site specific methods

In this chapter a range of methods outlined in Chapter 2 are adopted for use. GPR surveys were conducted in Spring 2012 using the methods outlined in section 2.4 . Surveys were undertaken transverse to the orientation of the moraine, surveying from the ice-proximal to ice-distal slope. Surveys were undertaken uniformly across the moraine to optimise the coverage. Structural glaciological features were identified on historical aerial and ground level imagery using the methods outlined in Section 2.6. Sedimentological surveys were conducted in July 2014 using methods outline in section 2.5. Clast

macrofabric analysis was, however, not conducted at this site. Samples were taken semi-randomly from excavations undertaken across the moraine system. UAV surveys were also conducted in July 2014. Details on these surveys are provided in Section 6.3.6.

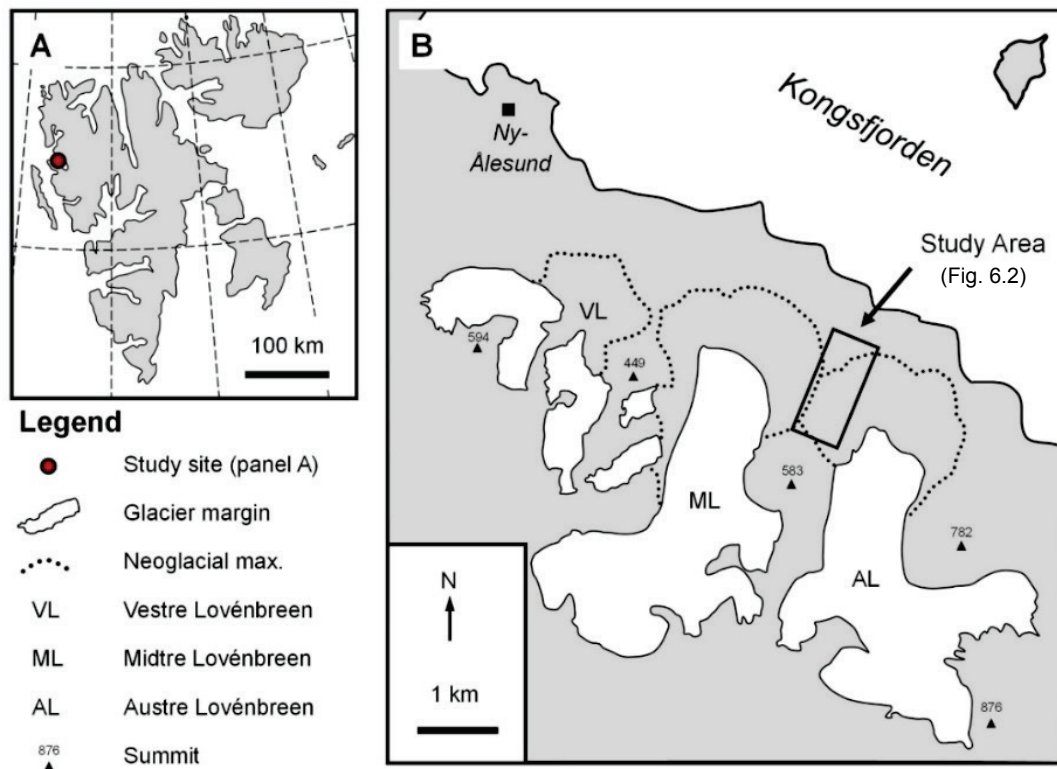


Fig. 6.1 Location of the landforms studied in this research. (A) The location of Kongsfjorden in relation to Svalbard. (B) The position of Austre Lovénbreen in relation to Ny-Ålesund and adjacent glaciers.

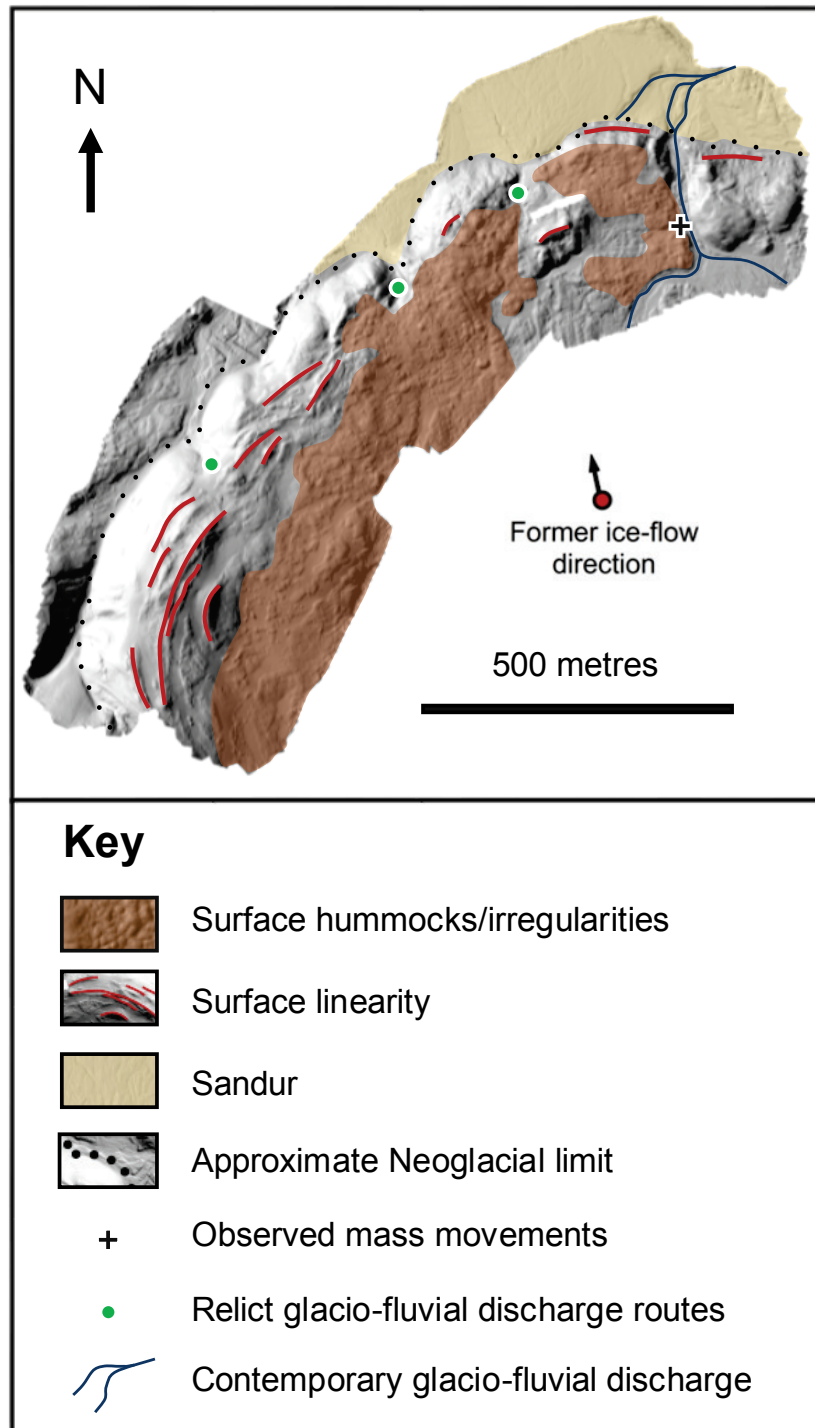
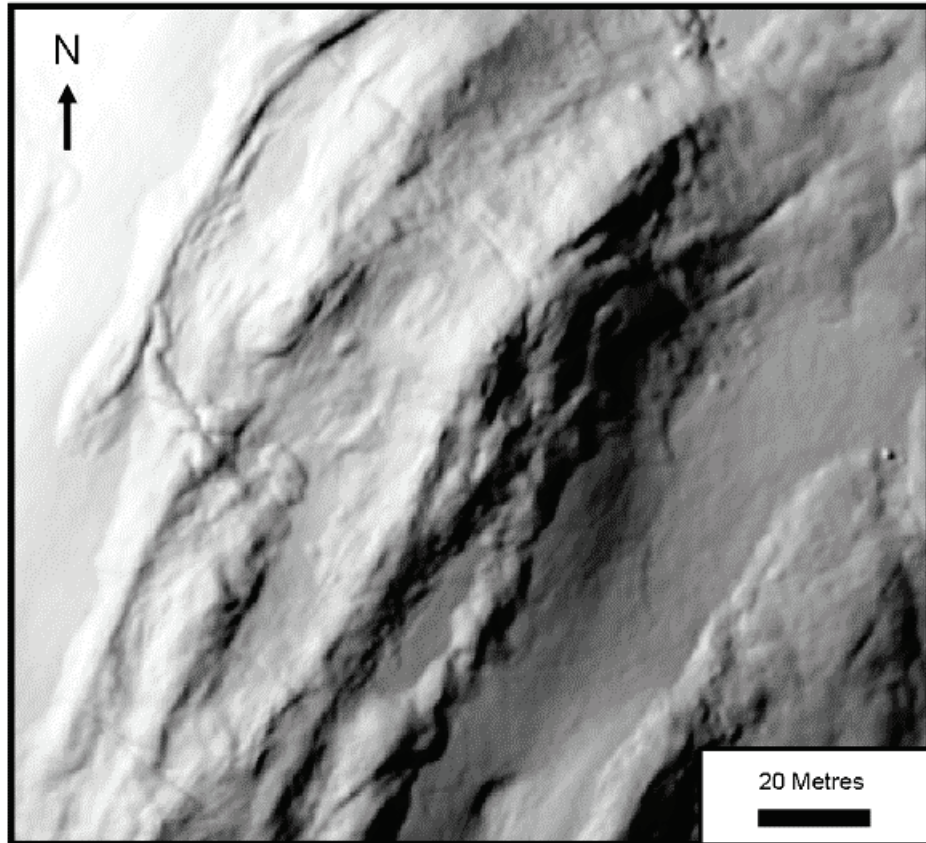


Fig. 6.2 Geomorphological interpretation of the Austre Lovénbreen lateral-frontal complex from 2014 topographic data with the approximate locations of hillshaded DEMs as shown Fig. 6.3 A and B.

A



B

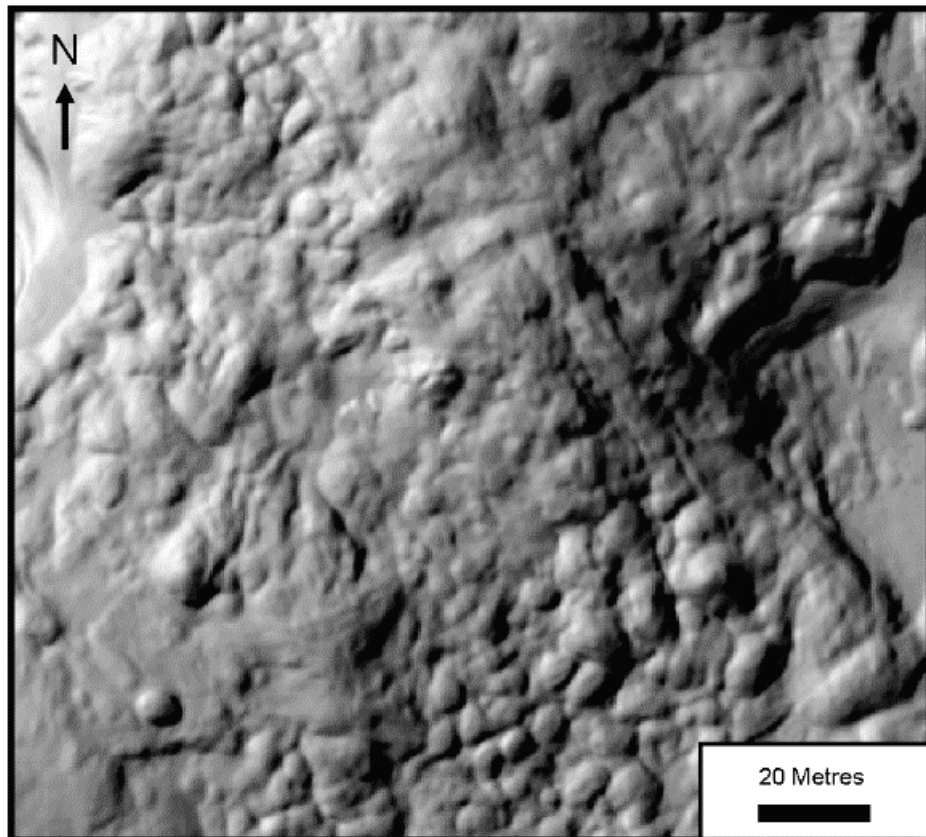


Fig. 6.3 Hill-shaded DEM illustrating morphological characteristics of the lateral-frontal complex. (a) Surface linearity. (b) Surface irregularity ('hummocks').

A



B



Fig. 6.4 Ground-level photograph illustrating morphological characteristics of the lateral-frontal complex. (A) Increasing topographic irregularity in frontal sections of the moraine complex. (B) Surface linearity in lateral sections of the landform.

6.3 Results

6.3.1 Internal structure

100 MHz reflection surveys were completed on the true-left lateral-frontal moraine complex. All reflection surveys dissect the moraine transversely. The locations of the survey transects are shown in Fig. 6.5. The nine transects are shown in their topographically corrected format in Fig. 6.6. Interpretations of the internal structure are available in Fig. 6.7.

Transects 1 to 6 all have clearly identifiable dipping reflectors. The predominant apparent angle of dip of reflectors at the moraine surface within these transects ranges between 41 and 50°. Whilst still exhibiting dipping reflectors, transect 1 exhibits lower apparent dip angles typically within the 11 to 20° range. Signal attenuation progressively increases from a lateral to frontal position on the moraine complex. Profiles 8 and 9 show the highest signal attenuation which have restricted penetration, and therefore limits structural interpretation of near-surface features at depth within the landform. This increase in signal attenuation also coincides with increased abundance of hyperbolae within the substrate. Transect 6 displays a moderate quantity of overlapping hyperbolae. Transects 7 to 9 appear to be more structurally homogenous with overlapping hyperbolae dominant throughout. Surface parallel reflectors are visible in transects 7, 8 and 9, but are absent on all other profiles. A synclinal arrangement of reflectors is also identified within the moraine. This is most clearly seen in transect 6 between approximately 60 and 150 m. Similar structure can be observed with less clarity on transects 1, 3, 4 and 5.

6.3.2 Radar wave propagation velocities

Radar propagation velocity was investigated using CMP analysis on each 100 MHz reflection transect. Example CMP plots are shown in Fig. 6.8. Here, the difference in radar wave propagation wave velocity is clearly delimited. On plot (a) between the *c.* 100 and 330 ns two-way travel time velocities of 0.16-0.17 m ns⁻¹ are detected. This is in contrast to plot (b) which exhibits velocities of 0.13-0.14 m ns⁻¹ at depth. Within both plots, velocities in excess of 0.19 m ns⁻¹ are detected in the first 50 ns time-window. Results from all surveys are displayed in Table 6.1. Radar wave propagation velocity decreases with distance down-moraine. Transects 1-5 all exhibit propagation velocities within the 0.16-0.17 m ns⁻¹ range. In contrast, transects 6 and 7 have a propagation velocity of 0.15 m ns⁻¹. The lowest propagation velocity was found in transect 9. This is located at the most

'frontal' position surveyed with the GPR. Here, the propagation velocity was recorded at 0.13 to 0.14 m ns⁻¹.

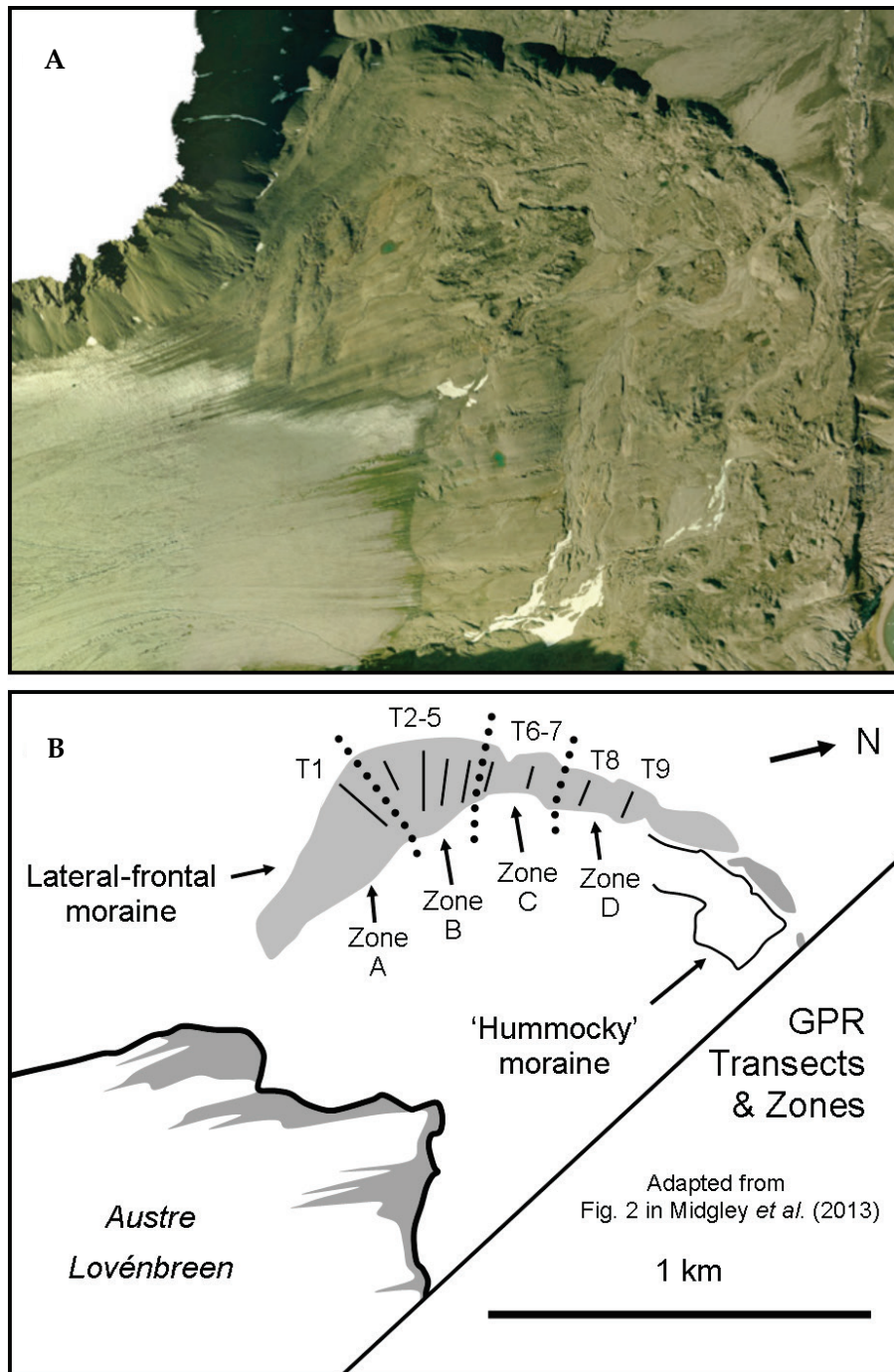


Fig. 6.5 The locations of nine GPR reflection surveys on the eastern lateral-frontal moraine in relation to the glacier terminus.

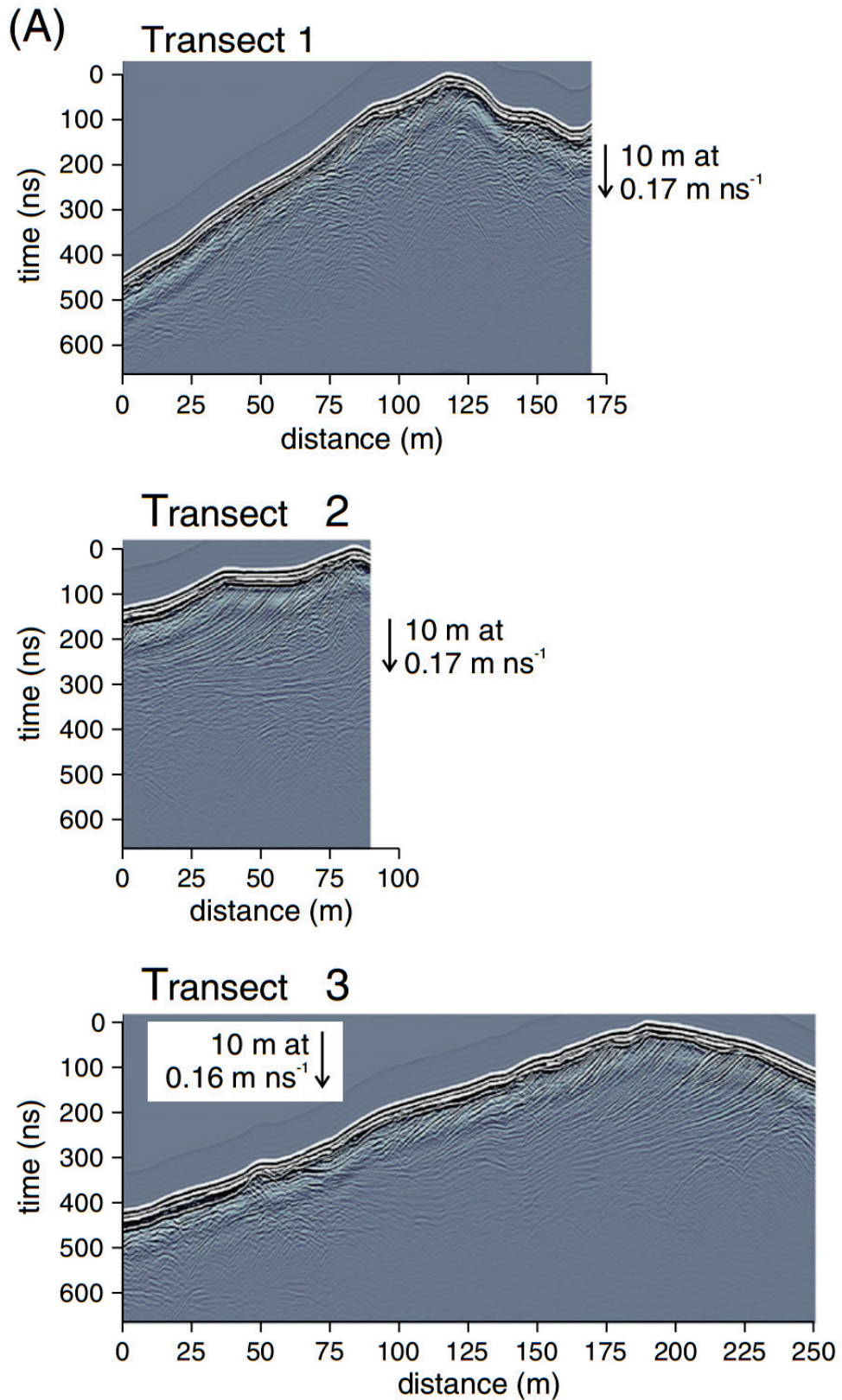


Fig. 6.6 100 MHz Reflection surveys transversely dissecting the western lateral-frontal ridge. (A) Transects 1-3. (B) Transects 4-6. (C) Transects 7-9 (Fig. 4 in Midgley *et al.*, 2013).

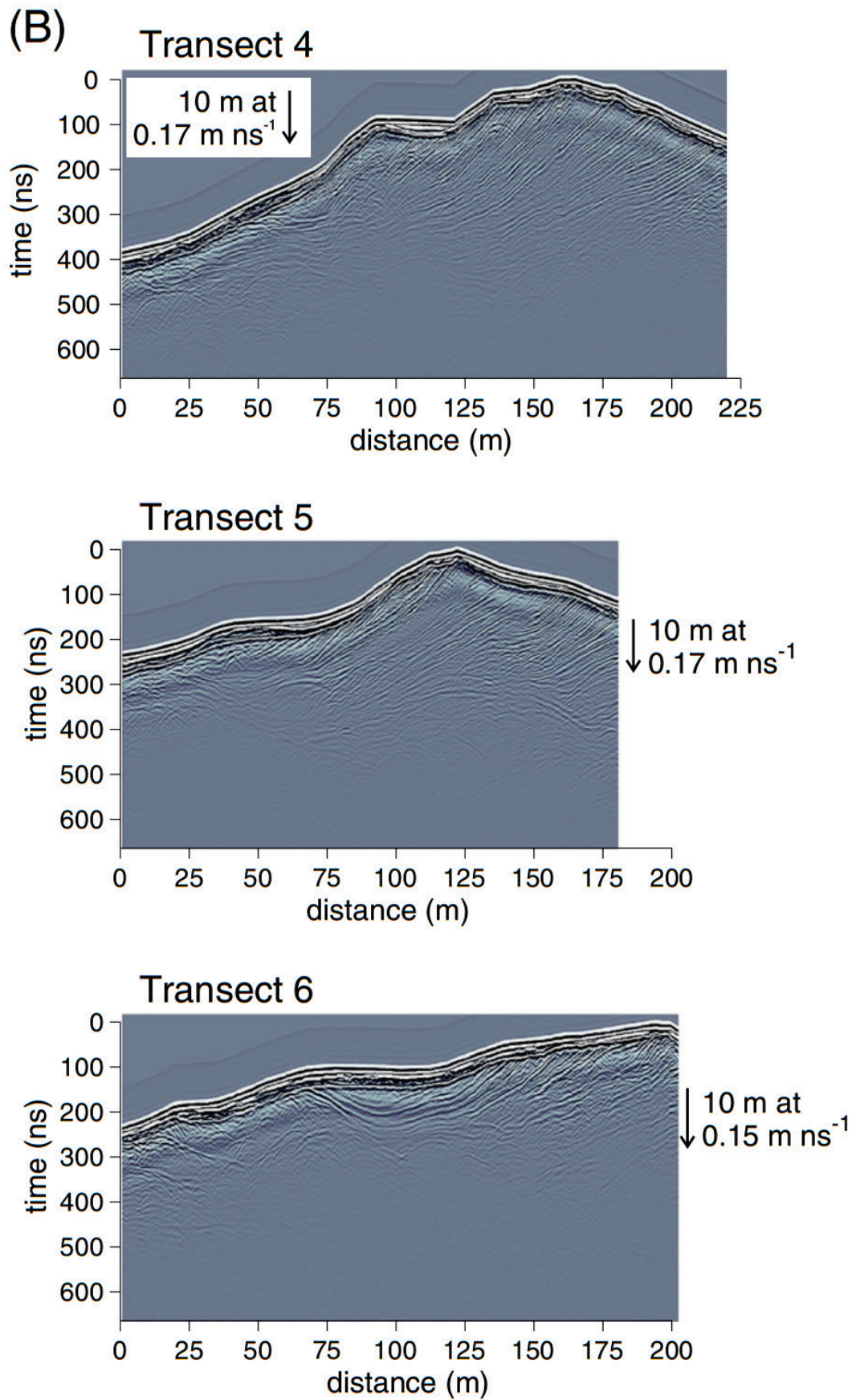


Fig. continued.

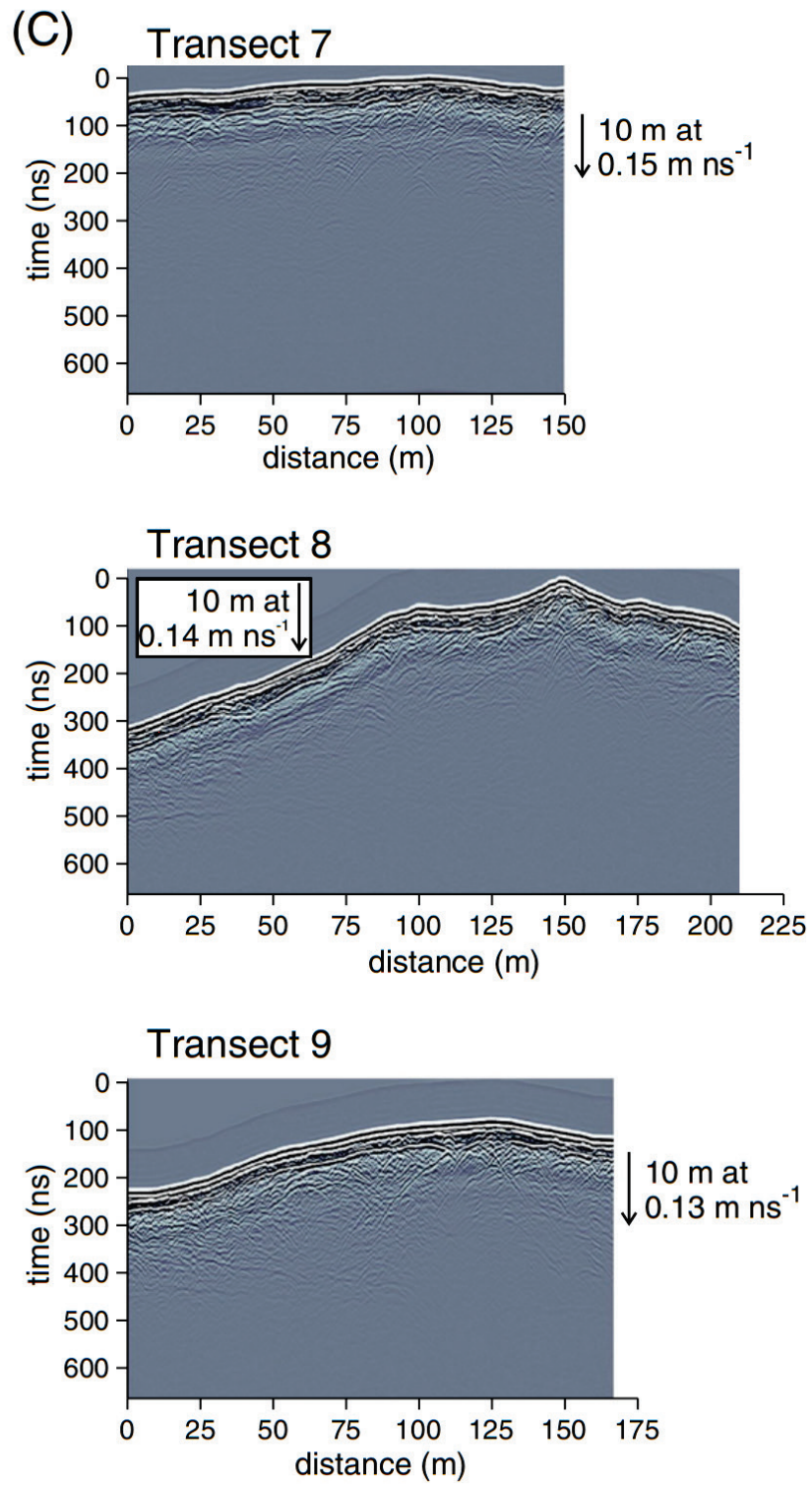


Fig. continued.

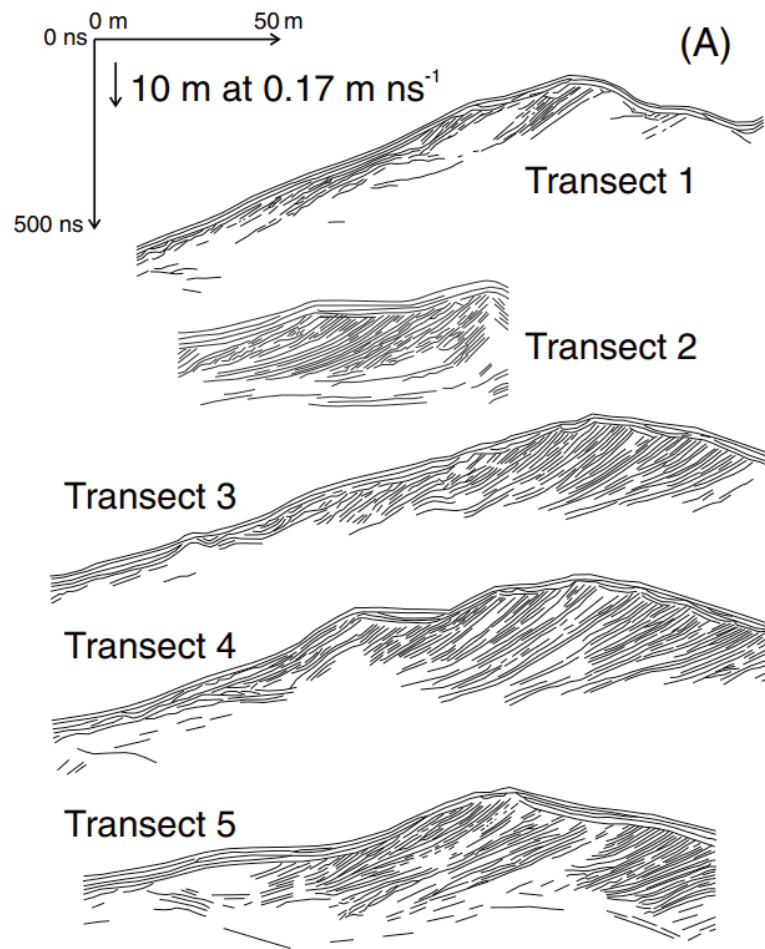


Fig. 6.7 Interpreted radar grams of the 9 100 MHz Reflection surveys (Fig. 4 in Midgley *et al.*, 2013). The radargrams were qualitatively assessed.

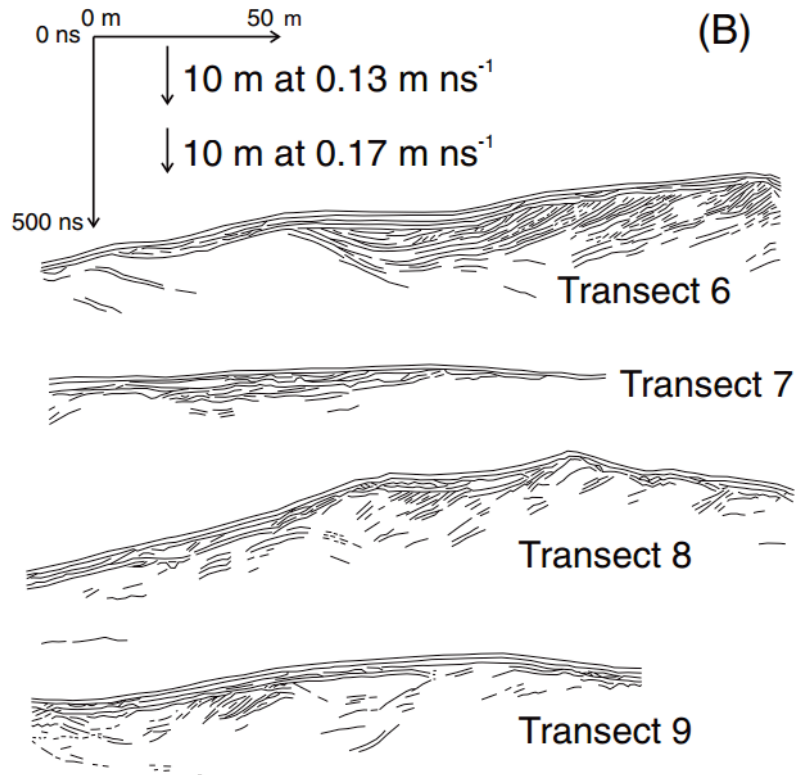


Fig. continued.

Table 6.1 Semblance analysis of CMP data obtained along 100 MHz radar transects 1-9. Note the decline in CMP velocity with increasing distance along the moraine rampart (Table 1 in Midgley *et al.*, 2013).

Transect	CMP velocity (m ns ⁻¹)
1	0.17
2	0.16 & 0.17
3	0.16
4	0.17
5	0.17, 0.16, 0.16, 0.17 & 0.17
6	0.15 & 0.15
7	0.15
8	0.14
9	0.14, 0.14 & 0.13

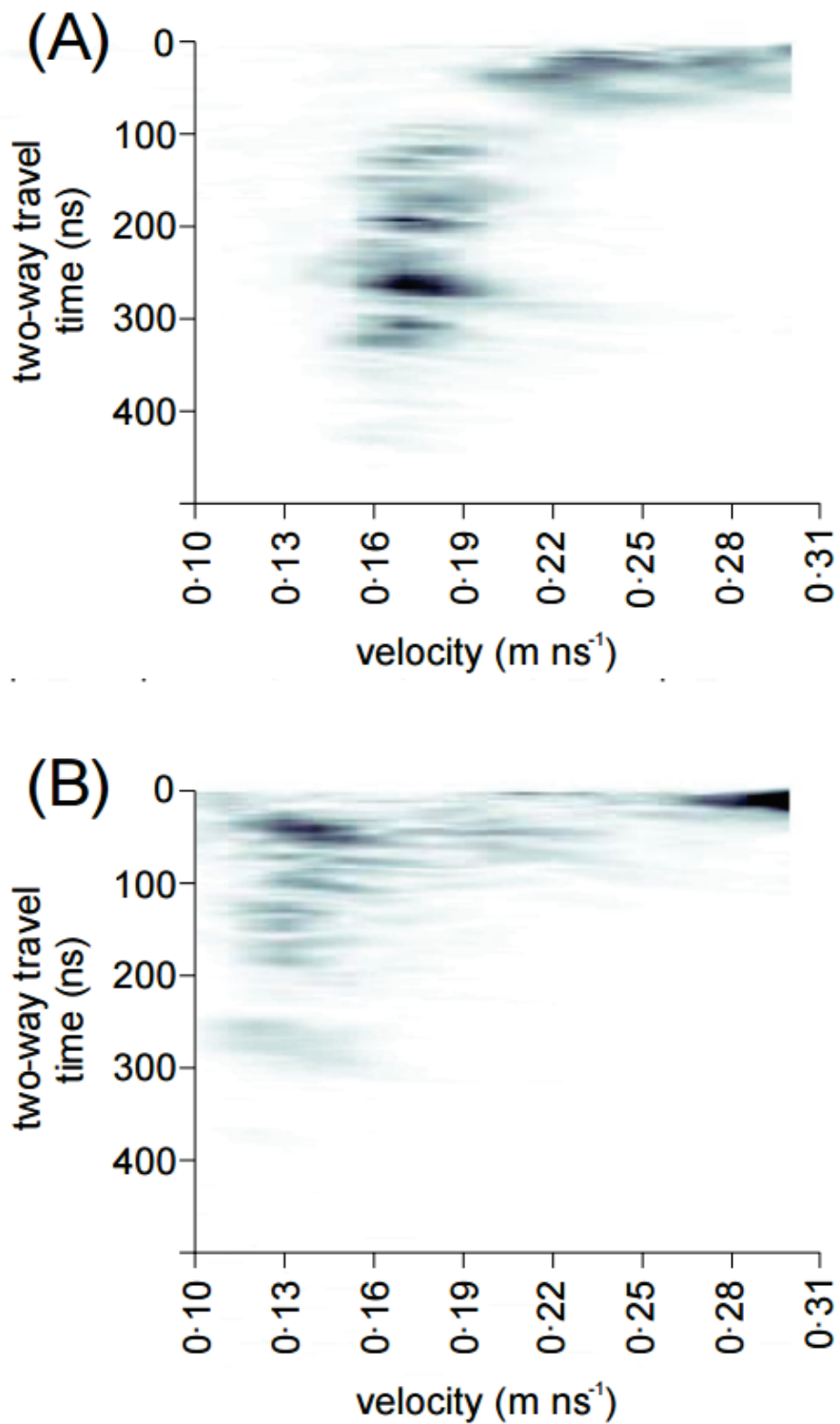


Fig. 6.8 Examples of CMP semblance analysis from (a) transect 2 and (b) transect 9 (Fig. 3 in Midgley *et al.*, 2013). Radar-wave velocity is not consistent across the study area, indicating variable subsurface characteristics.

6.3.3 Glacier change and moraine development: 1892-2003 AD

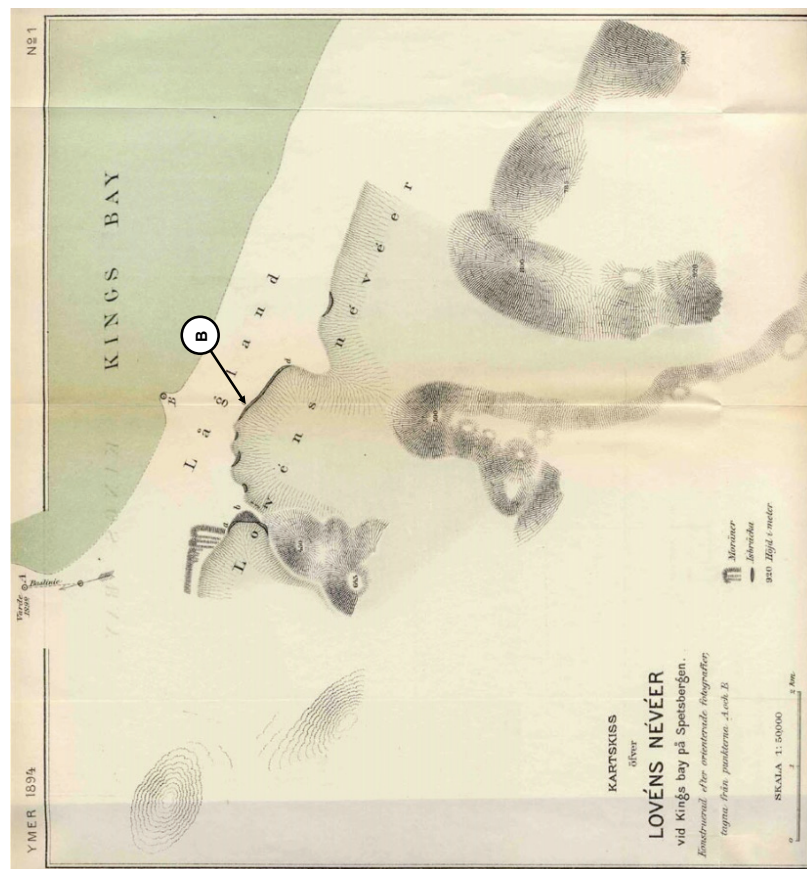
6.3.3.1 Overview

Historical evidence of glacier change in relation to the development of the Austre Lovénbreen lateral-frontal moraine is reported here. Evidence is supplemented with data from neighbouring Midtre Lovénbreen due to the glaciers similar glaciological contexts.

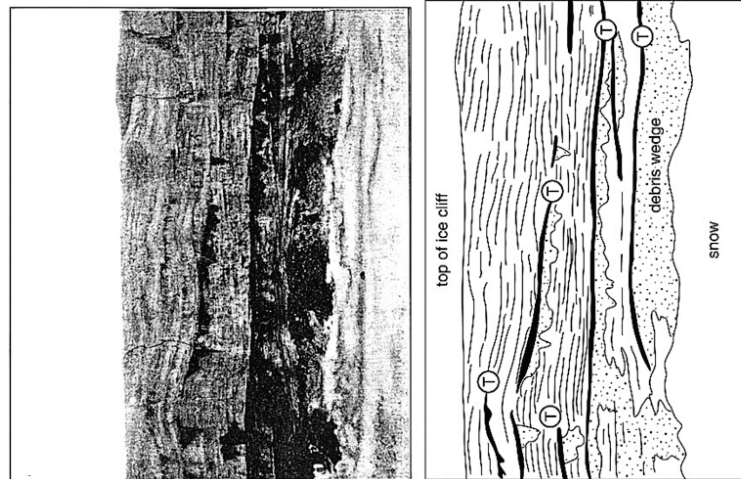
6.3.3.2 1892 AD

Description: Photographs and a photogrammetrically produced map of the termini of Austre, Midtre and Vestre Lovénbreen in 1892 are reported in Hamberg (1894). The map depicts debris-covered termini ('moraine') at these glaciers (Fig. 6.9A). Near vertical ice-margins are documented in the area which is inferred to be the outer moraine-mound complex of Midtre Lovénbreen (Fig. 6.9B). Hambrey *et al.* (2005) estimate that the ice-cliff extends 20-35 m above the moraine. Debris bands are visible at the terminus of Midtre Lovénbreen. Material is streaked below these linear debris bands, with material clearly delimited at the base of the ice-cliff.

Interpretation: These features are likely to represent debris-bearing thrusts located in frontal locations of Midtre Lovénbreen (Hambrey *et al.*, 2005). The mapping of debris-coverage ('moraine') at the terminus of Austre Lovénbreen is likely to imply that debris-bearing thrusts were emerging from the terminus of Austre Lovénbreen at the Neoglacial maximum. The elevation of basal material and flowage from the steepened ice-margin is interpreted to contribute to outer moraine development at Austre Lovénbreen. The sedimentary signature of frontal deposits are likely to represent this structural control on debris transport.



A



Debris-bearing thrusts; ice below debris-smear
 Debris-free thrust-related fractures

B

Fig. 6.9 (A) Vestre, Midtre and Austre Lovénbreen in 1892 as mapped by Hamberg (1894). (B) Debris-bearing features emerging from the terminus and subsequently contributing to moraine construction at Midtre Lovénbreen (Fig 9. in Hambrey *et al.*, 2005).

6.3.3.3 1907 AD

Description: Two images from August 29th 1907 are reported on (Fig. 6.10). These images are taken from Isachsen (1912) who reports on the expedition of the Prince Albert I of Monaco in 1907. The first image can be seen in Fig. 6.10a. This image was taken from the west. The terminus of Austre Lovénbreen can be seen in the middle distance. The glacier appears to be abutting the lateral-frontal complex. In places, the glacier may be topographically prominent over the ridge. Clear moraine distal snowbanks are also noted. Due to the low resolution and quality of this scanned image, no glacier structures are visible. The second image can be seen in Fig. 6.10b. This image was taken from the Bloomstrand, which is located to the north, on the adjacent shore of Kongsfjorden. Austre Lovénbreen is seen exhibiting a 'domed' piedmont glacier fronts. Similarly, due to the distance at which the glacier was photographed, and quality and resolution of the scanned image, no additional features are delimited.

Interpretation: Moraines appear to be visible in these images, potentially implying initial moraine genesis by 1907. However it is unclear whether the moraines represent a supraglacial debris cover, ice-contact dump ridges (e.g. Graham, 2002) or an embryonic ice-cored 'controlled' ridge. These images are also interpreted as evidence that by 1907, Austre Lovénbreen remained close to its Neoglacial maximum.

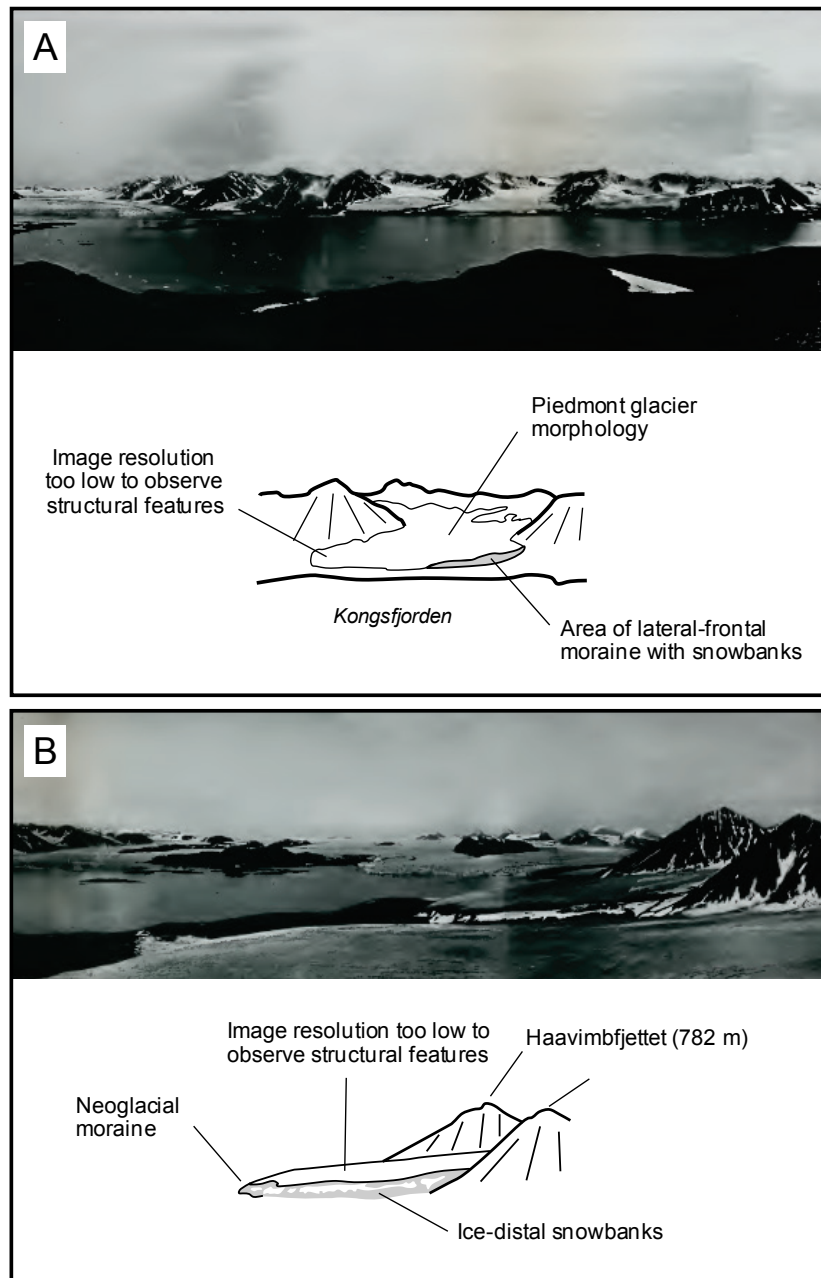


Fig. 6.10 Early historical imagery and interpretation of Austre Lovénbreen in 1907 taken from Isachsen (1912). (A) Austre Lovénbreen viewed from Bloomstrand. (B) Austre Lovénbreen viewed from the west.

6.3.3.4 1918 AD

Description: Although this is an image of Midtre Lovénbreen and not Austre Lovénbreen, there are similarities between the two glaciers and thus this image has been included for comparative purposes. The image is taken from ground-level, looking at Midtre Lovénbreen from Ny-Ålesund to the west (Fig. 6.11). In this photograph, Midtre Lovénbreen is seen abutting its true-left lateral-frontal moraine. The moraine, like much of the landscape visible in this photograph, is snow-covered. A steepened ice-cliff is visible at the terminus. Here, debris can be seen emerging, especially at more frontal positions along the terminus. In places, emerging debris appears to be organised into linear debris bands.

Interpretation: The linear debris structures are interpreted to represent either primary stratification emerging at terminus or emerging thrust related features. Thrust related features emerging at the steepened terminus of Midtre Lovénbreen have been interpreted from earlier ground-level historical imagery (see Hambrey *et al.*, 2005). Specifically, Fig. 9 in Hambrey *et al.* (2005) contains a structural interpretation of a photograph dated to 1892 (included in Hamberg, 1894) at the glacier terminus. In the 1918 photo, it is likely that emerging debris is subject to slumping at the terminus, and thus is contributing to moraine development. Here however, the scanned resolution of the image, and lack of scale impedes further analysis in relation to the structural glaciology of Midtre Lovénbreen and moraine development. One key interpretation is that Midtre Lovénbreen abutted the moraine rampart in 1918. A similar situation at Austre Lovénbreen is therefore highly likely given its similar size, geometry and thermal properties.

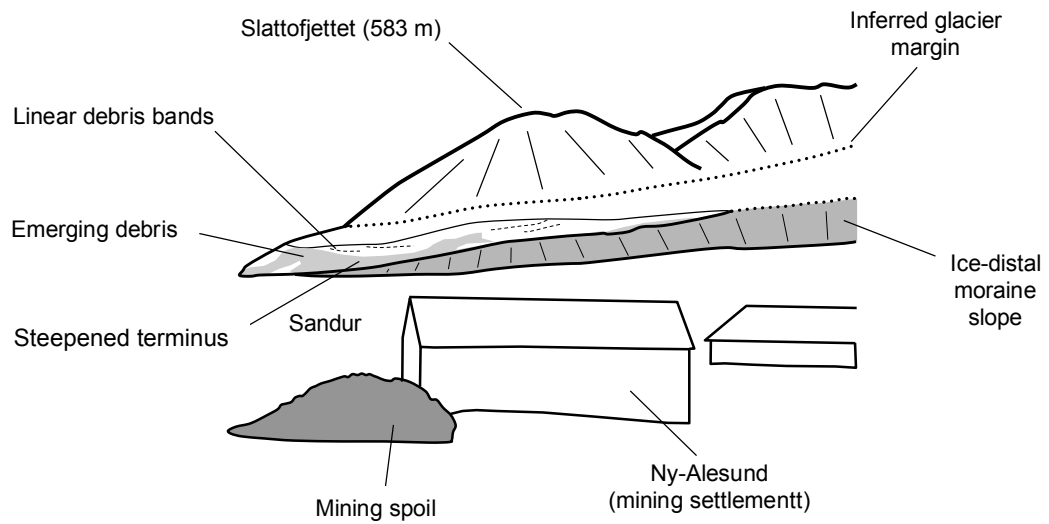
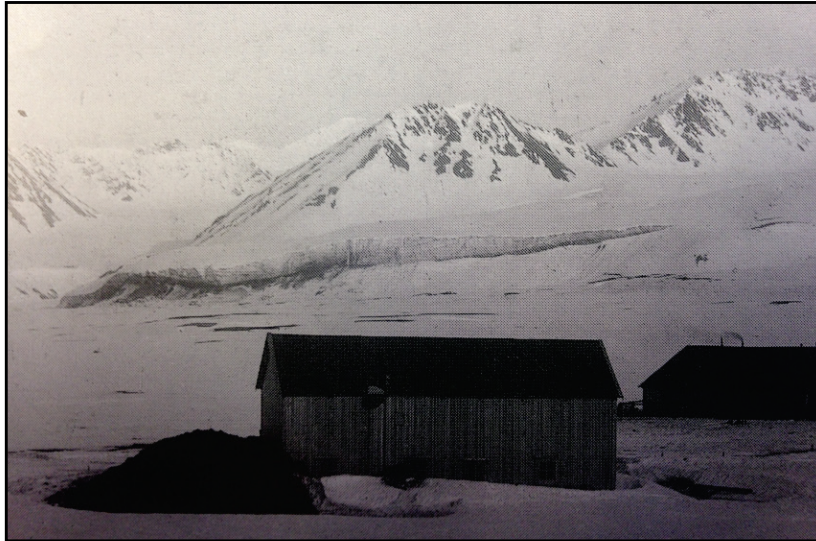


Fig. 6.11 Neighbouring Midtre Lovénbreen in 1918 as viewed from Ny-Ålesund. Note the steep glacier terminus, with emerging debris structures visible above the Neoglacial moraine rampart.

6.3.3.5 1936 AD

Description: An oblique aerial image was acquired in 1936 by the Norwegian Polar Institute (aerial photograph S36 1553). The cropped image and interpretation can be seen in Fig. 6.12. In this image, Austre Lovénbreen appears to have visibly down wasted since 1907. The terminus has been subject to limited recession when compared to the 1907 images. Limited structural characteristics can be observed on the lower 1 km of the terminus. Arcuate and linear planar structures are visible across the terminus. These features are highly visible on the true-left of the glacier. In addition to the mapped arcuate planar structures are more discrete linear to arcuate debris concentrations, which are noted on the true-left of the glacier. Longitudinal planar structures are visible across the terminus and appear to terminate into areas of continuous debris coverage down-glacier. The true-right of the glacier appears to show an irregularity, which can be described as a surface 'bulge'. This irregularity is also evident when tracing longitudinal planar structures to the glacier terminus. In some locations, the linearity of these features is distorted by the surface 'bulge'. Shadowing on the lateral-frontal complex delimits the location of an ice-proximal slope on this landform. This landform appears to contain several well defined ridges. Up-glacier, the distinction between supraglacial debris and the landform is less readily made.

Interpretation: Arcuate planar structures are interpreted as primary stratification resulting from layering of snow, and debris layers in the accumulation areas. The arcuate character of these features is likely to represent compression within individual flow units. Longitudinal planar structures are interpreted as longitudinal foliation occurring where primary stratification has been folded into ice-parallel linear bands. The positions of these structures is interpreted to signify three major flow units on this glacier. The termination of longitudinal foliation implies that the emergence of these structures is important with regard to the delivery of sediment to the glacier surface. The surface irregularity is highly indicative of surge-type behaviour within a flow unit on the true-left of the glacier. Surge-type behaviour is widely reported to occur on glaciers in Svalbard (e.g. Hagen *et al.*, 1993; Jiskoot *et al.*, 2000; Murray *et al.*, 2000). The potential for surge-type behaviour at adjacent glaciers on Brøggerhalvøya has been discussed (e.g. Hagen *et al.*, 1993; Hansen, 2003; Glasser *et al.*, 2004; Hambrey *et al.*, 2005). However, the classification of Midtre

Lovénbreen as a surge-type glacier has been disputed (e.g. Jiskoot *et al.*, 2000; King *et al.*, 2008).

Debris-bearing fractures are interpreted as englacial thrust features. Such features are reported to occur in high-Arctic valley glaciers. The abundance and appearance of the debris-bearing fractures in this imagery may represent recent propagation onto the glacier surface following significant down-wastage of the terminus. Down-wastage of the terminus is also visible, as shadowing allows for a developing ice-proximal slope on the lateral-frontal complex to be delimited. This is interpreted to signify differential ablation of buried ice, with regard to debris-coverage.

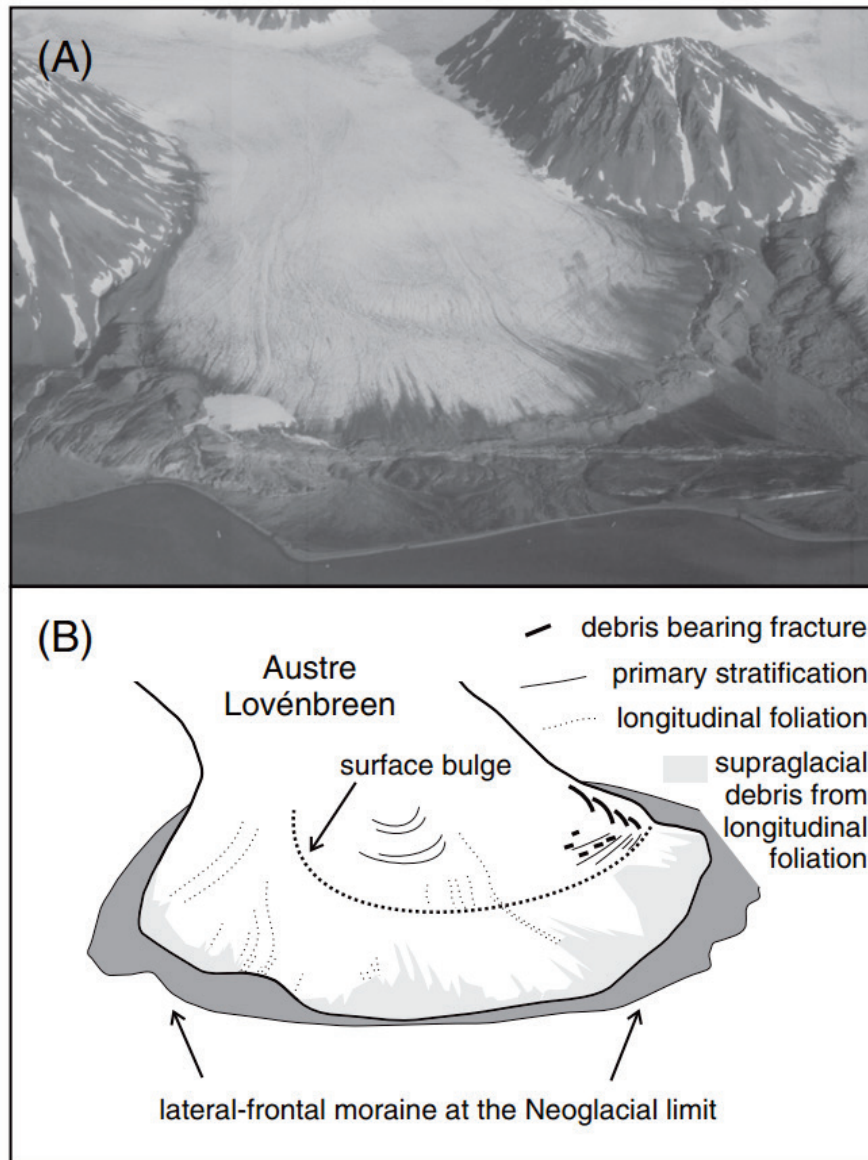


Fig. 6.12 Interpretation of Austre Lovénbreen in 1936 from an oblique aerial image obtained from the Norwegian Polar Institute (image S36 1553). This diagram appears in Midgley *et al.* (2013) as Fig. 6. (A) Original image. (B) Interpretation.

6.3.3.6 1948 AD

Description: This image was obtained by the Norwegian Polar Institute on September 9th 1948 (Fig. 6.13). This is a single aerial image, therefore is effected by camera distortion. The scale will vary across the image. Similar structural characteristics to the 1936 imagery are noted. Specifically, four main structures are observed: (1) arcuate planar structures; (2) longitudinal planar structures; (3) debris-bearing fractures; and (4) supraglacial debris coverage. Shading from adjacent mountains (e.g. Slattofjellet) limits structural and geomorphological description in the area of interest. A key observation is the recession of the glacier terminus from the lateral-frontal complex. A series of proglacial drainage channels appear to have developed between the moraines ice-proximal slope and the glacier margin. In more lateral positions, Austre Lovénbreen still appears to abut its true-left moraine rampart.

Interpretation: Similar to the 1936 imagery, the four main glaciological structures are interpreted as: (1) primary stratification; (2) longitudinal foliation; (3) englacial thrusts; (4) and supraglacial debris. In relation to the 1936 image, the 'thrust' features appear to have migrated down-glacier. Due to the oblique nature of the 1936 image, and lack of orthorectification on the 1948 image the displacement of these features over the 12 years is unknown, however, a combination of transport via glacier flow and exhumation related to down-wastage of the glacier terminus is likely to have contributed to the modification of these features. This image also highlights that by 1948, recession of Austre Lovénbreen was significant enough for the lateral-frontal complex and glacier margin to appear as separate entities. However, it is likely that buried glacier-ice appeared discontinuously through the deglaciating forefield at this time period. Differential ablation resulting from debris coverage is inferred to be important here with regard to the stabilisation of ice-cored 'controlled' ridge in the glacier forefield.

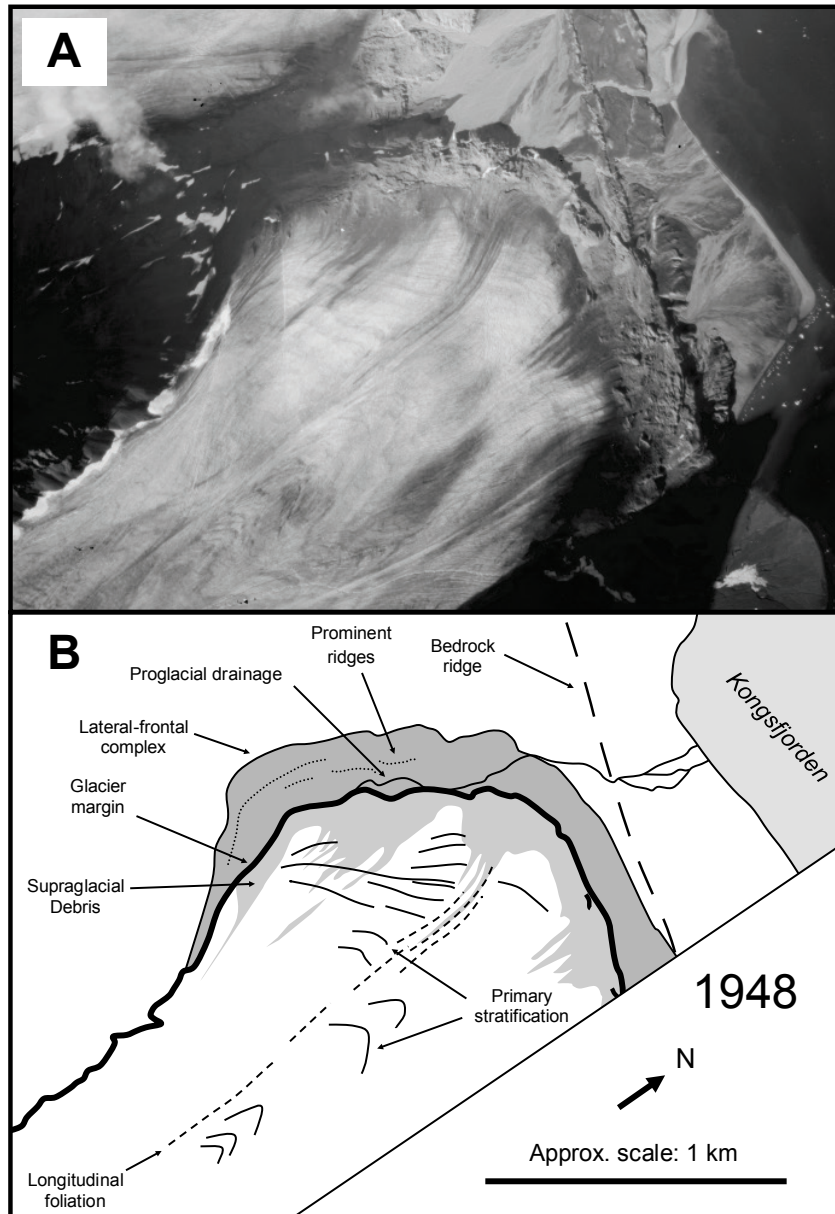


Fig. 6.13 Interpretation of Austre Lovénbreen in 1948 from aerial imagery obtained from the Norwegian Polar Institute (image S48 752). (A) Original image. (B) Interpretation.

6.3.3.7 2003 AD

Description: This image is derived from a series of orthorectified NERC ARSF aerial images from August 2003 (Fig. 6.14). The glacier terminus is clearly visible *c.* 1km up valley from its Neoglacial Maximum position. The lateral-frontal moraine complex is clearly developed in the glacier forefield and appears to be a detached unit from the glacier margin. The quality of this imagery has permitted detailed structural interpretation. The non-genetic structures identified in previous image sets are visible here. These include arcuate and longitudinal planar structures. The quality of this imagery allows for two types of fracture to be observed: debris-bearing fractures which are only visible on the true-right of the glacier and fractures free from debris which are distributed across the entire glacier margin. Fractures are highly abundant on the true-left of the glacier.

Interpretation: Similar to previous interpretations, longitudinal planar structures are likely to represent longitudinal foliation, resulting from folding and lateral compression of primary stratification between flow units. On this basis, the two bands of well-defined longitudinal foliation are interpreted to indicate the boundaries between three major flow units. The concentration of supraglacial debris into these flow unit boundaries is likely to be a key control on proglacial linear debris stripes (e.g. Hambrey and Glasser, 2003), which appear to have developed on deglaciated terrain. Folded arcuate planar structure between areas of longitudinal foliation are interpreted as primary stratification which have been subject to lateral compression within their various flow units. Fractures are interpreted to represent crevasses occurring at the terminus. These could represent both open and closed crevasses, which represent stress within the glacier. A key aspect in relation to the development of the lateral-frontal moraine is that the moraine is now visible as a discrete unit, which from plan view appears to be detached from the glacier terminus.

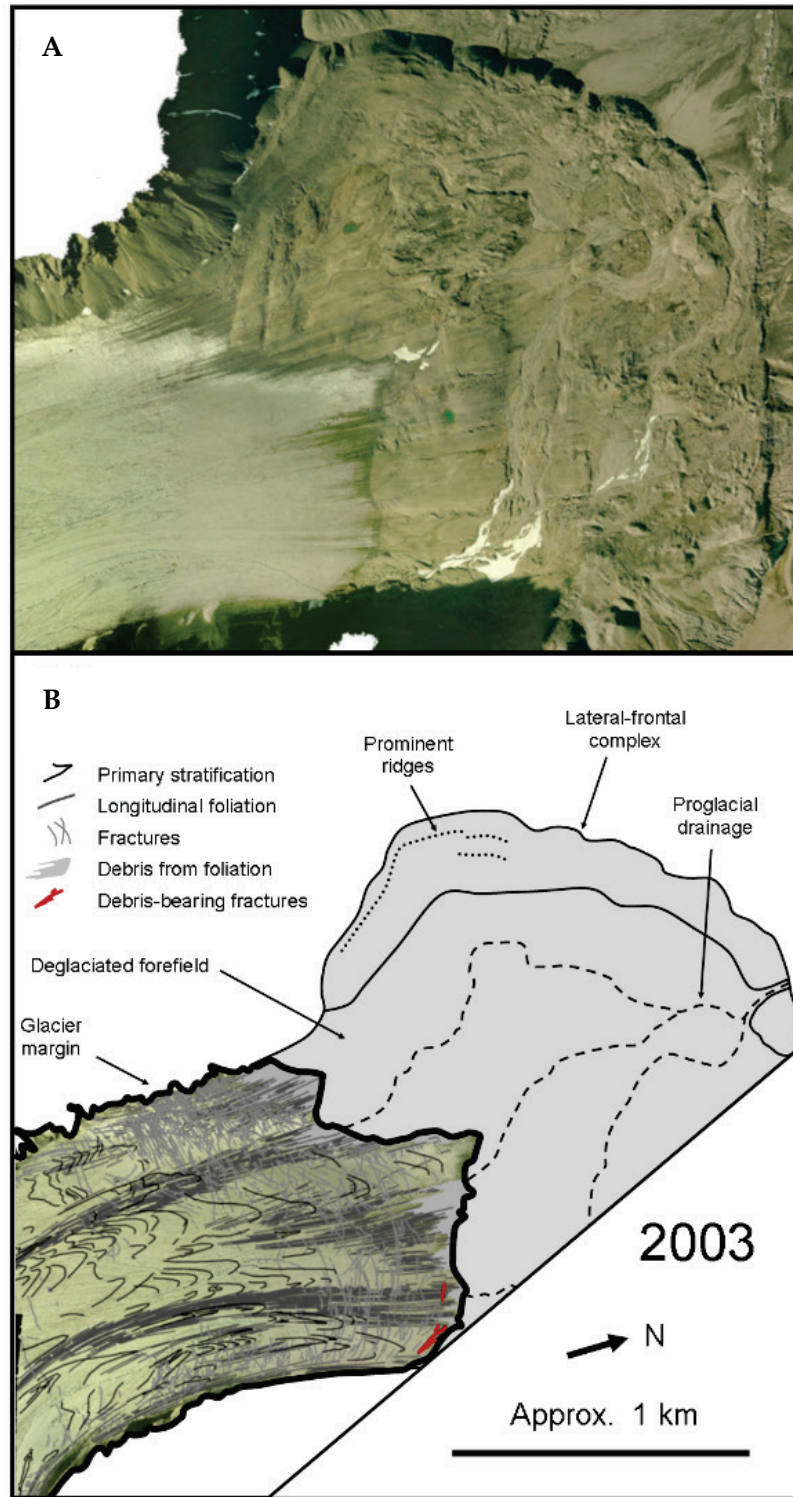


Fig. 6.14 Interpretation of Austre Lovénbreen in 2003 from orthorectified aerial imagery obtained by the NERC ARSF. (a) Original image. (b) Interpretation.

6.3.4 Lithofacies descriptions

6.3.4.1 Overview

Summaries of the key lithofacies on the lateral-frontal moraine are presented. Four facies were assessed: clast-rich sandy diamicton ($n = 12$), surface angular gravel ($n = 9$), clast-rich muddy diamicton ($n = 2$) and buried ice ($n = 1$). Table 6.2 contains a summary of sample locations and the facies logged at each site. The sample locations are displayed in Fig. 6.15 and sedimentary logs are presented in Fig. 6.16, highlighting key sedimentary exposures. Summaries of the results are displayed in tabular format (Tables 6.3-6.5).

6.3.4.2 Surface angular gravel ($n = 9$)

Surface facies of angular gravel were found at nine sample sites. The gravels were typically devoid of granular material; however three sub-types of gravel are distinguished. The most abundant is a coarse clast-supported gravel devoid of granular (or finer) material. An additional facies of clast-supported gravel with high (86 %) sand, and low mud (14 %) content was assessed at WP007 (Fig. 6.15). WP020 was distinguishable from other coarse surface gravels by its lack of material within the >2 mm fraction, but abundance of granular sized clasts. Surficial deposits of gravel were typically 10-20 cm in depth with excavations at five sites with angular gravel extensive enough to reveal underlying diamicton facies (Fig. 6.15). However, the thickness of this surficial deposit appears to be spatially variable. For example, an 80 cm excavation at WP020 revealed a single facies of clast-supported gravel. The roundness characteristics of this facies are variable. RA indices for sampled clasts typically fall within the 92-100 range. The gravel sampled at WP007 has an anomalously low % RA (56) in comparison to it other surficial gravels. At WP028 (Fig. 6.15), a lobate surface feature was assessed for its sedimentology. The feature contained muddy gravel. Clasts were almost exclusively angular or very angular (% RA = 90) and exhibited a moderate C_{40} index of 48. The <2mm fraction varied with surface facies containing 96 % mud, whereas subsurface material contained 98% mud. The mean class for both matrix samples was medium silt.

6.3.4.3 Clast-rich sandy diamicton ($n = 12$)

Clast-rich sandy diamicton was the most abundant lithofacies sampled on the lateral-frontal moraine ridge and was assessed at 11 locations (Table 6.2; Fig. 6.15) across the lateral-frontal complex. Excavations at WP002 and WP027 contain multiple inclined units

of matrix supported clast-rich sandy diamicton (Fig. 6.15). At WP002, upper and lower facies were distinguished by their respective colourations. At WP027, an up glacier dipping facies of angular gravel divides the upper and lower diamicton facies (Fig. 6.15). The clast form properties show high variability between facies. Clasts extracted from frontal excavations (e.g. WP027; upper diamicton) exhibit low angularity (% RA = 34), are frequently striated (26 %), and are typically more blocky in terms of their morphology (% C₄₀ = 30). This is of stark contrast to more lateral sites (e.g. WP002; upper diamicton) which are predominantly angular (% RA = 100), less blocky (C₄₀ = 88) and contain low proportion of striated clasts (2 %).

6.3.4.4 *Clast-rich muddy diamicton (n = 2)*

Clast-rich muddy diamicton was assessed at WP003 and WP015. The exposure at WP003 was dug on a small hummock located on a more frontal position on the moraine complex (Fig. 6.15). The diamicton was found to be matrix supported and structurally massive. Clasts sampled from this facies were dominantly angular (% RA = 62) and found to exhibit a moderate C₄₀ index (C₄₀ = 52). A small proportion of clasts were also found to exhibit striae (4%). Analysis of the >2mm fraction found the matrix to contain 33% sand, and 67% mud by volume. At WP015 a matrix supported clast rich muddy diamicton is found under a surface deposit of sandy gravel. Clasts within this diamicton were found to exhibit high angularity (% RA = 92) and a moderate C₄₀ index of 60. One clast (2% of the sample) was found to exhibit striae.

Table 6.2 Summary table of assessed lithofacies on the Austre Lovénbreen true-left lateral-frontal moraine complex and their structural configuration

Waypoint	Coordinates*	Lithofacies**
WP001	437797; 8759320	Clast-rich sandy diamicton overlain by gravel unit
WP002	437803; 8759432	Gravel overlying two facies of clast-rich sandy diamicton and sampled ice
WP003	438525; 8760181	Clast-rich muddy diamicton
WP004	438479; 8760104	Clast-rich sandy diamicton
WP005	438460; 8760070	Gravel overlying clast-rich sandy diamicton
WP006	438295; 8760043	Clast-rich sandy diamicton
WP007	438268; 8759920	Sandy Gravel
WP008	438071; 8759819	Clast-rich sandy diamicton
WP009	438076; 8759746	Clast-rich sandy diamicton
WP010	437965; 8759731	Gravel overlying Clast-rich sandy diamicton
WP011	438048; 8759658	Clast-rich sandy diamicton
WP012	438072; 8759523	Clast-rich sandy diamicton
WP013	437878; 8759567	Gravel
WP014	437793; 8759519	Gravel
WP015	437878; 8759453	Sandy Gravel overlying clast-rich muddy diamicton
WP016	437822; 8759178	Gravel
WP020	437824; 8759462	Gravel
WP027	438673; 8760084	Inclined units of clast-rich sandy diamicton (x2) and gravel
WP028	N/A	Muddy Gravel

* Presented using WGS 84 UTM Grid 33x

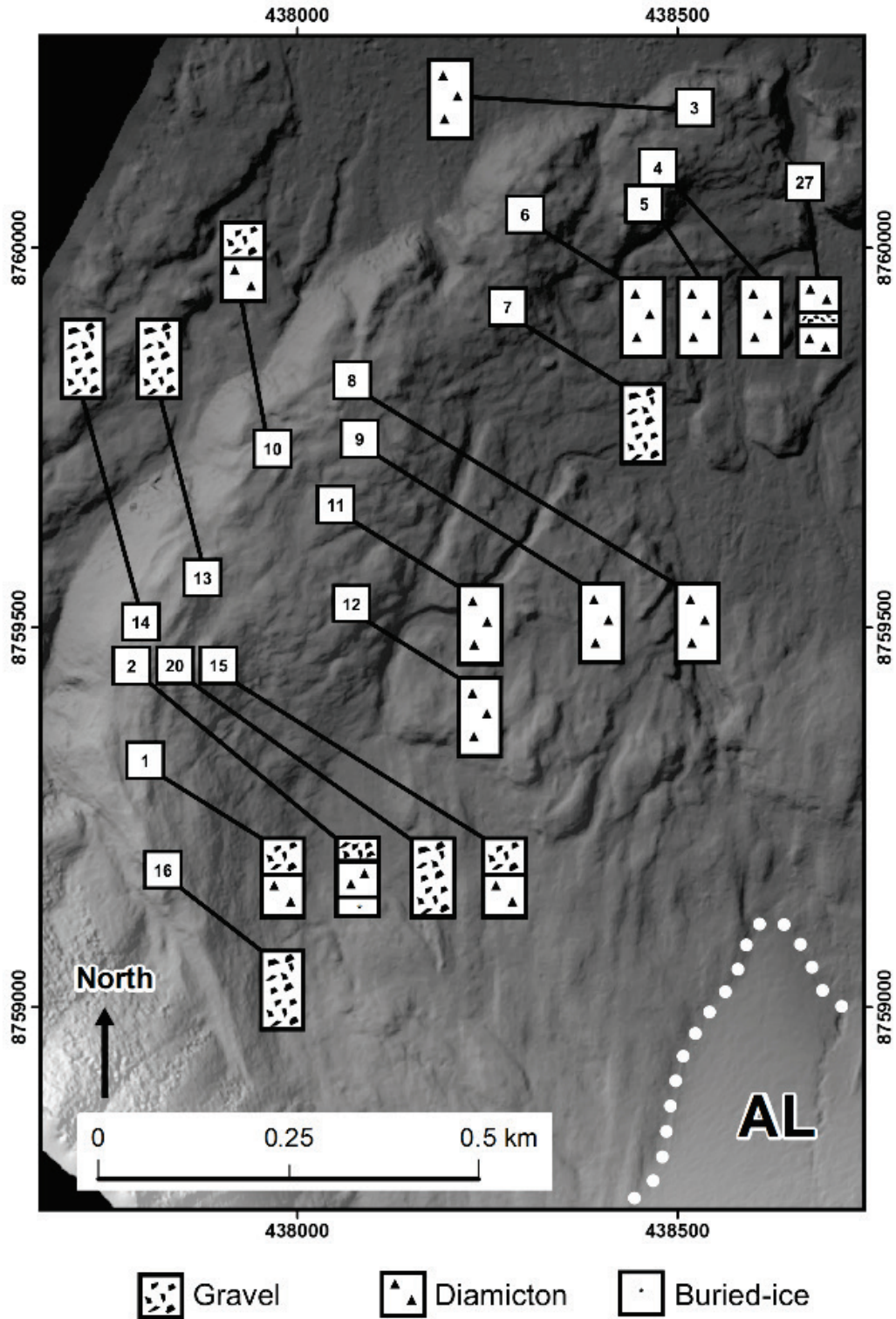


Fig. 6.15 Locations of excavations (numbered) across the lateral-frontal moraine with the position of the glacier terminus is noted (AL). Hillshaded DEM extracted from aerial imagery acquired in 2003 by the UK Natural Environment Research Council (NERC) Airborne Research and Survey Facility (ARSF) are provided courtesy of NERC via the NERC Earth Observation Data Centre (NEODC).

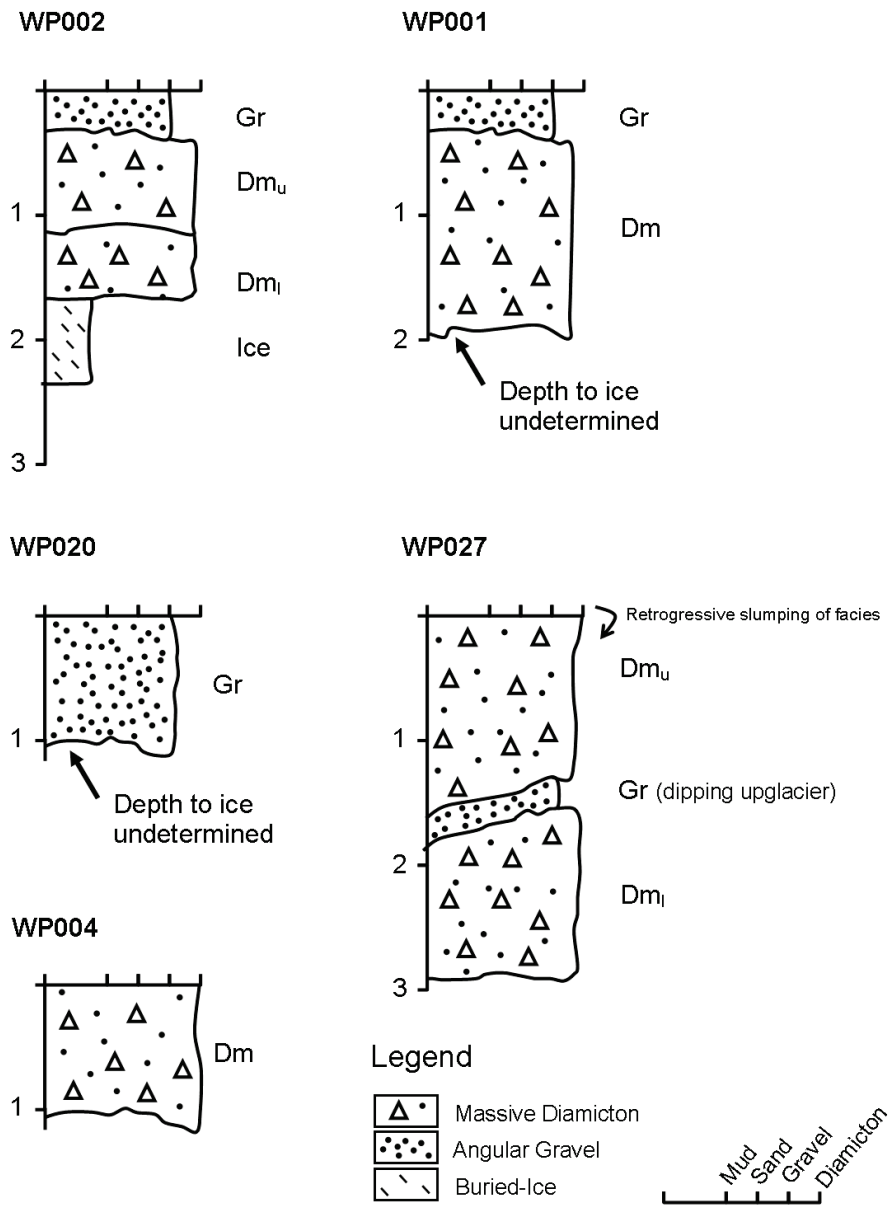


Fig. 6.16 Summary of the structural relationships between lithofacies on the Austre Lovénbreen lateral-frontal moraine complex. Scale increments in metres.

Table 6.3 Summary of clast-rich sandy diamicton facies

ID	% RA	% C ₄₀	% S	Matrix (<2mm Fraction)	
				% Sand	% Mud
WP001	98	70	0	74	26
WP002-U	100	88	2	81	19
WP002-L	94	76	2	--	--
WP004	50	40	2	67	33
WP005	80	42	0	83	17
WP006	70	38	4	79	21
WP008	84	60	0	72	28
WP009	46	52	4	72	27
WP010	72	34	0	78	22
WP011	66	46	2	71	29
WP012	96	46	0	77	32
WP027-U	34	30	26	87	13
WP027-L	44	16	20	67	33

Table 6.4 Summary of surface gravel facies

ID	Character	% RA	% C ₄₀	% S	Matrix (<2mm Fraction)	
					% Sand	% Mud
WP001	Coarse	100	76	0	--	--
WP002	Coarse	100	68	0	--	--
WP005	Coarse	78	60	0	--	--
WP010	Coarse	100	56	0	--	--
WP013	Coarse	98	76	0	--	--
WP014	Coarse	96	64	0	--	--
WP016	Coarse	92	68	0	--	--
WP020	Granular matrix	96	74	0	--	--
WP007	With sand	56	44	6	86	14
WP015	Sandy Gravel	*	*	*	90	10
WP028	Muddy gravel	90	48	0	2-4	96-98

* Clast form data missing

Table 6.5 Summary of clast-rich muddy diamicton facies

ID	% RA	% C ₄₀	% S	Matrix (<2mm Fraction)	
				% Sand	% Mud
WP015	92	60	2	14	86
WP003	62	52	4	33	67

6.3.4.5 Buried-ice ($n = 1$)

Buried ice was assessed at WP002, where an excavation revealed it to be present at a depth of 160 cm (Fig. 6.16). The bottom 0.3 m of diamicton covering the buried ice was found to be frozen, thus required significant effort to excavate through. Clast form data and a visual interpretation of the sampled ice is available in Fig. 6.17. The ice was found to contain 5% debris by volume. The debris consisted of dispersed silt aggregates within the >2 mm fraction. Coarser granular and pebble size debris were also present within the sampled ice. A total of 43 clasts were extracted and assessed for roundness. The material was predominantly angular in character (% RA = 95.3) with the modal roundness category identified as angular (% A = 58; Fig. 6.17). Of the 43 sampled clasts, 17 were large enough (pebble sized or greater) to be measured for shape. The C_{40} index for this sample was 100. Of the sampled clasts measured for shape, the most common shape classes were very-bladed and very-platy which account for 35 % and 29 % of the sample respectively. Debris appears to be crudely concentrated in layers (Fig. 6.17). The ice sample also contained some bubbles. These bubbles were >1 mm in diameter.

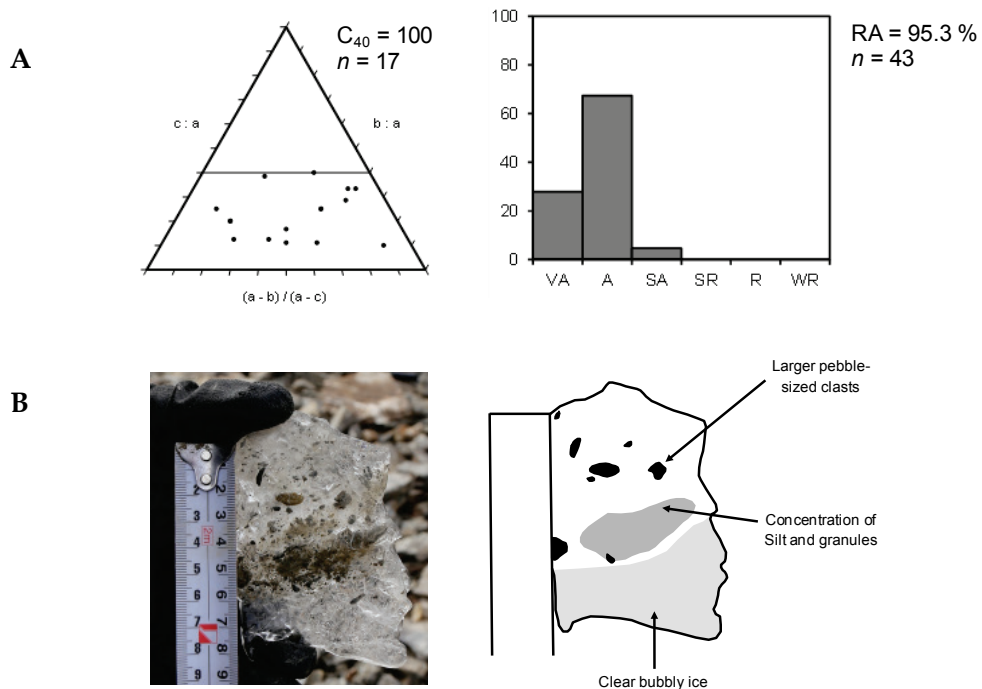


Fig. 6.17 Physical properties of the ice sample extracted from the Austre Lovénbreen true-left lateral-frontal moraine. (A) Shape and roundness of clasts removed from the ice. (B) Photograph and interpretation of sampled ice.

6.3.5 Clast-form analysis

Control samples: The control samples were taken from extraglacial, glacio-fluvial, and subglacial locations. Three glacio-fluvial samples were gathered. One from the west stream channel located within the glacier-forefield, c. 200 m from the current glacier terminus (FLU1). The additional two were taken outside the Neoglacial moraine complex, from an abandoned braided stream channel on the sandur (FLU2 and FLU3). The glacio-fluvial samples exhibit low-moderate RA (14-36) and C_{40} values (22-44). Sandur derived glacio-fluvial controls (FLU1 and FLU2) have both higher angularity and shape indices (% RA = 20-36; % C_{40} = 34-44). All glacio-fluvial samples were not striated. Subglacial control samples (SUB1 and SUB2) were taken from a stream dissected, and recently deglaciated diamicton plain located <50 m from the current glacier terminus. The samples have both low RA (20-22) and C_{40} (18-24) indices. The samples form a cluster, which partially overlaps with glaciofluvial control samples. However, a distinguishable characteristic of these subglacial controls is the frequency of clasts within the sample populations that carry striae. A total of 22 % of clasts within SUB1 exhibited striae. Similarly, 32 % of clasts within the sample SUB2 carried striae. Extraglacial debris was sourced from scree deposits located adjacent to the left-lateral-frontal complex (EXG1, EXG2 and EXG3). Extraglacial debris show contrasting clast-form characteristics to other reference samples. Samples were highly angular (% RA = 92-98) and had moderate-high shape indices (% C_{40} = 68-92).

Moraine samples: These samples relate to the lithofacies assessed in section 6.3.4. Within Fig. 6.18 moraine samples are split in to three main categories: ice ($n = 1$), diamicton ($n = 15$) and gravel ($n = 11$). Moraine samples form a cluster between extraglacial control populations (high RA and C_{40} indices), and subglacial and glaciofluvial control populations (low-moderate RA and C_{40} indices). Further visualisation of clast form parameters was investigated by plotting the % RA against the % striae within each clast sample (Fig. 6.19). Here, further discrimination is provided. Notably, samples WP027U and WP027L show similar, albeit slightly higher % RA (34-44), and comparable levels of striae to subglacial control samples (20-26). With the exception of WP007 (% RA = 56), gravels are generally more angular in character (% RA = 78-100) than diamicton samples. Gravel samples also show a tendency to exhibit less 'blocky' shape characteristics (48-90; excluding WP007). However, diamicton samples show wide variability in terms of both

roundness (% RA = 34-100), and shape (% C₄₀ = 16-88) indices. Diamicton samples appear to exhibit a roundness gradient down-moraine (Fig. 6.19).

Kolmogorov Smirnov two-tailed test: In four locations clasts were sampled from diamicton facies, which were overlain by a coarse angular gravel facies devoid of fine material (see section 6.3.4). To aid interpretation of the surficial gravel facies, and elucidate its likely origin, a two-tailed Kolmogorov Smirnov test was employed to compare the roundness cumulative distribution functions of samples in relation to their underlying diamicton facies. The four sample sites tested were: WP001, WP002, WP005, WP010; each of which comprise two samples of $n = 50$ from an upper coarse angular gravel facies and underlying diamicton facies. When tested, the two tailed Kolmogorov Smirnov failed to distinguish between the CDF of samples WP001, WP002 and WP005 at the 99 % confidence interval (Table 6.6). The d_{max} for these samples is 0.22, 0.12, and 0.2, respectively. WP001, and WP002 have identical % RA indices (100). At WP005 the RA index differs by 2% (% RA = 78 and 80) (Table 6.6). However, for the two clast samples at WP010, the two-tailed Kolmogorov Smirnov only failed to distinguish between the roundness CDF at the 95% confidence level. Unlike at other sample sites, the overlying gravel at WP010 (% RA = 100) is more angular than the underlying diamicton facies (% RA = 72).

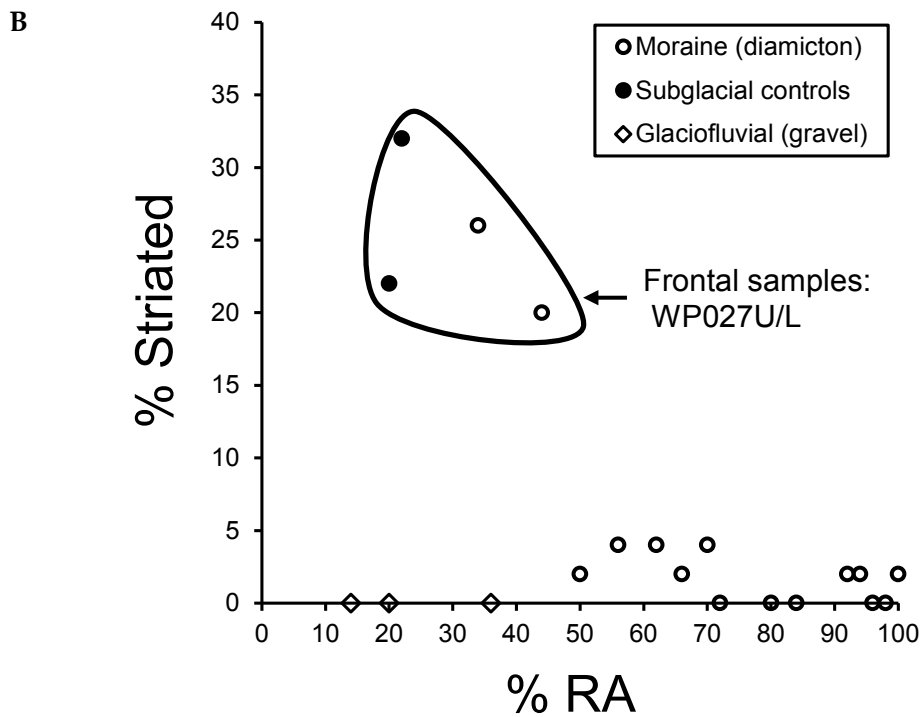
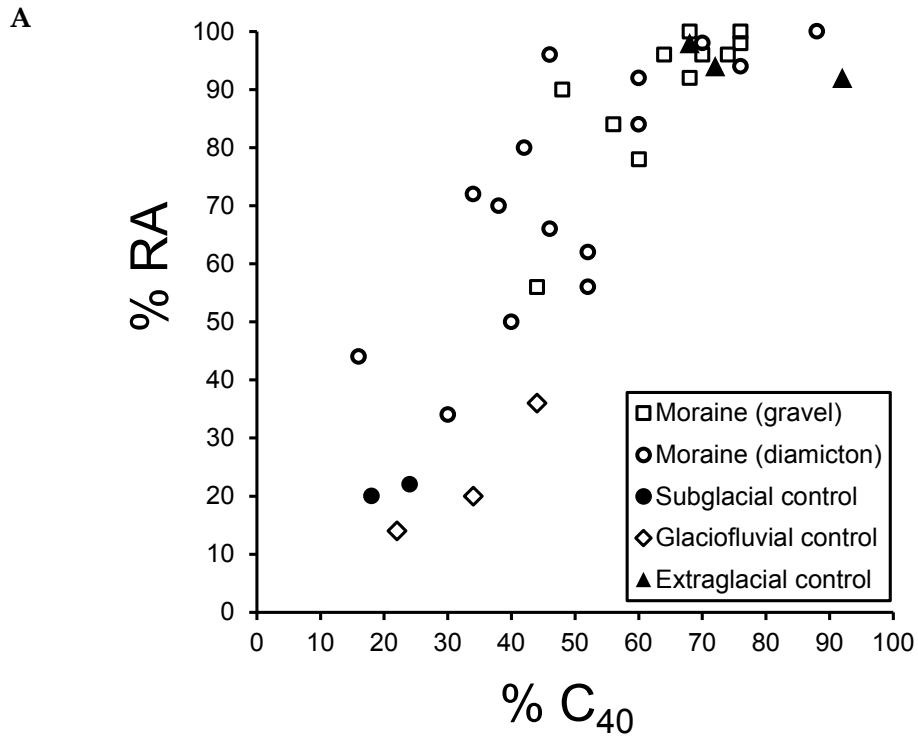


Fig. 6.18 Clast form plots from Austre Lovénbreen. (a) RA/C₄₀ plot. (b) The % RA plotted against the % striated discriminating samples obtained from two locations: subglacial controls and two samples from the frontal zone of the moraine.

Table 6.6 Statistical differences between the CDF of four sets of two clast samples taken from a coarse surficial angular drupe and an underlying diamicton facies.

Exposure	CDF d_{max}	Significance	% RA	
			Gravel	Diamicton
WP001	0.22	P > 0.01	100	100
WP002	0.12	P > 0.01	100	100
WP005	0.02	P > 0.01	78	80
WP010	0.32	P > 0.05	100	72

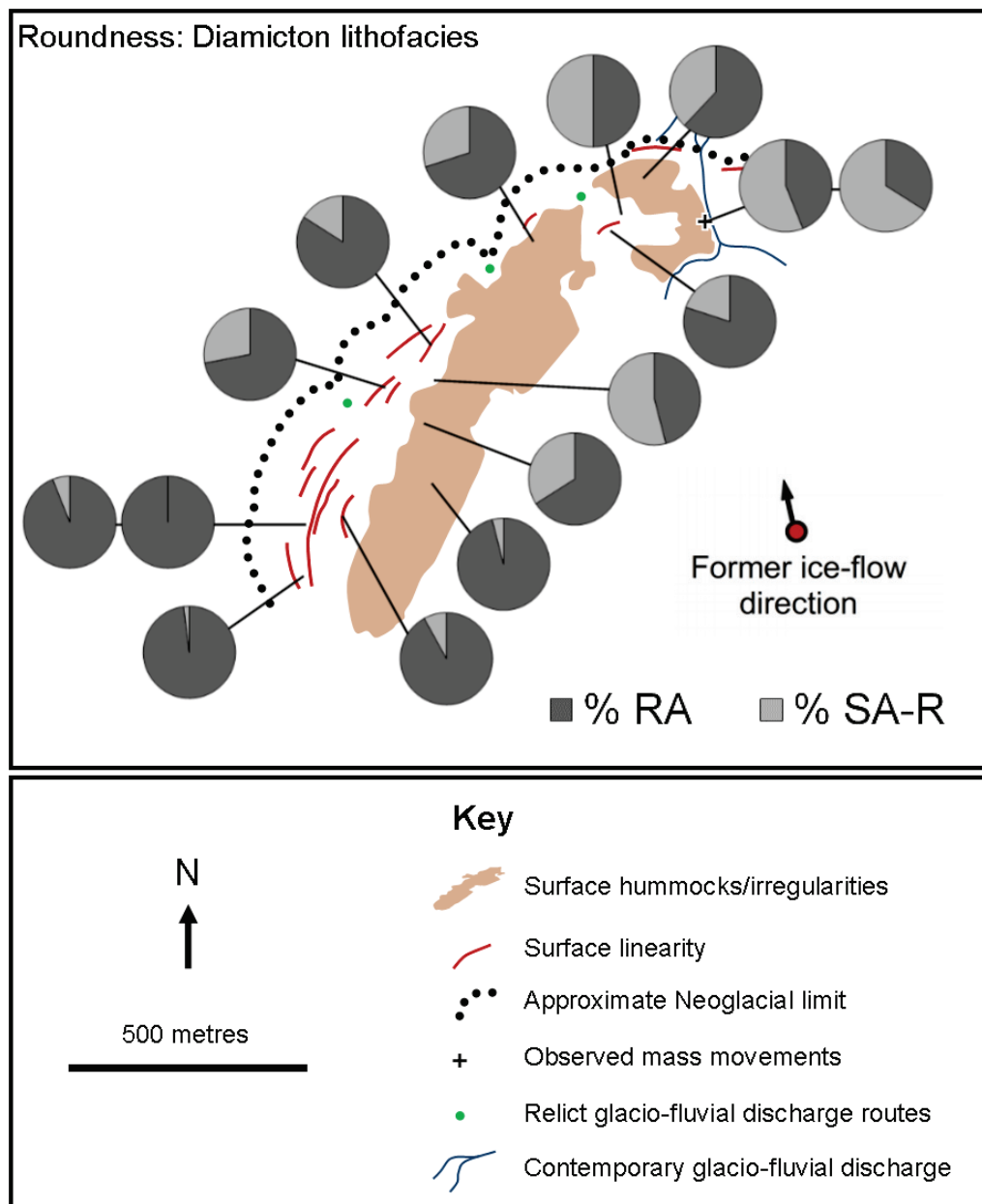


Fig. 6.19 Clast roundness on the lateral-frontal complex. Note the increase in SA-R clasts towards frontal sections of the landform. Geomorphology as mapped in section 6.2.

6.3.6 Moraine evolution: 2003-2014

6.3.6.1 Data acquisition

Five images from 2003 were obtained for DEM production. These images were collected by the UK Natural Environment Research Council (NERC) Airborne Research and Survey Facility (ARSF) on August 9th 2003 from a Dornier 228 aircraft. In 2014, 10 UAV sorties were flown over a two day survey period (15th and 16th July 2014). The total area covered by this survey was *c.* 676,000 m². The moraine was partially snow-covered when the surveys were undertaken. A DJI S800 multi-rotor UAV equipped with an 18 MP Canon EOS-M consumer-grade digital camera was used for image acquisition during the 2014 survey. Further details on the survey setup and validation against a total station derived survey are documented in Tonkin *et al.* (2014). A total of 1,856 images from this survey were used for DEM production.

Ground control was applied to both datasets using a Leica 1200 dGPS. For the 2003 imagery, three ground control points were used to georeference the point cloud and to assign it to the 'real-world' UTM 33x coordinate system. Ground-control was applied using surveyed boulders which were visible on the original scanned image prints and also readily identified in the field. As the glacier forefield could potentially be geomorphologically unstable (e.g. Irvine-Fynn *et al.*, 2011), control points were located outside the Neoglacial limit. Control points were corrected against RiNEX data obtained from Ny-Ålesund (see http://www.epncb.oma.be/_networkdata/). The 2014 imagery was georeferenced using 27 ground control-points. Ground control-points were placed on snow-free areas of the moraine. Illuminous A3 size paper targets are used to ensure adequate visibility on the resulting low-altitude aerial imagery.

6.3.6.2 Image processing

Image processing was conducted in Agisoft Photoscan (v. 1.1.5). A total of 2,035 tie-points were automatically identified on the five images from 2003. For the 2014 imagery, processing was split between two chunks that were merged to form a single DEM of the lateral-frontal moraine. Photoscan identified a total of 5,660,015 tie points from the 1,856 images with the resulting DEM produced from a dense point cloud of 106,484,427 points. Both SfM DEMs were produced at 0.5 m per pixel resolution. The periphery of the 2014 DEM was constructed from low (two or less) image overlap, so was considered less

reliable and was therefore removed. On the 2003 DEM, moraine distal slopes were subject to shading, resulting in excessively interpolated elevation data. Zones identified with these errors were removed prior to analysis.

6.3.6.3 Error assessment

Measurement of error on the DEMs was analysed using a minimal level of detection (minLOD) as a threshold for observable change whereby changes below this threshold were considered potentially erroneous and discarded. Error (dz) was calculated using RMSE (root mean squared error) as a measure of vertical difference between the datasets. Validation of the 2003 DEM was achieved through the use of spot heights from the 2003 LiDAR survey conducted by NERC, simultaneously with the aerial image collection (e.g. Arnold *et al.*, 2006). The NERC LiDAR survey produced a vertical RMSE of 0.888 m ($n = 768,296$; $\sigma = 0.812$ m). As the two datasets were obtained simultaneously, it was assumed that the vertical difference is limited. It is acknowledged that the LiDAR dataset will also contain errors, but for this purpose, serves as an independent dataset for validating the 2003 DEM. For the 2014 DEM, the error analysis was calculated from 12 dGPS surveyed check points. Sub-decimetre vertical error was reported for the 2014 DEM (RMSE = 0.048 m; $n = 12$).

6.3.6.4 DEM differencing and minimum levels of detection

DEM differencing was conducted using the GCD (Geomorphologic Change Detection, ver. 6) plugin of Wheaton *et al.*, (2010) in ArcGIS 10.2.1. DEM differencing is conducted by subtracting concurrent raster grid cells from each other. The GCD plugin facilitates this process by allowing for more robust error assessment through the use of minLOD, which were calculated using a propagated error value on error assessments undertaken on both topographic surfaces (e.g. Braslington *et al.*, 2003). The minLOD technique assumes error within datasets are spatially uniform, and discards changes below this threshold. For the 2003-2014 time period vertical differences under 0.89 m were regarded as potentially erroneous. Three zones (Z_1 , Z_2 and Z_3) were clipped from the differenced DEM and used to report on spatial variations in geomorphological change across the landform (Fig. 6.20).

6.3.6.5 Results

A total area of 461,429 m² was assessed for surface elevation change. Surface change is displayed in Fig. 6.20A. The lateral-frontal moraine shows a level of geomorphological stability, with change detected in just over half of the study area (52%; 238,476 m²). Ninety-six percent of detected change was related to surface lowering. The total volume difference for the study area is reported as $-377,490 \pm 201,292$ m³. The maximum rate of surface lowering is recorded at -5.14 m over the study period (Fig. 6.20B). The maximum average rate of surface lowering, therefore, did not exceed 0.47 ma⁻¹ on the lateral-frontal complex between 2003 and 2014. This is based on a 131 month (August 2003 – July 2014) gap between surveys.

A clear spatial trend dominates the landform. The lateral up-glacier sections are subject to higher rates of surface lowering. Average net surface change in Z₁ is reported at -2.56 ± 0.89 m for the study period. Nearly all grid cells in this area were observed outside the minimum level of detection. Z₂ and Z₃, which are located in more frontal positions show diminishing rates of detectable change (92.2 and 19.9 % of each study area respectively) and lower rates of surface change (-1.49 ± 0.89 m and -0.52 ± 0.89 m respectively). Profiles 1, 2, and 3 in Fig. 6.21 also demonstrate reduced surface lowering in frontal positions. On profile 1, surface lowering is clearly evident on the moraine ridge crest, but less extensive on the ice-proximal and distal slopes. Variability on the ice distal slope (340-380 m along profile 1) relate to poorly resolved topography on the 2003 SfM DEM. Profiles 2 and 3 show limited geomorphological change with a significant proportion of change falling close to or below the minLOD (Fig. 6.21). Detectable change on the outwash-plain is limited. Areas of deposition principally occur on moraine distal slopes and in proximity to glaciofluvial drainage systems. The average depth of deposition across the study area is 1.42 ± 0.89 m. However, the deposition is extremely spatially and volumetrically limited, only accounting for the movement of $17,952 \pm 11,267$ m³ of material (4% of the area of detectable change) opposed to $413,394 \pm 212,243$ m³ of change associated with surface lowering across the study area. It should be noted that c. 11 % of the study area was covered by exceptionally late-lying snow, which was typically located in sheltered areas between pronounced ridges, but was snow free in 2003. Values presented here therefore represent a minimum estimate for moraine surface lowering over the study period.

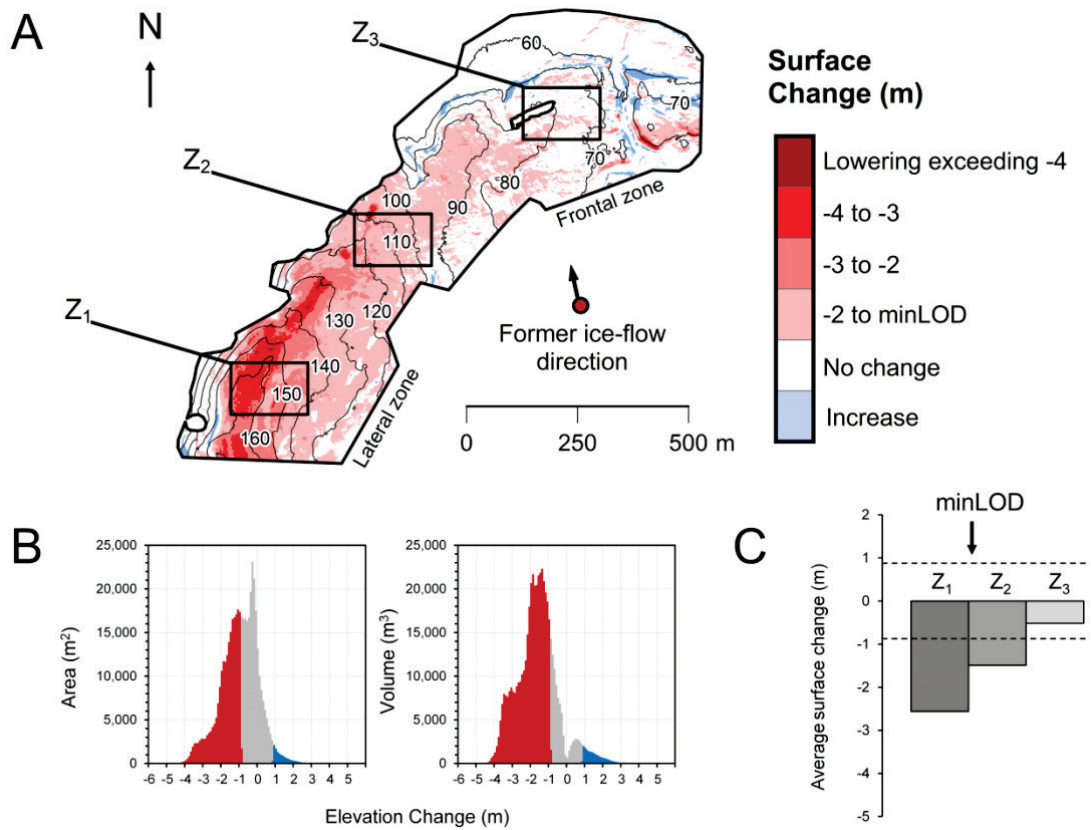


Fig. 6.20 (A) DEM of differences for 2003-2014. Contour data are derived from the 2014 DEM and are displayed in metres. The locations of three additional zones of analysis (Z₁, Z₂ and Z₃) are shown. (B) Surface change from 2003 to 2014 in relation to area and volume. Red represents surface lowering, gray represents thresholded change (error) and blue represents surface gain. (C) Average net surface change from 2003 to 2014 for areas Z₁, Z₂ and Z₃. This appears as Fig. 3 in Tonkin *et al.* (2016).

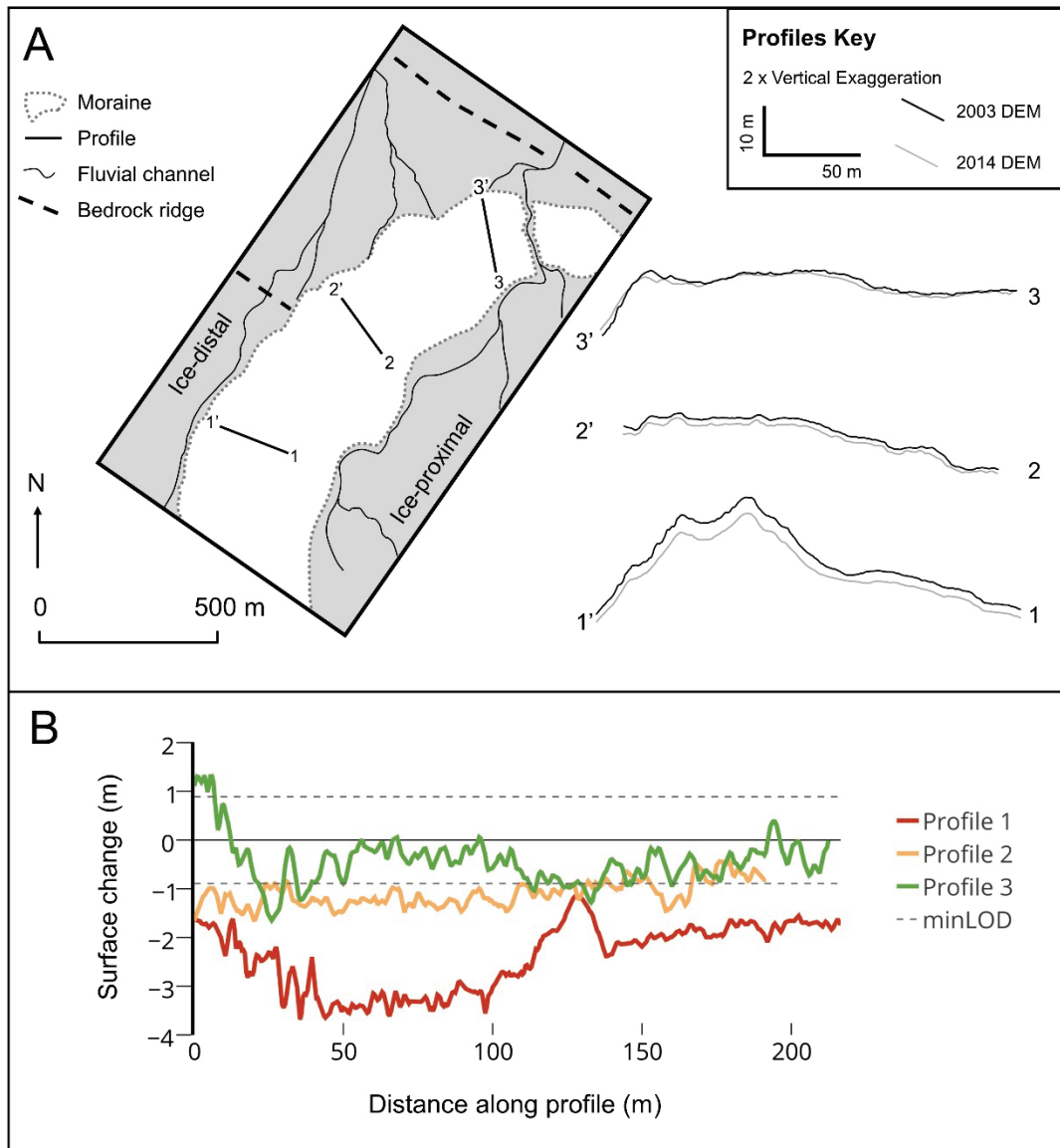


Fig. 6.21 Surface evolution over the 11-year study period demonstrated by three topographic profiles. (A) The locations of the three profiles. (B) Surface change along profiles 1-3 between 2003 and 2014. This appears as Fig. 4 in Tonkin *et al.* (2016).

6.4 Discussion

6.4.1 Structural character and origin of buried-ice

The origin of buried-ice structures within the Austre Lovénbreen true-left lateral moraine was considered in Midgley *et al.* (2013). Three potential origins were discussed with dipping structures representing: (1) primary stratification; (2) relict debris laden englacial thrusts planes; or (3) basal-ice structures (Midgley *et al.*, 2013). Midgley *et al.* (2013) favoured the basal ice origin for dipping ice structures identified within the lateral-frontal moraine. Despite the presence of debris-bearing thrusts within the 1936 aerial imagery, the features presented within the radar profiles are clearly dissimilar to structures reported from radar survey on other Svalbard glaciers. For example, Murray and Booth (2010) used ground-penetrating radar to image englacial-structures within the surge-type glacier Kongsvegen. When imaged at 100 MHz, these structures appeared as clearly spaced (~20 m or more) radar reflectors. Similar to the geometry of the buried ice-structures, thrusts imaged by Murray and Booth (2010) display asymptotic, dipping profiles (~37–52°). However, the thrusts imaged at Kongsvegen lack the dense layering associated with reflectors present within the Austre Lovénbreen moraines. Due to the dissimilarity of the buried-ice structures to features documented at other high-Arctic sites, an englacial thrust origin of these features is unlikely.

In light of the available evidence, Midgley *et al.* (2013) considered buried-ice structures to originate as debris-laden basal ice. Regelation, supercooling and freeze-on were cited as potential processes permitting the development of stacked debris-rich layers within buried-ice. Furthermore, Midgley *et al.* (2013) highlighted that physical conditions such as the subglacial topography (e.g. the overdeepening identified by Midgley *et al.* (2013) from the glacier radar profile of Saintainoy *et al.* (2013)), potential surge-type behaviour (e.g. the surface 'bulge' seen in the 1936 imagery), and the glacier margin could all have acted to promote high longitudinal compression within the glacier (Midgley *et al.*, 2013).

The sedimentary signature of basal ice has previously been investigated (e.g. Adam and Knight, 2003; Cook *et al.*, 2011). Basal ice facies have been associated with high proportions of sub-angular clasts and a tendency for more equidimensional shape characteristics (e.g. low C_{40} indices) (Adam and Knight, 2003). Specifically, the sedimentology from basal ice (and of melted out ice-marginal sediments) formed by both glaciohydraulic supercooling and regelation were investigated by Cook *et al.* (2011). Here,

regardless of the basal ice origin, entrained clasts exhibited low RA and C_{40} indices. This is of stark contrast to the highly angular and blocky parameters of clasts extracted from the Austre Lovénbreen ice sample.

Evans (2009) highlighted that englacial debris transport is important for the development of controlled moraine formation. Passive debris transport from the transfer of debris in primary stratification and the entrainment of basal debris at thermal boundaries represent important inputs for controlling the presence of englacial debris within a glacier, and therefore the formation of controlled moraine (Evans, 2009). Since the publication of Midgley *et al.* (2013) field sampling has provided new data which may allow for basal-ice hypothesis to be discounted (Table 6.7). However, it should be acknowledged that rejecting the favoured hypothesis of Midgley *et al.* (2013) would rest on the analysis of one ice-sample taken from WP002. Clasts from this sample were mostly angular or very angular in character (RA = 95%), which can be interpreted as evidence of passive supraglacial or englacial debris transport rather than basal debris transport and subsequent entrainment. Due to logistical constraints (e.g. limited time available for excavation and sampling) and safety concerns (polar bears and pit collapse), only one ice-sample was obtained. The ice from this sample was taken from a limited exposure (>50 cm²) at the bottom of a ~160 cm deep excavation. Further sampling may reveal ice-facies exhibiting evidence of basal-ice formation. Limited ice-sampling was primarily a result of misleading geophysical data. For example, discrepancies were found to exist between the depth of the buried-ice as documented by the 100 MHz GPR profiles (~50 cm), and the actual depth of the buried-ice (>160 cm). Ground-penetrating radar used at 100 MHz may underestimate the depth of surface debris when surveying buried ice. Further-work investigating may be warranted.

Table 6.7 Summary table of evidence used to deduce the likely origin of buried-ice structures within the Austre Lovénbreen left-lateral-frontal moraine

Evidence		Potential Origin		
		Englacial thrusts	Basal-ice	Primary-stratification
GPR	Dipping structures	✓	✓	✓
GPR	Thinly banded layering		✓	✓
Ice-sampling	Angular and very angular clasts indicative of passive debris transport			✓
Ice-sampling	Blocky clast-shape indicative of passive debris transport			✓
Aerial Imagery (1936)	Primary stratification visible in proximity to the terminus			✓
Aerial Imagery (1936)	Debris-bearing fractures visible in proximity to the terminus	✓		

6.4.2 Lateral-zone formation and evolution

Conceptual models have been developed to account for moraine development (Fig. 6.22) and potential changes to landform stability over time (Fig. 6.23). Fig. 6.22A depicts the status of the lateral moraine during (or close to) the Neoglacial Maximum (*c.* 1900), in 1936 and under present day conditions. During the Neoglacial Maximum, high percentages of angular clasts organised within primary foliation are concentrated at the glacier terminus. Increased top-melt releases debris into the overlying substrate. Once at a sufficient thickness, debris shields buried glacier-ice at the terminus from further ablation (e.g. Østrem, 1959) and reduces the climatic sensitivity of the moraine (Fig. 6.22A). Differential ablation permits the isolation of buried-glacier ice as the glacier thins. Folding of buried-ice occurs as the embryonic ice-cored moraine acts as a topographic barrier for a minor glacier fluctuation (e.g. the down-glacier propagation of a surge-front) resulting in the development of a syncline on ice-proximal sections of the lateral-frontal moraine (Fig. 6.22B). Glacier recession results in the complete isolation of the ice-cored lateral-frontal moraine, which is subject to degradation via down wastage. Debris

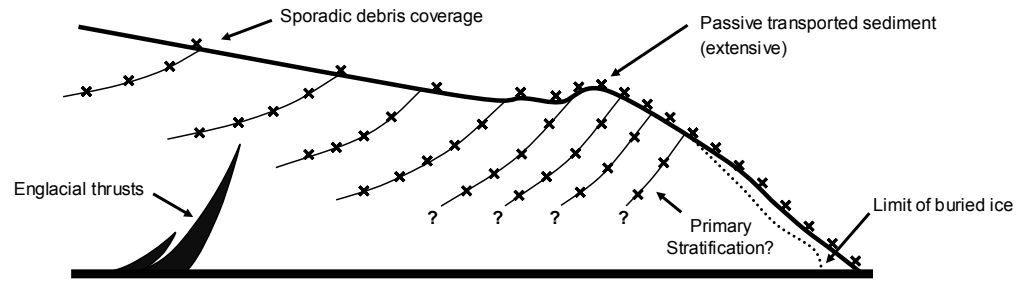
released from the buried glacier-ice forms a thick layer of clast-rich diamicton (e.g. Kjær and Krüger, 2001).

This development of the moraine can also be visualised schematically (Fig. 6.23). Three phases of secondary deglaciation (e.g. Everest and Bradwell, 2003) are defined. The first phase refers to initial increased ablation under thin debris coverage. Here, a thin covering of debris serves to increase initial melt rates through re-radiating incoming solar insolation. Once sufficient thickness is achieved, overlying debris serve to protect the buried-ice, allowing for its preservation. At this stage ice-melt proceeds, but climatic and debris related controls may serve to increase or decrease the rate of melt. For example, increasing temperatures may increase moraine degradation, whereas debris release may limit the rate of top-melt. The Austre Lovénbreen moraine complex is inferred to be at this stage (Fig. 6.24C) in its development at present, principally due to observations of increasing mean summer air temperature experienced by Svalbard over the study period. During the final stage of moraine development, two end-forms are envisaged: (1) a fully stabilised ice-cored moraine, which is in equilibrium with its environment; or (2) an ice-free lateral-frontal moraine complex. It is unclear whether the first scenario is plausible.

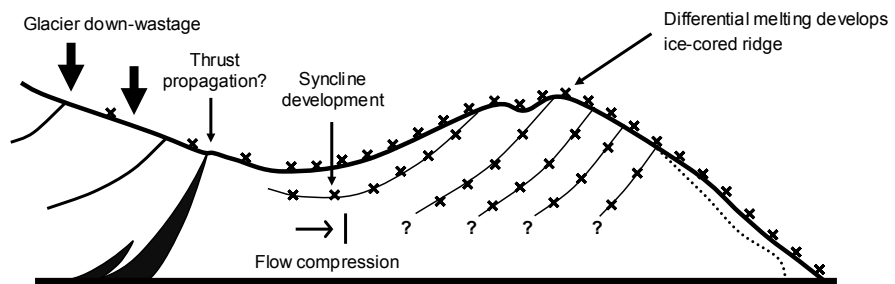
6.4.3 Frontal-zone formation

An alternative model for the development of frontal zone is presented in Fig. 6.24. This model differs from the lateral zone as buried-ice is not included within the structure of the moraine. The model is developed from interpretation of a fluvially cut exposure located at WP027. Slumping of debris from the steepened ice-margin was observed in historical photos of Midtre Lovénbreen in 1892 (Hamberg, 1894). Given the similarity between the two glaciers, this moraine forming process is inferred to also occur here (Fig. 6.24). The basal origin of this sediment is interpreted from the clast-form parameters of sediment sampled from WP027 which overlap from subglacial control samples (section 6.3.5). Recession or minor oscillation of the ice-margin forms an additional deposit of diamicton also derived from dumping basally transported debris, leaving an inclined stacked diamicton structure which represents the former moraine ice-proximal slope (Fig. 6.24).

A Neoglacial maximum (c. 1900)



B c.1936



C Present day

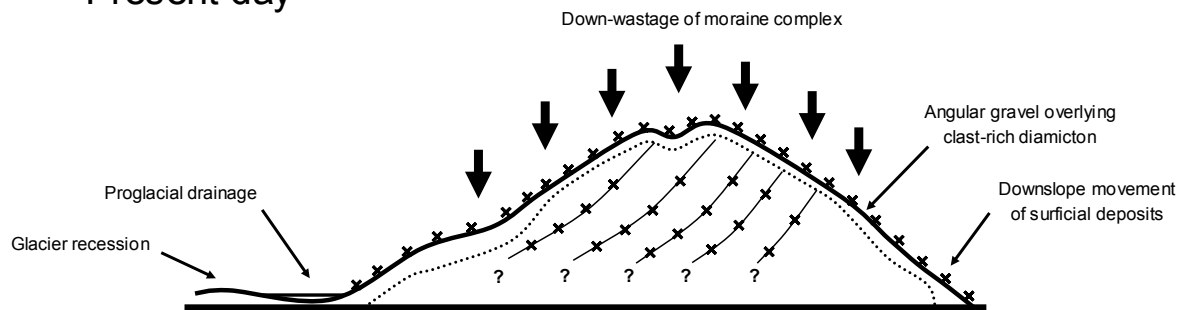


Fig. 6.22 A process-form model for the development of the ice-cored lateral moraine complex at Austre Lovénbreen. Glacier flow occurs obliquely to the cross-section. (A) Supraglacial debris transport and concentration at the Neoglacial Maximum. (B) Thinning of the terminus. (C) Present day downwastage following extensive glacier recession. For illustrative purposes the bed is depicted as horizontal. In reality it is gently sloping down-glacier.

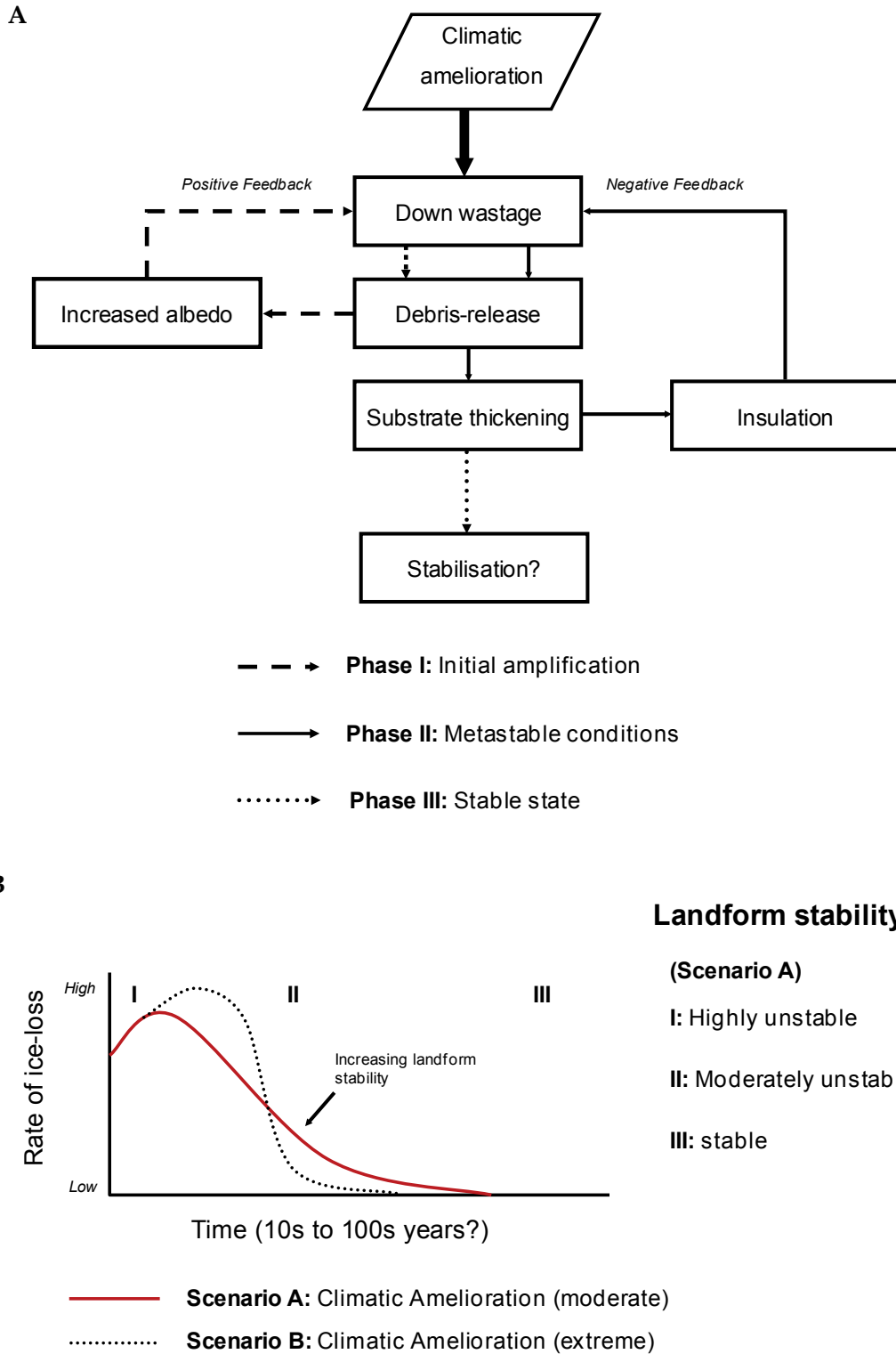


Fig. 6.23 Conceptual flow diagram showing pertinent feedbacks controlling the deglaciation process of ice-cored 'controlled' moraine. (A) Positive and negative feedbacks involved in the degradation of ice-cored moraine and (B) the rate of ice loss over time in relation to two hypothetical warming scenarios.

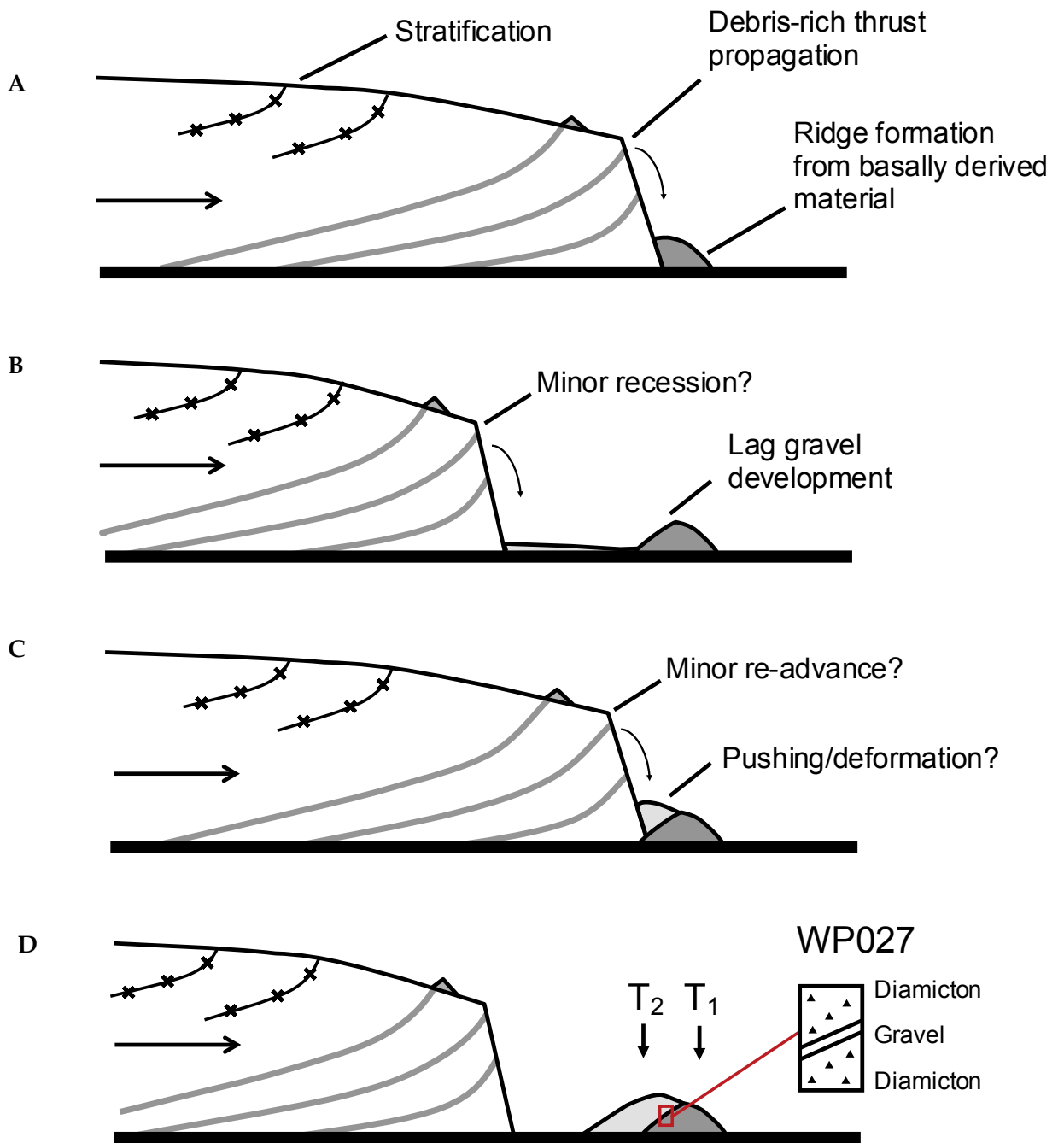


Fig. 6.24 A potential process-form model for the development of ice-free frontal sections of the moraine complex related to the oscillation of the glacier terminus and the supply of basally derived material via debris-rich thrust propagation at the terminus (e.g. Hamberg, 1894). Material is dumped from the steepened ice-cliff. T₁ and T₂ indicate the chronology of the two moraine deposits, with T₁ formed first.

6.4.4 Influences on rates of moraine disintegration

Here, rates of landform degradation appear to be limited in comparison to other sites. For example, Irvine-Fynn *et al.* (2011) reported a moraine surface lowering rate of -0.65 ± 0.2 ma⁻¹ at neighbouring Midtre Lovénbreen between 2003 and 2005. Longer-term changes (1984-2004) at Holmstrombreen are reported to have occurred at a rate of -0.9 ma⁻¹ (Schomacker and Kjær, 2008). Rates of surface lowering in temperature Icelandic glacial environments are variable (0.015-1.4 ma⁻¹; e.g. Krüger and Kjær, 2000; Schomacker and Kjær, 2007; Bennett and Evans, 2012). Whilst the maximum rate of surface lowering was calculated at -0.47 ma⁻¹, on average, surface lowering for the entire study area was considerably lower (-0.16 ma⁻¹) than reported at other sites. Even in areas with high levels of surface lowering (e.g. Z₁), only modest rates of surface lowering per year were detected (-0.23 ma⁻¹). A proportion of the study area (52%) was below the minimum level of detection implying no or exceptionally limited geomorphological change between 2003 and 2014.

Moraines in the high-Arctic glacial environment are understood to be highly vulnerable to thermo-erosion and mass movement facilitated by fluvial undercutting. This can result in high rates of landform transformation (Ewertowski and Tomczyk, 2015). Such surface processes are suggested to be less important with regard to the transformation of the lateral frontal moraine at Austre Lovénbreen. A surface excavation in proximity to Z₁ showed that the debris mantle was surprisingly thick at 1.6 m. At this site, and potentially others, whilst rates of moraine degradation may be high, a relatively thick and evenly distributed debris-layer can permit the meta-stabilisation of ice-cored moraine where the coupling of slope and fluvial process (e.g. Etzelmüller, 2000) exert less influence on moraine transformation. This is largely due to the less topographically confined setting of the lateral-frontal complex at Austre Lovénbreen. The result is a low level of transformational activity, which principally occurs via down-wasting (e.g. Ewertowski and Tomczyk, 2015). An implication of this study is that the ice-cored moraines formed at Austre Lovénbreen, and potentially other valley glaciers in Svalbard, may have higher preservation potential than previously thought possible as insulating debris is not reworked and remains *in situ*. Two scenarios (or a combination of the two) related to de-icing progression at Austre Lovénbreen are envisaged. The moraines may stabilise in relation to recent climatic amelioration. This scenario requires a thick debris mantle to

develop that exceeds the permafrost active layer allowing buried-ice to be a persistent landscape feature over decadal-centurial timescales. Alternatively, the active layer may continue to exceed the depth of the debris mantle for the duration of the secondary deglaciation process, resulting in continued and complete melting of buried-ice despite an increasing debris thickness.

During the final stage of moraine development, two end-forms are envisaged: (1) a fully stabilised ice-cored moraine, which is in equilibrium with its environment; or (2) an ice-free lateral-frontal moraine complex. It is unclear whether the first scenario is plausible. Currently, ice-cored 'controlled' moraines are understood to be poorly preserved in the geomorphological record (Evans, 2009). Buried-ice up to 200 years of age has been documented in moraines at the margins of temperate Icelandic glaciers (e.g. Everest and Bradwell, 2003). Examples where the preservation of buried-ice has been permitted on longer timescales include formally glaciated continental settings (e.g. Ingólfsson and Lokrantz, 2003; Murton *et al.*, 2005), and cold deserts where buried-ice is suggested to have existed several millennia under permafrost conditions (Sugden, 1995; Schäfer *et al.*, 2000). Waller *et al.* (2012) highlighted that the preservation of buried-ice may be permitted on geological timescales if it is located at depths unaffected by seasonal thaw. However, the high-Arctic glacial environment in Svalbard is known for its highly unstable ice-cored moraine, and rapidly progressing mass wasting processes (Bennett *et al.*, 2000; Schomacker, 2008; Irvine-Fynn *et al.* 2011; Ewertowski and Tomczyk, 2015). Schomacker (2008) showed that climatic variables are only weakly correlated with rates of ice-cored back wastage occurring at 14 different glaciers; the implication being that surface processes and topography are more important determinates of moraine disintegration. However, it should be noted that as Schomacker (2008) only investigated rates of back wasting, it may not be directly applicable to Austre Lovénbreen. Very limited field evidence of ice-cored moraine disintegration via back wastage was found at Austre Lovénbreen in 2014, 2009 and 1999 (Midgley pers. Comms).

The physical properties of the insulating debris layer such as its thickness, water content and thermal conductivity influence rates of moraine down-wastage (Schomacker, 2008). Highly permeable substrates allow rain to advect heat down to buried-ice and facilitate top-melt (Reznichenko *et al.*, 2010). Conversely, block-rich material with high surface roughness has low thermal conductivity and can obstruct the development of winter

snow-cover depressing the lower limit of permafrost in mountain terrain (Etzelmüller and Frauenfelder, 2009). Whilst block-gravel is not recorded on the Austre Lovénbreen moraines, the substrate typically consists of clast-rich diamictos (e.g. Graham, 2002) which are typically overlain by gravels with a variable fine component. Diamictos are associated with variable porosity values (e.g. Parriaux and Nicoud, 1990; Kilfeather and Van der Meer, 2008; Burki *et al.*, 2010; Worni *et al.*, 2012). Diamictos with silt and clay components and frozen horizons will lower the permeability of the debris, and serve to impede heat advection by water during summer months, thus limiting ice-ablation (e.g. Reznichenko *et al.*, 2010).

Local topographic controls also influence air temperature and subsequently permafrost distribution (Harris *et al.*, 2009). Strong topographic shading has been reported as an influence on de-icing at other sites in Svalbard (e.g. Lønne and Lyså, 2001). Given the proximity of the landform to Slattofljettet (582 m), rates of moraine down-wastage in up-glacier sections of the landform may be influenced. Modelling of these shading effects is likely to be an interesting avenue of research in relation to moraine disintegration and more generally, permafrost distribution and properties in mountainous terrain.

A further confounding factor is snow-cover, which is known to limit the influence of atmospheric heat on ground temperature (Stieglitz *et al.*, 2003). At the time of the 2014 survey, late lying snow covered a *c.* 11% of the study area. Values reported here are therefore considered a minimum estimation of moraine down-wastage. Whilst in winter, snow may permit higher ground temperature in relation to mean air temperatures (Stieglitz *et al.*, 2003), late lying snow is likely to play an additional role limiting the susceptibility of buried-ice to surface warming. Further work investigating the influence of snow cover and snow-depth in relation to moraine down-wastage could elucidate how significant a role it plays in reducing down wastage.

An additional aspect of interest is the spatial component of landform transformation. Diminishing rates of landform disintegration from Z_1 to Z_3 correspond with an increase in the moraines debris component from lateral to frontal positions (Section 6.4.1 and Section 6.4.2; Midgley *et al.*, 2013). Spatially variable amounts of buried-ice imply that the mode of moraine formation is not consistent across the moraine complex (e.g. Hambrey and Glasser, 2012). Lateral sections conform to the 'controlled' ice-cored model of moraine formation where the release of material from debris-rich folia result in surface

linearity and form an insulating surface layer for underlying glacier-ice. The limited rates of ice melt in the frontal sections, and the presence of surface irregularities indicate that separate glaciological and geomorphological processes are responsible for the emplacement of moraine at different locations along the lateral-frontal complex. Here, structural glaciology and the preferential entrainment of basal debris in frontal locations is likely to be important. For example, studies have investigated the development of belts of moraine mounds ('hummocky moraine') in relation to the stacking of englacial material along thrusts planes (e.g. Hambrey *et al.*, 1996; 1997; Bennett *et al.*, 1998; Glasser and Hambrey, 2001; Graham, 2002; Midgley *et al.*, 2007; Cook *et al.*, 2015). The processes described in these papers may, in part, be responsible for areas of surface irregularity on the moraine complex and lower levels of ice incorporation. Additional processes such as pushing and permafrost deformation are documented to operate in ice-marginal environments in Svalbard (Etzelmüller *et al.*, 1996; Boulton, 1999). It is unclear whether such processes are important at this site.

6.4.5 Limitations and issues related to the application of UAV topographic surveys and SfM Photogrammetry

This research highlights the potential of UAV and SfM technologies and their application in relation to a range of geoscientific enquiries. Here, the use of the UAVs combined with SfM was limited to data acquisition of the 2014 DEM. The resulting SfM DEM derived from this field campaign appears to show excellent levels of both accuracy and precision. The integration with corrected dGPS ground-control has enabled the geo-registration of exceptionally high-resolution orthorectified aerial imagery, and associated DEM that can be used to assess future geomorphological change. If a future aerial survey is undertaken at a similar level of both accuracy and precision as obtained in 2014, it will enable a much lower error threshold than was obtained between 2003 and 2014. Total RMSE reported following application of dGPS derived checkpoints fell within the sub-decimetre range (minimum and maximum errors of 0.014-0.144 m). Elevation differences between the SfM DEM and the checkpoints yielded excellent vertical agreement. The achievable levels of precision flying at *c.* 100 m above ground level using a consumer-grade digital camera make the repeated deployment of an UAV a highly suitable piece of equipment for geomorphological investigations of this kind.

The use of a SfM photogrammetric approach to extract topographic data from the 2003 aerial image appears to be less straight-forward. The main issue encountered here was the achievable levels of accuracy from the 2003 images, which in turn, reflect high minimum levels of detection when applying error thresholds for DEM differencing. Two interrelated issues are likely to account for higher levels of error in these datasets: (1) the use of lower resolution imagery for reproducing the former geometry of the landforms and (2) the use of existing 'stable' features for ground-control.

The first issue mainly relates to the fact that the 2003 imagery was at a coarser resolution (contact prints scanned to give an approximate ground resolution of 0.2 m per pixel) than the sub-decimetre resolution imagery obtained by the UAV survey. Thus, minimum levels of detection can be expected to be at, or around the resolution of existing images. This may also have been problematic when using the dGPS to survey 'stable' boulders to use as ground-control. For example if a boulder is smaller than the resolution of the raw uncorrected imagery, then it is likely to be unidentifiable on the imagery. This limits GCP selection to only large boulders. Finding suitable spots on such boulders which both aid their identification during the SfM point cloud creation process, and limits discrepancy between the actual dGPS survey point location maybe problematic. The second issue relates to the limited selection of ground-control points in geomorphologically unstable terrain, an issue encountered in similar studies that use photogrammetry to produce DEMs of changing geomorphological systems (e.g. Staines *et al.*, 2014). In this study, areas on the lateral-frontal moraine complex are avoided, as the landform is geomorphologically active. In such circumstances, the resulting optimal distribution of GCPs is not possible. Furthermore, sub-optimal GCP placement are suggested to weaken reproducibility and introduce error (Clapuyt *et al.*, 2015). Given the range of issues involved, extracting topographic data from standard aerial imagery is still demonstrated to be useful for studies investigating the response of geomorphological systems to de-icing. The techniques described here are also applicable to other research areas that would benefit from high spatial resolution and potentially high temporal resolution imagery and associated DEMs.

6.5 Summary

A multidisciplinary approach is used to characterise a lateral-frontal moraine developed at the margin of a high-Arctic valley glacier in Svalbard. Semblance analysis of GPR

common-midpoint surveys reveals high rates of radar-wave propagation in lateral sections, and low rates of radar wave propagation in frontal sections. This demonstrates an ice-dominated lateral composition, which grades through to a debris-dominated frontal section. Up-glacier dipping reflectors and syncline structures are documented to occur in areas of buried-ice. The initial favoured origin of this ice, as discussed in Midgley *et al.* (2013), is reinterpreted in light of a sampled-ice and potential melt-out tills which carry high quantity of angular clasts implying high-level glacier transport. A conceptual model related to the deformation and burial of primary stratification is developed in this chapter. Formation processes across the moraine complex may not be consistent, with frontal sections dominated by addition structural glaciological processes (e.g. thrusting), and subaerial dumping and lateral sections forming due to ablation and release of buried glacier-ice ('controlled moraine'). This is reflected by the occurrence of basally transported clasts in frontal areas of the moraine.

SfM photogrammetry is used to produce repeat DEMs of the landform and report on rates of moraine evolution over an 11-year period. The maximum average rate of surface lowering observed was -0.47 ma^{-1} . Average surface lowering over the entire study area is reported at -0.16 ma^{-1} . Landform evolution occurs more rapidly on lateral sections than frontal sections of the landform which typically fall below the minimum level of detection. Unlike other sites in Svalbard, the moraine appears to be de-icing predominately by down wastage, affording the landform high levels of stability. Atypical of de-icing moraines in the high-Arctic, slope and fluvial driven change appears to be less significant. There is potential for the buried-ice to be stabilised and preserved as a palaeo-glaciological archive of former Neoglacial ice dynamics. The high-resolution UAV derived dataset serves as a benchmark for future ultra-high resolution and accurate surveys of the lateral-frontal moraine at Austre Lovénbreen. The use of SfM photogrammetry for extracting topographic data from a range of aerial imagery is demonstrated to be beneficial for monitoring environmental change and is likely to have wider applications in other geoscientific sub-disciplines.

7. Discussion and conclusions

7.1 Introduction

Whilst findings are discussed within their respective chapters, aspects of this study are synthesised here. This section highlights disparities between the glacier processes and products within each of the landsystems and the potential diagnoses of specific forms in the geomorphological record. In this thesis the structure, morphology and significance of three lateral-frontal landforms have been investigated. Findings contribute current understanding of the glaciological and geomorphological significance of these landforms providing data on the sedimentary character of contemporary glacial environments. Furthermore, to my knowledge, this study is amongst the first to integrate SfM and UAV technologies for the purpose of investigating moraine degradation within high-Arctic glacial environments.

7.2 Discussion of study objectives

Objective 1: To investigate the novel integrated use of UAV and SfM technologies for geomorphological research and apply the technique to contemporary glacial environments.

This thesis has investigated the use of UAVs for novel small-format low-level image acquisition in relict and contemporary glacial environments. As a result of this study, a greater understanding of the potential of this technique is now known including logistical considerations and the potential spatial resolutions of derivative data products (e.g. DEMs and orthophotos) (Chapter 3; Tonkin *et al.* 2014). This study is the first to integrate UAV derived imagery and SfM photogrammetry to investigate the degradation of ice-cored moraine Chapter 6; Tonkin *et al.*, 2016). Furthermore, some of the technical challenges related to the extraction of topographic data from conventional imagery for the purpose of assessing geomorphological change were appraised. For example, there are challenges related to the application of ground-control on historical imagery, where much of the terrain is undergoing post-glacial modification. Given the low number ($n = 3$) of ground control points available, SfM is still shown to enable the extraction of topographic data with validation datasets showing acceptable levels of error (RMSE = 0.888 m), allowing for surface change under 1 m to be assessed.

Objective 2: To assess the internal structure of lateral-frontal moraine using ground-penetrating radar (GPR) or direct observations

The internal structure of lateral-frontal moraine has been assessed at three sites (Schwarzberggletscher, Isfallsglaciären and Austre Lovénbreen). Field surveys show that the internal structure is dissimilar at all three sites. Alpine moraine are structurally organised into stacked inclined units of diamicton deposited in particular sequence, dependant on whether the glacier overrode or was obstructed by a pre-existing moraine rampart. The Alpine sites investigated appear to be largely devoid of buried-ice despite an abundance of supraglacial debris, with buried ice spatially restricted to ice-proximal locations, and short lived with regard to their preservation. Moraine building episodes, thus advances in the glaciers lateral extent, are indicated by units of diamicton overlaying palaeosols. This is of stark contrast to both Arctic sites. At Isfallsglaciären, structurally, the moraines appear to be dominated by large bouldery debris (e.g. hyperbolic reflectors in the GPR radar-grams), although bounding surface layers can be identified in frontal deposits, and indicate the deposition of sedimentary units on both the ice-distal and ice-proximal slopes. The stratigraphy of diamicton units is largely topographically determined, and relate to the former position of the glacial surface and whether material is superimposed on pre-existing ice-proximal slopes or accreted onto the ice-distal slope. Given the mountainous setting, with sparse or absent vegetation it is unclear whether such bounding layers could be a potential source of organic material which could be used to constrain glacier activity over the Holocene. Organic layers are common in Alpine moraine (Ivy-Ochs *et al.*, 2009), reflecting long formational histories over several glacier advance stages, but are infrequently identified in Arctic lateral-frontal moraine located in continental Scandinavia (e.g. Hormes *et al.*, 2004). Furthermore, higher radar velocities are identified in lateral zones of the Isfallsglaciären lateral-frontal moraines, and are interpreted to indicate the presence of ice within the internal structure, although the origin of the ice in terms of its depositional history may be different to high-Arctic landforms (e.g. Østrem, 1964).

Austre Lovénbreen offers an example of where, volumetrically, glacier ice represents a significant proportion of the landform. The findings reveal that glacier structures are exceptionally well-preserved, as demonstrated by 100 MHz GPR surveys. Whilst the GPR data show a limited surficial debris layer, the actual debris layer exceeds 1.5 m. The

findings also show that GPR may be ineffective at estimating the debris layer thickness on glaciers and ice-cored moraine when deployed using a 100 MHz antenna setup. Similar to Isfallsglaciären, ice within the landform appears to be limited to lateral zones of the landform. The dominance of debris in supraglacial transport at these positions promotes the isolation of ice at the terminus, and explains the spatial extent of buried ice as detected by the GPR.

This research highlights that based on structural configuration, 'controlled' ice-cored moraine as a term cannot be applied to the ice-cored moraine investigated at Isfallsglaciären. Additional descriptors such as 'Østrem' type moraine are likely to be useful in distinguishing these structurally diverse landforms, which are formed by glaciers with both dissimilar (e.g. non-surge type, continental climate, moderate relief setting, variable permafrost presence) and similar (e.g. polythermal structure) attributes.

Objective 3: To use sedimentological techniques to assess the debris transport histories and origin of material contained within moraine and to allow important moraine forming processes to be identified.

The relative importance of specific ice-marginal processes (glaciotectonism, dumping, and ablation) also vary across the three sites. At Austre Lovénbreen the ablation and the release of debris from glacier ice and transfer of supraglacial debris on to moraine via dumping are important processes controlling the development of the landform, although the importance of ablation as a process is more significant for the formation of the ice-cored lateral zones, rather than the frontal zones.

In contrast, Isfallsglaciären may represent a complex situation related to the relative importance of dumping, glaciotectonism (e.g. related to overriding of pre-existing moraine), and the formation of ice-contact fans (e.g. distal deposits on the outer-frontal ridge). Silt deposits on ice-proximal slopes also indicate how existing landforms act as a topographic barrier promoting the development of a low-energy depositional environment (e.g. ice-marginal lake development). The dumping and flowage from the lateral ice-margin are significant ice-marginal processes at Schwarzberggletscher which result in the production of crudely stratified diamictons, with strong-moderate macrofabrics dipping away from the former glacier surface. This is in accordance with previous models of moraine formation (e.g. Humlum, 1978; Small, 198). However, the

strength of the principle eigenvalue of clasts diminishes down-glacier, which may reflect glaciotectonic disturbance of initially dumped sediment units.

Common to all sites is the presence of diamicton and gravel facies as products of glacial transport and deposition. It is clear that the clast-form parameters vary across sites (Table 7.1). This in part represents lithological controls (e.g. Lukas *et al.*, 2014), but also debris transport pathways and potential re-working related to past glacier activity at different sites. Clast-form gradients are best observed at Austre Lovénbreen, but are also present at Isfallsglaciären and Schwarzberggletscher. Schwarzberggletscher has the least well developed clast-form gradient. Material appears to show distinguishable shape (C_{40}) and roundness (RA) indices but exhibits a reduction in the amount of VA clasts, and a surprising increase in clasts carrying striae within the lower-lateral complex. Various hypotheses were discussed regarding the origin and significance of the striae. The favoured hypothesis is the elevation of debris as the former glacier flowed over a steep bedrock slope, and initiation of debris transfer from the glacier bed (e.g. Swift *et al.* 2006). The transfer of basal material into lateral moraine has been suggested at other sites (Benn and Owen, 2002; Lukas and Sass, 2011; Lukas *et al.* 2012) and may be widely applicable to lateral moraine formed in high-mountain glacial environments. The RA and C_{40} indices decrease from lateral to frontal position at the high-Arctic glacier, Austre Lovénbreen, as does the occurrence of striated clasts. At Isfallsglaciären, material on the frontal moraine exhibits evidence of active transport in the form of sub angular and striated clasts, which are rare or absent on the lateral zones. The clast-form gradient, in part, highlights a disparity in occurrence of the glaciological processes responsible for the elevation of basal material to a supraglacial position for dumping at the ice-margin within each of the parent glaciers investigated, but also variation in terms of the quantity of debris input from extraglacial sources within each of the glacial landsystems. As debris transport, the transfer of basal material, and moraine construction are linked, the sedimentary signature of relict lateral-frontal moraine in the geomorphological record have the potential to be used to infer former debris transport pathways and character of former glaciers.

Objective 4: *To develop models of moraine formation to account for subsets of lateral-frontal moraine formation in Arctic and Alpine environments*

Whilst all the landforms investigated can be classified as lateral-frontal moraine, each site highlights how local conditions (topography, glacier thermal regime, dynamic status of

the parent glacier) are important with regard to the character and form of the resulting feature. These lateral-frontal moraines should therefore be considered as subsets of the typical 'valley glacier landsystem' model, exhibiting site specific nuances related to glaciological and environmental conditions (e.g. Boulton and Eyles, 1979; Benn *et al.*, 2003). Divergent models of moraine formation applicable to each site are presented within the previous chapters and are compared here.

For temperate high-mountain glacial landsystems, the findings presented in this thesis aid the verification of new models of landform development. Whilst aspects of these models satisfactorily explain the formations investigated here, debris supply and topography are demonstrated to be important controls on the character of Alpine lateral-frontal moraines. Predictive models of landform development that account for lateral-frontal ridges as a primary product of passive glacier transport do not necessarily fully account for all findings presented here. Passive glacier transport contributes significantly to moraine formation, however the structural glaciology of the parent ice is suggested to be important with regard to the provision of actively transported debris for moraine formation.

For the continental Arctic site (Isfallsglaciären), despite historically being amongst the first sites identified with 'ice-cored moraine', the results presented here show that they are structurally divergent from their high-Arctic counterparts. However, models of landform development for the glaciers of continental Scandinavia remain poorly developed, with uncertainty over the origin of the incorporated ice, the age of the incorporated ice, and the interaction of the parent glacier with permafrost in the proglacial area. At present, due to the overriding of pre-existing moraine, the chronology of the landforms is poorly constrained, and should be subject to future study to see whether they are in agreement with interpretations of Østrem type ridges from other sites (Matthews *et al.*, 2014). A range of ice-marginal processes are likely to have operated at the time of moraine genesis. The reoccupation of the moraine rampart of the late Holocene introduces additional complexities, for example, the ineffective self-censoring of pre-existing moraine within the forefield by later glacier advances. Given the importance of the glaciers of Tarfala valley in relation to long-term monitoring, future investigations seeking to understand their sedimentological record may help aid understanding of glacier response over the late Holocene.

Moraines developed by the Arctic polythermal glacier, Austre Lovénbreen, were formed following the isolation of buried ice from solar insolation by a debris cover of passively transported debris sourced from valley sides and the ablation of relatively debris-rich primary stratification contained within the ice. Whilst the initial formation of the ice-cored moraine may conform to existing models for the development of ice-cored moraine relating to the isolation of a body of glacier ice (Schomacker, 2008; Evans, 2009), the coupling of slope and fluvial processes in high-Arctic settings appear to be acting at a slower rate at this site, permitting a relatively stable secondary deglaciation processes with limited backwastage of exposed ice and debris flow activity. It is unclear whether the moraine has switched from an active to stable state (e.g. Ewertowski and Tomczyk, 2015), but given the lack of relict mass movement deposits, this may be unlikely. This has implications for the long-term persistence of ice-cored moraine in high-Arctic glacial environments.

Objective 5: *To assess how the morphology and internal composition of lateral moraine may change following climatic amelioration or deglaciation and identify any implications this may have on interpretations of the Quaternary landform record.*

Contemporary glacial landsystems can be seen as useful analogues for formerly glaciated areas (Benn and Lukas, 2006). There is therefore potential for landforms to inform researchers on past environmental and glaciological conditions. Alpine sites may be more readily identified due to their distinctive asymmetric morphology. The persistence of these landforms in the geomorphological record is beginning to be recognised, with moraine chronologies spanning the entire Holocene (e.g. Schimmelpfennig *et al.*, 2013). However, it is noted that topography may play a significant role in relation to the external censoring of these features (Barr and Lovell, 2014; Fig. 7.1) and also their resulting topographic expression. In chapter 4 lateral moraine at Schwarzberggletscher appears to be stabilising, with vegetated ice-proximal slopes and the infrequent occurrence of ice-proximal gullies.

In the high-Arctic environment, whilst external censoring has resulted in low preservation potential at some sites, results from Austre Lovénbreen highlight that topography is an important control on landform disintegration. Here, the coupling of fluvial and slope processes are less pronounced due to the topographic configuration of the terminal zone (topographically unconfined) (Fig. 7.1). Neoglacial ice within the

moraines appears to be degrading in a relatively stable manner, preserving glacier structures originating from the Neoglacial advance. The excellent preservation of glacier structures within lateral-frontal moraine provides a potential record of former glacier behaviour. Structures preserved within buried-ice may help elucidate subglacial processes including basal-ice formation and sediment entrainment, and subsequently the thermal composition of these glaciers during the Neoglacial. Given the modest rates of landform degradation and limited back wastage, reworking of debris is limited as it remains *in situ*. The western lateral-frontal moraine at Austre Lovénbreen is likely to be preserved, albeit as a less topographically prominent landform over centurial or potentially greater timescales if not subject to glacier self-censoring (e.g. a future advance removing moraines from the geomorphological record). Variability in terms of the extent of external censoring in high-Arctic settings imply that similar moraines in relict geomorphological environments may represent a fragmented palaeoenvironmental record of glaciation. Studies using moraine chronologies are recommended to evaluate the topographic controls on both the formation of moraines and the role it has on self and external censoring (e.g. Barr and Lovell, 2014).

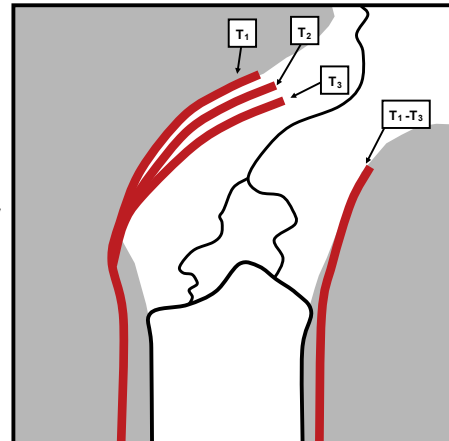
A key finding of this research is the presence of buried ice within lateral zones, but not within frontal zones of Arctic lateral-frontal moraines. A clear implication is that the frontal zones of ice-cored moraine are likely to be better preserved in the geomorphological record following complete de-icing, whereas lateral zones, which are subject to de-icing and potentially external censoring from slope processes, may be poorly preserved (e.g. Bennett, 1999), or completely removed from the geomorphological record. This may have implications for where the lateral reconstruction of former glaciers is attempted (e.g. glacier reconstruction for the British Younger Dryas; e.g. Carr *et al.*, 2010; Bendle and Glasser, 2012), especially if polythermal conditions, thus potential for ice-cored moraine generation, were widespread. The recognition of lateral ice-cored moraine in the geomorphological record is unclear, however, the volumetric content of the buried ice, and the role of topographic censoring is likely to be important with regard to the topographic prominence of deglaciated features. In some cases, where little debris is contained within buried ice, a thin veneer of angular and very angular debris may remain, which is similar to the sedimentary products and the proglacial morphology produced by the backwasting supraglacial lateral moraine on the true left of Schwarzberggletscher.

Table 7.1 Contrasting characteristics at the three sites investigated.

Topographic setting	Morphology	Structure	Moraine lithofacies	Debris transport	Stability
Schwarzberggletscher (Temperate)					
Valley-side and partially unconfined	Asymmetric cross profile; anastomoses into multi-crested feature in lower sections	Spatially limited to a supraglacial lateral-moraine; moraine complex devoid of ice	Predominately clast-rich diamicton	Weak roundness gradient; actively transported sediment found down-moraine	Landform undergoing limited gullying; down-glacier zones vegetated
Isfallsglaciären (Polythermal)					
Valley-side and partially unconfined	Complex: multi- and single-crested zones. Landform partially topographically subdued	Potential ice-debris mix within lateral zones	Boulder-gravel, gravel, mud and clast-rich diamicton	Largely passively transported debris. Frontal zones show evidence of active glacier transport.	Limited evidence of structure failure on ice-proximal slopes
Austre Lovénbreen (Polythermal)					
Valley side and unconfined	Variable: Linear ridges in lateral zones. Surface irregularities in frontal zones	Ice-core comprises a significant component of the landform but is spatially restricted to lateral zones	Gravel and clast-rich diamicton	Largely passively transported debris. Frontal zones show evidence of active glacier transport.	Actively degrading. Moraine subject to spatially variable amounts of down-wastage

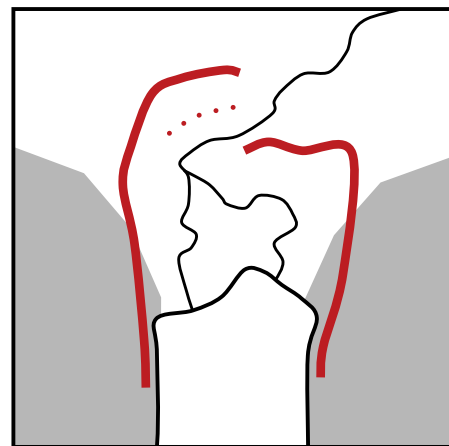
A High-mountain ('Alpine')

- Topographically confined terminus
- Moraine impedes subsequent advance(s).
- Strong moraine asymmetry driven by differential supply of debris on the true left of the basin
- Topography influences external censoring of moraine chronologies



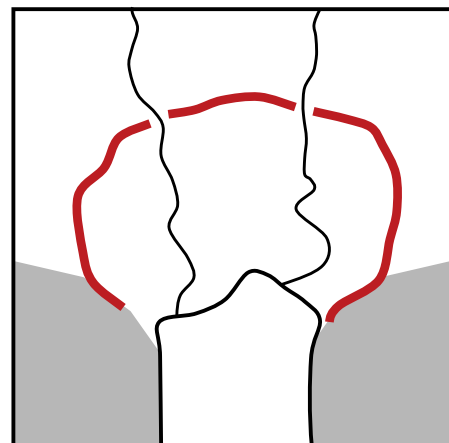
B Partially confined terminus

- Moraine formation partially controlled by topography
- Moraine impedes subsequent advance(s).
- Overriding of pre-existing moraines indicate ineffective glacier self-censoring of moraine chronologies.



C Unconfined with piedmont zone

- Moraine formation in unconfined topographic zone.
- Terminus sensitive to change
- Limited topographically driven external moraine censoring



Legend

- | | | |
|--|--|---|
|  Moraine |  T_3 Moraine chronology |  Confined topography |
|  Moraine (overridden) |  Stream |  Unconfined topography |

Indicative scale: 

Fig. 7.1 Summary figure illustrating confounding topographic factors influencing moraine characteristics and morphostratigraphy at the three investigated sites. (A) Schwarzberggletscher, (B) Isfallsglaciären and (C) Austre Lovénbreen.

7.3 Limitations

A fundamental limitation of this research is the paucity of observations of active moraine formation at the margins of contemporary glaciers. The negative mass balance of glaciers globally (e.g. WGMS, 2012) limit the opportunity to observe active moraine formation, as such, observations of active moraine formation are rarely reported (e.g. Whalley, 1973; Matthews *et al.*, 1995). In this thesis, the processes of moraine formation have been interpreted from the form and sedimentary character of lateral-frontal moraine, or via historical imagery. Consequently, uncertainty over the modes of moraine development still exist. Specifically the coarse, and often massive sedimentary structure of the Isfallsgläciären moraines impede precise understanding of how these glaciers interacted with proglacial permafrost, and how stress was transferred from the glacier terminus into the lateral-frontal ridges. Understanding of moraine formation and the glaciological and geomorphology significance of these moraines remains uncertain. At other sites (e.g. Schwarzberggletscher) findings appear to generally conform to existing predictive models of moraine formation, albeit with site specific nuances.

Site selection also presents a key limitation: in reality, due the practicalities of studying Arctic and Alpine glaciers such as cost, time, access and safety, large sample sizes are difficult to obtain for any given glacial environmental. Choosing a small number of glaciers to test existing models of landform development or basing generalisations regarding landform development on a few sites may result in an incomplete understanding of glacial processes and landform development. Models of landform development may be uniform in applicability or site specific. Generalisations based on a small number of sites may generate contention or disagreement regarding the validity of certain processes and their role in landform development (Lukas, 2005; Graham *et al.*, 2007). In this thesis, although site selection may limit a complete understanding of the complexity involved in moraine construction and modification, it still has merit in that it adds additional case studies for the respective glacial environments to the existing body of knowledge.

The use of mixed lithologies could be considered a further limitation of this study (e.g. Lukas *et al.*, 2013). Whilst the use of a single lithology is suggested to strengthen discrimination of debris transport pathways, the findings presented here show that moraine samples can show good discrimination between active and passive transport

pathways where lithologies are mixed. Given that the analysis of clast-form data is often semi-quantitative, and samples presented are readily discriminated, the value added from single lithology sampling is unclear. Lukas *et al.* (2013) suggested that similar lithologies in different basins do not respond uniformly to transport processes. Thus, the comparison of a single lithology across a range of basins may not yield meaningful comparisons. It is acknowledged that assessment of the lithology of each clast within a sample was not conducted. An abundance of certain lithologies within a facies may aid interpretation of source areas for material and the mode of subsequent glacier transport (e.g. Brugger, 1996).

7.4 Future research

Several research avenues merit investigation following on from the findings presented here.

- *The application of dating controls on Østrem type moraines:* Despite the application of GPR for documenting the structural configuration of these landforms, their genesis remains poorly understood. Potential issues with lichenometric dates, and a paucity of other datasets represent a significant gap in our knowledge of these landforms. Potential dating controls such as Schmidt rebound hammer exposure-age dating (e.g. Winkler, 2014; Matthews *et al.*, 2015) or cosmogenic dating would shed light on the significance of these landforms. Given the potential for reworking, glacier censoring, and para and periglacial processes at the margins of these glaciers, dating studies should be integrated with geomorphological interpretations. Specifically the interaction of advancing glaciers with permafrost in this region requires further investigation in relation to the censoring of lateral-frontal moraines.
- *Structure-from-Motion photogrammetry for measuring historical and contemporary glaciological and geomorphological change:* Research using this iterative automated approach presents a potential research frontier. The potential for the extraction of historical topographic surfaces from archived aerial photography has previously been realised. Where integrated with historical imagery, precise and accurate topographic information can be obtained. A key challenge here will be the collection of robust ground-control and check points for data validation on stable terrain. Through the appropriate use of error thresholding (e.g. Chapter 6;

Wheaton *et al.*, 2010; Tonkin *et al.*, 2016), reasonable estimates for past change are possible.

- *Ice-cored moraine degradation dynamics*: Studies investigating the dynamics of degrading of buried ice are of important for understanding debris covered glaciers, and relevant beyond glacier geomorphology, with vast quantities of buried ice present permafrost terrain in the Northern Hemisphere. A number of additional factors preclude understanding of the dynamics of de-icing. Future work using the high-resolution topography presented here as a baseline could investigate small scale processes which could be observed from sub-decimetre resolution datasets, for example on an intra-annual time scale. Additional work understanding the role shading, sedimentology and snow cover has on controlling the rates of down-wastage is required. Understanding of these variables will facilitate the production of numerical models; such models may allow for the prediction of geomorphological change over time in response to changing environmental conditions.
- *The use of UAVs and SfM for monitoring small-scale earth surface processes*: Where UAVs are integrated with SfM, ultra-high spatial resolutions are possible (e.g. Chapter 3; Tonkin *et al.*, 2014). Given how rapidly UAVs can be deployed, monitoring small-scale changes at both high temporal and spatial scales is now possible. Research applying these technologies to new problems is on-going. These technologies have the potential to revolutionise our understanding of the short-term dynamics of geomorphological and glaciological environments, affording geoscientists with low-cost but exceptionally high resolution (sub-decimetre) surface data. A wide range of geoscientific disciplines may also benefit from integrating these technologies into their research.

7.6 Conclusions

To conclude, the findings of this research demonstrate the value and potential of unmanned aerial vehicles and structure-from-motion photogrammetry for geoscientific studies. Validation of topographic data derived from small format, low-level aerial imagery is presented (e.g. Tonkin *et al.*, 2014), demonstrating excellent levels of accuracy and precision. SfM is shown to be suitable for monitoring changing environments (e.g. Tonkin *et al.*, 2016). Where archived aerial photography is used, there is future potential

to reconstruct evolving earth surface features in four dimensions. This is an exciting research avenue that has the potential to aid understanding of environmental change over the 20th and 21st Centuries.

This study presents valuable observations on the character of lateral-frontal moraine developed in a range of glaciological settings. Alpine type lateral-frontal moraine ridges investigated here are shown to develop as supraglacial dumped debris of mixed transport origin, implying that actively transported material was made available for moraine formation on the former lower terminus of the glacier. The potential origin of active debris is unclear, but may relate to the elevation of material via debris-bearing englacial septa. Further work is required (e.g. structural glaciological mapping from archive aerial imagery) before the significance of this mechanism of debris transfer in temperate alpine glaciers can be fully determined.

The Alpine landsystem differs from findings at continental Arctic and high-Arctic polythermal glaciers which contain ice within the moraine structure. Buried ice is, however, located in lateral zones of the moraines, implying a lower preservation potential for lateral moraine in the geomorphological record. This has implications where lateral moraine are identified and used for reconstructing the geometry of former glaciers. Furthermore, a disparity is evident at Arctic sites with buried-ice structures being exceptionally well-preserved in the high-Arctic environment, but not at the continental Arctic site investigated. Relict ice within high-Arctic moraine may provide a valuable insight into the former Neoglacial dynamics of these glaciers. Bounding structures were observed within landforms developed within the continental Arctic setting demonstrating multiple periods of moraine development, which may have longer formational histories than high-Arctic sites, and provide a rich Late Holocene record of glacier change.

In summary, the characteristics of moraines investigated are shown to be divergent, highlighting how earth surface and glaciological processes control moraine structure, form and sedimentology. However, the topographic setting is an important control on moraine development and external censoring (preservation). By documenting the character of various lateral-frontal moraine subsets, this study facilitates the use of moraines as indicators of past glacier response and aids studies seeking to use moraines for determining the geochronology of past glacier change.

8. References

- Aber, J.S., Marzolff, I., Ries, J.B. 2010. Small-format aerial photography: Principles, techniques and geoscience applications. Elsevier, Amsterdam, pp 268.
- Ackert, R.P. 1984. Ice-Cored Lateral Moraines in Tarfala Valley, Swedish Lapland. *Geografiska Annaler*, 66A (1-2), 79-88.
- Adam, W.G. and Knight, P.G. 2003. Identification of basal layer debris in ice-marginal moraines, Russell Glacier, West Greenland. *Quaternary Science Reviews*, 22, 1407-1414.
- Addison, K. 1988. *The Ice Age in Cwm Idwal*, 2nd edition. Shropshire, pp 16.
- Agassiz, L., 1840. *Études sur les Glaciers*. Neuchâtel.
- Agisoft. 2013. Agisoft PhotoScan User Manual: Professional Edition. Retrieved 23/10/2013: <http://www.agisoft.ru/products/photoscan/professional/>
- Alley, R.B., Cuffey, K.M., Evenson, E.B., Strasser, J.C., Lawson, D.E., Larson, G.J., 1997. How glaciers entrain and transport basal sediment: physical constraints. *Quaternary Science Reviews*, 16, 1017-1038.
- Allmendinger, R. W., Cardozo, N., and Fisher, D. 2012. *Structural geology algorithms: Vectors and tensors in structural geology*. Cambridge University Press, Cambridge.
- Anderson, K and Gaston, K.J. 2013. Lightweight unmanned aerial vehicles will revolutionize spatial ecology. *Frontiers in Ecology and the Environment*, 11 (3), 138-146.
- Annan, A.P. 2003. Ground Penetrating Radar: Principles, Procedures & Applications. Sensors & Software Inc. Canada.
- Appleby, J.R., Brook, M.S., Vale, S.S. and MacDonald-Creevey, A.M. 2010. Structural glaciology of a temperate, maritime glacier: Lower Fox Glacier, New Zealand. *Geografiska Annaler*, 92A (4), 451-467.
- Arnold N.S., Rees, W.G., Devereux, B.J. and Amable., G.S. 2006. Evaluating the potential of high-resolution airborne LiDAR data in glaciology. *International Journal of Remote Sensing*, 27 (6), 1233-1251.
- Bakker, M.A.J. and Van Der Meer, J.J.M. 2003. Structure of a Pleistocene push moraine revealed by GPR: the eastern Veluwe Ridge, The Netherlands. In: Bristol, C.S. and Jol, H.M. (eds.) *Ground Penetrating Radar in Sediments*, 221, 143-151.
- Baltsavias, E.P. 1999. A comparison between photogrammetry and laser scanning. *ISPRS Journal of Photogrammetry and Remote Sensing*. 54 (2-3), 83-94.
- Banard, P.L., Owen, L.A. and Finkel, R.C. 2004. Style and timing of glacial and paraglacial sedimentation in a monsoon-influenced high Himalayan environment, the upper Bhagirathi Valley, Garhwal Himalaya. *Sedimentary Geology*, 165, 199-221.
- Barr, I.D. and Lovell, H. 2014. A review of topographic controls on moraine distribution. *Geomorphology*, 226, 44-64.
- Barsch, D. 1971. Rock Glaciers and Ice-Cored Moraines, *Geografiska Annaler*, 53 (3-4), 203-206.

- Beckman Coulter, Inc. 2011. LS 13 320 Laser Diffraction Particle Size Analyzer Instructions For Use. Retrieved: 23/01/2015. <https://www.beckmancoulter.com/wsrportal/techdocs?docname=B05577AB.pdf>
- Beedle, M.J., Menounos, B., Luckman, B.H. and Wheate, R. 2009. Annual push moraines as climate proxy, *Geophysical Research Letters*, 36, L20501.
- Bendle, J.M and Glasser, N.F. 2012. Palaeoclimatic reconstruction from Lateglacial (Younger Dryas Chronozone) cirque glaciers in Snowdonia, North Wales. *Proceedings of the Geologists' Association*, 123, 130-145.
- Benedict, J.B. 1993. A 2000-year lichen-snowkill chronology for the Colorado Front Range, USA, *The Holocene*, 3 (1), 27-33.
- Benediktsson, Í.Ö., 2012. Polyphase structural evolution of a fine-grained, fold-dominated end moraine, Bruarjökull surge-type glacier, Iceland. *Jökull*, 62, 167-184.
- Benn, D.I. 1989. Debris transport by Loch Lomond Readvance glaciers in northern Scotland: basin form and within-valley asymmetry of lateral moraines. *Journal of Quaternary Science*, 4, 243–54.
- Benn, D.I. 1994. Fabric shape and the interpretation of sedimentary fabric data. *Journal of Sedimentary Research*, A64, 910-915.
- Benn, D.I. 2004a. Clast morphology. In: Evans, D.J.A. and Benn, D.I. (eds.) *A Practical Guide to the Study of Glacial Sediments*. Arnold, London, pp 77-92.
- Benn, D.I. 2004b. Macrofabric. In: Evans, D.J.A and Benn, D.I. (eds.) *A Practical Guide to the Study of Glacial Sediments*. Arnold, London, pp 93-114.
- Benn, D.I. 2006. Interpreting glacial sediments. In: Knight. P.G (ed.) *Glacier science and environmental change*, Wiley-Blackwell, Chichester, pp 434-439.
- Benn, D.I. and Ballantyne, C.K. 1993. The description and representation of particle shape. *Earth Surface Processes and Landforms*, 18 (7), 665–672.
- Benn, D.I. and Ballantyne, C.K. 1994. Reconstructing the transport history of glacial sediments – a new approach based on the co-variance of clast form indices. *Sedimentary Geology*, 91 (1–4): 215–227.
- Benn, D.I. and Evans, D.J.A. 2010. *Glaciers and Glaciation*. Taylor and Francis, London.
- Benn, D.I. and Lehmkuhl, F. 2000. Mass balance and equilibrium-line altitudes of glaciers in high-mountain environments. *Quaternary International*, 65-66, 15-29.
- Benn, D.I. and Owen, L.A. 2002. Himalayan glacial sedimentary environments: a framework for reconstructing and dating the former extent of glaciers in high mountains. *Quaternary International*, 97-98, 3-25.
- Benn, D.I., Kirkbride, M.P., Owen, L.A., Brazier, V., 2003. Glaciated valley landsystems. In: Evans, D.J.A. (Ed.), *Glacial Landsystems*. Oxford University press, 372–406.
- Benn, D.I. and Lukas, S. 2006. Younger Dryas glacial landsystems in North West Scotland: An assessment of modern analogues and palaeoclimatic implications. *Quaternary Science Reviews*, 25, 2390-2408.

- Bennett, G.L. and Evans, D.J.A. 2012. Glacier retreat and landform production on an overdeepened glacier foreland: the debris-charged glacial landsystem at Kviárjökull, Iceland. *Earth Surface Processes and Landforms*, 37 (15), 1584-1602.
- Bennett, M.R. 1999. Paraglacial and periglacial slope adjustment of a degraded lateral moraine in Glen Torridon, *Scottish Journal of Geology*, 35, 79-83.
- Bennett, M.R. 2001. The morphology, structural evolution and significance of push moraines, *Earth-Science Reviews*, 53 (3-4), 197-236.
- Bennett, M.R. and Glasser, N.F. 2009. *Glacial Geology: Ice sheets and landforms*, 2nd Edition. Wiley-Blackwell, Chichester.
- Bennett, M.R., Hambrey, M.J. and Huddart, D. 1997. Modification of clast shape in high-Arctic glacial environments. *Journal of Sedimentary Research*, A67 (3): 550-559.
- Bennett, M.R., Hambrey, M.J., Huddart, D. and Glasser, N.F., 1998. Glacial thrusting and moraine-mound formation in Svalbard and Britain: the example of Coire a' Cheudchnoic (Valley of hundred hills), Torridon, Scotland. *Quaternary Proceedings*, 6, 17-34.
- Bennett, M.R., Huddart, D., Glasser, N.F. and Hambrey, M.J. 2000. Resedimentation of debris on an ice-cored lateral moraine in the high-Arctic (Kongsvegen, Svalbard). *Geomorphology*, 35 (1-2), 21-40.
- Bennett, M.R., Huddart, D., Hambrey, M.J. and Ghienne, J.F. 1996. Moraine Development at the High-Arctic Valley Glacier Pedersenbreen, Svalbard. *Geografiska Annaler. Series A, Physical Geography*, 78 (4), 209-222.
- Bennett, M.R., Waller, R.I., Glasser, N.F., Hambrey, M.J. and Huddart, D. 1999b. Glacigenic clast fabrics: genetic fingerprint or wishful thinking? *Journal of Quaternary Science*, 14, 124-135.
- Bernhardsen, T. 2002. *Geographic Information Systems: An Introduction*. John Wiley & Sons, New York, pp 448.
- Berthling, I. 2011. Beyond Confusion: Rock glacier as cryo-conditioned landforms. *Geomorphology*, 131. 98-106.
- Beuselinck, L., Govers, G., Poesen, J., Dagraer, G. and Froyen, L. 1998. Grain-size analysis by laser diffractometry: comparison with the sieve-pipette method. *Catena*, 32 (3-4), 193-208.
- Bircher, W. 1982: *Zur Gletscher- und Klimageschichte des Saas-tales*. Unpublished PhD thesis, Zurich University.
- Birnie, R.V. 1977. A snow-bank push mechanism for the formation of some "annual" moraine ridges. *Journal of Glaciology*, 18 (78), 77-85.
- Bishop, M.P., James, L.A., Shroder Jr, J.F. and Walsh, S.J. 2012. Geospatial technologies and digital geomorphological mapping: Concepts, issues and research. *Geomorphology*, 137 (1), 5-26.
- Blott, S.J. and Pye, K. 2001. GRADISTAT: a grain size distribution and statistics package for the analysis of unconsolidated sediments. *Earth Surface Processes and Landforms*, 26: 1237-1248.

- Blott, S.J., Croft, D.J., Pye, K., Saye, S.E. and Wilson, H.E. 2004. Particle size analysis by laser diffraction. In: Pye, K. and Croft, D. (eds.), *Forensic Geoscience: Principles, Techniques, and Applications*. Geological Society London, Special Publications, 232, pp 63-73.
- Borradaile, G.J. 2003. *Statistics of Earth Science Data*. Springer-Verlag, Berlin.
- Boulton, G, van der Meer, JJM, Beets, DJ, Hart, JK & Ruegg, GHJ 1999. The sedimentary and structural evolution of a recent push moraine complex: Holmstrombreen, Spitsbergen. *Quaternary Science Reviews*, 18, 339-371.
- Boulton, G. S. and Eyles, N. 1979. Sedimentation by valley glaciers: a model and genetic classification. In: Schlüchter, C. (ed.) *Proceedings of an INQUA symposium on genesis and lithology of Quaternary deposits, Zurich , 10- 20 September 1978. Moraines and varves: origin, genesis, classification*. Balkema, Rotterdam, pp 11-23.
- Boulton, G.S. 1972. Modern Arctic glaciers as depositional models for former ice sheets. *Journal of the Geological Society*, 128, 361-93.
- Bradwell, T., Sigurðsson, O. and Everest, J. 2013. Recent, very rapid retreat of a temperate glacier in SE Iceland. *Boreas*, 42 (4), 959-973.
- Brandt, O., Langley, K., Kohler, J. and Hamran, S-K. 2007. Detection of buried ice and sediment layers in permafrost using multi-frequency Ground Penetrating Radar: A case examination on Svalbard. *Remote Sensing of the Environment*, 111 (2-3): 212-227.
- Brasington, J., Langham, J. and Rumsby B. 2003. Methodological sensitivity of morphometric estimates of coarse fluvial sediment transport. *Geomorphology*, 53 (3-4), 299-316.
- Brook, M. and Lukas. S. 2012. A revised approach to discriminating sediment transport histories in glacial sediments in a temperate alpine environment: a case study from Fox Glacier, New Zealand. *Earth Surface Process and Landforms*, 37 (8), 895-900.
- Brook, M.S. and Paine, S., 2012. Ablation of ice-cored moraine in a humid, maritime climate: Fox Glacier, New Zealand. *Geografiska Annaler: Series A, Physical Geography*, 94, 339-349.
- Brugger, K.A. 1996. Implications of till-provenance studies for glaciological reconstructions of the paleoglaciers of Wildhorse Canyon, Idaho, U.S.A. *Annals of Glaciology*, 22, 93-101.
- Burki, V. 2009. Glacial remobilization cycles as revealed by lateral moraine sediment, Bødalsbreen glacier foreland, western Norway. *The Holocene*, 19 (3), 415-426.
- Burki, V., Hansen, L., Fredin, O., Andersen, T.A., Beylich, A.A., Jaboyedoff, M., Larsen, E., Tønnesen, J.-F. 2010. Little Ice Age advance and retreat sediment budgets for an outlet glacier in western Norway. *Boreas*, 39 (3), 551-566.
- CAA. 2012. CAP722 Unmanned aircraft system operations in UK airspace - guidance (5th Edition). The Stationery Office, Norwich, pp 110.
- Carr, S.J., Lukas, S. and Mills, S.C. 2010. Glacier reconstruction and mass-balance modelling as a geomorphic and palaeoclimatic tool. *Earth Surface Process and Landforms*, 35, 1103-1115.

- Carrivick J.L., Geilhausen, M., Warburton, J., Dickson, N.E., Carver, S.J., Evans, A.J. and Brown, L.E. 2012b. Contemporary geomorphological activity throughout the proglacial area of an alpine catchment. *Geomorphology*, 188, 83-95.
- Carrivick, J.L. Bethan, B.J., Glasser, N.F., Nývlt, D. and Hambrey, M.J. 2012a. Late-Holocene changes in character and behaviour of land-terminating glaciers on James Ross Island, Antarctica. *Journal of Glaciology*, 58 (212), 1176-1190.
- Carrivick, J.L., Smith, M.W., Quincey, D.J. and Carver, S.J. 2013b. Developments in budget remote sensing for the geosciences. *Geology Today*, 29 (4), 138-143.
- Cassidy, N.J. 2009. Ground Penetrating Radar Data Processing, Modelling and Analysis. In *Ground Penetrating Radar: Theory and Applications*. Jol, H.M. (Ed.). Elsevier.
- Chandler, D.M. and Hubbard, B. 2008. Quantifying sample bias in clast fabric measurements. *Sedimentology*, 55, 925-938.
- Chesworth, W., Perez-Alberti, A. and Arnaud, E. 2008. Ice Erosion. In: Chesworth, W. (ed.) *Encyclopedia of Soil Science*. Springer-Verlag, New York, pp 333-338.
- Clapuyt, F., Vanacker, V., Van Oost, K. 2015. Reproducibility of uav-based earth topography reconstructions based on structure-from-motion algorithms. *Geomorphology*, In press.
- Clark, D.H., Clark, M.M. and Gillespie, A.R. 1994. Debris-Covered Glaciers in the Sierra Nevada, California, and Their Implications for Snowline Reconstructions. *Quaternary Research*, 41 (2), 139-153.
- Collomb, E., 1847. Preuves de l'existence d'anciens glaciers dans les vallées des Vosges. Victor Masson, Paris, pp 246.
- Conyers, 2012. *Interpreting Ground-penetrating Radar for Archaeology*. Left Coast Press Inc., California.
- Cook S.J., Graham, D.J., Swift, D.A., Midgley, N.G. and Adam, W.G. 2011. Sedimentary signatures of basal ice formation and their preservation in ice-marginal sediments. *Geomorphology*, 25 (1), 122-131.
- Cook S.J., Porter, P.R. and Bendall, C.A. 2013. Geomorphological consequences of a glacier advance across a paraglacial rock avalanche deposit. *Geomorphology*, 189, 109-120.
- Cook, S.J., Tonkin, T.N., Midgley, N.G. and Wicikowski, A. 2015. Analysis of 'hummocky moraine' using Structure-from-Motion photogrammetry. *North West Geography*, 15 (1), 9-18.
- Curry, A. and Ballantyne, C.K. (1999) Paraglacial modification of hillslope glacial drift. *Geografiska Annaler*, 81A, 409-419.
- Curry, A.M., Cleasby, V., and Zukowskyj, P. 2006. Paraglacial response of steep, sediment-mantled slopes to post-'Little Ice Age' glacier recession in the central Swiss Alps. *Journal of Quaternary Science*, 21 (3), 211-225.
- Curry, A.M., Sands, T.B. and Porter, P.R. 2009. Geotechnical controls on a steep lateral moraine undergoing paraglacial slope adjustment. In: *Periglacial and Paraglacial*

- Processes and Environments* (eds. Knight, J. and Harrison, S.). Geological Society, Special Publication, 320, pp 181-197.
- Dandois, J.P. and Ellis, E.C. 2013. High spatial resolution three-dimensional mapping of vegetation spectral dynamics using computer vision. *Remote Sensing of Environment*, 136, 259-276.
- Darwin, C. 1842. Notes on the effects produced by the ancient glaciers of Caernavonshire, and on boulders transported by floating ice. *Philosophical Magazine*, 3, 180-188.
- Davis, J.L., and A.P. Annan 1989. Ground-penetrating radar for high resolution mapping of soil and rock stratigraphy, *Geophysical Prospecting*, 37, 531-551.
- Dewitte, O., Jasselette, J.-C., Cornet, Y., Van Den Eeckhaut, M., Collignon, A., Poesen, J. and Demoulin, A. 2008. Tracking landslide displacements by multi-temporal DTMs: A combined aerial stereophotogrammetric and LIDAR approach in western Belgium. *Engineering Geology*, 99 (1-2), 11-22.
- DJI. 2013. WooKong-M Waypoint-Altitude Offset Setting. Retrieved: 23/02/2014. http://wiki.dji.com/en/index.php/WooKong-M_Waypoint-Altitude_Offset_Setting
- Dowdswell, J.A. and Sharp, M. 1986. Characterisation of pebble fabrics in modern terrestrial glacial sediments. *Sedimentology*, 33, 699–710.
- Driscoll, F.G. 1980. Wastage of the Klutlan ice-cored moraines, Yukon Territory, Canada. *Quaternary Research*, 14 (1), 31-49.
- ETH-Bibliothek's Image Archive. 2013. E-Pics image database. Retrieved: 02/09/2013. <http://www.e-pics.ethz.ch/>
- Eklund, A. and Hart, J. K. 1996. Glaciotectonic deformation within a flute from the glacier Isfallsglaciären, Sweden. *Journal of Quaternary Science*, 11, 299-310.
- Escritt, E.A. 1971. Plumbing the depths of Idwal's moraines. *Geographical Magazine*, 44, 52-55.
- Eshel, G., Levy, G.J., Mingelgrin, U. and Singer, M.J. 2004. Critical Evaluation of the Use of Laser Diffraction for Particle-Size Distribution Analysis. *Soil Science Society of America Journal*, 68 (3), 736-743.
- Etienne, J.L., Glasser, N.F. and Hambrey, M.J. 2003. Proglacial Sediment—Landform Associations of a Polythermal Glacier: Storglaciären, Northern Sweden. *Geografiska Annaler: Series A*. 85 (2), 149-164.
- Etzelmüller, B. 2000. Quantification of thermo-erosion in pro-glacial areas - examples from Svalbard. *Zeitschrift Fur Geomorphologie*, 44, 343-361.
- Etzelmüller, B. and Frauenfelder, R. 2009. Factors Controlling The Distribution of Mountain Permafrost in The Northern Hemisphere and Their Influence on Sediment Transfer. *Arctic, Antarctic, and Alpine Research*, 41 (1), 48-58.
- Etzelmüller, B. and Hagen, J.O. 2005. Glacier permafrost interaction in arctic and alpine environments – examples from southern Norway and Svalbard. In: Harris, C. & Murton, J. (eds.). *Cryospheric systems – Glaciers and Permafrost*. British Geological Society, Special Publications, 242, pp 11-27.

- Etzelmüller, B., Hagen, J.O., Vatne, G., Ødegård, R.S., Sollid, J.L. 1996. Glacier debris accumulation and sediment deformation influenced by permafrost, examples from Svalbard. *Annals of Glaciology*, 22, 53-62.
- Evans DJA. 1999. Glacial debris transport and moraine deposition: a case study of the Jardalen cirque complex, Sogn-og-Fjordane, western Norway. *Zeitschrift für Geomorphologie*, 43, 203-234.
- Evans, D.J.A and England, J. 1991. High-Arctic thrust block moraines. *The Canadian Geographer*, 35 (1), 93-97.
- Evans, D.J.A. 2009. Controlled moraines: origins, characteristics and palaeoglaciological implications. *Quaternary Science Reviews*, 28 (3-4), 183-208.
- Evans, D.J.A. 2010. Controlled moraine development and debris transport pathways in polythermal plateau icefields: examples from Tungnafellsjökull, Iceland. *Earth Surface Processes and Landforms*, 35, 1430-1444.
- Evans, D.J.A. and Hiemstra, J.F. 2005. Till deposition by glacier submarginal, incremental thickening. *Earth Surface Processes and Landforms*, 30 (13), 1633-1662.
- Evans, D.J.A., Shulmeister, J. and Hyatt, O. 2010. Sedimentology of latero-frontal moraines and fans on the west coast of South Island, New Zealand. *Quaternary Science Reviews*, 29, 3790-3811.
- Everest, J. and Bradwell, T. 2003. Buried glacier ice in southern Iceland and its wider significance. *Geomorphology*, 52 (3-4), 347-358.
- Everest, J. and Kubik, P. 2006. The deglaciation of eastern Scotland: cosmogenic ¹⁰Be evidence for a Lateglacial stillstand. *Journal of Quaternary Science*, 21 (1), 95-104.
- Ewertowski M., Kasprzak L., Szuman I., Tomczyk A.M., 2012. Controlled, ice-cored moraines: sediments and geomorphology. An example from Ragnarbreen, Svalbard. *Zeitschrift für Geomorphologie*, 56 (1), 53-74.
- Ewertowski, M. and Tomczyk, A.M. 2015. Quantification of the ice-cored moraines' short-term dynamics in the high-Arctic glaciers Ebbabreen and Ragnarbreen, Petuniabukta, Svalbard. *Geomorphology*, 234, 211-227.
- Ewertowski, M. 2014. Recent transformations in the high-Arctic glacier landsystem, Ragnarbreen, Svalbard. *Geografiska Annaler: Series A (Physical Geography)*, 96, 265-285.
- Eyles, N. 1983. The glaciated valley landsystem. In: N. Eyles (Ed.). *Glacial Geology*, Pergamon, Oxford, pp 91-110.
- Ezter, F.M. and Deanne, R. 1997. Particle size analysis: A comparison of various methods ii. *Particle and Particle Systems Characterisation*, 14 (6), 278-282.
- Fisher, P.F. and Tate, N.J. 2006. Causes and consequences of error in digital elevation models. *Progress in Physical Geography*, 30 (4), 467-489.
- Fonstad, M.A., Dietrich, J.T., Courville, B.C., Jensen, J.L., Carbonneau, P.E. 2013. Topographic structure from motion: a new development in photogrammetric measurement. *Earth Surface Processes and Landforms*, 38, 421-430.

- Friedt, J.-M., Tolle, F., Bernard, É., Griselin, M., Laffy, D and Marlin, C. 2012. Assessing the relevance of digital elevation models to evaluate glacier mass balance: application to Austre Lovénbreen (Spitsbergen, 79° N). *Polar Record*, 48 (244), 2-10.
- Galloway, R.W. 1956. The structure of moraines in Lyngsdalen, North Norway. *Journal of Glaciology*, 2, 730-733.
- Gibbons, A.B., Megeath, J.D., Pierce, K.L. 1984. Probability of moraine survival in a succession of glacial advances. *Geology*, 12, 327-330.
- Glasser, N.F. and Hambrey, M.J. 2001. Styles of sedimentation beneath Svalbard valley glaciers under changing dynamic and thermal regimes. *Journal of Geological Society*, London, 158 (4), 697-707.
- Glasser N.F., Hambrey, M.J., Crawford K.R., Bennett M.R., Huddart D. 1998. The structural glaciology of Kongsvegen Svalbard and its role in landform genesis. *Journal of Glaciology*, 44 (146), 136-148.
- Glasser, N.F. and Hambrey, M.J. 2003. Ice-marginal terrestrial landsystems: Svalbard polythermal glaciers in D.J.A. Evans (Ed.), *Glacial Landsystems*. Hodder Arnold, London, pp 65-88.
- Glasser, N.F., Coulsen, S.J., Hodkinson, I.D. and Webb, N.R. 2004. Photographic evidence of the return period of a Svalbard surge-type glacier: a tributary of Pedersenbreen, Kongsfjord. *Journal of Glaciology*, 50 (169), 307-308.
- Goodsell, B., Hambrey, M.J. and Glasser, N.F. 2002. Formation of band ogives and associated structures at Bas Glacier d'Arolla, Valais, Switzerland. *Journal of Glaciology*, 48 (161), 287-300.
- Goodsell, B., Hambrey, M.J., Glasser, N.F. 2005b. Debris transport in a temperate valley glacier: Haut Glacier d'Arolla, Valais, Switzerland. *Journal of Glaciology*, 51, 139-146.
- Goodsell, B., Hambrey, M.J., Glasser, N.F., Nienow, P., Mair, D. 2005a. The structural glaciology of a temperate valley glacier: Haut Glacier d-'Arolla, Valais, Switzerland. *Arctic Antarctic and Alpine Research*, 37, 218-232.
- Goudie, A. and Viles, H. 2010. *Landscapes and Geomorphology: A Very Short Introduction*. Oxford University Press, Oxford.
- Graham, D.J. 2002. Moraine-mound formation during the Younger Dryas in Britain and the Neoglacial in Svalbard. PhD thesis University of Wales, Aberystwyth.
- Graham, D.J. and Midgley, N.G. 2000a. Moraine-mound formation by englacial thrusting: the Younger Dryas moraines of Cwm Idwal, North Wales. In: A.J. Maltman, B. Hubbard and M.J. Hambrey (eds.), *Deformation of Glacial Materials*. London: Geological Society, pp. 321-336.
- Graham, D.J. and Midgley, N.G. 2000b. Graphical representation of particle shape using triangular diagrams: an Excel spreadsheet method. *Earth Surface Processes and Landforms*, 25 (13): 1473-1477.
- Graham, D.J. Bennett, M.R., Glasser, N.F., Hambrey, M.J., Huddart, D. and Midgley, N.G. 2007. Comment on: "A test of the englacial thrusting hypothesis of 'hummocky' moraine formation." *Boreas*, 36 (1), 103-107.

- Gray, J.M. 1982. The last glaciers (Loch Lomond Advance) in Snowdonia, North Wales. *Geological Journal*, 17, 111-133.
- Grech, V.I and Semenenok, S.H. 1969. The modern dams of Switzerland. *Hydrotechnical Construction*. 3 (5), 463-473.
- Grove, J.M. and Switsur, R. 1994. Glacial geological evidence for the medieval warm period. *Climatic Change*, 26 (2-3), 143-169.
- Gulley, J. and Benn, D.I. 2007. Structural control of englacial drainage systems in Himalayan debris-covered glaciers. *Journal of Glaciology*, 53 (182), 399-412.
- Gusmeroli, A., Jansson, P., Pettersson, R. and Murray, T. 2012. Twenty years of cold surface layer thinning at Storglaciären, sub-Arctic Sweden, 1989-2009. *Journal of Glaciology*, 58 (207), 3-10.
- Haeberli, W., Kääh, A., Paul, F., Chiarle, M., Mortara, G., Mazza, A., and Richardson, S. 2002. A Surge type movement at Ghiacciaio del Belvedere and a developing slope instability in the east face of Monte Rose, Macugnaga, Italian Alps, *Norwegian Journal of Geography*, 56 (2), 104-111.
- Hagen, J.O., Liestøl, O., Roland, E., and Jørgensen, T. 1993. *Glacier Atlas of Svalbard and Jan Mayen*. Norsk Polarinstitutt Meddelelser, 129, Oslo.
- Hamberg, A. 1894. En resa till norra Ishafvet sommaren 1892. *Ymer*, 14, 25-61.
- Hamberg, A., Rabot, C., & Mercanton, P.L., 1930. *Commission UGGI des glaciers: Rapport pour 1914 – 1928*. Venezia 1930. 1–53.
- Hambrey, M.J and Ehrmann, W. 2004. Modification of sediment characteristics during glacial transport in high-alpine catchments: Mount Cook area, New Zealand. *Boreas*, 33 (4) 300-318.
- Hambrey, M.J. 1994. *Glacial Environments*. UCL Press, London.
- Hambrey, M.J. 2011. Structural Glaciology. In Singh, V.P. Singh, P., and Haritashya, U.K. *Encyclopedia of Snow, Ice and Glaciers*. Springer, Dordrecht, pp 1089-1091.
- Hambrey, M.J. and Glasser, N.F. 2003. The role of folding and foliation development in the genesis of medial moraines: examples from Svalbard glaciers, *Journal of Geology*, 111 (4), 471-485.
- Hambrey, M.J. and Glasser, N.F. 2012. Discriminating glacier thermal and dynamic regimes in the sedimentary record, *Sedimentary Geology*, 251–252, 1–33.
- Hambrey, M.J. and Lawson, W. 2000. Structural styles and deformation fields in glaciers: a review. *Geological Society, London, Special Publications*, 176, 59-83
- Hambrey, M.J., Dowdeswell, J.A., Murray, T., Porter, P.R., 1996. Thrusting and debris entrainment in a surging glacier: Bakaninbreen, Svalbard. *Annals of Glaciology*, 22, 241-248.
- Hambrey, M.J., Huddart, D., Bennett, M.R. and Glasser, N.F. 1997. Genesis of "hummocky moraines" by thrusting in glacier ice: evidence from Svalbard and Britain. *Journal of the Geological Society, London*. 154, 623-632.

- Hambrey, M.J., Murrery, T., Glasser, N.F., Hubbard, A., Hubbard, B., Stuart, G., Hansen, S. and Kohler, J. 2005. Structure and changing dynamics of a polythermal valley glacier on a centennial time-scale: midre Lovénbreen, Svalbard. *Journal of Geophysical Research: Earth Surface*, p. F010006.
- Hambrey, M.J., Quincey, D.J., Glasser, N.F., Reynolds, J.M., Richardson, S.J., Clemmens, S. 2008. Sedimentological, geomorphological and dynamic context of debris-mantled glaciers, Mount Everest (Sagarmatha) region, Nepal. *Quaternary Science Reviews*, 27 (25-26), 2361-2389.
- Hansen, S. 2003. From surge-type to non-surge type glacier behaviour: Midre Lovénbreen, Svalbard. *Annals of Glaciology*, 36, 97–102.
- Harris, C., Arenson, L.U., Christiansen, H.H., Etzelmüller, B., Fraunfelder, R., Gruber, Haeberli, W., Hauck, C., Hölzle, M., Humlum, O., Isaksen, K. Kääb, A., Kern-Lütschg, M.A., Lehning, M., Matsuoka, N., Murton, J.B., Nötzlie, J., Philips, M., Ross, N., Seppälä, M., Springman, S.M. and Mühl, D.V. 2009. Permafrost and climate in Europe: Monitoring and modelling thermal, geomorphological and geotechnical responses. *Earth-Science Reviews*, 92 (3-4), 117-171.
- Hart, J.K. 1990. Proglacial glaciotectonic deformation and the origin of the Cromer Ridge push moraine complex, North Norfolk, England, *Boreas*, 19 (2), 165-180.
- Harwin, S. and Lucieer, A. 2012. Assessing the Accuracy of Georeferenced Point Clouds Produced via Multi-View Stereopsis from Unmanned Aerial Vehicle (UAV) Imagery. *Remote Sensing*, 4, 1573-1599.
- Head K.H. 1992. *Manual of Soil Laboratory Testing* (Volume 1: soil classification and compaction tests) 2nd Edition. Pentech Press, London.
- Heyman, J. and Hättestrand, C. 2006. Morphology, distribution and formation of relict marginal moraines in the Swedish mountains. *Geografiska Annaler: Series A*, 88 (4): 253–265.
- Hicock, S.R., Goff, J.R., Lian, O.B. and Little, E.C. 1996. On the interpretation of subglacial till fabric. *Journal of Sedimentary Research*, 66: 928-945.
- Hladik, C. and Alber, M. 2012. Accuracy assessment and correction of a LIDAR-derived salt marsh digital elevation model. *Remote Sensing of Environment*. 121, 224-235.
- Hoey, T.B. 2004. The size of sedimentary particles. In: Evans, D.J.A and Benn, D.I. (eds.), *A Practical Guide to Glacial Sediments*. Arnold, London, pp 53-77.
- Holmlund, P, Karlin, W. and Grudd, H., 1996: Fifty years of mass balance and glacier front observations at the Tarfala Research Station. *Geografiska Annaler: Series A*, 78 (2-3), 105-114.
- Holmlund, P. and Jansson, P. 1999. The Tarfala Mass Balance Programme. *Geografiska Annaler: Series A*, 81 (4), 621-631.
- Hooke, R.L. 1973. Flow near the Margin of the Barnes Ice Cap, and the Development of Ice-Cored Moraines. *Geological Society of America Bulletin*, 84 (12), 3929-3948.

- Hormes A., Karlén, W. and Possnert, G. 2004. Radiocarbon dating of palaeosol components in moraines in Lapland, northern Sweden. *Quaternary Science Reviews*, 23 (18-19), 2031-2043.
- Hubbard, B. and Glasser, N. 2005. *Field techniques in glaciology and glacial geomorphology*. John Wiley & Sons, New York.
- Huddart, D. and Hambrey, M. J. 1996. Sedimentary and tectonic development of a high-arctic, thrust-moraine complex: Comfortlessbreen, Svalbard. *Boreas*, 25, 227-243.
- Hugenholtz, C.H. 2010. Topographic changes of a supply-limited inland parabolic sand dune during the incipient phase of stabilization. *Earth Surface Processes and Landforms*, 35, (14), 1674-1681.
- Hugenholtz, C.H., Whitehead, K., Brown, O.W., Barchyn, T.E., Moorman, B.J., LeClair, A., Riddell, K., Hamilton, T. 2013. Geomorphological mapping with a small unmanned aircraft system (sUAS): Feature detection and accuracy assessment of a photogrammetrically-derived digital terrain model. *Geomorphology*, 194, 16-24.
- Humlum, O. 1978. Genesis of Layered Lateral Moraines: Implications for palaeoclimatology, and Lichenometry. *Geografisk Tidsskrift*, 77: 65-72.
- Ingólfsson, Ó and Lokrantz, H. 2003. Massive ground ice body of glacial origin at Yugorski Peninsula, arctic Russia. *Permafrost and Periglacial Processes*, 14 (3), 199 – 215.
- Irvine-Fynn, T.D.L., Barrand, N.E., Porter, P.R., Hodson, A.J., and Murray, T. 2011. Recent High-Arctic proglacial sediment redistribution: a process perspective using airborne lidar. *Geomorphology*, 125, 27-39.
- Isachsen, G. 1912. Exploration du Nord-Ouest du Spitsberg entreprise sous les auspices de S.A.S. le Prince de Monaco par la Mission Isachsen. Fascicule XL. Imprimerie de Monaco.
- Ivy-Ochs, S., Kerschner, H., Maisch, M., Christl, M., Kubik, P.W. and Schlüchter, C. 2009. Latest Pleistocene and Holocene glacier variations in the European Alps. *Quaternary Science Reviews*, 28, 2137-2149.
- Ivy-Ochs, S. and Kober, F. 2008. Surface exposure dating with cosmogenic nuclides. *Quaternary Science Journal*, 57 (1-2), 157-189.
- James, M.R and Robson, S. 2012. Straightforward reconstruction of 3D surfaces and topography with a camera: Accuracy and geoscience application. *Journal of Geophysical Research*, 117: F03017.
- Javernick, L., Brasington, J. and Caruso, B. 2014. Modelling the topography of shallow braided rivers using Structure-from-Motion photogrammetry. *Geomorphology*, In press. Corrected Proof.
- Jennings, S.J.A., Hambrey, M.J. and Glasser, N.F. 2014. Ice flow-unit influence on glacier structure, debris entrainment and transport. *Earth Surface Processes and Landforms*, 39 (10), 1279-1292.
- Jiskoot, H., Murray, T. and Boyle, P.J. 2000. Controls on the distribution of surge-type glaciers in Svalbard. *Journal of Glaciology*, 46 (154) 412–422.

- Joerin, U.E., Stocker, T.F. and Schluchter, C. Multicentury glacier fluctuations in the Swiss Alps during the Holocene, *The Holocene*, 16 (5), 697-704.
- Johnson, P.G. 1971. Ice Cored Moraine Formation and Degradation, Donjek Glacier, Yukon Territory, Canada. *Geografiska Annaler. Series A, Physical Geography*, 53 (3-4), 198-202.
- Jones, A.F., Brewer, P.A., Johnstone, E. and Macklin, M.G. 2007. High-resolution interpretative geomorphological mapping of river valley environments using airborne LiDAR data. *Earth Surface Processes and Landforms*, 32 (10): 1574-1592.
- Karlén, W. 1973. Holocene glacier and climatic variations, Kebnekaise mountains, Swedish Lapland. *Geografiska Annaler*, 55A, 29-63.
- Karlén, W. 1988. Scandinavian glacial and climatic fluctuations during the Holocene, *Quaternary Science Reviews*, 7 (2), 199-209.
- Karlén, W. and Kuylenstierna, J. 1996. On solar forcing of Holocene climate: evidence from Scandinavia. *The Holocene*, 6, 359-365.
- Kaser, G., Cogley, J.G., Dyurgerov, M.B., Meier, M.F. and Ohmura. 2006. Mass balance of glaciers and ice caps: Consensus estimates for 1961–2004. *Geophysical Research Letters*, 33 (19), L19501.
- Kerschner, H. and Ivy-Ochs, S. 2008. Palaeoclimate from glaciers: Examples from the Eastern Alps during the Alpine Lateglacial and early Holocene. *Global and Planetary Change*, 60 (1-2), 58-71.
- Kerschner, H., Ivy-Ochs, S. and Schlüchter, C. 1999. Palaeoclimatic interpretation of the early late-glacial glacier in the Gschnitz valley, Central Alps, Austria. *Annals of Glaciology*, 28, 135-140.
- Kerschner, H., Kaser, G. and Sailer, R. 2000. Alpine Younger Dryas glaciers as palaeoprecipitation gauges. *Annals of Glaciology*, 31, 80-84.
- Kilfeather, A.A. and van der Meer, J.J.M. 2008. Pore size, shape and connectivity in tills and their relationship to deformation processes. *Quaternary Science Reviews*, 27 (3–4), 250–266.
- King, E.C., Smith, A.M., Murray, T. and Stuart, G.W. 2008. Glacier-bed characteristics of midtre Lovénbreen, Svalbard, from high - resolution seismic and radar surveying, *Journal of Glaciology*, 54, 145-156.
- Kirkbride, M.P. and Winkler, S. 2012. Correlation of Late Quaternary moraines: impact of climate variability, glacier response, and chronological resolution. *Quaternary Science Reviews*, 46: 1-29.
- Kjær, K.H. and Krüger, J. 2001. The final phase of dead-ice moraine development: processes and sediment architecture, Kötlujökull, Iceland. *Sedimentology*, 48 (5), 935-952.
- Knight, J., Mitchell, W.A. and Rose, J. 2011. Geomorphological field mapping. In: Smith, M.J., Paron, P. and Griffiths, J. (eds) *Geomorphological Mapping: a handbook of techniques and applications*. Elsevier, London, pp 151-187.

- Knight, P.G. 1997. The basal ice layer of glaciers and ice sheets. *Quaternary Science Reviews*, 16 (9), 975-993.
- Kohler, J., James, T.D., Murray, T., Nuth, C., Brandt, O. Barrand, N.E., Aas, H.F. and Luckman, A. 2007. Acceleration in thinning rate on western Svalbard glaciers. *Geophysical Research Letters*, 34 (18), L18502.
- Konert, M. and Vandenberghe, J. 1997. Comparison of laser grain-size analysis with pipette and sieve analysis: a solution for the underestimation of the clay fraction. *Sedimentology*, 44, 523- 535.
- Krüger J. 1994. Glacial processes, sediments, landforms and stratigraphy in the terminus region of Myrdalsjökull, Iceland. *Folia Geographica Danica*, 21, 1-223.
- Krüger J. 1995. Origin, chronology and climatological significance of annual-moraine ridges at Myrdalsjökull, Iceland. *The Holocene*, 5, 420–427.
- Krüger, J. 1985. Formation of a Push Moraine at the Margin of Höfdabrekkujökull, South Iceland. *Geografiska Annaler*. 67A (3-4). 199-212.
- Krüger, J. and Kjær, K.H. 2000. De-icing progression of ice-cored moraines in a humid, subpolar climate, Kötlujökull, Iceland. *The Holocene*, 10 (6), 737-747.
- Krüger, J., Kurt, K.H. and Meer, J.J.M., 2002. From push moraine to single-crested dump moraine during a sustained glacier advance. *Norsk Geografisk Tidsskrift*, 56, 87-95.
- Krüger, J., Schomacker A., and Benediktsson, Í.Ö. 2010. Ice-marginal environments: geomorphic and structural genesis of marginal moraines at Mýrdalsjökull. In: A.Schomacker, J. Krüger and K. H. Kjær eds. *The Mýrdalsjökull Ice Cap, Iceland. Glacial processes, sediments and landforms on an active volcano. Developments in Quaternary Science*, 13, 79–104.
- Krzyszowski, D. and Zieliński, T. 2002 The Pleistocene end moraine fans: controls on their sedimentation and location. *Sedimentary Geology*, 149 (1-3), 73-92.
- Laliberte, A.S. and Rango, A. 2009. Texture and Scale in Object-Based Analysis of Subdecimeter Resolution Unmanned Aerial Vehicle (UAV) Imagery. *IEEE Transactions on Geoscience and Remote Sensing*, 47 (3), 761-770.
- Lamplugh, G.W. 1911. On the shelly moraine of the Sefstromglacier and other Spitsbergen phenomena illustrative of British glacial conditions. *Proceedings of the Yorkshire Geological Society*, 17: 216-341.
- Lane, S.N. 2000. The measurement of river channel morphology using digital photogrammetry. *Photogrammetric Record*, 16 (96), 937-961.
- Le Roy, M., Nicolussi, K., Deline, P., Astrade, L. Edouard. J-L., Miramont, C. and Arnaud, F. 2015. Calendar-dated glacier variations in the western European Alps during the Neoglacial: the Mer de Glace record, Mont Blanc massif. *Quaternary Science Reviews*, 108, 1-22.
- Lee, J.R., Phillips, E., Booth, S.J., Rose, J., Jordan, H.M., Pawley, S.M., Warren, M., Lawley, R.S. 2013. A polyphase glacetectonic model for ice-marginal retreat and terminal moraine development: the Middle Pleistocene British Ice Sheet, northern Norfolk, UK. *Proceedings of the Geologists' Association*, 124, 753-777.

- Leica. 1997. *TC600/800 Electronic Total Station User Manual*. Leica Geosystems, Heerbrugg, pp 135.
- Lindhorst, S. and Schutter, I. 2014. Polar gravel beach-ridge systems: Sedimentary architecture, genesis, and implications for climate reconstructions (South Shetland Islands/Western Antarctic Peninsula). *Geomorphology*, 221, 187-203.
- Lønne, I. and Lyså, A. 2005. Deglaciation dynamics following the Little Ice Age on Svalbard: Implications for shaping of landscapes at high latitudes. *Geomorphology*, 72 (1-4), 300-319.
- Lucieer, A., de Jong, S.M., and Turner, D. 2013. Mapping landslide displacements using Structure from Motion (SfM) and image correlation of multi-temporal UAV photography. *Progress in Physical Geography*, 38 (1), 97-116.
- Lucieer, A., Turner, D., King, D.H. and Robinson, S.A. 2014. Using an Unmanned Aerial Vehicle (UAV) to capture micro-topography of Antarctic moss beds. *International Journal of Applied Earth Observation and Geoinformation*, 27A, 53-62.
- Lui, X. 2008. Airborne LiDAR for DEM generation: some critical issues. *Progress in Physical Geography*. 32 (1), 31-49.
- Lukas, S. 2005. A test of the englacial thrusting hypothesis of 'hummocky' moraine formation: case studies from the northwest Highlands, Scotland. *Boreas*, 34 (3), 287-307.
- Lukas, S., Benn, D.I., Boston, C.M., Brook, M., Coray, S., Evans, D.J.A., Grafe, A., Kellerer-Pirklbauer, A., Kirkbride, M.P., Krabbendam, M., Lovell, H., Machiedo, M., Mills, S.C., Nye, K., Reinardy, B.T.I., Ross, F.H. and Signere, M. 2013. Clast shape analysis and clast transport paths in glacial environments: A critical review of methods and the role of lithology. *Earth-Science Reviews*, 121, 96-116.
- Lukas, S., Graf, A., Coray, S. and Schlüchter, C. 2012. Genesis, stability and preservation potential of large lateral moraines of Alpine valley glaciers – towards a unifying theory based on Findelengletscher, Switzerland. *Quaternary Science Reviews*, 38, 27-48.
- Lukas, S., Nicholson, L.I. and Humlum, O. 2007. Comment on Lønne and Lyså (2005): Deglaciation dynamics following the Little Ice Age on Svalbard: Implications for shaping of landscapes at high latitudes, *Geomorphology*, 72, 300 – 319.
- Lukas, S., Nicholson, L.I., Ross, F.H. and Humlum, O. 2005. Formation, meltout processes and landscape alteration of High-Arctic ice-cored moraines—examples from Nordenskiöld Land, Central Spitsbergen. *Polar Geography*, 29 (3), 157–187.
- Lukas, S., Sass, O., 2011. The formation of Alpine lateral moraines inferred from sedimentology and radar reflection patterns: a case study from Gornergletscher, Switzerland. *Geological Society, London, Special Publications*, 354, 77-92.
- Lütschg, D and Kasser, P. 1973. Map of the Mattmark Glaciers. In: PSFG. 1973. *Fluctuations of Glaciers 1965-1970 (Vol. II)*. P. Kasser (ed.), IAHS (ICSU) / UNESCO, Permanent Service on Fluctuations on Glaciers, Zurich, Switzerland: 357 pp.
- Lyså, A. and Lønne, I. 2001. Moraine development at a small High-Arctic valley glacier: Rieperbreen, Svalbard. *Journal of Quaternary Science*, 16 (6), 519–529.

- Mancini, F., Dubbini, M., Gattelli, M., Stecchi, F., Fabbri, S. and Gabbianelli, G. 2013. Using Unmanned Aerial Vehicles (UAV) for High-Resolution Reconstruction of Topography: The Structure from Motion Approach on Coastal Environments. *Remote Sensing*, 5, 6880-6898.
- Marzolf, I. and Poesen, J. 2009. The potential of 3D gully monitoring with GIS using high-resolution aerial photography and a digital photogrammetry system. *Geomorphology*, 111 (1-2), 48-60.
- Masiokas, M.H., Villalba, R., Luckman, B.H., Lascano, M.E., Delgado, S. and Stepanek, P. 2008. 20th-century glacier recession and regional hydroclimatic changes in northwestern Patagonia. *Global and Planetary Change*, 60 (1-2): 85-100.
- Matthews, J.A. and Petch, J.R. 1982. Within-valley asymmetry and related problems of Neoglacial lateral moraine development at certain Jotunheimen glaciers, southern Norway. *Boreas*, 11 (3), 225-247.
- Matthews, J.A. and Shakesby, R.A. 1984. The status of the 'Little Ice Age' in southern Norway: relative-age dating of Neoglacial moraines with Schmidt hammer and lichenometry. *Boreas*, 13 (3), 333-346.
- Matthews, J.A. Winkler, S. and Wilson, P. 2014. Age and origin of ice-cored moraines in Jotunheimen and Breheimen, southern Norway: insights from Schmidt-hammer exposure-age dating. *Geografiska Annaler: Series A, Physical Geography*, 96 (4), 531-548.
- Matthews, J.A., McCarrol, D. and Shakesby, R.A. 1995. Contemporary terminal-moraine ridge formation at a temperate glacier: Styggedalsbreen, Jotunheimen, southern Norway. *Boreas*, 24 (2), 129-139.
- Mattson, L.E. and Gardner, J.S. 1991. Mass Wasting on Valley-Side Ice-Cored Moraines, Boundary Glacier, Alberta, Canada. *Geografiska Annaler. Series A*, 73 (3/4), 123-128.
- McKillop, R.J. and Clague, J.J. 2007. Statistical, remote sensing-based approach for estimating the probability of catastrophic drainage from moraine-dammed lakes in southwestern British Columbia. *Global and Planetary Change*, 56, 153-171.
- Miall, A. 2010. *The Geology of Stratigraphic Sequences*. Springer-Verlag, Berlin.
- Midgley, N.G., Cook, S.J., Graham, D.J. and Tonkin, T.N. 2013. Origin, evolution and dynamic context of a Neoglacial lateral-frontal moraine at Austre Lovénbreen, Svalbard. *Geomorphology*, 198, 96-106.
- Midgley, N.G., Glasser, N.F. and Hambrey, M.J., 2007. Sedimentology, structural characteristics and morphology of a Neoglacial high-Arctic moraine-mound complex: midre Lovénbreen, Svalbard. In: Hambrey, M.J., Christoffersen, P., Glasser, N.F. and Hubbard, B (eds.), *Glacial Sedimentary Processes and Products*, International Association of Sedimentologists. Blackwells, Oxford, pp 11-22.
- Millar, S.W.S. and Nelson, F.E. 2001a. Sampling-surface orientation and clast macrofabric in periglacial colluvium. *Earth Surface Process and Landforms*, 26 (5), 523-529.
- Millar, S.W.S. and Nelson, F.E. 2001b. Clast Fabric in Relict Periglacial Colluvium, Salamanca Re-Entrant, Southwestern New York, USA. *Geografiska Annaler*, 83A (3), 145-156.

- Millar, S.W.S. and Nelson, F.E. 2003. Influence of Clast Axial Ratio on Macrofabric Strength in Periglacial Colluvium. *Journal of Sedimentary Research*, 73 (5): 720-724.
- Mitasova, H., Overton, M.F., Recalde, J.J., Bernstein, D.J and Freeman, C.W. 2009. Raster-Based Analysis of Coastal Terrain Dynamics from Multitemporal Lidar Data. *Journal of Coastal Research*, 25 (2), 507-514.
- Moncrieff, A.C.M. 1989. Classification of poorly-sorted sedimentary rocks. *Sedimentary Geology*, 65, (1-2), 191-194.
- Monnier, S. and Kinnard, C. 2013. Internal structure and composition of a rock glacier in the Andes (upper Choapa valley, Chile) using borehole information and ground-penetrating radar. *Annals of Glaciology*, 54 (64), 61-72.
- Murray, T., Booth, A.D. 2009. Imaging glacial sediment inclusions in 3-D using ground-penetrating radar at Kongsvegen, Svalbard. *Journal of Quaternary Science*, 25, 754-761.
- Murray, T., Strozzi, T., Luckman, A., Jiskoot, H. and Christakos, P. 2000. Is there a single surge mechanism? Contrasts in dynamics between glacier surges in Svalbard and other regions. *Journal of Geophysical Research: Solid Earth*, 108, 2237, B5.
- Murton J.B., Whiteman, C.A., Waller, R.I., Pollard, W.H., Clark, I.D. and Dallimore, S.R. 2005. Basal ice facies and supraglacial melt-out till of the Laurentide Ice Sheet, Tuktoyaktuk Coastlands, western Arctic Canada. *Quaternary Science Reviews*, 24 (5-6), 681-708.
- Napieralski, J., Harbor, J. and Li, Y. 2007. Glacial geomorphology and geographic information systems. *Earth-Science Reviews*, 85 (1-2): 1-22.
- Neal, A. 2004. Ground-penetrating radar and its use in sedimentology: principles, problems and progress. *Earth-Science Reviews*, 66, 261-330.
- Nesje, A. 1992. Younger Dryas and Holocene glacier fluctuations and equilibrium-line altitude variations in the Jostedalbreen region, western Norway. *Climate Dynamics*, 6, 221-227.
- Nesje, A. 2009. Latest Pleistocene and Holocene alpine glacier fluctuations in Scandinavia. *Quaternary Science Reviews*, 28, 2119-2136.
- Nesje, A., Bakke, J., Dahl, S.O., Lie, Ø., and Matthews, J.A. 2008. Norwegian mountain glaciers in the past, present and future. *Global Planetary Change*, 60 (1-2), 10-27.
- Niethammer, U., James, M.R., Rothmund, J.S., Travelletti, J. and Joswig, M. 2012. UAV-based remote sensing of the Super-Sauze landslide: Evaluation and results. *Engineering Geology*, 128, 2-11.
- Nobes, D.C. 2011. Ground penetrating radar measurements over glaciers. In Singh, V.P and Iaritashya, U.K. (eds.). *Encyclopedia of Snow, Ice and Glaciers*. Springer, Dordrecht.
- Núñez-Nieto, X., Solla, M., Novo, A., Lorenzo, H. 2014. Three-dimensional ground penetrating radar methodologies for the characterization and volumetric reconstruction of underground tunnelling. *Construction and Building Materials*, 71, 551-560.

- Oguchi, T., Hayakawa, Y.S. and Wasklewicz, T. 2011. Data Sources. In: Smith, M.J., Paron, P. and Griffiths, J. (eds) *Geomorphological Mapping: a handbook of techniques and applications*. Elsevier, London, pp 151-187.
- Osborn, G., McCarthy, D., LaBrie, A. and Burke, R. 2015. Lichenometric dating: Science or pseudo-science? *Quaternary Research*, 83 (1), 1-12.
- Osborn, G.D. 1978. Fabric and origin of lateral moraines, Bethartoli Glacier, Garhwal Himalaya, India. *Journal of Glaciology*, 20, 547-553.
- Osborn, G.D. 1986. Lateral-moraine stratigraphy and neoglacial history of Bugaboo Glacier, British Columbia. *Quaternary Research*, 26 (2), 171-178.
- Østrem, G. 1959. Ice melting under a thin layer of moraine, and the existence of ice cores in moraine ridges. *Geografiska Annaler*, 41A: 228-230.
- Østrem, G. 1963. Comparative crystallographic studies on ice from ice-cored moraine, snow banks and glaciers. *Geografiska Annaler*, 45, 210-40
- Østrem, G. 1964. Ice-cored moraines in Scandinavia. *Geografiska Annaler*, 46: 282-337.
- Østrem, G. 1965. Problems of Dating Ice-Cored Moraines. *Geografiska Annaler*, 47A (1), 1-38.
- Østrem, G. 1971. Rock Glaciers and Ice-Cored Moraines, a Reply to D. Barsch. *Geografiska Annaler*, 53A (3-4), 207-213.
- Østrem, G. and Arnold, K. 1970. Ice-Cored Moraines in Southern British Columbia and Alberta, Canada. *Geografiska Annaler, Series A*. 52 (2), 120-128.
- Ouédraogo, M.M., Degré, A., Debouche, C. and Lisein, J. 2014. The evaluation of unmanned aerial system-based photogrammetry and terrestrial laser scanning to generate DEMs of agricultural watersheds. *Geomorphology*, 214, 339-355.
- Overgaard, T and Jakobsen, P.R. 2001. Mapping of glaciotectionic deformation in an ice marginal environment with ground penetrating radar. *Journal of Applied Geophysics*, 47 (3-4), 191-197.
- Parriaux, A. and Nicoud, G.F. 1990. Hydrological behaviour of glacial deposits in mountainous areas, in: L. Molnár (Ed.), *Hydrology of Mountainous Areas*. International Association of Hydrological Sciences, Publication 190, pp 291-311.
- Paul, F., Kääb, A., Maisch, M., Kellenberger, T. and Haeberli, W. 2004. Rapid disintegration of Alpine glaciers observed with satellite data. *Geophysical Research Letters*, 31 (21), L21402.
- Pellicer, X.M. and Gibson, P. 2011. Electrical resistivity and Ground Penetrating Radar for the characterisation of the internal architecture of Quaternary sediments in the Midlands of Ireland. *Journal of Applied Geophysics*, 75 (4), 638-647.
- Pettersson, R. Jansson, P. and Holmlund, P. Cold surface layer thinning on Storglaciären, Sweden, observed by repeated ground penetrating radar surveys. *Journal of Geophysical Research: Earth Surface*, 108 (F1).
- Pickard, J. 1983. Surface lowering of ice-cored moraine by wandering lakes. *Journal of Glaciology*, 29, 338-342.

- Pomeroy, J.A. 2013. The sedimentary and geomorphic signature of subglacial processes in the Tarfala Valley, northern Sweden, and the links between subglacial soft-bed deformation, glacier flow dynamics, and landform generation. Unpublished PhD Thesis. Loughborough University.
- Powers, M.C. 1953. A new roundness scale for sedimentary particles. *Journal of Sedimentary Research*, 23 (2), 117-119.
- Price, R.J. 1970. Moraines at Fjallsjökull, Iceland. *Arctic and Alpine Research*, 2 (1), 27-42.
- Pyle, C.J., Richards, K.S. and Chandler, J.H. 1997. Digital photogrammetric monitoring of river bank erosion. *The Photogrammetric Record*, 15, 753-764.
- Ramage, J.M., Smith, J.A., Rodbell, D.T. and Seltzer, G.O. 2005. Comparing reconstructed Pleistocene equilibrium-line altitudes in the tropical Andes of central Peru. *Journal of Quaternary Science*, 20 (7-8), 777-788.
- Rango, A., Laliberte, A., Herrick, J.E., Winters, C., Havstad, K., Steele, C. and Browning, D. 2009. Unmanned aerial vehicle-based remote sensing for rangeland assessment, monitoring and management. *Journal of Applied Remote Sensing*, 3, 1-15.
- Reinardy, B., Leighton I. and Marx, P. 2013. Glacial thermal regime linked to processes of annual moraine formation at Midtdalsbreen, southern Norway. *Boreas* 42 (4), 896-911.
- Reyes, A.V., Wiles, G.C., Smith, D.J., Barclay, D.J., Allen, S., Jackson, S., Larocque, S., Laxton, S., Lewis, D., Calkin, P.E. and Clague, J.J. 2006. Expansion of alpine glaciers in Pacific North America in the first millennium A.D. *Geology*, 34 (1), 57-60.
- Reynolds, J.M. 2011. Chapter 12: An Introduction to Applied and Environmental Geophysics. John Wiley & Sons, New York.
- Reznichenko, N., Davies, T., Shulmeister, J. and McSaveney, M. 2010. Effects of debris on ice surface melting rates: an experimental study. *Journal of Glaciology*, 56 (197), 384-394.
- Rhind, P. and Jones, B. The vegetation history of Snowdonia since the Last Glacial Period. *Field Studies*, 10, 539-552.
- Rippin, D.M., Carrivick, J.L., and Williams, C. 2011. Evidence towards a thermal lag in the response of Kårsaglaciären, northern Sweden, to climate change. *Journal of Glaciology*, 57 (205), 895-903.
- Roberson S. and Hubbard B. 2010. Application of borehole optical televiewing to investigating the 3-D structure of glaciers: implications for the formation of longitudinal debris ridges, midre Lovénbreen, Svalbard, *Journal of Glaciology*, 56 (195), 143-156.
- Roberson, S. 2008. Structural composition and sediment transfer in a composite cirque glacier: Glacier de St. Sorlin, France. *Earth Surface Processes and Landforms*. 33 (13), 1931-1947.
- Robinson, M., Bristow, C., McKinley, J. and Ruffel, A. 2013. Section 1.5.5: GPR. In: Clarke, L.E & Nield, J.M. (Eds.) *Geomorphological Techniques* (Online Edition). British Society for Geomorphology; London, UK. ISSN: 2047-0371.

- Rood, D.H., Burbank, D.W. and Finkel, R.C. 2011. Chronology of glaciations in the Sierra Nevada from ^{10}Be surface exposure dating. *Quaternary Science Reviews*, 30, 646-661.
- Rosnell, T and Honkavaara, E. 2012. Point Cloud Generation from Aerial Image Data Acquired by a Quadrocopter Type Micro Unmanned Aerial Vehicle and Digital Still Camera. *Sensors*, 12, 453-480.
- Röthlisberger, F. and Schneebeli, W. 1979. Genesis of lateral moraine complexes, demonstrated by fossil soils and trunks: indicators of postglacial climatic fluctuations. In: Schlüchter, C. (ed.), *Moraines and Varves*. Balkema, Rotterdam, 387-419.
- Röthlisberger, F., Haas, P., Holzhauser, H., Keller, W., Bircher, W. and Renner F. 1980. Holocene climatic fluctuations - radiocarbon dating of fossil soils (fAh) and woods from moraines and glaciers in the Alps. *Geographica Helvetica*, 35, 21-52.
- Ryan, J.C., Hubbard, A.L., Box, J.E., Todd, J., Christoffersen, P., Carr, J.R., Holt, T.O., Snooke, N. 2015. UAV photogrammetry and structure from motion to assess calving dynamics at Store Glacier, a large outlet draining the Greenland ice sheet. *The Cryosphere*, 9, 1-11.
- Sadura, S., Martini, I.P., Endres, A.L. and Wolf, K. 2006. Morphology and GPR stratigraphy of a frontal part of an end moraine of the Laurentide Ice Sheet: Paris Moraine near Guelph, ON, Canada. *Geomorphology*, 75: (1-2), 212-225.
- Saintenoy, A., Friedt, J.-M., Booth, A.D., Tolle, F., Bernard, E., Laffly, D., Marlin, C. and Griselin, M. 2012. Deriving ice thickness, glacier volume and bedrock morphology of Austre Lovénbreen (Svalbard) using GPR. *Near Surface Geophysics*, 11 (2), 253-26.
- SCNAT 2015. *Glaciological reports (1881-2015) The Swiss Glaciers, 1880-2010/11*, Yearbooks of the Cryospheric Commission of the Swiss Academy of Sciences (SCNAT), 1-132. Published since 1964 by VAW-ETH Zürich.
- Schäfer, J.M., Heinrich, B., Denton, G.H., Ivy-Ochs, S., Marchant, D.R., Schlüchter, C. and Rainer, W. 2000. The oldest ice on Earth in Beacon Valley, Antarctica: new evidence from surface exposure dating. *Earth and Planetary Science Letters*, 179 (1), 91-99.
- Schiefer, E. and Gilbert, R. 2007. Reconstructing morphometric change in a proglacial landscape using historical aerial photography and automated DEM generation. *Geomorphology*, 88 (1-2), 167-178.
- Schimmelpfennig, I., Schaefer, J.M., Akçar, N., Koffman, T., Ivy-Ochs, S., Schwartz, R., Finkel, R.C., Zimmerman, S. and Schlüchter, C. 2014. A chronology of Holocene and Little Ice Age glacier culminations of the Steingletscher, Central Alps, Switzerland, based on high-sensitivity beryllium-10 moraine dating. *Earth and Planetary Science Letters*, 393, 220-230.
- Schimmelpfennig, I., Schaefer, J.M., Akçar, N., Ivy-Ochs, S., Finkel, R.C and Schlüchter, C. 2013. Holocene glacier culminations in the Western Alps and their hemispheric relevance. *Geology*, 40, 891-894.
- Schomacker, A. 2008. What controls dead-ice melting under different climate conditions? A discussion. *Earth-Science Reviews*, 90 (3-4), 103-113.

- Schomacker, A. and Kjær, K.H. 2007. Origin and de-icing of multiple generations of ice-cored moraines at Brúarjökull, Iceland. *Boreas*, 36 (4), 411-425.
- Schomacker, A. and Kjær, K.H. 2008. Quantification of dead-ice melting in ice-cored moraines at the high-Arctic glacier Holmströmbreen, Svalbard. *Boreas*, 37 (2): 211-225.
- Schwamborn, G., Heinzl, J., Schirrmeyer, L. 2007. Internal characteristics of ice-marginal sediments deduced from georadar profiling and sediment properties (Brøgger Peninsula, Svalbard). *Geomorphology*, 95 (1-2), 74-83.
- Schytt, V. 1959. The Glaciers of the Kebnekajse-Massif. *Geografiska Annaler*, 41 (4), 213-227.
- Schytt, V. 1962. A tunnel along the bottom of Isfallsglaciären. *Geografiska Annaler*, 44 (3-4), 411-412.
- Schytt, V. 1966. Notes on Glaciological Activities in Kebnekaise, Sweden during 1965. *Geografiska Annaler*, 48 (1), 43-50.
- Shakesby, R.A., Dawson, A.G. and Matthews, J.A. 1987. Rock glaciers, protalus ramparts and related phenomena, Rondane, Norway: a continuum of large-scale talus derived landforms. *Boreas*, 16, 306-317.
- Shakesby, R.A., Matthews, J.A. and Winkler, S. 2004. Glacier variations in Breheimen, southern Norway: relative-age dating of Holocene moraine complexes at six high-altitude glaciers. *The Holocene*, 14 (6), 899-910.
- Sletten, K., Lyså, A. and Lønne, I. 2001. Formation and disintegration of a high - arctic ice - cored moraine complex, Scott Turnerbreen, Svalbard. *Boreas*, 30, 272-284.
- Small, R.J. 1983. Lateral moraines of Glacier De Tsidjore Nouve: form, development and implications. *Journal of Glaciology*, 29 (102), 250-259.
- Small, R.J. 1987. The Glacial Sediment System: An Alpine Perspective. In: Gurnell, A.M. (ed.) *Glacio-fluvial Sediment Transfer*. John Wiley and Sons Ltd, Chichester, pp 199-203.
- Smith, D.G. and Jol, H.M. 1995. Ground penetrating radar: antenna frequencies and maximum probable depths of penetration in Quaternary sediments. *Journal of Applied Geophysics*, 33, 93-100.
- Smith, M.J., Chandler, J. and Rose, J. 2009. High spatial resolution data acquisition for the geosciences: kite aerial photography. *Earth Surface Processes and Landforms*, 34, 155-161.
- Snaveley, N., Seitz, S.M. and Szeliski, R. 2008. Modelling the World from Internet Photo Collections. *International Journal of Computer Vision*, 80 (2), 189-210.
- Sneed, E.D. and Folk, R.L. 1958. Pebbles in the lower Colorado River, Texas, a study of particle morphogenesis. *Journal of Geology*, 66 (2), 114-150.
- Spaete, L.P., Glenn, N.F., Derryberry, D.R., Sankey, T.T., Mitchell, J.J., and Hardegree, S.P. 2011. Vegetation and slope effects on accuracy of a LiDAR-derived DEM in the sagebrush steppe. *Remote Sensing Letters*, 2 (4), 317-326.

- Spedding, N. and Evans, D.J.A. 2002. Sediments and landforms at Kvíárjökull, southeast Iceland: a reappraisal of the glaciated valley landsystem. *Sedimentary Geology*, 149, 21–42.
- Staines, K.E., Carrivick, J.L., Tweed, F.S., Evans, A.J., Russell, A.J., Jóhannesson, T. and Roberts, M. 2014. A multi-dimensional analysis of proglacial landscape change at Sólheimajökull, southern Iceland. *Earth Surface Processes and Landforms*, 40 (6), 809-822.
- Stieglitz, M., Déry, S.J., Romanovsky, V.E., Osterkamp, T.E. 2003. The role of snow cover in the warming of arctic permafrost. *Geophysical Research Letters*, 30 (13), 1721.
- Sugden, D.E., Marchant, D.R., Potter Jr. N., Souchez, R.A., Denton, G.H., Swischer III, C.C. and Tison, J.-L. 1995. Preservation of Miocene glacier ice in East Antarctica. *Nature*, 376, 412–414.
- Swift, D.A., Evans, D.J.A. and Fallick, A.E. 2006. Transverse englacial debris-rich ice bands at Kvíárjökull, southeast Iceland. *Quaternary Science Reviews*, 25 (13-14), 1708-1718.
- Swisstopo. 2014. Swisstopo: swissALTI3D. Available at URL: <http://www.swisstopo.admin.ch/internet/swisstopo/en/home/products/height/swissALTI3D.html>. Retrieved: 21/05/2014.
- Tarolli, P. 2014. High-resolution topography for understanding Earth surface processes: opportunities and challenges. *Geomorphology*, 216, 295-312.
- Tonkin, T.N., Midgley, N.G., Graham, D.J. and Labadz, J.C. 2014. The potential of small unmanned aircraft systems and structure-from-motion for topographic surveys: A test of emerging integrated approaches at Cwm Idwal, North Wales. *Geomorphology*, 226, 35-43.
- Tonkin, T.N., Midgley, N.G., Cook, S.J and Grahan, D.J. 2016. Ice-cored moraine degradation mapped and quantified using an unmanned aerial vehicle: a case study from a polythermal glacier in Svalbard. *Geomorphology*, 158, 1-10.
- Turner, D., Lucieer, A. and Watson, C. 2012. An Automated Technique for Generating Georectified Mosaics from Ultra-High Resolution Unmanned Aerial Vehicle (UAV) Imagery, Based on Structure from Motion (SfM) Point Clouds. *Remote Sensing*, 4, 1392-1410.
- Van der Wateren, F.M., 2002, Processes of Glaciotectonism, invited chapter in Menzies, J., ed., *Glacial Environments: Processes, Sediments and Landforms*. Butterworth-Heinemann, Oxford, pp 417-443.
- Waller, R.I., Murton, J.B. and Kristensen, L. 2012. Glacier-permafrost interactions: Processes, products and glaciological implications. *Sedimentary Geology*, 255, 1-28.
- Watts, A.C., Smith, S.E., Burgess, M.A., Wilkinson, B.E., Szantoi, Z., Ifju, P.G. and Franklin Percival, H. 2010. Small Unmanned Aircraft Systems for Low-Altitude Aerial Surveys. *Journal of Wildlife Management*: 74 (7), 1614-1619.
- Wechsler, S.P. 2007. Uncertainties associated with digital elevation models for hydrologic applications: a review. *Hydrology and Earth System Sciences*, 11, 1481-1500.

- Weertman, J. 1961. Mechanism for the formation of inner moraines found near the edge of cold ice caps and ice sheets. *Journal of Glaciology*, 3, 965-978.
- Wentworth, C.K. 1922. A scale of grade and class terms for clastic sediments. *The Journal of Geology*, 30: 377-392.
- Wester-Ebbinghaus, W. 1980. Aerial Photography by radio controlled model helicopter. London. England. *The Photogrammetric Record*. Vol. X No. 55.
- Westoby, M., Brasington J, Glasser, N.F., Hambrey, M.J. and Reynolds, M.J. 2012. Structure-from-Motion photogrammetry: a low-cost, effective tool for geoscience applications. *Geomorphology*, 179, 300-314.
- WGMS. 2012. Fluctuations of Glaciers 2005-2010 (Vol. X). Zemp, M., Frey, H., Gärtner-Roer, I., Nussbaumer, S.U., Hoelzle, M., Paul, F. and W. Haeberli (eds.), ICSU (WDS) / IUGG (IACS) / UNEP / UNESCO / WMO, World Glacier Monitoring Service, Zurich, Switzerland, pp 1-336.
- Whalley, W.B. 1973. Correspondence: An exposure of ice on the distal side of a lateral moraine. *Journal of Glaciology*, 12 (65), 327-329.
- Whalley, W.B. 1975. Abnormally steep slopes on moraines constructed by valley glaciers. In: Proceedings of the Midland Soil Mechanics and Foundation Engineering Society Symposium: The engineering behaviour of glacial materials, University of Birmingham, 21st -23rd April, 1975, 60-66.
- Whalley, W.B. 2009. On the interpretation of discrete debris accumulations associated with glaciers with special reference to the British Isles. *Geological Society, London, Special Publications*. 320, 85-102.
- Whalley, W.B. 2012. Using Discrete Debris Accumulations to Help Interpret Upland Glaciation of the Younger Dryas in the British Isles. In: Piacentini, T. and Miccadei, E. (eds.), *Studies on Environmental and Applied Geomorphology*. 1-21.
- Whalley, W.B. and Martin, H.E. 1992. Rock glaciers : II models and mechanisms. *Progress in Physical Geography*. 16 (2), 127-186.
- Wheaton, J.M., Brasington, J., Darby, S.E. and Sear, D.A. 2010. Accounting for uncertainty in DEMs from repeat topographic surveys: improved sediment budgets. *Earth Surface Processes and Landforms*, 35 (2), 136-156.
- Whitehead, K., Moorman, B.J. and Hugenholtz, C.H. 2013. Brief Communication: Low-cost, on-demand aerial photogrammetry for glaciological measurement. *The Cryosphere*, 7, 1879-1884.
- Williams, R.D. 2012. Section 2.3.2: DEMs of difference (using DODs to quantify landscape change and uncertainty analysis in DoDs). In: Clarke, L.E & Nield, J.M. (Eds.) *Geomorphological Techniques* (Online Edition). British Society for Geomorphology, London, UK. ISSN: 2047-0371.
- Winkler, S. and Matthews, J.A. 2010. Observations on terminal moraine-ridge formation during recent advances of southern Norwegian glaciers. *Geomorphology*, 116 (1-2): 87-106.

- Worni, R., Stoffel, M., Huggel, C., Volz, C., Casteller, A. and Luckman, B. 2012. Analysis and dynamic modeling of a moraine failure and glacier lake outburst flood at Ventisquero Negro, Patagonian Andes (Argentina). *Journal of Hydrology*, 444–445, 134–145.
- Zemp, M., Jansson, P. Holmlund, P. Gärtner-Roer, I. Koblet, T., Thee, P. and Haeberli, W. 2010. Reanalysis of multi-temporal aerial images of Storglaciären, Sweden (1959 – 99) – Part 2: Comparison of glaciological and volumetric mass balances. *The Cryosphere*, 4, 345-357.
- Zemp, M., Paul, F., Hoelzle, M. and Haeberli, W. 2006. Glacier fluctuations in the European Alps 1850– 2000: an overview and spatiotemporal analysis of available data, In: *The Darkening Peaks: Glacial Retreat in Scientific and Social Context*, (eds.) Orlove, B., Wiegandt, E. and Luckman. Berkeley University Press, Berkeley.